1991

A micro-simulation of heat and fluid flow to determine thermal fluctuation at the mold/plastic interface during plastic injection molding.

Xuong T. Nguyen
University of Windsor

NOTICE

The quality of this microform is heavily dependent upon the quality of the original thesis submitted for microfilming. Every effort has been made to ensure the highest quality of reproduction possible.

If pages are missing, contact the university which granted the degree.

Some pages may have indistinct print especially if the original pages were typed with a poor typewriter ribbon or if the university sent us an inferior photocopy.

Reproduction in full or in part of this microform is governed by the Canadian Copyright Act, R.S.C. 1970, c. C-30, and subsequent amendments.

AVIS

La qualité de cette microforme dépend grandement de la qualité de la thèse soumise au microfilmage. Nous avons tout fait pour assurer une qualité supérieure de reproduction.

S'il manque des pages, veuillez communiquer avec l'université qui a conféré le grade.

La qualité d'impression de certaines pages peut laisser à désirer, surtout si les pages originales ont été dactylographiées à l'aide d'un ruban usé ou si l'université nous a fait parvenir une photocopie de qualité inférieure.

La reproduction, même partielle, de cette microforme est soumise à la Loi canadienne sur le droit d'auteur, SRC 1970, c. C-30, et ses amendements subséquents.

A MICRO-SIMULATION OF HEAT AND FLUID FLOW TO DETERMINE THERMAL FLUCTUATION AT THE MOLD/PLASTIC INTERFACE DURING PLASTIC INJECTION MOLDING

by

XUONG T. NGUYEN

A thesis

Submitted to the Faculty of Graduate Studies and Research

Through The Department of Mechanical Engineering

In Partial Fulfillment of the Requirements for

the Degree of Master Applied Science

in Engineering Materials at the

University of Windsor.

Windsor, Ontario, Canada

1991

ISBN 0-315-65140-7

ABSTRACT

In most of Computer-Aided-Engineering (CAE) packages used in injection molding, the assumption of an isothermal boundary and/or perfect thermal contact along the mold wall interface is very commonly used to facilitate the filling flow analysis as well as the thermal analysis of the process. Each analysis is carried out as a separate work. The objective of this thesis is to bring the cavity domain of the plastic part and the mold part together as a composite domain, to take the thermal resistance of the interface into account and to simulate the basic stages of the total cycle time of injection molding, especially the thermal characteristics of the interface.

A two-dimensional mathematical model has been developed using a generalized Newtonian fluid for the problem. A stable finite difference method (FDM) scheme has been developed with an interpolation approach for the streamline velocity profile, instead of the iterative method which is implemented by many researchers in dealing with this type of analysis. The program analysis in this thesis can determine the cross-sectional velocity profile of the flowing plastic along the flow-direction during the filling stage. The effects of varying the contact conductance, part thickness, injection speed and mold temperature were examined. The results of the thermal analysis show that for the filling flow, the isothermal cavity boundary should be relocated somewhere inside the mold wall, away from the cavity surface. For a constant contact conductance Hr, the discontinuative temperature gap at the interface diminishes hyperbolically with time.

DEDICATION

This Work is Affectionately Dedicated to

My Schools and My Teachers

ACKNOWLEDGEMENTS

The author wishes to gratefully thank the following persons for their help in various aspects of this work:

Dr. D.F. Watt for his research grant, his indispensable supports

Dr. N. Zamani for his discussions and suggestions on mathematical aspects of the thesis.

Dr. D. O. Northwood for his personal advices during this master program.

Dr. T. W. McDonald for his suggestions throughout all parts of this thesis.

without your helps, the thesis can be accomplished so.

CONTENTS

Abstract iii

Dedication iv

Acknowledgements v

List of Tables ix

List of Figures x

Nomenclature xii

Chapter I: INTRODUCTION 1

THE INJECTION MOLDING MACHINE AND OPERATION 1
Injection Molding Machines 2
The Injection Molding Process 3
CAE IN INJECTION MOLDING 6
Mold Filling Analysis 7
Cooling and Solidification Analysis 9
Summary of CAE in Injection Molding 9
THE OBJECTIVES OF THIS THESIS 10

Chapter II: LITERATURE REVIEW 11

MAIN COMMERCIAL INJECTION MOLDING PACKAGES 11
TMCONCEPT Expert System 11
MOLDFLOW Packages 18
Micro Analysis 18
Macro Analysis: 21
Mold Cooling Analysis 25
POLYCOOL 2 Packages 27
Coupling of The Part and Mold Analysis: 30
MOLDCOOL package: 31
C-FLOW Packages 33
MCKAM-2 Package 33
Summary of Current State of CAE 34
REVIEW OF TECHNICAL ACADEMIC PUBLICATIONS 35
Heat Transfer with a Freezing Boundary 35

Fluid Flow And Heat Transfer in Injection Molding Processes . . . 37
Fluid Flow Equations . . . 37
Heat Transfer Equations . . . 39
Work of H. Van Wijngaarden, J. F. Dijksman and P.Wesseling [17] . . . 39
Other Publications . . . 40

Chapter III: DEVELOPMENT OF THE MODEL . . . 44

PRELIMINARY STUDIES . . . 44
THE MAIN PURPOSE OF THE THESIS . . . 46
THE PHYSICAL MODEL AND THE MATHEMATICAL MODEL . . . 48
The Mathematical Model Equations . . . 53
The Simplified Model Equations . . . 58
THE NUMERICAL FDM ALGORITHM . . . 62
The Nodal Grid Scheme . . . 63
The Finite Difference Scheme . . . 67
The Post Filling Calculation . . . 72
MAIN COMPUTER PROGRAMING ASPECTS . . . 73

Chapter IV: RESULTS AND DISCUSSIONS . . . 78

INPUTS . . . 78
RESULTS . . . 83
Group A: Transient start up cyclic behaviour . . . 85
Group B: The effect of varying the mean injection velocity (V) . . . 103
Group C: The effect of varying the cavity thickness (2h) . . . 114
Group D: The effect of varying the contact conductance (Hr) . . . 121
Group E: The effect of varying the mold sink temperature (To) . . . 133
DISCUSSION OF RESULTS . . . 139
Group A: Transient cyclic behaviour . . . 139
Group B: Effect of varying the mean injection velocity (V) . . . 142
Group C: Effect of varying the cavity thickness (2h) . . . 145
Group D: Effect of varying the thermal contact conductance (Hr) . . . 148
Group E: Effect of varying the initial mold temperature (To) . . . 150
Some suggestions for the flow analysis . . . 151
Possible sources of error in the model analysis . . . 152
Critique of the main program . . . 154

Chapter V: CONCLUSIONS AND RECOMMENDATIONS . . . 157

CONCLUSIONS . . . 157
RECOMMENDATIONS . . . 158

Chapter VI: POSSIBLE APPLICATIONS AND FUTURE WORKS . 159

APPLICATIONS 159
FUTURE WORKS 168
Domain decoupling 168
Possible Extend of the Model Development 170
Experimental Works 172

Appendix A: Some Results of The Third Preliminary Study: 180

Appendix B: The Approximation of Thermal Contact Conductance Value Hr 187

The Radiation Across The Interface Air Gap: 187
The Conduction Across The Interface Air Gap: 188

Appendix C: The Simplified Freezing Boundary Condition 189

Appendix D: The Derivations of Velocity and Pressure Gradient Integrations 191

Appendix E: Simpson's Rule For Numerical Integration of Unequal Spaced X-Data 193

Appendix F: The Polymer Orientation in Injection Molded Objects . . . 194

VITA AUCTORIS 197

LIST OF TABLES

DATA TABLE 1: The physical properties of the mold and polymer part 80

DATA TABLE 2: The table of change in values chosen for some process parameters 82

LIST OF FIGURES

Fig.1.1: Basic elements of injection molding process..... 2

Fig.1.2: Molding machine function 4

Fig.1.3: Injection molding cycles 5

Fig.2.1: FA1 Calculation model..... 16

Fig.2.2: FA2 Calculation model 17

Fig.2.3: Flow path divided into sections 18

Fig.2.4: Single slice 18

Fig.2.5: Starting positions 26

Fig.2.6: Optimized cooling lines 26

Fig.3.1a: An injection moulding model of a thin rectangular plastic sheet 49

Fig.3.1b: The macro-analysis of the filling stage for the thin rectangular mould cavity 50

Fig.3.2 (a & b) : The 2-dimensional micro-analysis for the cross-section along the flow direction 51

Fig.3.3: The simple sketch of the model and nodal mesh 64

Fig.3.4: Definition of Δx , Δy , Δs..... 67

Fig.3.5: Flow Chart For Computational Scheme 74

Fig.A.N.n: Group A, Results of Transient Start Up Behaviour 85

Fig.B.N.n: Group B, Results of The Effect of Varying The Mean Injection Speed (V) 103

Fig.C.N.n: Group C, Results of The Effect of Varying The Cavity Thickness (2h) 114

Fig.D.N.n: Group D, Results of The Effect of Varying The Contact Conductance (Hr) 121

Fig.E.N.n: Group E, Results of The Effect of Varying The Initial Mold Temperature (To) 133

Fig.6.n : The values of the program compared with those of the empirical formula for the temperature gap at the interface 161

NOMENCLATURE

A	temperature coefficient
C_p	heat capacity of liquid polymer (J/kg.K)
C_{p_s}	heat capacity of solidified polymer (J/kg.K)
C_{p_m}	heat capacity of mold steel (J/kg.K)
2h	cavity thickness (m)
Ha	heat transfer coefficient of surrounding air (W/m.m.K)
Hc	heat transfer coefficient of coolants (W/m.m.K)
Hr	thermal contact conductance at mold/plastic interface (W/m.m.K)
k_l	thermal conductivity of liquid polymer (W/m.K)
k_s	thermal conductivity of solidified polymer (W/m.K)
k_m	thermal conductivity of mold steel (W/m.K)
k_1	thermal conductivity of solid 1 (W/m.K)
k_2	thermal conductivity of solid 2 (W/m.K)
l_m	distance from mold surface to heat sink (m)
l_c	length of cavity (m)
l^*	location of flow front during filling (m)
m_o	coefficient of Power-law model ($Pa.sec^n$)
n	Power law index

P	pressure (Pa)
P_{max}	maximum attainable pressure at entrance (Pa)
Q^*	volumetric flow rate through gate (m^3/sec)(1/m)
t	time (sec)
T	temperature (Celsius)
T_s	temperature in solid (Celsius)
T_l	temperature in liquid (Celsius)
T_m	transition temperature (Celsius)
T_b	injection temperature (Celsius)
To	mold isothermal heat sink temperature (Celsius)
u_1 , u_2	velocity components in the x_1– and x_2-directions, respectively
V	mean injection velocity (m/sec)
v_n	normal velocity of freezing boundary (m/sec)
x_1 , x_2	coordinates; x_1 flow direction, x_2 transverse direction (m)
δ	x_2-coordinate of freezing boundary (m)
λ	latent heat of fusion of polymer (J/kg)
ρ	density of liquid polymer (kg/m.m.m)
ρ_s	density of solidified polymer (kg/m.m.m)
ρ_m	density of mold steel (kg/m.m.m)
α_1 , α_2	thermal diffusivities of solid 1 and solid 2 respectively (m.m/sec)
Δ_y^m	step size in y-direction of mold steel (m)
Δ_x^m	step size in x-direction of mold steel (m)

Δt	time step (sec)

Dimensionless symbols

Q	gate flux = $Q^* / 2hV$
s	natural coordinate along streamline
u	velocity component x-direction = u_1/V
v	velocity component y-direction = $u_2/\varepsilon V$
$\bar{v}$	velocity component of freezing boundary in y-direction
x	coordinate in the flow direction = x_1/l_c
y	coordinate in the transverse direction = x_2/h
X_k	x-coordinate grid line
Y_k^l	y-coordinate intersection of grid line X_k with streamline l
α	y-coordinate of freezing boundary = δ/h
β	number needed to define entrance grid points
$\dot{\gamma}$	shear rate
Δs	step size along streamline
ΔX	step size in x-direction
$\Delta\tau$	time step chosen
ε	asymptotic parameter = h/l_c
π	pressure = $\varepsilon P / \rho V^2$
π_o	ambient pressure
π_{max}	maximum pressure
τ	time = Vt / l_c

θ temperature = $(T-T_b)/(T_m-To)$

θ_k^l temperature at intersection of grid line X_k and streamline l

θ^* interpolated temperature for previous time step

Dimensionless numbers

$Re = \rho hV/\eta_o$

$Gz = \varepsilon Pe = \varepsilon\rho C_p Vh/k$

$Gz_s = \varepsilon\rho_s C_{Ps} Vh/k_s$

$Br = \eta_o V^2/\{k(T_m-To)\}$

$Ste = C_p(T_m-To)/\lambda$

with : $\eta_o = m_o(V/h)^{n-1}$

A few other symbols are locally defined or self explained.

Chapter I
INTRODUCTION

Plastic processing is one of the world's fastest growing industries. The two major processing methods are injection molding and extrusion. Approximately, 32% by weight of all plastics processed goes through injection molding machines, 36% through extruders, and the remaining 32% is formed by other plastic processing methods.

Injection molding is principally a mass-production method producing unlimited quantities of complicated shaped plastic parts with little or no finishing operations. The surface of injection moldings are as smooth and bright or as grained and engraved as the surface of the mold cavity in which they were prepared.

1.1 THE INJECTION MOLDING MACHINE AND OPERATION

The following paragraphs are a basic description of the injection molding process, summarized from reference [1].

An injection molding machine converts, processes, and forms raw plastic material fed in as powder or pellets or regrind to produce a part of desired shape and configuration. The process of injection molding consists of heating plastic material until it melts, and then forcing this melted plastic into a mold where it cools and solidifies.

1.1.1 INJECTION MOLDING MACHINES

An injection molding machine consists of the three main components working together in the injection molding process as shown in Figure 1.1.

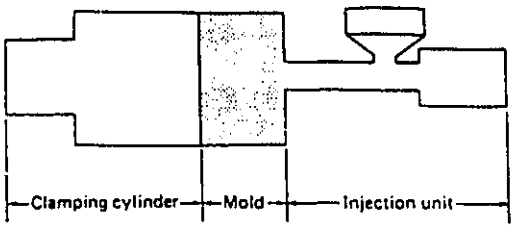

Figure 1.1: Basic elements of injection molding process [1].

(a) The injection unit. This portion of an injection machine converts a plastic material from a solid state to a homogeneous semi-liquid phase by raising its temperature. It then maintains the plastic material at a preset temperature, and forces it upon demand, through an injection unit nozzle into a mold cavity. Nowadays, the reciprocating screw injection unit, which is a combination of the high plasticizing capacity of the screw extruder with the high pressure and fast filling characteristics of ram-type machine, is in widespread use.

(b) The mold. The function of the mold is twofold. It imparts the desired shape to the plasticized polymer and it cools the injection molded part. For more details about mold design, see Ref.[1] .

(c) The clamping device. This is the portion of an injection molding machine in which the mold is mounted and which provides the motion and forces necessary to open and close the mold, and to hold the mold closed during the injection and packing phases. The clamping device must have sufficient locking force to resist the tendency of fluid plastic moving at high pressure to force apart the mold halves.

1.1.2 THE INJECTION MOLDING PROCESS

In the injection molding process, the following basic operations exist:

1. Raising the temperature of a plastic to a point where it will flow under pressure. This is usually done by simultaneously heating and masticating granular solid until it forms a melt at an elevated and uniform temperature. Today this is accomplished in the cylinder of the injection unit with a reciprocating screw. This step is called plasticizing of the material.

2. Injecting the liquid, molten plastic from the injection cylinder of the machine through various flow channels (sprue, runner) to fill all the cavities of the mold.

3. Allowing the plastic to solidify in the mold while keeping the material confined under pressure as the heat (which was added to the material to liquefy it) is removed into the mold, thus allowing the plastic to freeze permanently into the shape desired.

4. Opening the mold and ejecting the molded part.

5. Closing the mold in readiness for the step 2.

What makes this apparently simple operation complex is the limitations of the hydraulic circuitry used in the actuation of the injection plunger of the injection unit, the complicated flow paths involved in the filling of the mold and the cooling action in the mold.

A simplified description of the molding machine functions in operation is shown in Figure 1.2.

Figure 1.2: Molding machine function [1].

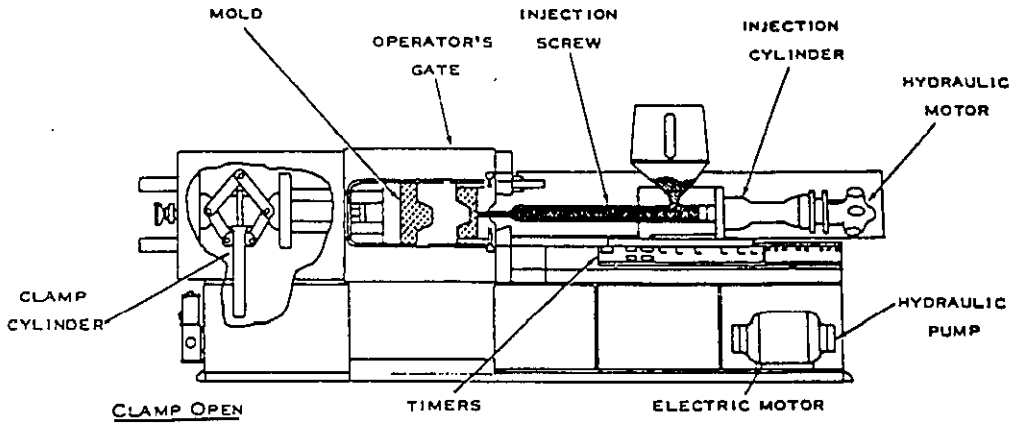

	ELECTRICAL	HYDRAULIC	MECHANICAL
1.	MOTOR SWITCH "ON"	PUMP PRESSURIZES SYSTEM	
2.	CLOSE OPERATOR'S GATE AND START CYCLE	OIL FLOWS TO CLAMP CYLINDER FROM HYDRAULIC MANIFOLD	CLAMP CLOSES
3.	CLOSING CLAMP TRIPS LIMIT SWITCH DIRECTING OIL TO INJECT	OIL FLOWS TO INJECTION CYLINDER	INJECTION RAM FORWARD TO INJECT

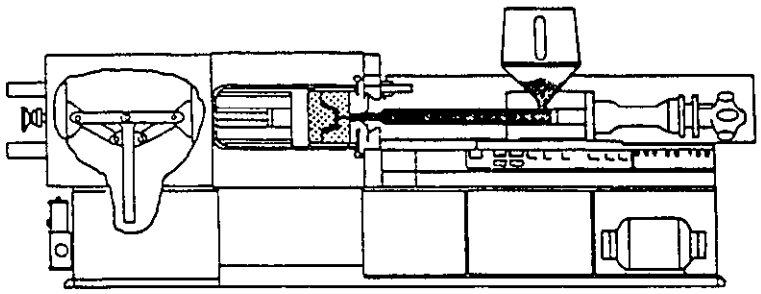

CLAMP CLOSED

4.	INJECTION TIMES OUT	OIL FLOWS TO SCREW DRIVE MOTOR	SCREW PUMPS ITSELF BACK AS PARTS COOL IN MOLD
5.	CLAMP COOLING TIMES OUT AND SCREW TRIPS SHOT SIZE LIMIT SWITCH	OIL FLOWS TO CLAMP CYLINDER ROD	SCREW STOPS ROTATING AND CLAMP OPENS
6.	EJECTION LIMIT SWITCH IS TRIPPED	OIL FLOWS TO EJECTOR CYLINDER	PART IS EJECTED FROM MOLD
7.	RECYCLE TIMER TIMES OUT	START CYCLE ETC.	

These steps must be properly coordinated together in the processing. The prime determinant of the productivity of an injection molding process is the manufacturing speed . This will depend on how fast we can heat the plastic to the molding temperature, inject it into mold cavity, how long it takes to cool the product in the mold, and how long it takes to eject the part and reseal the mold. A cycle time of a typical overall injection molding process is represented by Figure 1.3.

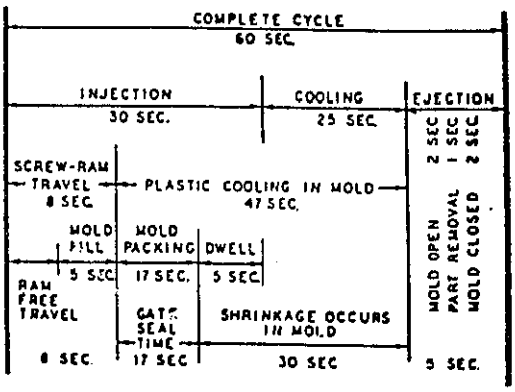

Figure 1.3: Injection molding cycle [1].

Optimum productivity is achieved as a balance between production speed and quality control. Both of these are dependent upon the proper coordination of the above steps, and the determination of the correct plastic temperature, injection pressure, cavity filling speed, mold temperature and cooling characteristics. These are usually determined by a combination of analytical and experimental studies.

1.2 CAE IN INJECTION MOLDING

The following review of the use of CAE (Computer-Aided-Engineering) in the injection molding industry is a condensed report of reference [2].

The complexity of the injection molding makes successful production start up on the first attempt a rare occurence. The combination of a viscoelastic molding material, an irregular mold geometry, steep temperature gradients and other criteria, such as appearance and dimensional tolerances, makes mold design a difficult task even for recognized experts. Optimum productivity and short start up times are required to be competitive in injection molding. Numerous iterations in prototyping a plastic part prior to satisfactory molding are costly in terms of engineering time to resolve the problem and the delay in getting the part to the customer.

In the past, very little was known about what was happening inside these familiar processing machines. Only with the begining of a deeper understanding of the process mechanism and the underlying physical laws (gained through close cooperation between theorists and technologists) has the plastic processing technology and mold design made any real progress. In recent years, many publications of scientific investigations of the rheological and thermodynamic phenomena occurring during the injection have been made making considerable use of computer simulations. In addition to the proliferation of computational capability of powerful advanced computers for numerical analysis of these mathematical modelings, computer aids for injection molding have been developed and have been accepted by the processing industry to improve productivity, part quality, performance, and to shorten start up times. There have

been rapid advances in the development, sophistication and acceptance of computational algorithms expert system and artificial intelligence (AI). These are all components of what is known as Computer Aided Engineering (CAE). This technology is having, and will continue to have, a major impact on polymer engineering and mold design. It holds the promise of achieving human expert levels of performance based on their capacity for compiled knowledge.

Now we are still at an early stage of the implementation of CAE in the injection molding industry; computational algorithms with little or no inferential capabilities. These algorithms however are growing in number and sophistication and they provide strong incentives for their use at this time. They are also establishing the necessary credibility that is an important component of a successful implementation, and thereby paving the way for more advanced problem solvers that will follow. Some of the benefits of implementing a CAE algorithm are insights into part and mold design, material and equipment selection, process economics and overall process optimization. In many cases, the realization of any of these benefits can pay for the cost of the analysis, often including all associated hardware and software costs [2].

1.2.1 Mold Filling Analysis

The most popular type of software in terms of commercial offerings is mold filling analysis. This software simulates the polymer flow into the cavity, predicting pressure drops and shear rates as the cavity fills. Its widespread acceptance is understandable in that this phase of the process is the most technically complicated and difficult to predict even for an experienced mold designer. Mold filling analysis can take into account many parameters such as:

material properties, section thickness, injection pressure, injection temperature, mold surface temperature, and others that influence flow behaviour. A mold filling analysis package allows a designer to weigh all of these parameters based on the actual physics of the flow as approximated by the solution algorithm of the analysis.

Generally, for such a 2-D (two-dimensional) flow analysis package, we need to specify the following inputs, then the program provides the indicated quantities as outputs:

(a) The Inputs: flow path geometry, plastic properties, injection pressure or injection rate, mold surface temperature, injection temperature.

(b) The Outputs: flow rate or pressure drop, temperature distribution, shear stress along flow path, velocity profile; the temperatures, pressures and locations of the flow fronts. Even the molecular orientation and degree of crystallization can be predicted with the appropriate material constitutive relationship.

For 3-D flow types, we do not need to specify the flow path leading into the mold cavity, otherwise the inputs and outputs are similar to those of 2-D flow types above.

The proper use of a program requires the user to be familiar with the limitations of the analysis. Care must be taken to ensure that the results of the analysis are properly interpreted. Computational time and cost for complete 3-D solutions can be prohibitive. Mathematically rigorous solutions of complex parts can consume hours or days of relatively fast computer time at a cost of hundreds to thousands of dollars.

1.2.2 Cooling and Solidification Analysis

Solidification and cooling time of a plastic part is the largest component of the cycle time. Minimization of the solidification and cooling time is necessary to optimize productivity. Solidification analysis is a complex function of material selection, process parameters, part geometry, part quality and mold construction. Improper and unbalanced solidification is a principle cause of warpage and distortion of a molded plastic.

Thermal analysis programs generally consider the section thickness, the size and location of coolant channels, the heat transfer characteristics of the coolant flow, and the mold material. Some programs can also be used to evaluate the crystallization and morphology development during the solidifying time.

Solution of the transient 3-D temperature field in complex mold/plastic parts is extremely computation-intensive with machine time taking hours on relatively fast computers. So the analysis of selected one-dimensional sections representing thickness extremes are often adequate to establish an accurate prediction of cycle time as well as premature freeze off of critical areas.

1.2.3 Summary of CAE in Injection Molding

Generally, there are three basic types of analysis packages in CAE that provide major benefits to a user:

1. Flow analysis
2. Thermal solidification analysis
3. Economic analysis and optimization of the process

There are as many potential analysis packages in CAE for injection molding as there are aspects of the technology itself. Some packages perform a simple specific task such as:

(a) Gate, runner and sprue sizing.

(b) Shrinkage, mold cavity sizing.

(c) Selecting the plastic for a given set of mechanical, environmental, processing and economic criteria using an algorithm that intelligently searches through a compiled data bank of material properties to find suitable molding plastics for the criteria.

The key word in CAE is Aided; these analysis packages in no way replace skill or education in the basics of plastic material properties, mold design, or processing. What these tools do is supplement the knowledge of a trained analyst, making him more productive and more accurate in his predictions.

1.3 THE OBJECTIVES OF THIS THESIS

Hitherto, for many of the CAE packages used for injection molding, the mold filling analysis and the thermal/solidification analysis were separate works. In most of these packages, a common isothermal temperature assumption along mold/plastic interfaces was made. The assumption simply stated that there was perfect thermal contact at the plastic/mold interfaces and an isothermal temperature along these interfaces throughout the injection molding cycle.

The purpose of this thesis is to determine more accurate knowledge about the thermal fluctuation of the mold/plastic interface during the injection molding cycle. This thesis reports the results of an investigation into the cyclic temperature variation of a mold/plastic interface, the number of cycles required to achieve periodic steady-state operating conditions, and the way that various process parameters affecting this thermal fluctuation.

Chapter II
LITERATURE REVIEW

At first, a brief review of the most widely known packages currently used in the injection molding technology is presented to identify their mathematical and technical treatments of the mold filling and/or thermal analysis of the process and to indicate how they work. For our academic interests, the major point which we are looking for is how the numerical algorithms of these packages are built up and the minor point is the description of what the packages can or can not do. This section is largely condensed from reference [2].

2.1 MAIN COMMERCIAL INJECTION MOLDING PACKAGES

2.1.1 TMCONCEPT Expert System

So far, no single model can legitimately claim to cover all aspects of the injection molding process from the design concept to the economic production of desired product. A comprehensive analysis of a molding operation requires the use of several models and it also demands their closest possible integration. The TMCONCEPT system is made to create different models to analyze different aspects of the injection molding operation. Then the best workable integration of these models forms the basic of the TMCONCEPT system. This feature of the system assures that a good and comprehensive analysis is obtained. The

TMCONCEPT system models the entire injection molding process. It integrates the traditional purely scientific calculations with practical knowledge and experience. It ties the technical aspects intimately with the economic factors, leading to a true optimization of the process. It represents a methodology to handle the optimization of the quality-cost relationship in the production of desired plastic parts. The component program packages of this system are:

TMC-MS package for material selection

TMC-MCO package for molding and cost optimization

TMC-FA package for mold filling analysis

TMC-CSE package for cavity dimensioning

TMC-MTA package for mold thermal analysis

The first step for a full analysis of a design concept is the selection of the best candidate materials to be used. The TMC-MS carries out this task on the basis of "end use requirements". It does this in a unique way by using rating classifications, and a cost index per desired property.

Further discrimination among candidate materials must be made with respect to the processing considerations. This differentiation according to processability can be carried out in the TMC-MCO package for molding and cost optimization in these following steps.

In the first step of the TMC-MCO analysis, the MCO1 program quickly establishes the ease of molding to specified part tolerances based on the resin properties of candidate materials. It gives the opportunity for further refinement of the candidate material selection.

Next, the second step, the MCO2 program determines the single cavity molding specifications and provides a complete moldability analysis. It refines the molding conditions to determine the component of the molding cycle, and the holding pressure, desired tolerances, gate specifications and known process fluctuations.

In the third step, MCO3 is activated. The selection of the molding machine and the optimum number of cavities are computed, based on cycle time which includes mold opening, ejection and closing times of available machines.

If a deeper analysis of the mold filling phase is desired, the TMC-FA package can determine the optimum filling condition. The TMC-FA package is also used to position the weld line, to determine the quality of the weld and the available time for packing, the balance of flow, the average temperature, the frozen skin formation, shear rate, shear stress , etc . It is also used to optimize the dimensions of the sprue, runners, gate specification.

Knowing the optimum molding conditions and permissible process fluctuation, it is now possible to proceed to cavity dimensioning to compensate for shrinkage. The TMC-CSE package gives full consideration to flow orientation, and tool making quality. It provides a direct linkage between part dimensions, with their respective tolerances, mold dimensions, with their tolerances, and molding conditions with their permissible fluctuation. The TMC-FA provides accurate information on frozen skin and its orientation. So the TMC-FA contributes these results to the analysis of the TMC-CSE package for shrinkage evaluation.

The next phase is to look at the need for the mold thermal conditions. The TMC-MTA package handles this task. It deals not only with the quantity of heat to

be removed from the mold, but also assists in determining the means required to maintain the mold surface temperature within specified limits. The shrinkage is dependent on the mold temperature, and tolerances are the result of shrinkage variations so the TMC-MTA can identify those areas of the mold which really need to have a close control of the mold surface temperature.

It is worth mentioning that heat exchange calculations alone can not be used to establish attainable cycle times. The best cycle is determined not only by mold temperature and part configuration but above all by the desired part quality. The TMCONCEPT gives proper consideration to all of these variables in its TMC-MCO packages.

For the final solution, the user is back to the TMC-MCO package to obtain the definite and optimized cost figures and complete molding/material/processing specifications of the total analysis for the designed part with desired quality.

The technical structure of the TMC-FA package is presented here in more details as follows:

TMC-FA package processes the mold filling analysis into two step procedure; Preparation and Flow Analysis.

A. Preparation

This step consists of:

a. *Flow Schematization*: To describe the pattern of flow paths into the mold cavity with the proper segmentization of the flow domain, the domain is broken into permissible segments according to the standard geometries of the program, and these segments are numbered to indicate the order of the segment filling.

b. *Dimensioning*: The dimensions of the various flow segments of the "flow schematization" are defined with respect to their geometries, surface temperature, and angles relative to the preceding segment and to the mold parting line.

This preparation has been made essentially error proof. In case the user makes a mistake in this schematization, the output of pressures of interconnected flows will alert him by showing illogical pressure distributions. He can then easily correct his segmentation of flow paths to remedy this defect.

B. Flow Analysis

In mold filling analysis, the complete analysis is usually separated into two aspects, macro analysis and micro analysis, in order to obtain the most comprehensive analysis. The EMC-FA package offers the user flow analysis programs for both of these analysis aspects.

For the macro analysis, the FA1 calculation model describes the procedure for the calculation of defined segments of flow as shown in Figure 2.1. The starting temperature is the temperature of the preceding segment. The calculation is performed in time steps and looks for convergences of results in temperature and pressure.

When the flow front moves in several branches of different segment lengths and/or geometries, differences in the pressure drops to the flow fronts are computed, and a maximum permissible difference can be set as a target for the convergence calculations.

Figure 2.1: FA1 Calculation model [3].

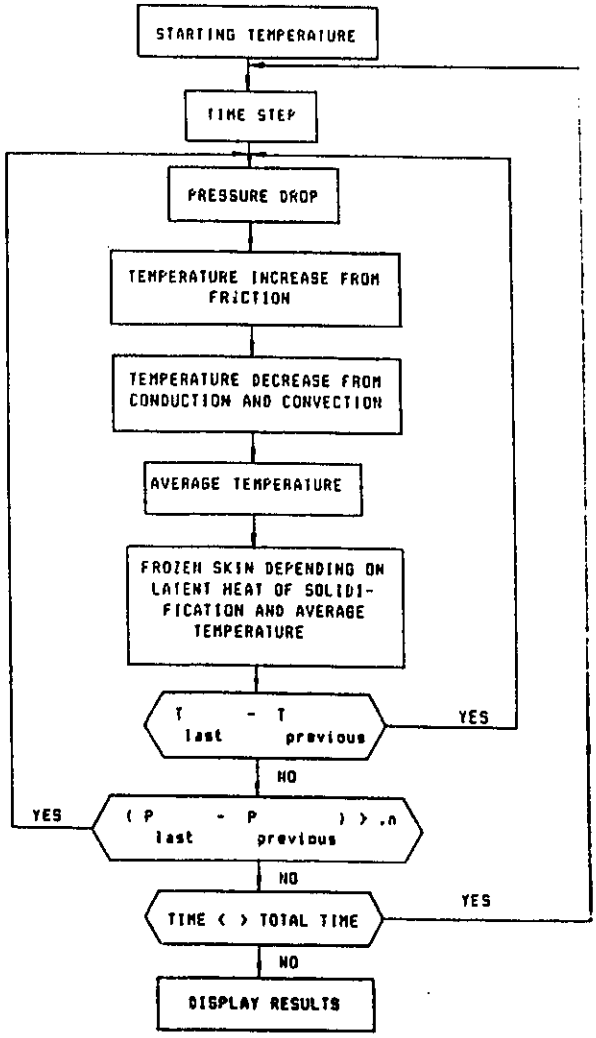

The results of FA1 will be refined further with FA4 program. This program computes the dynamic change of conditions at any instant. The conditions monitored are flow rate, position of the flow front, pressure, temperature, frozen skin, shear stress and shear rate. These values are reported for each filled segment or partially filled. This analysis program FA4 uses finite difference techniques and integral equations [3],[4].

Figure 2.2: FA2 Calculation model [3].

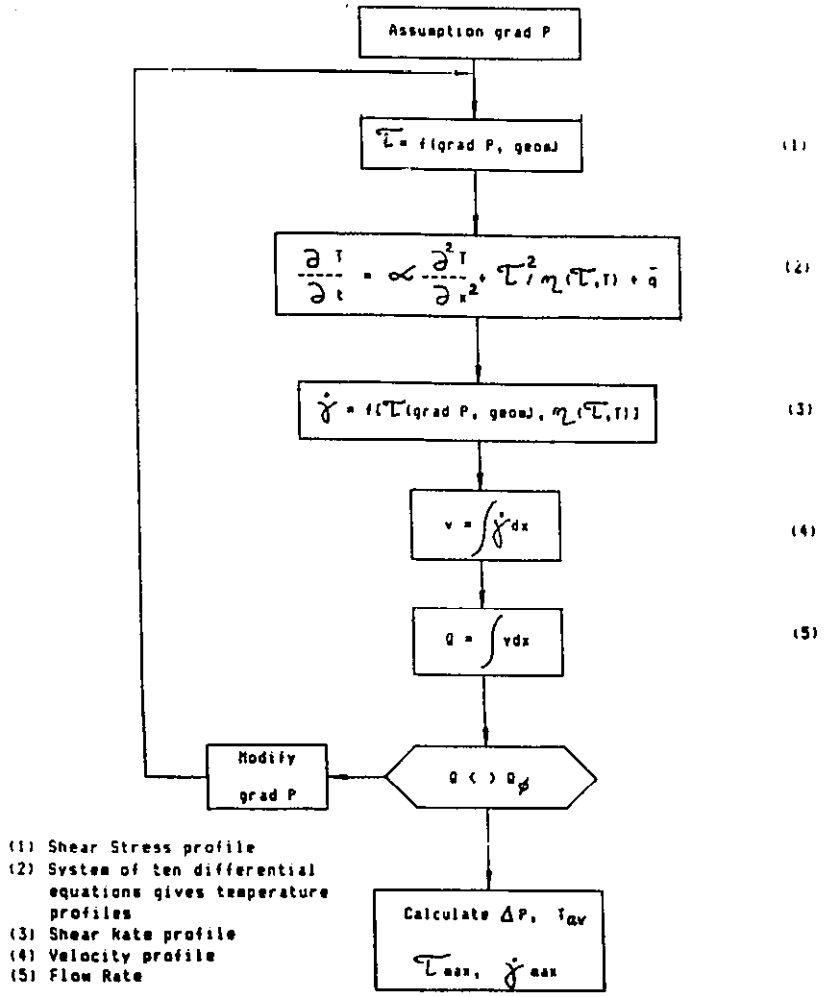

The FA2 program is used for the micro analysis in this package. The FA2 is used to add the computations of profiles of shear rate, shear stress and temperature distributions through segment cross sections. It also identifies the peak temperature and the amount of frozen skin formation of each segment. FA2 takes longer to run. It seeks the numerical solutions through finite difference techniques with the system of the differential integral equations of continuity, momentum,

energy and rheological constitutive equations. The FA2 calculation model describes the procedure of the calculation of defined segments as shown in Figure 2.2. For more details about the applications of the finite difference techniques in injection mold filling process, an interested reader can review the reference [4] at the end of this thesis.

2.1.2 MOLDFLOW Packages

This package also divides the complete analysis of injection mold filling into two areas. The first can be referred to as micro or sectional analysis and the second as macro or part analysis. Micro analysis involves methods of predicting the pressure, temperature, shear rate distribution over a single thickness section. Macro analysis is the development of a total scheme to predict pressure, average temperature and flow patterns of a complex part molding, given the ability to predict pressure and temperature along the weld line.

2.1.2.1 Micro Analysis

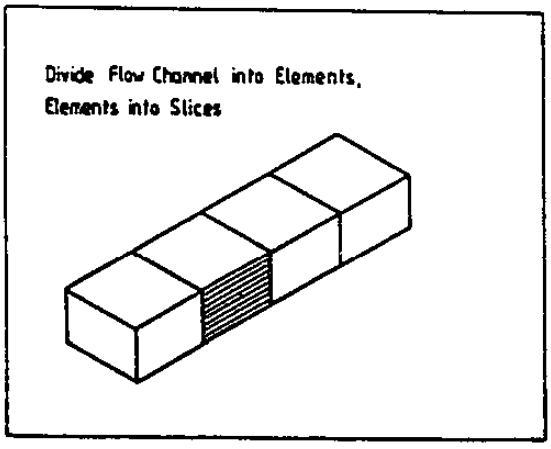

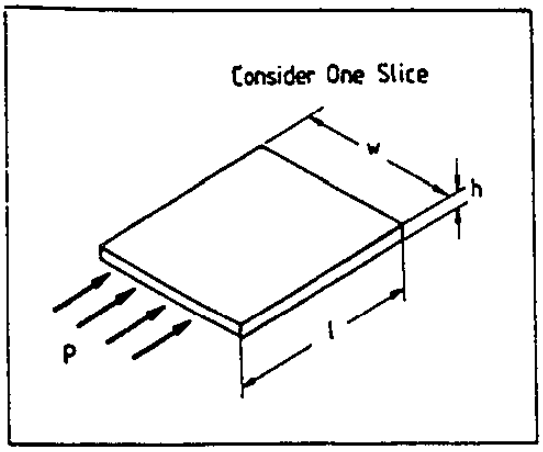

Stress = Pressure drop * thickness/(2 * length).

Fig.2.3:Flow path divided into sections. Fig.2.4: Single slice [5].

The micro analysis program concentrates on solving the simultaneous heat transfer and fluid flow equations using single flow path models in which the flow rate was known. This approach is based on a finite difference scheme. Flow paths are defined by simple strip geometries which are broken into sections, see Fig.2.3. These sections are divided into a number of slices each of which has its own temperature, shear rate and viscosity, see Fig.2.4.

The energy equation for each slice is calculated using normal heat transfer equations and the momentum equations are solved by numerical integration over the section. The relationship between pressure and shear stress across the section is:

Shear stress = (pressure drop * thickness(h)) / (2 * length(l))

This is a fundamental relation which is solely based on resolving forces, and is independent of material or flow characteristics. The pressure drop is available from the macro analysis. The shear rate can be computed with the shear stress above if the viscosity is known. Apply this to the strip geometry where the sections are divided into slices as Fig.2.3 The marching approach is employed to calculate the velocity profile. Calculations start from the outer edge where the velocity of the plastic is assumed to be zero. The velocity of the outer face of the outer slice is zero. The increase in velocity over that slice is (shear rate) * (thickness of slice). The basic definition of shear rate is the increase in velocity per unit thickness (du/dy). The velocity of the inner face is now known. Moving into the next slice, the increase in velocity across this slice can be calculated in the same way and added to the velocity of the first slice to arrive at the velocity of the second slice. When this is done for every slice, the complete velocity distribution

is known across the section. Multiplying the average velocity of every slice by its cross sectional area gives the volumetric flow in every slice. These are then added together to give the total flow rate.

To summarize, knowing the temperature distribution across the section and some relation between shear rate and shear stress and viscosity, the flow rate is calculated for a set pressure.

The heat transfer into and out each slice is calculated as follows:

1. Heat in/out by conduction:

   This can be calculated as the heat change (per time increment) = thermal conductivity * area * temperature difference/slice thickness

2. Heat in by flow:

   The plastic entering the section is at a different temperature to that leaving. The change in heat content again can be calculated as heat change = velocity * slice area (flow rate) * density * specific heat * temperature difference

3. Viscous heating :

   This is equal to the time rate of work done which is simply equal to (acting force) * (average velocity).

   where the acting force = (shear stress) * (slice area)

The problem remains that to do the heat transfer analysis, the flow calculations must have been completed, yet to do the flow calculations, the temperature distribution must be known. This can be solved by first calculating the velocity of the plastic as it starts to enter the section before any heat transfer has occurred and the temperature is equal to the melt temperature. This establishes

a velocity distribution from which a new temperature distribution can be calculated for a small time difference later. Based on this new temperature profile a revised velocity distribution can be developed for the same time increment, and so on until the mold is filled.

Although these finite difference schemes have worked well in most applications, they suffer from two disadvantages:

1. A significant amount of computer power is required to run them.
2. The results are very dependent on the analysis near the frozen layer where conditions of high shear and low temperature prevail and experimental results are most prone to error.

2.1.2.2 Macro Analysis:

In the micro analysis, a flow path consists of a strip of sequential sections so the flow rate in every section is known. Now using a branching flow concept, flow is described as a series of elements which continuously divide into a number of diverging flow paths. The elements are connected together in such a way that plastic flow enters one element and at the end of that element can be divided between any number of elements, which in turn can feed any number of elements, the only limitation being that the elements can not converge. Because the flow divides, the flow rate in each flow path is not immediately known. However, the basic flow laws (conservation of matter) mean that the flow rate into each section or element must equal the flow rate out of that section. This gives a boundary condition which allows the flow pattern to be calculated [5].

There are two ways of analysing this scheme, either the flow is assumed to be "steady state" where every flow path fills at the same instant in time, or a fully

dynamic situation is analysed with the position of the flow front determined at time intervals throughout filling stage. Both the systems have advantages and disadvantages. The "steady state" analysis is simple and is perfectly valid for fully balanced flow paths calculations. It enables automatic balancing of runners to be simply achieved. But it does not have the transient information on the flow front. The fully dynamic analysis is based on injecting a known volume of plastic at discrete time intervals throughout filling. The distance the plastic moves along each flow path is initially guessed and the pressure drop to the end of each flow path analysed. Based on these results, the length of each flow path is adjusted until the total pressure drop in every flow path is the same. Once the flow rate at any point in time has been determined, each section can be micro-analysed so that the combined results yield a total flow analysis.

The above "steady state" analysis implements the finite element method with an iterative scheme. This analysis gives only the solution of the conditions at the instant of filling and a stable final fill pattern. The reader can find more information about this approach in reference [6].

The fully dynamic analysis of filling using a finite element method will be represented with more technical details. The flow analysis procedure is best explained by developing the procedure step by step in the following paragraphs.

The cavity geometry of the flow domain is constructed by some CAD package such as I-DEAS, CADKEY, or ALGOR.

The cavity is broken into a number of triangles of finite elements by a mesh generator program. Then stiffness equations are developed which give the flow resistance. In order to develop these equations, certain assumptions must be made.

The most convenient way to visualize this situation is to consider a large sheet of flowing plastic which contains the nodes that make up the elements. Within this sheet the flow rate is assumed to be constant, and viscosity is a known function. Knowing the flow, the pressure gradient and later temperature gradient can be calculated. By resolving the pressure at each node, and considering the flow crossing the boundaries, it is possible to generate total flow equations, relating nodal pressure and nodal flow.

Note that nodal flow is used to describe external nodal flow, i.e., when flow enters or leaves the system. There will be internal flow even if the external flow is zero (similar to external force and internal force in stress analysis). The sum of internal flows crossing a node is zero as the elements are assembled together.

To solve these equations, it is necessary to determine boundary conditions, such as:

(a) The flow at the gate is known, the pressure unknown

(b) The flow crossing all intermediate nodes is zero, the pressure unknown

(c) The pressure of the frontal nodes is known as zero, the frontal flow is to be determined.

These boundary conditions are needed to provide adequate information to solve the family of simultaneous stiffness equations. With these boundary conditions, the program is then able to compute the pressure distribution over the flowing plastic sheet. Then from these pressure values, the nodal flow at each node can be closely approximated.

It is useful to highlight key problems to be solved in finite element models of plastic flow in a cold cavity. These are the mathematical boundary problems caused by:

(a) Non-linear material properties (viscosity, thermal conductivity)

(b) Free and moving boundary condition of flow fronts.

The first problem can be overcome through appropriate iteration techniques which utilize the computing power of a computer to solve the non-linear system.

The second poses a more difficult challenge. The finite element technique needs information on the boundary location of the advancing flow fronts, but the flow fronts in unsteady flow are not readily known.

The solution to this problem lies in making a starting assumption of a reasonable location of the flow front at a given time, and verifying whether the starting hypothesis is consistent with the boundary condition of the flow front (the ambient pressure at the flow front). The pressure drop must be the same from the melt inlet to every point along the front. If this is not the case, the starting assumption must be corrected and the calculation repeated, until convergence is achieved. When the convergence is reached, a new flow front is created by including the newly generated elements with the filled elements of the preceding time step calculation. The procedure is repeated until the mold cavity is filled. This is one of the most sophisticated approaches for the macro analysis of mold filling, but it requires extensive computational time.

2.1.2.3 Mold Cooling Analysis

The MOLDFLOW cooling package has been developed to aid a user to design a cooling system of injection molding that satisfies the two basic requirements:

(a) The capacity of the cooling system is able to remove the heat load from plastic to mold at the required rate.

(b) The configuration of the cooling system ensures that the cooling of the part will be uniform.

The total heat load from plastic to the mold surfaces can be closely approximated as:

(Plastic mass) * [*heat of fusion* + (*specific heat*) * (*inject temperature* – *eject temperature*)]

The total heat load from the plastic through the mold metal and into the water lines has to be analysed as one entire system in order to obtain an efficient cooling system.

The heat transfer through the mold metal is determined by the classical differential equation of steady state conductive heat transfer in 3 dimensions. The heat transfer into the water lines is determined by the characteristics of the coolant flow, inlet/outlet temperatures of coolant, the surface area of the cooling channels and dimensions of the cooling channels.

In a 2-D case, the procedure for the heat transfer analysis is illustrated with the following example in the "T" shape mold shown with a thin top and a thicker leg in Fig.2.5 and Fig.2.6, next page. In Figure 2.5, the surface temperature will be highest at the internal corners, lower down the thick leg, and a minimum on the thin top bar. To achieve a uniform temperature, the cooling channels must be placed as near as possible to the hot corners (zone1, Figure 2.6). In zone2 the

channel should be placed further away. While in zone3 the cooling channels should be at an even greater distance to achieve more uniform temperature on the surface of the mold [5].

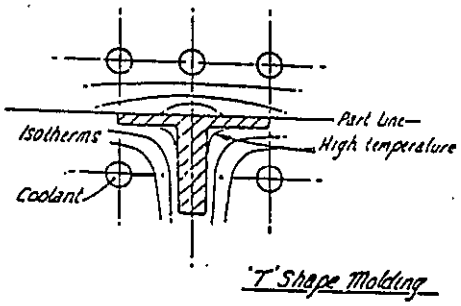

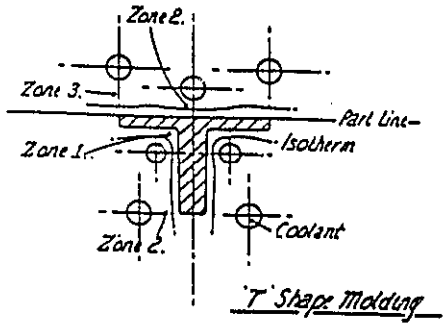

Fig.2.5:Starting positions: Fig.2.6:Optimized cooling lines[5].

This 2-D case can be handled quite adequately by the finite element approach. The cross section above can be easily meshed in 2-D. The heat load at each node of the surface is determined by the thickness and temperature of the plastic, remembering that the sum of the heat loads of all the surface nodes must be equal to the total heat load from plastic to the mold surface calculated previously, the temperature of the nodes near the cooling channel are determined from the water temperature. We assume a uniform heat flux on the surface of cooling channels. This gives sufficient information for the heat transfer analysis to calculate the temperature distribution of the mold surface. If the results of the analysis show that the temperature of the mold surface is not uniformly distributed, the user has to relocate the cooling channel, and rerun the analysis until the acceptable temperature distribution of the surface obtained. This temperature distribution can be used as the thermal cavity boundary for mold filling analysis.

The real problem of the thermal analysis occurs as a result of the complex 3-D geometry inherent in plastic injection molding. The finite element approach becomes less practical since it is necessary to form a solid element mesh, which can result in modelling and computational problems.

2.1.3 POLYCOOL 2 Packages

POLYCOOL 2 is a computer program from SDRC (Structural Dynamic Research Corporation) which simulates the cooling and solidification of injection-molded plastic parts. The simulation is based on a transient analysis of the part and the mold, and a steady state description of the coolant. A non-linear thermal analysis of the part is performed in the time domain using a 1-D explicit finite difference method (FDM). This analysis is iteratively coupled with the mold analysis, which is performed in the frequency domain using a 3-D linear boundary integral equation method (BIE), also known as the boundary element method (BEM). POLYCOOL 2 is designed to be run in connection with several other tools of CAE; a geometric modeler and a mesh generator for the shell model of the part (I-DEAS) and a flow simulator (MOLDFLOW) to generate the temperature distribution of the part at the instant of fill.

Now a brief review of the major algorithms in POLYCOOL 2 is presented here. An interested reader can review Ref[7] for more details of this package.

The thermal fields in the mold are governed by the 3-D transient diffusion equation with constant properties. The time coordinate has been removed through the use of a Fourier transform, appropriate for steady state cyclic operation of a warm mold set. The field equation is:

$$\frac{\partial^2 T}{\partial x^2} + \frac{\partial^2 T}{\partial y^2} + \frac{\partial^2 T}{\partial z^2} = \Omega_k T \quad (2.1)$$

where Ω is a constant for each Fourier number k.

This field equation is solved by the boundary integral equation method (BIE) also known as boundary element method. In this technique, only the mold surface needs to be meshed. Temperature and heat flux are evaluated at the centroid of each element.

The boundary element approach for heat transfer in 3-D can be explained at the conceptual level in a simple way. Consider a heat source in a continuous solid, and then derive a simple formula showing how the temperature profile will drop away as we move away from the heat source.

Every element on the surface of the mold can be considered as a heat source on which there is a known heat flux. The effect of that heat source on every mold node can be calculated by considering a triangular prism coming out from that node to the heat source. That can establish the set of relations between that node and every surface element of the mold. In this calculation, the boundary conditions are that the heat load by the plastic to the mold surfaces is equal to the heat removal by the water lines. This assumes that only a small fraction of heat is lost throughout the outside surface of the mold. This enables us to write a complete family of equations expressing the effect of the heat load on every surface element, conducted throughout the mold, and onto the temperature of every node in the cooling system [8]. Solving this set of simultaneous equations gives the relative temperature distribution on the surface of the cavity.

In technical terms, there are several basic steps involved in the formulation and numerical implementation of the boundary element method.

The governing differential equation to be solved, with the use of the divergence theorem, is transformed into an integral equation on the boundary by utilizing some type of "special test" function. In a linear problem, the test function is the fundamental solution of original differential equation. Since the transformation is performed analytically no approximation is used at this stage.

The basic integral equation on the boundary is discretized to obtain the approximation boundary element representation. This involves the use of nodes, elements, shape functions, natural coordinates of boundary elements, much like the finite element method. First, discretize the domain boundary into finite elements, each containing a prescribed number of nodes. The field variables within each element are then approximated by interpolating shape functions and the integral reduced to partial sums by the appropriate quadrature. The final system of linear algebraic equations for the unknown variables is formed by using the partial sums in the original boundary integral equation and imposing the prescribed boundary conditions at the appropriate nodes. Once the system of these discrete equations is set up, Gaussian elimination can be used to get the solution. Subsequently, solution at any interior point of the solution domain can be recovered by performing a simple boundary quadrature.

The solidifying plastic part is governed by the transient thermal diffusion equation in 1-D with variable properties. The field equation to be solved in the part is :

$$\frac{\partial^2 T}{\partial z^2} + \frac{\dot{q}}{k} = \frac{1}{\alpha} \frac{\partial T}{\partial t} \qquad (2.2)$$

where z is the coordinate through the thickness of the part, $\dot{q}$ is the heat generation rate, k is thermal conductivity, α is the thermal diffusivity. The k and α properties can be linear functions of temperature. To transform this differential equation into a difference equation, each triangular finite element representing the part is sliced parallel to the mid plane into several layers, the temperature being assumed constant within each layer. The difference equation is solved by a modified explicit method.

The flow in cooling lines is governed by conservation of mass and an empirical equation relating pressure drop to mass flow rate, geometry, and materials properties. The thermal field in cooling lines is governed by the conservation of energy and an empirical equation relating the film coefficient to the mass flow rate, geometry, and materials properties. All coolant properties: viscosity, density, specific heat, and thermal conductivity are functions of temperature alone; pressure sensitivity is considered to be small.

2.1.3.1 Coupling of The Part and Mold Analysis:

The package solves separately the transient thermal fields in the part and the mold metal using radically different techniques as discussed above. Briefly, the melt part analysis with explicit FDM is first carried out using an assumed melt/mold interface temperature variation over the cycle time. This gives a heat flux variation with time along the interface. Then this interface heat flux variation is used to carry out the mold thermal analysis with Fourier transformation equations. The interface temperature variation with time, calculated in the mold analysis, is then compared with that used in the initial melt analysis. The two must be iterated until convergence. If they are within a small specified difference

(say 0.1 K), then the calculation is stopped. Otherwise, the iterative process is repeated until convergence is obtained.

The solutions of the flow and temperature fields in the coolant simply lag behind the thermal field analysed above.

One of the limitations of the POLYCOOL 2 package is that the thermal contact between part and mold is assumed to be perfect, between injection and ejection. Thus the temperatures of plastic and metal are assumed to be equal all along the part-mold boundary. In fact, many plastics shrink enough during the latter part of the cooling period to open a gap between the part and mold, and this greatly impedes the flow of heat. The solution to this problem is being studied for the further development of POLYCOOL 2.

2.1.4 MOLDCOOL package:

This package was developed over ten years ago by AEC (Application Engineering Co.) in USA. Nowadays, the package is available for use on time sharing basis worldwide.

The package mainly focuses on designing an optimum cooling system (parallel/series configuration of the circuitry and flow conditions of the cooling system) by considering the heat load from plastic throughout the mold metal to the cooling passages without directly solving the thermal field of the mold metal. It is the implementation of many theoretical/empirical relationships and finite difference techniques of heat transfer to design the cooling system in injection molding [9].

The variables involved in this analysis package are:

1. Geometry and properties of plastic/mold: average thickness, total surface area, part weight, thermal parameters.
2. Injection and ejection temperature of plastic part.
3. Mold/plastic interface temperature.
4. The mean temperature of the cooling medium.
5. Overall heat transfer coefficient, configuration and properties of the coolant.

The program can handle or assist the user in the following design steps:

1. Calculation of the total heat load for a particular application.
2. Calculation of various channel sizes, thermal equivalent lengths, and pitch required to handle the calculated heat load above.
3. Circuiting the mold designer's cooling channels layout to provide equal pressure drops along coolant and uniform heat transfer characteristics throughout the mold.
4. Optimization of flow rate, pressure, and temperature of coolant.
5. Calculation of cooling times for both the theoretical minimum time and the approximate time by numerical method.
6. Prediction of cavity surface temperature if the cooling time is specified.

2.1.5 C-FLOW Packages

This is a package consisting of C-Flow, C-Pack, C-Cool software. C-Flow can analyse, using the finite element method, the symmetrical flow pattern into a thin cavity of any geometric complexity in 3-D domain with high level interactive graphics during the filling stage [10]. C-Pack uses the results of C-Flow analysis to continue the simulation of polymer melt behavior into the post filling stage. These consist of a very short packing phase and a relatively long holding and cooling phase. The quality of parts can be improved by changing gate size and packing pressure, thereby controlling shrinkage and warp. Gate size is determined to assure the cavity is well packed before freeze off. Clamp force and shot weight can be reduced by optimizing the packing pressure profile. C-Cool simulates heat transfer between the cavity and the cooling channels in a mold geometry, utilizing the boundary element method.

2.1.6 MCKAM-2 Package

This package which has been developed at McGill University is very sophisticated and useful for the micro analysis of the molded part during the injection molding cycle. Its filling algorithm includes optional fountain, viscoelastic and curing reaction effects. It further simulates packing/holding, solidification and cooling. However, the package at this stage of development is restricted in its use to basic simple shapes: disc, semi-circular disc, rectangular, and cylindrical cavities[11].

2.1.7 Summary of Current State of CAE

A brief review providing insight into some of the most well known commercial computer packages used in the injection molding industry has been presented. Each package has its own special features, as well as its limitations. For instance the TMCONCEPT expert system has the best capability for analysis and integration of all the basic economic considerations as well as design steps for the complete injection molding operation from the design concept to the optimum production. On the other hand it requires that the user should have the necessary skills and experience to be able to define the flow paths manually for the filling analysis, and to decide which is the next move to be done to refine the integration between various current analyses. The MOLDFLOW package is capable of analysing the mechanical stress in parts as a result of molding conditions. It models the mold filling and cooling with macro and micro analysis with sophisticated implementations of finite element/finite difference techniques. It can also determine the orientation and crystallinity of molded plastics and relate them to the shrinkage calculation. It also requires a skillful and experienced user for efficient application of the package.

In summary, we can say that each package has its own distinguishing features and algorithms to aid a user in design and making other decisions about certain aspects of the complex injection molding operation. The best use of any of these programs requires that a user should have a basic knowledge of the algorithms of that package.

2.2 REVIEW OF TECHNICAL ACADEMIC PUBLICATIONS

There are numerous technical papers dealing with numerical and theoretical analysis, and of experimental studies in the area of injection molding. In this section, the author will briefly present a basic review of many important research works in this field, and the theoretical background that will be used later in the thesis.

2.2.1 Heat Transfer with a Freezing Boundary

In injection molding, the polymer starts freezing after being injected into mold cavity. For a solid/liquid phase change with a sharp fusion point, the applicable differential equations for 1-D heat flow with constant thermal properties in both the solid and liquid regions are:

$$\frac{\partial \theta_s}{\partial t} = \alpha_s \frac{\partial^2 \theta_s}{\partial x^2} \quad (\textit{The solid region}) \quad (2.3)$$

$$\frac{\partial \theta_l}{\partial t} = \alpha_l \frac{\partial^2 \theta_l}{\partial x^2} \quad (\textit{The liquid region}) \quad (2.4)$$

The α_s, α_l are the thermal diffusivities of the solid and the liquid respectively.

The θ_s, θ_l are the temperatures of the solid and the liquid respectively.

At the fusion boundary, these equations are coupled due to the latent heat of fusion by:

$$\frac{d\varepsilon}{dt} = \frac{1}{\rho\lambda} \left\{ k_s \frac{\partial \theta_s}{\partial x} - k_l \frac{\partial \theta_l}{\partial x} \right\} \quad (2.5)$$

where $d\varepsilon/dt$ is the rate of travel of the fusion front, and λ is the latent heat of fusion. The densities of plastic are $\rho_s = \rho_l = \rho$

Analytical solutions of these kinds of problems are limited to very simple initial and boundary conditions only.

The limitations imposed on the available analytical solutions can be overcome by either fully numerical or by lumped parameter techniques [12]. There are two basic numerical schemes in the FDM for phase change problems that will be briefly mentioned.

The first approach utilizes a traveling space network where the fusion front travel can be accurately determined, but local temperature-time history within the medium must be interpolated. This approach focuses attention on the temperature-time substantial derivative of each nodal point.

The second method uses the conventional complete difference equations for fixed network spacing. The slopes of the solid and liquid sides at the fusion front are derived from the first two terms of the difference form of the Taylor' expansion about the fusion front[13].

For polymers, the fusion temperature usually varies over a range of temperatures and hence the results of the analyses for pure substances are not valid. For such cases, an effective heat capacity concept may be used. The merit of this method is that a single heat flow equation can accommodate both the solid and liquid phases as well as the glassy state [14].

2.2.2 FLUID FLOW AND HEAT TRANSFER IN INJECTION MOLDING PROCESSES.

From the first principles of conservation laws, one can derive the general differential expressions for fluid and heat flow: the continuity, momentum and energy equations. The derivations can be found in any standard textbook of heat transfer and fluid mechanics [15],[16]. For polymer flow, the appropriate constitutive equations (viscosity law, viscoelastic parameters) have to be used to embody the particular characteristics of a polymer being studied into the above differential expressions, or additional terms (viscoelastic and/or chemical reaction terms) are used to modify the momentum and/or energy expressions if they are required.

In general, injection molding involves non-Newtonian and non-isothermal flow behaviour associated with the heat transfer during solidification. In the simulation of flow behaviour, attention is focused on the non-linearity of polymer melt properties. In modeling the heat transfer behaviour, the effective heat capacity approach is usually used to reduce the number of the governing equations for covering the liquid, solid and glassy states of the polymer.

2.2.2.1 Fluid Flow Equations

The field description for fluid particles is governed (in Cartesian-tensor notation) by:

$$\frac{\partial \rho}{\partial t} + \frac{\partial(\rho\, u_j)}{\partial x_j} = 0 \quad (\textit{Continuity Equation}) \quad (2.6)$$

$$\frac{\partial(\rho\, u_i)}{\partial t} + \frac{\partial(\rho\, u_i\, u_j)}{\partial x_j} = \frac{\partial \sigma_{ji}}{\partial x_j} + \rho B_i \quad (\textit{Momentum Equation}) \quad (2.7)$$

where B_i is the body force in the ith direction; ρ is the density of the polymer melt; t is the time; x_j is a displacement in the jth coordinate direction; u_j is the velocity component in the jth direction; and σ_{ji} represents the stress component due to surface forces acting on the j surface in the ith direction. The repeated subscripts imply a summation over all the coordinate directions. Certainly, equations (2.6) and (2.7) are not open to question, for they are mathematical statements of well known conservation laws. However, the constitutive equations for the components of the total stress tensor σ_{ji} are more complicated when dealing with non-Newtonian fluids (in this case a macromolecular polymeric fluid). Generally, these constitutive expressions for polymeric fluids are nonlinear in the velocity gradients and may contain information about the time dependent mechanical response of viscoelastic behavior. Thus the determination of these constitutive expressions is a central problem in dealing with non-Newtonian viscoelastic fluid mechanics.

Usually, molten polymers are pseudoplastics, that is the non-Newtonian viscosity, η, depends on the instantaneous state of shear stress such as the power law of viscosity. In some cases, the dependence of viscosity on pressure can not be neglected. For instance, the viscosity of polystyrene is very sensitive to pressure due to the large toluene side groups preventing close packing. Detailed information on the constitutive equations can be found in Ref.[14],[16].

2.2.2.2 Heat Transfer Equations

The governing energy equation for flowing molten polymer that was derived with the effective heat capacity approach and enthalpy method can be written as

$$\rho C_e\left[\frac{\partial T}{\partial t} + u_j \frac{\partial T}{\partial x_j}\right] = \frac{\partial}{\partial x_j}\left(k \frac{\partial T}{\partial x_j}\right) + \eta \phi \quad (2.8)$$

where C_e, the effective heat capacity is

$$C_e = C_p + \frac{e\lambda}{T_l - T_s} \quad (2.9)$$

where $e = 1$ if $T_s \le T \le T_l$, *otherwise* $e = 0$

T_s and T_l are the solidus and liquidus temperatures of the polymer respectively

and ϕ is the dissipation function given as $\phi = \frac{1}{2}\left(\frac{\partial u_i}{\partial x_j} + \frac{\partial u_j}{\partial x_i}\right)^2$

More details of these derivations can be found in Ref.[14].

2.2.3 WORK OF H. VAN WIJNGAARDEN, J. F. DIJKSMAN AND P.WESSELING [17].

The authors presented a stable numerical scheme of calculation for the non-isothermal flow of a non-Newtonian fluid into a narrow rectangular cavity. The effects of solidification of polymer melt on the walls of the cavity during filling and viscous heating were taken into account. The viscosity of the model used was shear rate and temperature dependent.

Their mathematical model was sectional analysis. It considered 2-D flow of a molten polymer with a sharp fusion temperature. Variations across the width of

the cavity were ignored. The original governing equations, which were derived from the generalized Newtonian fluid model, were transformed into dimensionless forms and then further simplified with the assumption of the asymptotic channel approximation (ε = (1/2thickness) / length of cavity : ε is much less than unity)

The solution algorithm of their computation scheme was as follows:

(a) Define the nodal mesh of the flow domain: grid lines and grid points.

(b) Compute the temperature field of the flow domain with the finite difference scheme.

(c) Integrate the pressure field.

(d) Integrate the velocity field.

(e) The above steps must be repeated until the positions of the grid points on each grid line are in the instantaneous streamlines.

With this algorithm, it is necessary to carry out an iteration scheme in order to find the streamline grid points on each grid line which can be treated one by one, starting from the entrance to the new frontal grid. This process was repeated until the flow front reached the end of the cavity. The algorithm is comparable to that of the Fig.2.2 calculation model on page 17. Some basic ideas of this paper are implemented in this thesis. The interested reader can review the paper to have an better insight into the thesis analysis.

2.2.4 OTHER PUBLICATIONS

As mentioned previously, there are numerous technical papers that analyze many different aspects of the injection molding processes from many universities around the world. Most of the papers concerned with the numerical analysis of the filling and packing stages assume an isothermal temperature of the cavity wall,

and/or perfect thermal contact at the mold/plastic interface. It is impossible to cover all aspects of an injection molding process during an injection molding cycle in a single mathematical model. So most papers attempt to deal with some particular aspects of the injection molding process. Therefore appropriately chosen governing equations were employed, along with certain acceptable simplifying assumptions imposed, to disclose the specified information being sought. These calculations can generally classified into two groups:

1. MACRO ANALYSIS:

   Pressure field, melt-front advancement, temperature field. [18], [19] [20], [21], [28], [29].

2. MICRO ANALYSIS:

   Fountain effects: [22], [23], [24], [32].

   Chemical reaction effects: [23], [25].

   Microstructure development: [26], [27], [31], [33].

   Viscoelastic effects: [30], [32].

Most of these papers use finite element techniques for part analysis and finite difference techniques for sectional analysis. Generally speaking, there are different approaches and/or numerical algorithms to implement the finite element method to analyze the flow pattern of polymer melt and the moving front boundary into the cavity during filling stage of injection molding.

The Finite Element/Control Volume approach is a very widely used method for modeling 3-D thin plastic parts. Briefly, this approach employs the popular Generalized Hele-Shaw model. After some mathematical manipulation, the equations of momentum and continuity for this model are embodied in one

equation known as the Reynolds equation with only pressure as the primary unknown variable. Then the finite element technique of minimizing functional analysis is implemented to solve this Reynolds equation subject to the appropriate boundary conditions. This approach is powerful and yields a very good approximation for inelastic symmetrical flow with small variation in the thickness of the mold cavity.

For viscoelastic and/or asymmetrical flow, we have to use the Galerkin Weighed Residual treatment of the model differential equations and integrate by parts to obtain the weak form of the Galerkin equations. Then the representations of the finite element approximation with chosen element type and shape functions for interpolation of the velocity components and pressure over each element are introduced to obtain the Galerkin finite element equation for each element. In this formulation approach, the velocity components and pressure are both primary unknowns. The Penalty Method can be used to eliminate pressures as primary variables in the problem. The technical details are much more involved with various mathematical treatments, especially with element types; and developing an efficient numerical algorithm for determining the moving front boundary is a formidable task.

The finite difference technique applied to a control volume is usually employed by the researchers to solve the energy equation for the plastic part, either explicitly or implicitly, due to the ease of understanding and formulation of the approach.

A few papers discuss experimental studies [34-36]. Others are thermal analyses of the cooling system in injection molding [37-39].

It is worth mentioning that care must be taken to use wisely the rheological and thermal data of a molten polymer. These are usually obtained from the supplier's standard tests of the polymer. To apply these to a particular injection molding case in practice, a user should know how to adjust or interpolate these standard test data in order to get better computed results from his simulation. The user should have a basic knowledge of molten polymer behaviour in terms of rheological characteristics, thermodynamics, molecular structures and the experimental measurement of these standard test data. An interested reader can review this information in Ref. [40-42].

Chapter III
DEVELOPMENT OF THE MODEL

For the sake of completeness, a brief review of the sequence of preliminary studies towards the main work of the thesis will be presented first.

3.1 PRELIMINARY STUDIES

Let us visualize that a mold block and a plastic part at different temperature levels are brought into contact. What thermally happens at the mold/plastic interface when there is non-perfect thermal contact?

First Analysis : Two semi-infinite solids, namely solid 1 and solid 2, which are initially at different uniform temperatures, say T_1 and T_2 respectively at time t = 0, are brought into contact. A thermal contact conductance Hr (the reciprocal value of a thermal contact resistance), exists at their interface. The analytic solution of this case is found in [43]. It is a complicated expression in terms of thermal properties: k_1 , α_1 , T_1 , k_2 , α_2 , T_2 respectively and Hr and the error function, exponential function and time t.

Second Analysis . This analysis is similar to the first except that the two solids have a finite rectangular form of the same width and length but different thickness (height). Let's say the upper solid (1) is a hot and thin layer squarely and fully superimposed on the top of the lower solid (2) which is cooler and thicker. A thermal contact conductance Hr is imposed at their interface boundary. The

bottom boundary of the solid (2) which is parallel to the interface is assumed to maintain a constant isothermal temperature or constant heat transfer coefficient. The remaining outline surface boundaries are assumed to be adiabatic. For simplicity, it can be considered as 1-D diffusive heat flow from the top thin solid (1) to the cool thick solid (2) through the interface. The solution is found by the explicit finite difference method.

Third Analysis . This study was for instantaneous contact between a molten polymer sheet (the upper solid (1)) and a mold block (the lower solid (2)). This time, the solution calculation takes the heat of fusion of the solid/liquid plastic phase change into account, and is extended to carry out the cyclic computational scheme towards the periodic steady-state for the mold block. In this scheme, it is assumed that at the initial time $t = 0$, a molten polymer sheet is put on the top of the mold block. Let the sheet sit there until the solidification and cooling phases are completed, then take the sheet off the mold block. The freshly opened mold surface is exposed to the convection of surrounding air for a few seconds before another polymer melt sheet is brought into the top of the mold to begin the next computational cycle. The computational cycle repeats itself n times until the temperature distribution along the mold block reaches periodic steady state. Some of the outputs of this study are presented in Appendix A.

Fourth Analysis . In this final stage of the development, a two dimensional analysis was carried out, which also takes into account the influence of the molten polymer flow on the temperature field of the plastic part during the filling stage of the cycle.

The physical value chosen for the thermal contact conductance Hr at the plastic/mold interface is of crucial importance in this investigation. An experimental value of Hr is not available in research literature, so a rough theoretical approximation of the Hr value was calculated. This calculation is presented in the Appendix B.

3.2 THE MAIN PURPOSE OF THE THESIS

Recall that the major purpose of the thesis is to investigate the thermal fluctuation of the interface between the mold cavity surface and the plastic surface, and to examine how the process parameters (melt temperature, mold temperature, etc.) affect the thermal fluctuation of the interface.

A basic physical understanding of the process is essential to mathematical modeling as it helps, not only in identifying important factors and setting up the equations and their boundary conditions, but also in interpreting the model solution and applying the model in practice. The following is a physical description of the major steps in the thermal cooling action that occurs within the mold body during a typical injection molding cycle: A hot molten polymer, under pressure, flows out of the nozzle of the injection cylinder, through the sprue, runner, gate, and finally fills the mold cavity. The cooling action of the mold plates starts as soon as the melt enters the mold cavity. The hot molten polymer acts as a moving heat source flowing into the cavity. The cooling channels, embedded not far away from the mold cavity surfaces inside the mold plates, act as heat sinks. The thermal field of the injected molten plastic is a function of time and the spatial coordinates. After the mold cavity is filled and held under pressure,

further solidification and cooling take place. During this phase creeping flow can occur to compensate for cooling shrinkage. The mold then opens, the plastic part is ejected. The mold closes and the system is once more ready to repeat the molding cycle.

The thermal behaviour of the cooling cycle can be divided into the following three main steps :

1. Cooling during mold filling
2. Cooling after mold filling
3. Cooling during opening and ejection of the molded part

In the first two cooling steps, heat flows from the plastic part through the mold body to the cooling channels. These channels are located some distance from the mold/plastic interface, and are positioned so as to achieve a reasonably uniform temperature distribution along the plastic surface at as high a cooling rate as possible.

In the literature review, we have seen that the mold filling analysis and thermal solidification and cooling analysis are usually treated as completely separate calculations. A few research groups have tried to couple these two analyses together in order to obtain a more "detailed and complete" picture of the process. In these coupling analyses they assume a perfect thermal contact of the mold/plastic interface to facilitate their computational algorithms. At the present time, data is lacking about the thermal contact resistance at the interface.

Since the thermal resistance at the interface becomes important during the latter part of the cooling period when many plastics shrink enough to open a gap between plastic part and cavity surface, that greatly impedes the flow of heat from

the plastic to the mold, the main analysis of the thesis will examine the perfect thermal contact assumption and replace it with some constant value of thermal contact resistance at the interface. Then the thermal contact resistance can be a function of time, pressure or degree of shrinkage. This study will also attempt to coherently couple the two analyses as one "composite" problem to disclose the thermal fluctuation of the interface.

A simple and appropriate mathematical model must be set up that can disclose the thermal behaviour of both the plastic and the mold, especially their interface, during a typical injection molding cycle. The procedure followed will be presented using a step by step approach.

3.3 THE PHYSICAL MODEL AND THE MATHEMATICAL MODEL

At first, one can attempt to set up a simple physical model as shown in Figure 3.1(a). The physical model can be employed to experimentally study the process and to verify the validity of any computer simulation for the model. Figure 3.1(b) shows how the plastic is expected to flow into the thin gap rectangular cavity with three circular end gates as an example of the macro-analysis of the process.

Since the major interest of this work is the micro-analysis of the model, a 2-D mathematical model of the micro-analysis of the process has been set up in which the temperature variation across the width of the cavity was ignored for simplicity. As a result, the central cross section along the length of the physical model for this work, shown in Fig.3.2.a. was mathematically modelled as shown in Fig.3.2.b where symmetry is assumed about a plane passing through the z and x-coordinates and the cooling lines are replaced by an isothermal boundary heat sink at a constant temperature (or constant heat transfer coefficient).

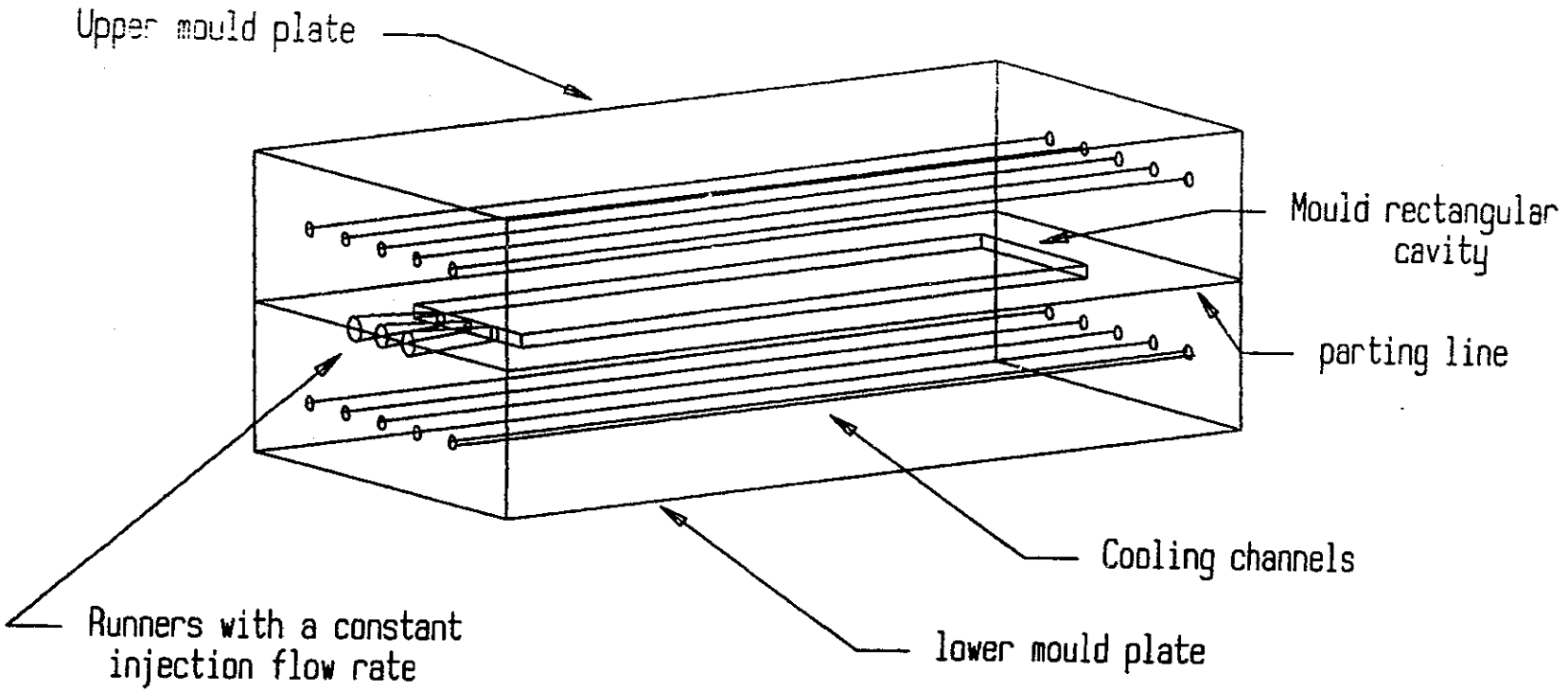

Fig.3.1a: Injection moulding model of a thin rectangular plastic sheet.

The macro analysis of the model is done to determine the flow pattern, the pressure and temperature distributions but ignoring these variations across the thickness.

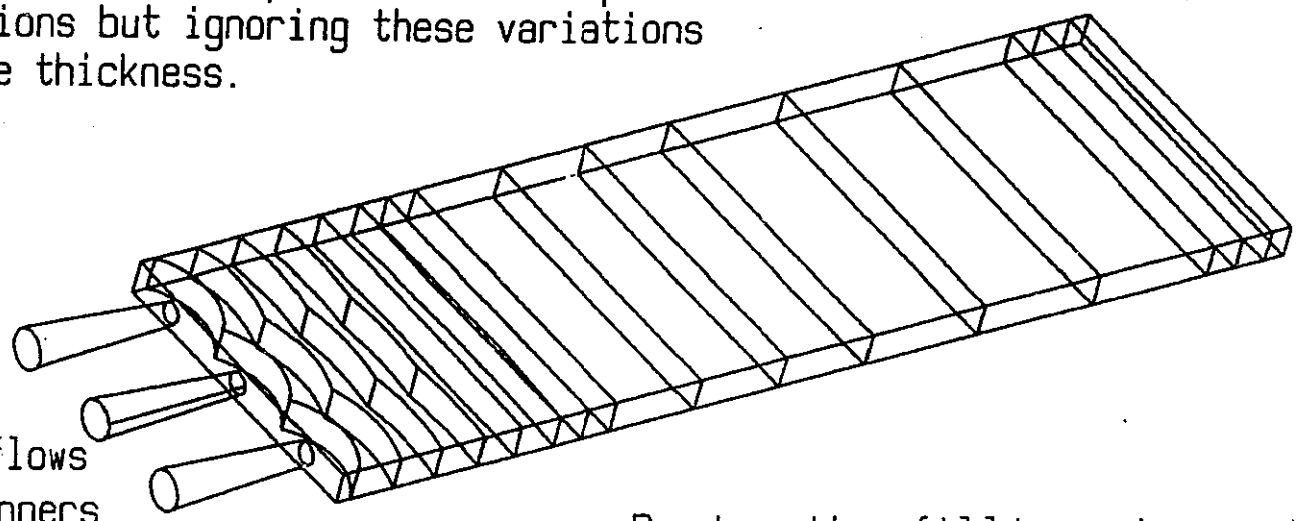

Polymer melt flows into these runners

During the filling stage, the flow front gets straightened as it moves away from the gate.

Fig.3.ib: The macro-analysis of the filling stage for the thin rectangular mould cavity.

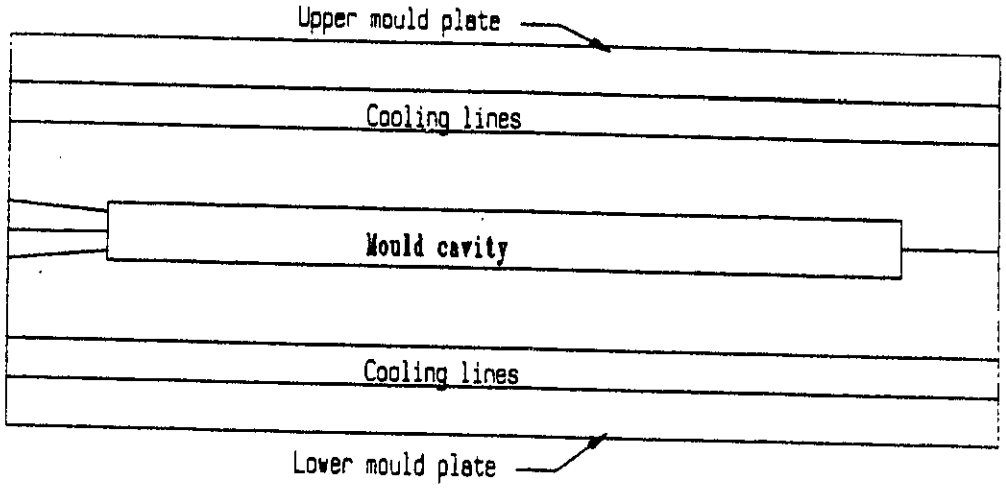

Fig.3.2a

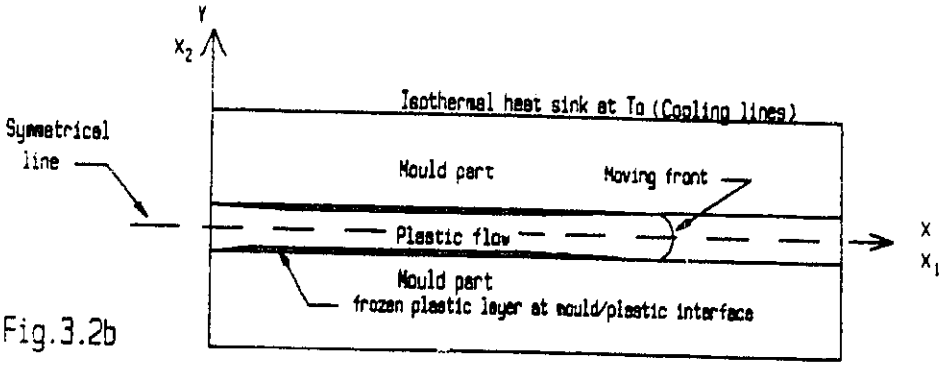

Fig.3.2b

The 2 dimensional micro-analysis for the cross section along the flow direction. (3.2a) the side view of the model cross section; (3.2b) the mathematical model of the model cross section for the 2-D micro-analysis.

The two vertical ends of the mold part are assumed adiabatic, which means the heat loss to the surrounding air by convection is assumed negligible.

Since there is immediate solidification on the cavity wall during filling, the domain of the calculation must be divided into three physical sub-domains; molten plastic, solidified plastic and the mold. The molten plastic and solidified plastic are separated by an interface called the freezing boundary. A thermal resistance is imposed at the interface between the mold and the solidified plastic part.

For most injection molding processes, the flow rate through the entrance of the cavity is constant up to the moment that the maximum injection pressure is reached. After that instant, the pressure is kept constant at its maximum value and the flow decreases rapidly. In order to avoid an "incompleted shot", and to obtain high rate of production, the injection pressure and injection temperature of the melt are maintained high enough that the observation time (total filling time) is long enough to have a low Deborah number, which is defined as the ratio between the (relaxation) retardation time of the fluid and the observation time of the flow. This means one may safely assume that the behaviour of the molten polymer during the filling period is essentially that of a fluid without a viscoelastic effect. The viscoelastic effect becomes considerable wherever there is an abrupt change in the cross section of the flow domain, but such is not the case for the model used in this thesis.

3.3.1 The Mathematical Model Equations

The general governing equations for an incompressible, generalized Newtonian fluid in the 2-D non-isothermal flow of the plastic and for the heat flow of the mold for the model selected can be written as follows (neglecting body forces):

(a) For The Liquid Polymer Domain :

$$\frac{\partial u_i}{\partial x_i} = 0 \qquad (3.1)$$

$$\rho\left(\frac{\partial u_i}{\partial t} + u_j\frac{\partial u_i}{\partial x_j}\right) = -\frac{\partial P}{\partial x_i} + \frac{\partial}{\partial x_j}\eta\left(\frac{\partial u_i}{\partial x_j} + \frac{\partial u_j}{\partial x_i}\right) \qquad (3.2)$$

$$\rho C_p\left(\frac{\partial T}{\partial t} + u_j\frac{\partial T}{\partial x_j}\right) = k\frac{\partial^2 T}{\partial x_j\,\partial x_j} + \eta\dot{\gamma}^2 \qquad (3.3)$$

$$\dot{\gamma}^2 = \frac{1}{2}\left(\frac{\partial u_i}{\partial x_j} + \frac{\partial u_j}{\partial x_i}\right)^2 \qquad with:\ i=1,2\ \ \&\ \ j=1,2 \qquad (3.4)$$

(Bird, Armstrong, & Hassager [44])

(b) For The Solidified Polymer Layer :

$$\rho_s C_{ps}\frac{\partial T}{\partial t} = k_s\frac{\partial^2 T}{\partial x_j\,\partial x_j} \qquad (3.5)$$

(c) For The Mold :

$$\rho_m C_{pm}\frac{\partial T}{\partial t} = k_m\left(\frac{\partial^2 T}{\partial x_j\,\partial x_j}\right) \qquad (3.6)$$

Equation (3.1) is satisfactory for the condition of an incompressible fluid.

In the momentum equation (3.2), the first term and the second term on the left-hand-side are the local mass-times-acceleration term and the convective transport term due to bulk flow respectively. The right-hand-side is the total surface force. The first term is due to pressure-force, and the second term is the viscous force term due to interactions and motions of molecules. The unit of all terms are in force per unit volume.

The correspondance between terms in equation (3.2) and the more general equation (2.7) are as follows:

* The term of total stress tensor due to surface forces:

$$\sigma_{ji} = -P + \eta\left(\frac{\partial u_i}{\partial x_j} + \frac{\partial u_j}{\partial x_i}\right) \quad (\textit{Generalized Newtonian fluid})$$

* The term of convective transport due to bulk flow:

$$\frac{\partial(\rho u_i u_j)}{\partial x_j} = \rho u_j \frac{\partial u_i}{\partial x_j} \quad (\textit{Incompressible fluid}).$$

The major point of the definition of generalized Newtonian fluid is that the "apparent" viscosity η is a function of the scalar invariants of the rate-of-deformation tensor $\{\dot{\gamma}\}$ (or of the viscous momentum flux tensor $\{\tau\}$).

Equation (2.9), uses the effective heat capacity instead of the constant pressure specific heat capacity as in the energy equation (3.3). The effective heat capacity has to be a function of temperature as defined in equation (2.9).

The constitutive equation of viscosity chosen for this model obeys the Ostwald and de Waele power law for shear rate dependence and an Arrhenius-exponential type expression for temperature dependence. Hence the

viscosity function of the model can be written as [17]:

$$\eta = m_o EXP\left(\frac{-A(T-T_b)}{(T_m-To)}\right)\dot{\gamma}^{n-1} \qquad (3.7)$$

We assume that m_o , A , n , C_p , C_{p_s} , C_{p_m} , k_s , k_m , ρ , ρ_s , ρ_m are all constants.

These above equations are subjected to the following initial and boundary conditions of the model:

(a) At the flow front $x_1 = l^*$, only the pressure is prescribed, which is arbitrarily defined to be zero (ambient pressure):

$$P(l^*, x_2) = 0$$

(b) The central symmetrical conditions:

$$\frac{\partial T}{\partial x_2}(x_1, 0) = \frac{\partial u_1}{\partial x_2}(x_1, 0) = u_2(x_1, 0) = 0$$

(c) At the entrance $x_1 = 0$, we prescribe the temperature and either the value of the entrance volume flow rate or the maximum pressure:

$$T(0, x_2) = T_b$$

$$If\ P(0, x_2) < P_{max}\ \ then\ \ 2\int_0^h u_1(0, x_2)dx_2 = Q^*$$

Q^* is the constant entrance volume flow rate.

Otherwise: $P(0, x_2) = P_{max}$

(d) At x_2 = h , there exists a thermal contact conductance Hr along the mold/plastic interface line at (x_1, h).

(e) At $x_2 = h + l_m$, there exists an isothermal temperature line of heat sink at a constant temperature To .

(f) The two vertical ends of the mold (at $x_1 = 0$ and $x_1 = l_c$) are assumed adiabatic boundaries: $\partial T / \partial x_1 = 0$.

(g) At the moving boundary where the plastic layer is freezing, the velocity with which the solid/liquid boundary moves depends upon the temperature gradients in the liquid and solid phases at the moving boundary.

$$\lambda \rho v_n = k_s \frac{\partial T_s}{\partial n} - k \frac{\partial T_l}{\partial n} \qquad (3.8)$$

where λ is the latent heat of the phase change, $\partial / \partial n$ means differentiation normal to the freezing boundary, which is positive towards the wall, and v_n is the velocity in the direction normal to the freezing boundary. To obtain the boundary conditions along the moving boundary we use conservation of mass for a small portion of the plastic domain with length Δx_1 just after the flow front has passed.

During the time increment Δt, the freezing boundary location, denoted as δ, is displaced through a distance $v_n \Delta t$ in the direction of the normal. Due to the difference in the specific mass between the solid and the liquid phase, the total mass M per unit depth in the plastic domain within the length Δx_1 changes as follows:

$$\frac{dM}{dt} = (\rho - \rho_s) \Delta x_1 \frac{\partial \delta}{\partial t} \qquad (3.9)$$

The parameter function of the moving boundary δ is given by $x_2 = \delta(x_1, t)$. The conservation of mass requires:

$$\frac{dM}{dt} = \left[\rho\int_0^{\delta} u_1 dx_2\right]_{x_1+\Delta x_1}^{x_1} \qquad (3.10)$$

Combining (3.9) and (3.10) and letting Δx_1 approach 0 results in:

$$(\rho - \rho_s)\frac{\partial \delta}{\partial t} = -\rho u_1(x_1, \delta)\frac{\partial \delta}{\partial x_1} + \rho u_2(x_1, \delta) \qquad (3.11).$$

where we have used the continuity equation $\partial u_1 / \partial x_1 + \partial u_2 / \partial x_2 = 0$.

The no slip condition along the moving boundary reads:

$$u_1(x_1, \delta) + u_2(x_1, \delta)\frac{\partial \delta}{\partial x_1} = 0 \qquad (3.12)$$

Simultaneously solving (3.11) and (3.12) for $u_1(x_1, \delta)$ and $u_2(x_1, \delta)$ one finds [45]:

$$u_1(x_1, \delta) = -\left(1 - \frac{\rho_s}{\rho}\right)\frac{\dfrac{\partial \delta}{\partial x_1}}{1 + \left(\dfrac{\partial \delta}{\partial x_1}\right)^2}\frac{\partial \delta}{\partial t} \qquad (3.13)$$

$$u_2(x_1, \delta) = \left(1 - \frac{\rho_s}{\rho}\right)\frac{1}{1 + \left(\dfrac{\partial \delta}{\partial x_1}\right)^2}\frac{\partial \delta}{\partial t} \qquad (3.14)$$

For simplicity, one can assume that $\rho_s = \rho$, and considering the fact that the temperature of the moving boundary equals the melting temperature, one can write:

$$T(x_1, \delta) = T_m \quad ; \quad u_1(x_1, \delta) = u_2(x_1, \delta) = 0$$

3.3.2 The Simplified Model Equations

Since it is always desirable to have simple and reasonable model equations for a specific problem whose solutions can be obtained with minimal time and effort and within an acceptable accuracy, one usually (if not always) tries to simplify the equations before beginning to solve them analytically or numerically. An appropriate model simplification can usually be achieved from the consideration of the engineering and the physics of the process, the material behaviour, the geometry of the problem and the mathematical manipulation. To assist this simplifying procedure, the general governing equations are nondimensionalized as follows:

For the plastic domain

$$\varepsilon = \frac{h}{l_c} \;;\; x = \frac{x_1}{l_c} \;;\; y = \frac{x_2}{h} \;;\; \tau = \frac{V t}{l_c} \;;\; Q = \frac{Q^*}{2 V h}$$

$$u = \frac{u_1}{V} \;;\; v = \frac{u_2}{\varepsilon V} \;;\; \pi = \frac{\varepsilon P}{\rho V^2} \;;\; \theta = \frac{T - T_b}{T_m - \mathrm{To}}$$

Assuming quasi-steady state, the momentum equations can be written as:

The x-component:

$$\varepsilon \rho h V\left(u\frac{\partial u}{\partial x} + v\frac{\partial u}{\partial y}\right) = -\rho V h\frac{\partial \pi}{\partial x} + 2\varepsilon^2\frac{\partial}{\partial x}\eta\left(\frac{\partial u}{\partial x}\right) + \frac{\partial}{\partial y}\eta\left(\varepsilon^2\frac{\partial v}{\partial x} + \frac{\partial u}{\partial y}\right) \quad (3.15)$$

The y-component:

$$\varepsilon^3 \rho V h\left(u\frac{\partial v}{\partial x} + v\frac{\partial v}{\partial y}\right) = -\rho V h\frac{\partial \pi}{\partial y} + \varepsilon^2\frac{\partial}{\partial x}\eta\left(\varepsilon^2\frac{\partial v}{\partial x} + \frac{\partial u}{\partial y}\right) + 2\varepsilon^2\frac{\partial}{\partial y}\eta\frac{\partial v}{\partial y} \quad (3.16)$$

One now assumes that the cavity is long and narrow, thus ε is much smaller than unity (e.g. ε is about 1/100). This assumption is exploited to obtain the

asymptotic channel approximation solution for the flow field. As ε approaches zero, one obtains:

$$-\rho V h \frac{\partial \pi}{\partial x} = \frac{\partial}{\partial y}\left(\eta \frac{\partial u}{\partial y}\right) \quad (3.17)$$

$$\frac{\partial \pi}{\partial y} = 0 \quad (3.18)$$

They can be considered as a consistent first order approximation of their original equation (3.2). It means that the sensitivity of the flow field with respect to the velocity component v is negligible when compared to the velocity component u as long as ε is much smaller than unity. We can check the validity of this asymptotic approximation by substituting the physical values of the input data involved, and then consider the relative magnitudes of all terms in the original equation (3.2). Finally, the viscosity function is put into use and one obtains:

$$\frac{\partial \pi}{\partial x} = \mathrm{Re}^{-1} \frac{\partial}{\partial y} e^{-A\theta} \left|\frac{\partial u}{\partial y}\right|^{n-1} \frac{\partial u}{\partial y} \quad (3.19)$$

where Re is the Reynolds number defined below.

Similarly, the *continuity equation*:

$$\frac{\partial u}{\partial x} + \frac{\partial v}{\partial y} = 0 \quad (3.20)$$

and the *energy equation* with conduction in the flow direction neglected:

$$\frac{\partial \theta}{\partial \tau} + u\frac{\partial \theta}{\partial x} + v\frac{\partial \theta}{\partial y} = \frac{1}{Gz}\frac{\partial^2 \theta}{\partial y^2} + \frac{Br}{Gz} e^{-A\theta} \left|\frac{\partial u}{\partial y}\right|^{n+1} \quad (3.21)$$

$$\frac{\partial \theta_s}{\partial \tau} = \frac{1}{Gz_s}\frac{\partial^2 \theta_s}{\partial y^2} \quad \text{for } \textit{Solidified Plastic} \qquad (3.22)$$

The Reynolds, Graetz, and Brinkman numbers are defined by:

$$\mathrm{Re} = \frac{\rho h V}{\eta_o} \;;\; Gz = \frac{\varepsilon \rho C_p V h}{k} \;;\; Br = \frac{\eta_o V^2}{k(T_m - \mathrm{To})} \;;\; \eta_o = m_o\left(\frac{V}{h}\right)^{n-1}$$

For the mold domain, the 2-D heat flow equation with only temperature nondimensionalized can be written as:

$$\rho_m C_{Pm}\frac{\partial \theta}{\partial t} = k_m\left(\frac{\partial^2 \theta}{\partial x_1^2} + \frac{\partial^2 \theta}{\partial x_2^2}\right) \qquad (3.23)$$

It is now necessary to solve for u , $\partial\pi / \partial x$ and θ using the model equations: (3.18) to (3.23) with the following dimensionless boundary conditions:

(a) **For the plastic domain :**

$\pi(l^*/l_c, y) = \pi_o = 0$ *where* π_o is the dimensionless pressure at the flow front

$$v(x,0) = \frac{\partial u}{\partial y}(x,0) = \frac{\partial \theta}{\partial y}(x,0) = 0 \quad \textit{the symmetry condition}$$

$\theta(0,y) = \theta_b$ *where* θ_b is a specified dimensionless temperature at the entrance

$$\textit{If } \pi(0,y) < \pi_{max} \textit{ then } \int_0^1 u(0,y)\,dy = 1 \quad \textit{otherwise } \pi(0,y) = \pi_{max}$$

(b) **For the interface :**

$$\left(\frac{k_s}{h}\frac{\partial \theta}{\partial y}\right)_{(x,1^-)} = \left(k_m\frac{\partial \theta}{\partial x_2}\right)_{(x_1,h^+)} = -Hr\,(\theta_{(x,1^-)} - \theta_{(x_1,h^+)}) \qquad (3.24)$$

(c) **For the mold :**

$\theta(x_1 , h+l_m) = \theta_o$ *where* θ_o is the dimensionless temperature of the heat sink

$$\frac{\partial \theta}{\partial x_1}(0 , x_2) = \frac{\partial \theta}{\partial x_1}(l_c , x_2) = 0$$

(d) **At the freezing boundary :**

$u(x,\alpha) = v(x,\alpha) = 0 \quad , \quad \theta(x,\alpha) = \theta_m$

$$\bar{v} = \left[\frac{Ste}{Gz} \frac{\partial}{\partial y} \left(\frac{k_s}{k} \theta_s - \theta \right) \right]_{y=\alpha} \qquad (3.25)$$

where $\bar{v} \approx (v_n) / (\varepsilon V)$ and α is the dimensionless coordinate of the freezing boundary in the y-direction.

Appendix C presents a detailed derivation of equation (3.25)

Integration of the equation of motion in the y-direction yields, under the assumption that $\partial \pi / \partial x < 0$,

$$\frac{\partial \pi}{\partial x}(x,\tau) = \frac{Q^n}{\mathrm{Re}} \left[\int_0^{\alpha} e^{\frac{A\theta}{n}} y^{(1+1/n)} dy \right]^{-n} \qquad (3.26)$$

where $Q = Q^* / 2 V h$, for the case of constant volume flow rate at the entrance then $Q = 1$. And

$$u = Q \frac{\int_y^{\alpha} e^{\frac{A\theta}{n}} y^{1/n} dy}{\int_0^{\alpha} e^{\frac{A\theta}{n}} y^{(1+1/n)} dy} \qquad (3.27)$$

As soon as the temperature field θ is known, the pressure gradient and velocity profile can be found by evaluation of the expressions (3.26) and (3.27).

Appendix D presents a detailed derivation of equations (3.26) and (3.27).

The additional assumptions made for model simplification are as follows:

1. Fully developed flow, which means that the entrance effect upon the flow field is negligible
2. The fountain effect during the filling and the shrinkage during the cooling do not have a significant effect on the temperature distribution in the plastic part.
3. The molten plastic begins freezing as soon as it comes into contact with the wall of the cavity.

3.4 THE NUMERICAL FDM ALGORITHM

Generally, there are four main steps in this numerical analysis scheme:

1. Discretize the solution domain by setting up an appropriate nodal grid scheme.
2. Derive the algebraic finite difference equations from the model thermal equation and boundary conditions for each node of the mesh and set them up in a matrix form. Solve for the temperature field. Then calculate the pressure gradient and velocity field using numerical integration and interpolation methods
3. Encode the above two schematic steps into a computer program to facilitate the computational procedure for the solution.

4. Produce appropriate graphical outputs so that interpretation of the outputs can proceed.

3.4.1 THE NODAL GRID SCHEME

Since the melt flows into the cavity at a uniform volumetric rate and the cross sectional flow area of the cavity is constant and the rectangularity of the total solution domain, the flow front moves a fixed distance down the cavity during each (constant) time interval. Figure 3.3 shows a nodal grid scheme where the flow rate and time interval are such that the cavity fills in 12 time intervals. The nodal grid scheme was set up such that the first grid line at $x = X_1$ was at the mid position of the plastic at the end of the first time increment and perpendicular to the direction of flow. Then each subsequent grid line was 1/12 of the cavity length further down the cavity.

Therefore during the filling stage, in mathematical terms, we define the grid lines at time level $\tau = \tau_i$ as follows.

Let the grid lines $x = X_k$, $k = 1, 2, 3, ..., (i - 1)$. be the same as the grid lines of previous time level $\tau = \tau_{i-1}$, and let $x = X_i$ be the new grid line of the advancing flow front. When the injection volumetric flow rate Q is known, the position of this new line can be calculated as:

$$\Delta X_i = X_i - X_{i-1} = \int_{\tau_{i-1}}^{\tau_i} Q(\tau)\, d\tau \qquad (3.28)$$

If Q is constant then

$$\Delta X = Q\, \Delta\tau$$

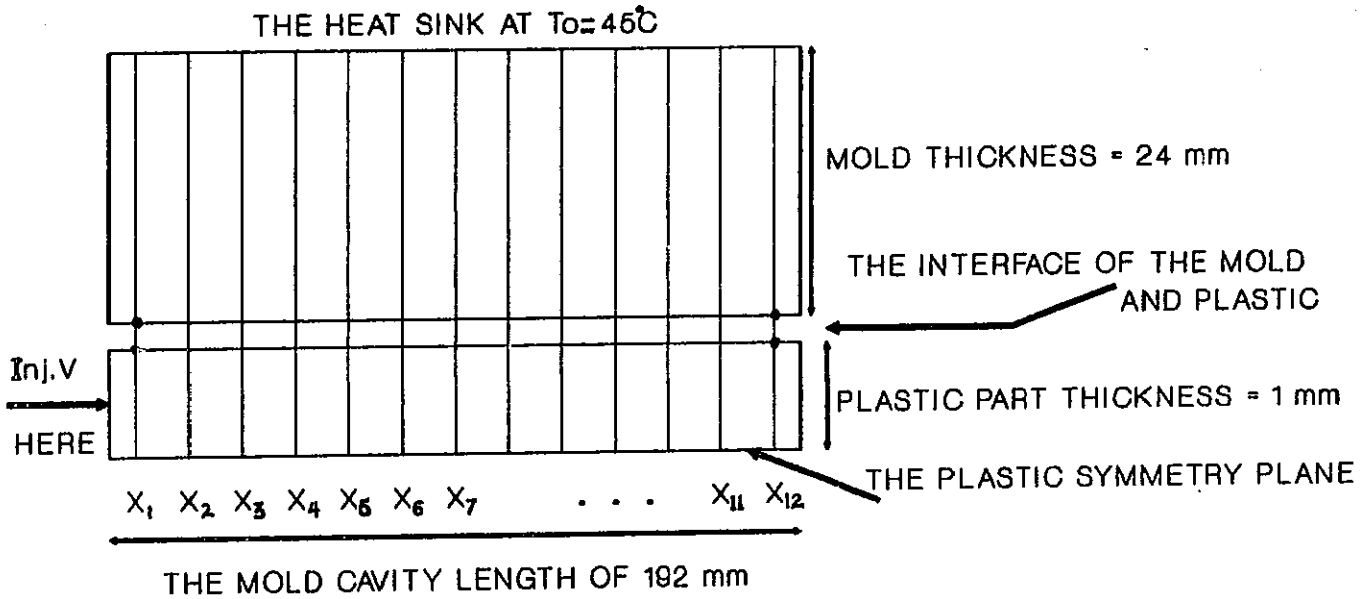

——— X_k's denote grid lines which are consecutively set up perpendicular to the direction of flow as the flow front advances time step by time step during the filing stage.

(X_k ; k = 1, 2, 3,... l-1, l.)

(The filling time: 1.2 sec; time step value: 0.10 sec.)

NODES PER GRID: (# IN MOLD) + (# IN SOLID PLASTIC) + (# IN LIQUID PLASTIC)

Hence THE TOTAL NODAL # = (# OF GRIDS) TIMES (# OF NODES PER GRID)

Fig.3.3: **THE SIMPLE SKETCH OF THE MODEL AND NODAL MESH**

The nodal scheme could be modified to set up multiple grid lines after each time step if it were required.

The total number of nodes on each grid line was arbitrarily chosen. The nodal scheme of grid points in the mold domain and solidified plastic layer was set up in a conventional manner with equally spaced steps in the x and y directions respectively. Due to the steep temperature gradient near the freezing boundary in the y direction, unequally spaced nodes in the liquid domain were used to set a high density of nodes near this freezing boundary.

For the flow domain, define on the entrance line $x = X_o$, the grid points $y = Y_0^l$, $l = 1, 2, 3, ..., L$; where Y_0^1 lies on the symmetrical line of the flow and Y_0^L on the interface. The intersections of the instantaneous streamlines through these points and the grid lines X_k's are the grid points Y_k^l in the liquid domain. One advantage of this definition is that the position of the freezing boundary is defined by the grid points Y_k^L as this boundary is a streamline. Another advantage is that the convection term in the energy equation can be expressed in a simple way:

$$u\,\partial\theta/\partial x + v\,\partial\theta/\partial y = u_s\,\partial\theta/\partial s \qquad (3.29)$$

Where s measures the distance along the streamline.

The main problem is now the calculation of the positions of the grid points so they correspond to streamlines. This calculation is based on the idea that the flux through two adjacent grid points at the entrance $x = X_o$ and two corresponding adjacent grid points on any other grid line must be equal. Suppose that we know the position, fluid velocity, and temperature at all grid points at the present time level $\tau = \tau_i$, but they are not on the streamline line positions. We can determine

these nodal values on the streamline position by interpolation. The interpolation procedure to find the arrangement of nodal points on each grid line, such that the streamline condition is satisfied, gives rise to two unknowns; the positions of the streamlines, and velocity values at these positions. So two equations are needed to solve for these unknowns. On a given grid line, by linear interpolation, we can write as follows:

$$u^*_{l+1} = u^*_l + \left(\frac{u_{l+1} - u^*_l}{Y_{l+1} - Y^*_l}\right) d^*_{l+1} \qquad (3.30)$$

$$1/2\,(u^*_{l+1} + u^*_l)\, d^*_{l+1} = \Delta Q_l \qquad (3.31)$$

where $d^*_{l+1} = (Y^*_{l+1} - Y^*_l)$

u^*_{l+1} , u^*_l : interpolated streamline velocities.

Y^*_{l+1} , Y^*_l : the two corresponding streamline positions.

u_{l+1} , Y_{l+1} : are the "not on streamline" values before interpolation.

ΔQ_l : the flux flow between the Y^*_{l+1} and Y^*_l positions.

In equations (3.30) and (3.31), Y^*_l and u^*_l are already known values from the previous calculation or the boundary condition. Y^*_{l+1} and u^*_{l+1} are unknown variables. Substitute (3.30) into (3.31) we obtain:

$$\frac{1}{2}\left(\frac{u_{l+1} - u^*_l}{Y_{l+1} - Y^*_l}\right)(d^*_{l+1})^2 + u^*_l d^*_{l+1} - \Delta Q_l = 0 \qquad (3.32)$$

which is a quadratic equation and can be solved for d^*_{l+1}.

Then

$$Y^*_{l+1} = Y^*_l + d^*_{l+1}$$

For each grid line, the calculation can begin from the symmetrical node $l = 1$ to interpolate the required values of the next node $l = 2$. The interpolation is repeated for the next node $l = 3$ and so on until $l = L - 2$.

The temperature of the old grid points are used to interpolate the temperature of the streamline grid points, e.g. linearly or by Aitken's method for iterative interpolation [48].

3.4.2 The Finite Difference Scheme

We will now consider the finite difference scheme for the temperature of the thermal equation. Since the Peclect number of this flow problem (Gz = εPe) is usually much greater than unity, then, at the point (X_k , Y^l_k), the convection term will be approximated with the upwinding differencing as follows (see Fig.3.4).

$$u_s \frac{\partial \theta}{\partial s} \approx u^l_{S(k-1)} \frac{\theta^l_k - \theta^l_{k-1}}{\Delta s} \qquad (3.33)$$

Notice that a subscript k denotes the grid line at the coordinate of x = X_k and a superscript l is the nodal index of a grid point on each grid line.

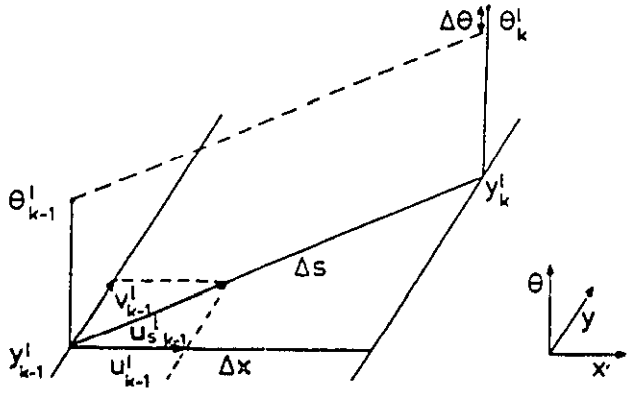

Fig.3.4: Definition of Δx , Δy , Δs

Unless stated otherwise, $\tau = \tau_i$, the current time level. Equation (3.33) is an implicit approximation. Now we have:

$$\frac{u^l_{S(k-1)}}{\Delta s} = \frac{u^l_{k-1}}{\Delta X} \quad (geometric\ similarity)$$

$$Hence \quad u_s \frac{\partial \theta}{\partial s} \approx u^l_{k-1} \frac{\theta^l_k - \theta^l_{k-1}}{\Delta X} \qquad (3.34)$$

For the approximation of the non-stationary terms in the energy equation we have to know the value $\theta = \theta^*$ *at* $\tau = \tau_{i-1}$ (previous moment) at the points (X_k, Y^l_k). As the positions of the grid points are time dependent, this value has to be interpolated e.g. linearly. The conduction term is approximated implicitly with central differences and the viscous heating term explicitly. This results in the following scheme:

$$\frac{\theta^l_k - \theta^*}{\Delta\tau} + u^l_{k-1} \frac{\theta^l_k - \theta^l_{k-1}}{\Delta X} = \frac{2}{Gz\,\Delta^l_k \Delta^{l+1}_k} \left(\frac{\Delta^l_k}{\Delta^{l+1}_k + \Delta^l_k} \theta^{l+1}_k - \theta^l_k + \frac{\Delta^{l+1}_k}{\Delta^{l+1}_k + \Delta^l_k} \theta^{l-1}_k \right)$$

$$+ \frac{Br}{Gz} e^{\frac{A}{n}\theta^*} \left(-\mathrm{Re}(\frac{\partial \pi}{\partial x})^* Y^l_k \right)^{(1+1/n)} \qquad (3.35)$$

Where $\Delta^l_k = Y^l_k - Y^{l-1}_k$ and the symbol * denotes the interpolated value for $\tau = \tau_{i-1}$ at the point (X_k, Y^l_k) of the present nodal grids.

In the solidified layer, the distance between the points on the same grid line are equal. The 1-D parabolic energy equation along each grid line was solved (the heat conduction in the x direction is negligible). This was done with an implicit central difference scheme.

For the mold domain, the 2-D energy equation was solved using nodal points at equal spacing along each grid line and the appropriate boundary conditions. At the interface, the general difference equation for a mold node can be written as:

$$(-Fmx)\theta^{l}_{k-1} + (-2Fmy\,Bmy)\theta^{l-1}_{k} + (1 + 2Fmy\,Bmy + 2Fmy + 2Fmx)\theta^{l}_{k} + (-2Fmy)\theta^{l+1}_{k} + (-Fmx)\theta^{l}_{k+1} = (\theta^{*})^{l}_{k}$$

where:

$$Fmx = \frac{\alpha_m \Delta t}{(\Delta^m_x)^2} \quad , \quad Fmy = \frac{\alpha_m \Delta t}{(\Delta^m_y)^2} \quad , \quad Bmy = \frac{Hr\,\Delta^m_y}{k_m} \quad , \quad \alpha_m = \frac{k_m}{(\rho\, C_p)_m}$$

A similar expression can be derived for a plastic node.

$$\left(-\frac{2}{Gz\,(\Delta^l_k)^2}\right)\theta^{l-1}_{k} + \left(1 + \frac{2}{Gzs\,(\Delta^l_k)^2} + \frac{2Bis}{Gzs\,(\Delta^l_k)}\right)\theta^{l}_{k} + \left(-\frac{2Bis}{Gzs\,(\Delta^l_k)}\right)\theta^{l+1}_{k} = \frac{(\theta^{*})^{l}_{k}}{\Delta\tau}$$

where

$$Bis = \frac{Hr}{k_s}h \quad , \quad Gzs = \frac{(C_p\rho)_s\, V\, \varepsilon\, h}{k_s}$$

For the calculation of the total solution domain at $\tau = \tau_i$ one problem remains; the determination of the position of the freezing boundary $\alpha(\tau_i, X_k)$. For this purpose equation (3.25) is used. With the solution of the previous time level $\tau = \tau_{i-1}$, the right hand side of equation (3.25) can be evaluated according to the numerical scheme just outline above. This right hand side is a function of α only, and is denoted by $g(\alpha(\tau_i, X_k))$. Therefore equation (3.25) can be approximated by a stiffly stable numerical scheme, namely the implicit Euler method as follows:

$$\alpha(\tau_i, X_k) = \alpha(\tau_{i-1}, X_k) + (\tau_i - \tau_{i-1})\, g(\alpha(\tau_i, X_k)) \qquad (3.36)$$

$$g(\alpha) = \left[\frac{k_s}{k} \frac{\theta_m - (\theta^*)_k^{l+1}}{\alpha - (Y^*)_k^{l+1}} - \frac{(\theta^*)_k^{l-1} - \theta_m}{(Y^*)_k^{l-1} - \alpha} \right] \frac{Ste}{Gz} \qquad (3.37)$$

$$g(\alpha(\tau_i, X_k)) \equiv g(\alpha)$$

This nonlinear equation is solved approximately by the Regular Falsi method combined with Aitken acceleration [46]. Let α_j , j = 0, 1, 2..., be successive approximations to $\alpha(\tau_i, X_k)$. The algorithm is defined as follows:

$$\alpha_o : = \alpha(\tau_{i-1}, X_k)$$

$$\alpha_1 : = 3/2\alpha_o - 1/2\alpha(\tau_{i-2}, X_k)$$

Regular Falsi: for $j = 2, 3$.

$$\alpha_j : = \frac{\{\alpha_o\, g(\alpha_{j-1}) - \alpha_{j-1}\, g(\alpha_o)\}}{\{g(\alpha_{j-1}) - g(\alpha_o)\}} \qquad (3.38)$$

Aitken acceleration:

$$\alpha_4 = \frac{(\alpha_1\alpha_3 - \alpha_2^2)}{(\alpha_1 + \alpha_3 - 2\alpha_2)}$$

The numerical algorithm just described enables us to solve the set of the finite difference equations numerically if the entrance injection volume flow rate Q is known.

For the case when the maximum pressure has been reached at the entrance of the cavity, the entrance flow rate Q is no longer constant and has to be adjusted. Integration of equation (3.26) yields

$$\pi_o - \pi_{entrance} = -\frac{Q^n}{\mathrm{Re}} \int_0^{\pi/l} \left[\int_0^{\alpha(\xi)} e^{\frac{A}{n}\theta} y^{(1+1/n)} dy \right]^{-n} dx \qquad (3.39)$$

It is found that the integral on the right hand side does not change very much if the variations of Q are not too large. This indicates that the time for the adjustment of the temperature distribution is much longer than the time scale for changes in Q, equation (3.39). Thus, the pressure at the entrance is approximately proportional to Q^n. Using this result a new Q can be obtained from

$$Q_{new} = Q_{prev.}\left(\frac{\pi_{max} - \pi_o}{\pi(Q_{prev.}) - \pi_o}\right)^{1/n} \qquad (3.40)$$

where $\pi(Q_{prev.})$ is the calculated value of π at the entrance for $Q = Q_{prev.}$. Then Q_{new} can be used to set up a new grid line of the advancing flow front.

The calculated nodal temperatures in the flow and equations (3.26) and (3.27) are used to calculate the pressure gradient $\partial\pi / \partial x$ and the velocity profile (u_k^l) on each grid line respectively. Because these grid points are not equally spaced, and for the simplicity, the trapezoidal method of numerical integration is implemented. The Simpson's rule of numerical integration with unequally spaced data is also derived and presented in Appendix E.

The cross-cavity transverse velocity component v_k^l can be approximated by [49]:

$$v_k^l \approx u_k^l\left(\frac{\partial\alpha_k}{\partial x}\right)\left(\frac{y_k^l}{\alpha_k}\right) \quad (k = 1,2,3,...,i \;\; ; \;\; l = 1,2,3,...,L) \qquad (3.41)$$

When the mold cavity is just filled, the filling stage ceases and the packing stage comes into account. During the packing and holding phase, a slow creeping plastic flow compensates for cooling shrinkage and the mold pressure is built up and transmitted to level off the pressure difference throughout the polymer in the

cavity. The response pattern of the mold pressure during the packing and holding stage can be modified by the process control settings for the operation of the injection molding cycle [47]. Since viscous heating during this phase is negligible, we can assume that the temperature field of the liquid plastic is shifted downstream very little. Hence, for the purpose of this investigation, we can treat the packing stage as part of the post filling analysis.

3.4.3 The Post Filling Calculation

In the solidification and cooling stage, the numerical algorithm is the same as that for the filling stage but we are dealing with the diffusive thermal equation only. There is no more flow in the liquid plastic. In the solidification phase, although there is still a liquid region, there is no flow and hence no convection and viscous heating terms in the finite difference equation. In the cooling phase, the latent heat effect vanishes once all the plastic solidifies. In the opening and ejection time, only the mold is analysed with the freshly opened surface exposed to cooling by the surrounding air.

The numerical analysis of the solidification and cooling stage is very similar to that of the preliminary third attempt, except that:

It is a 2-D analysis instead of 1-D.

It uses moving nodal points in the plastic domain during the solidification instead of fixed nodal points.

It is implicit instead of explicit.

It would be interesting to have time to compare the corresponding results of these two analyses!

Finally, the output of the mold temperature distribution at the end of one molding cycle will be the input for the next computational cycle until the thermal field of the mold part reaches periodic steady state.

3.5 MAIN COMPUTER PROGRAMING ASPECTS

The basic ideas and the sequence of the numerical algorithm in the last section are compactly represented in the flow chart shown in Fig.3.5 where i denotes the number of time steps, i = 1, 2, 3, ..., $I_{(total)}$, *where* $I_{(total)}$ represents the total number of time steps for one complete molding cycle.

Fig.3.5: The flow chart of the numerical algorithm.

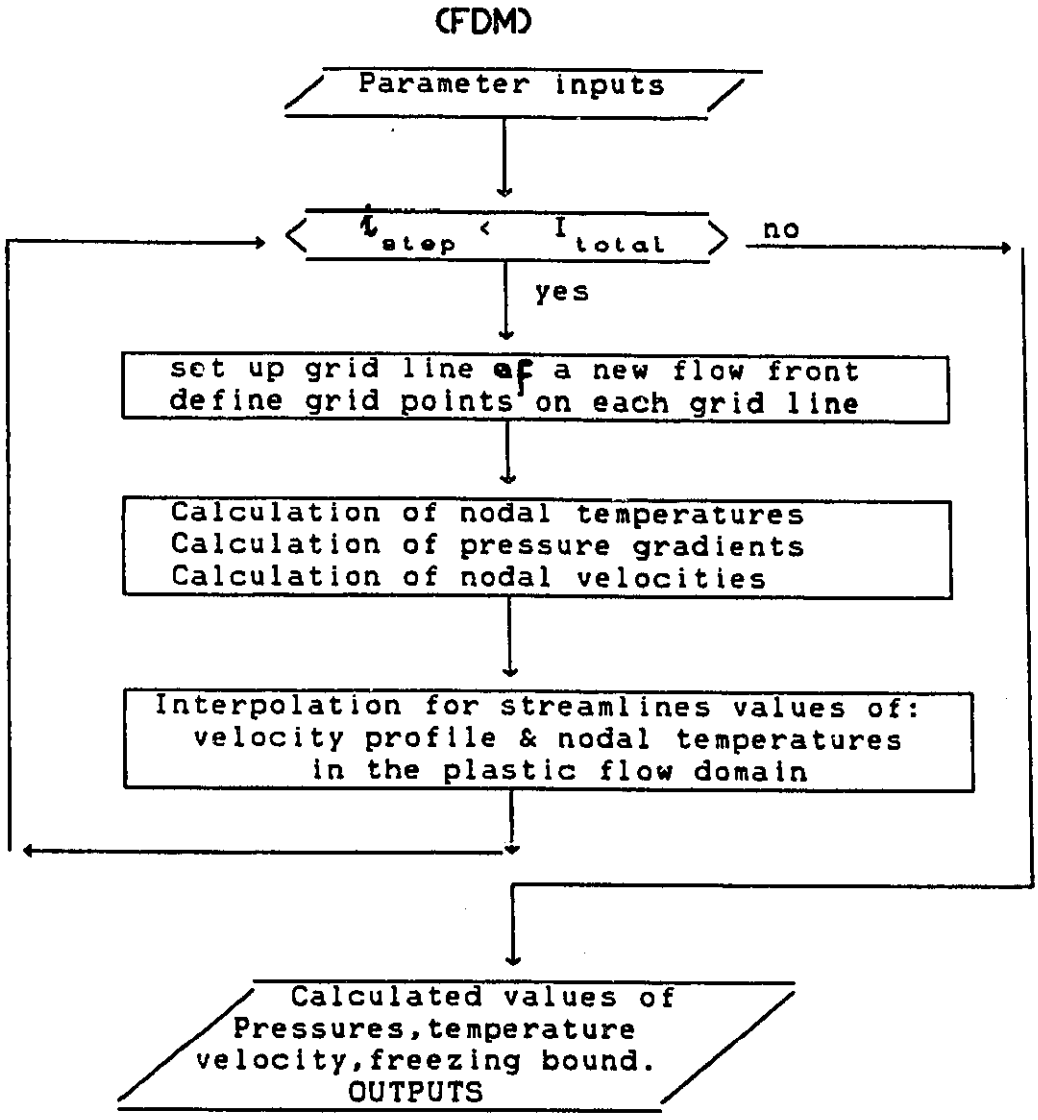

The development of numerical algorithm has evolved into a major research study. A research computer program usually emphasizes the demonstration of a technical idea, and is used for a specific purpose in research. It should be developed with a clearly determined theoretical background for maximum confidence in its correctness, with known limitations and requiring minimum programming effort. This research program was written in a natural tendency of "just writing the program" and getting on with the job without any preparation for program documentation.

The computer program was written in the standard Fortran language for program portability and for use in the batch mode. This thesis work provides enough information to serve as the theory manual and the documentation for this research program. The mainframe of the computer centre in the University of Windsor has the IBM 4381 computing system and the Fortran 77 compiler accessed by the Control Program (CP) and the operating system, Conversational Monitor System (CMS). The compiler is used to run and execute the program. It has a good debugging ability. The chosen outputs of the program can be formatted to become an interface file for external graphic software, as a post-processing program, or the program can include some plotting subroutines to do the graphics for the outputs (such as using the plotting subroutine of SAS/GRAPH, Statistical Analysis System, version 5, SAS institute, Carg. NC. in the mainframe).

The thesis is submitted with a floppy disc containing the program mounted inside the thesis back cover.

To help with interpretation, the research program can be considered as consisting of four main modules, namely Tau 1, Tau 2, Tau 3 and Gauss. These four modules will be described in the sequence in which they are encountered in the program structure:

Tau 1 This is the main program from which other module subroutines are called. Its main functions are: the processing of the inputs and outputs and the calling of its subroutines to carry out the desired computational work in the proper sequence. It takes in the initial data regarding molding conditions and domain geometry parameters with DATA/PARAMETER statements and READ statements. It performs preprocessing work to compute and store those desired values that are repeatedly used by the computational processing of the program. It shares global variables with other modules through COMMON statements. Its outputs are formatted PRINT statements.

The Primary Outputs are:

(a) The pressure gradients, and the nodal velocity profiles of the flow domain.

(b) The nodal temperature distribution of the total solution domain.

(c) The position of the freezing boundary.

With the primary outputs, we can calculate the secondary outputs such as the pressure field, the shear stress field of the flow domain, the amount of heat flow through the interface as a function of time , and so on .

Tau 2 This subroutine is used to compute the flow field and temperature field during the filling stage only. After it is called and receives the necessary input values from the main program it calculates the position of the freezing

boundary, the interpolated grid points, the coefficient matrix of nodal temperature unknowns from their finite difference equations, and then the pressure gradient and interpolated streamline velocity profile on each grid line. Each entry of the coefficient matrix is put into its intended location by using the IF-ELSEIF control structure. It calls the Gauss subroutine to solve for the nodal temperature unknowns. DO-LOOP control structures are used to do the numerical integration summation of the trapezoidal method and the interpolation for pressure gradient and streamline velocity profiles at each time step.

Tau_3 This subroutine handles the rest of the molding cycle: the solidification phase, the cooling phase, and the opening and closing phase. Its computational structure is similar to the Tau 2 but is simpler since there is no flow field involved. The IF-ELSEIF control structure used to determine whether it is the transition time to "switch" the computational action from one phase to the next phase of the cycle.

Gauss This subroutine is the direct solver of a system of linear algebraic equations. It employs the Gaussian elimination algorithm to directly solve for the solution of the system.

Chapter IV
RESULTS AND DISCUSSIONS

4.1 INPUTS

Some basic features of the input data will be emphasized in the following paragraphs to provide information necessary for those who attempt to run this program.

The input data required for the program are the physical values for a chosen molding condition. This includes the material properties for both the given polymer and the mold material, the descriptive geometry/nodal parameters of the composite domain and the chosen total cycle time. All the data inputs except the initial mold temperature input are fed into the program through the DATA statements in the first few lines of the main Program. It is much more convenient to treat this initial mold temperature data as an external input file through a READ statement because this data changes with each molding cycle; the output data from one cycle becomes the input for the next.

At the entrance gate, either the injection pressure or injection volume flow rate may be prescribed. The other can be calculated by the program. A liquid/solid transition temperature for the selected polymer is chosen such that there is no "apparent" flow in the polymer when the temperature falls below this transition point, and the heat of fusion is released at this temperature. The initial mold temperature must be less than the transition temperature in order for solidification

to occur. The injected polymer temperature must be sufficiently above the transition temperature so that the plastic flow will not be "frozen off" before it reaches to the end of the cavity. The program currently treats the thermal property values of the polymer and the mold as constants but they could be made functions of temperature with an additional subroutine in the pre-processing stage of the main program.

Unequally spaced nodes in the liquid plastic on the entrance grid are specified by setting the geometry index β to a number smaller than unity. If the geometry index is equal to unity, these nodes becomes equally spaced.

An historical overview of the thesis work has been presented. The capabilities of the program were then tested by running it with the inputs shown in Data Table 1. The values were chosen because they were available to the author.

The sensitivity of the results of the program analysis to the injection velocity "V" , the cavity thickness "2h" , the thermal contact conductance "Hr" , and the initial mold temperature "To" was studied by varying one of these parameters to the new values shown in Data Table 2, while holding all other parameters at their initial values. The program was then rerun to investigate the effect of varying these process parameters on the flow field as well as the thermal field.

THE DATA TABLE 1

THE PHYSICAL PROPERTIES OF THE MOLD AND POLYMER

(Very similar to physical properties of the polystyrene PS 678 DOW by H.VAN WIJNGAARDEN, J.F.DIJKSMAN, 1982[17])

DIMEMSIONS OF MOLD CAVITY			
Length (ℓ_c)	Thickness(2h)	Width(W)	Asymptotic Parameter ε
192 mm	2.0 mm	W >> 2h	(ε=h/ℓ_c):0.005208
MOLD THERMAL PROPERTIES			
Conductivity k_m	Density ρ_m	Specific heat C_{p_m}	Convective air
58.0 W/m.K	7860 Kg/m.m.m	440 J/Kg.K	Ha: 25 W/m.m.K
PLASTIC THERMAL PROPERTIES (SI units)			
Conductivity k	Density ρ	Specific heat C_p	Heat of fusion λ
Solid → 0.140	1060.0	1700.0	3800.0
Molten → 0.140	1060.0	1700.0	
BOUNDARY TEMPERATURES (Celsius)			
Inj.temp. T_b	Freez.temp. T_m	Init.mold T_o	Air temp. T_a
240.0	160.0	45.0	25.0

THE DATA TABLE 1 (Continued)

VISCOUS PROPERTIES OF THE MOLTEN POLYMER (SI units)			
Visco. coef. m_o	Thermal index A	Sh.rate index n	Injec. speed V
2500.0	0.85	0.356	0.160
THE NODAL MESH SCHEME			
# in mold	# in solidified	# in liquid	Geom. index β
10	6	7	0.85
Inj.CYC.	Time step	Mold thickness ℓ_m	Mold size step
22.0sec	0.10 sec	24 mm	2.4 mm

The viscosity law of non newtonian behavior of plastic melt:[7]

$$\eta = m_o EXP\left(\frac{-A(T-T_b)}{(T_m-To)}\right)\dot{\gamma}^{n-1} \qquad (3.7)$$

THE DATA TABLE 2

THE CHANGE IN VALUES CHOSEN FOR SOME PROCESS PARAMETERS

(SI units)

PARAMETERS	Initial value	first value	Second value
Injection speed V	0.16	0.08	0.32
(2h) THICKNESS (mm)	2	1	0.4
contact conductance Hr	2500	1000	10000
initial mold temperature T_0	45	65	85

4.2 RESULTS

The raw outputs generated by the computer were carefully checked to ensure there were no inconsistent numbers. The interesting aspects of the outputs were then chosen and plotted.

Nodal Temperatures, Pressure Gradients, Velocities, Freezing Boundaries, and Streamline Positions were all directly available from the computer program outputs. Shear Rates and Isothermal Lines, however, had to be calculated from the primary outputs with a hand calculator.

The results of this study are presented graphically in five groups according to the parameter being studied as follows.

1. Group A : Transient Start Up Cyclic Behaviour
2. Group B : The Effect of Varying the mean injection speed (V)
   the time step, and the grid size.
3. Group C : The Effect of Varying the Cavity Thickness (2h)
4. Group D : The Effect of Varying the Contact Conductance (Hr)
5. Group E : The Effect of Varying the mold sink temperature (To)

All of these results are presented together in order to facilitate comparisons between the studies. The results will be discussed in the next section. An extra fold out Figure 3.3 is attached to the back cover to assist the reader with the general layout of the 2-D model.

Generally, the flow profile, pressure gradient, the maximum shear rate line along the flow domain (from left to right) at the end of the filling stage were plotted. For the thermal field, the temperature distributions along the grid lines of k = 1 and k = 12; along the interface lines (mold faced and polymer faced); the

thermal responses of the interface nodes of k = 1 , k = 6 , k = 12 ; and the isothermal lines of the whole "composite" domain at the end of the filling stage were plotted when of interest.

4.2.1

GROUP A

Transient Start Up Cyclic Behaviour

(The inputs are from Data Table 1)

Figures A.I.1 to 8 : Mold temperatures along grids 1 and 12 at various times throughout the first and fifteenth cycles 86

Figures A.II.1 to 4 : Variation of the temperature distribution along the mold contact surface at various times throughout the first and fifteenth cycles 90

Figures A.III.1 to 4 : The thermal response of the interfacial nodes at grids 1 and 12 for the first and fifteenth cycles 92

Figure A.IV. : The pressure gradients and frozen thicknesses along the length of the cavity at the moment when the mold has just been filled for the first and fifteenth cycles 94

Figures A.V.1 and 2 : Isothermal profiles Within the plastic and the mold at the moment when the mold has just been filled for the first and fifteenth cycles 95

Figures A.VI.1 and 2 : The position of the solid/liquid plastic layer at various times during the first and fifteenth cycles 97

Figures A.VII.1 to 4 : The velocity profiles and streamlines of the liquid plastic when the plastic is about to reach the end of the cavity for the first and fifteenth cycles 99

Figure A.I.1 Mold temperatures along Grid #1 at various times during the first cycle.

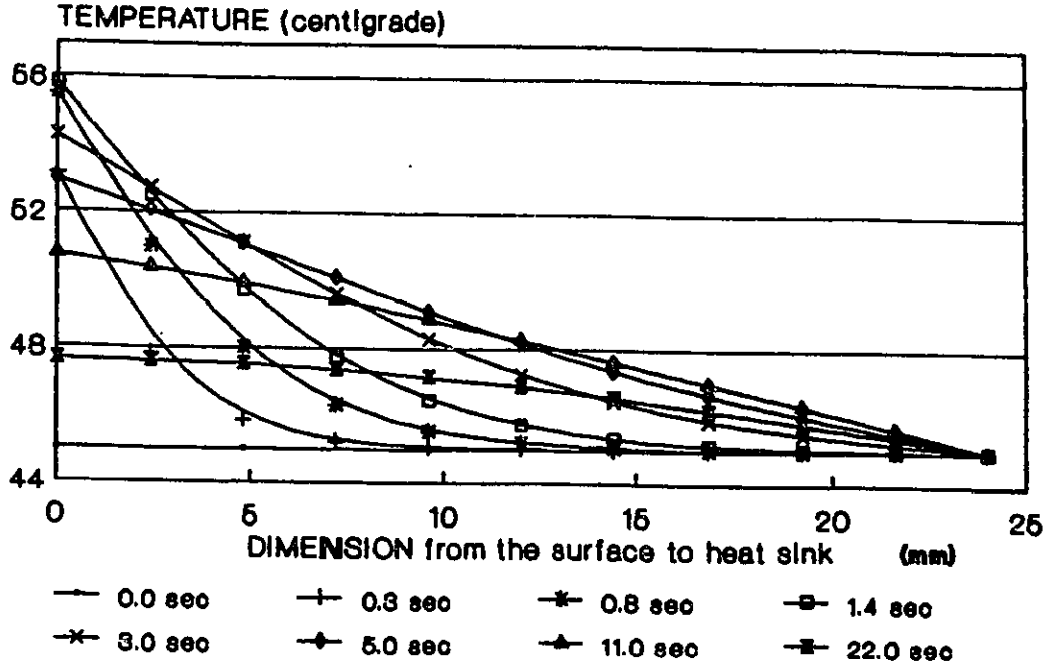

Figure A.I.2 Mold temperatures along Grid #1 at various times during the 15th cycle.

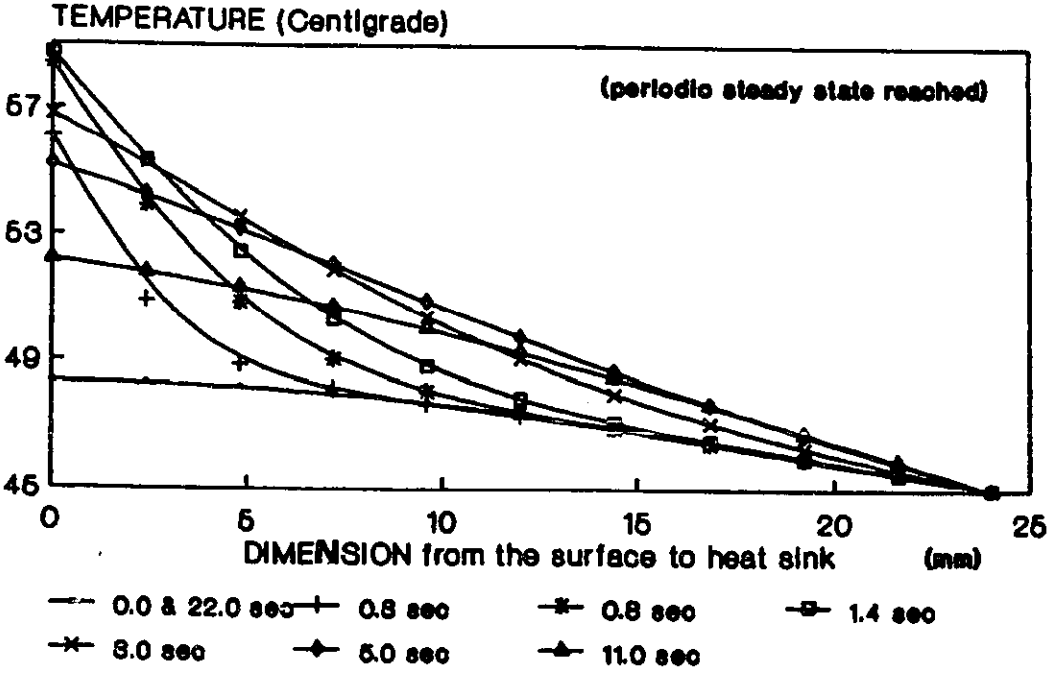

Figure A.I.3 Temperatures in the polymer along Grid #1 at various times during the first cycle.

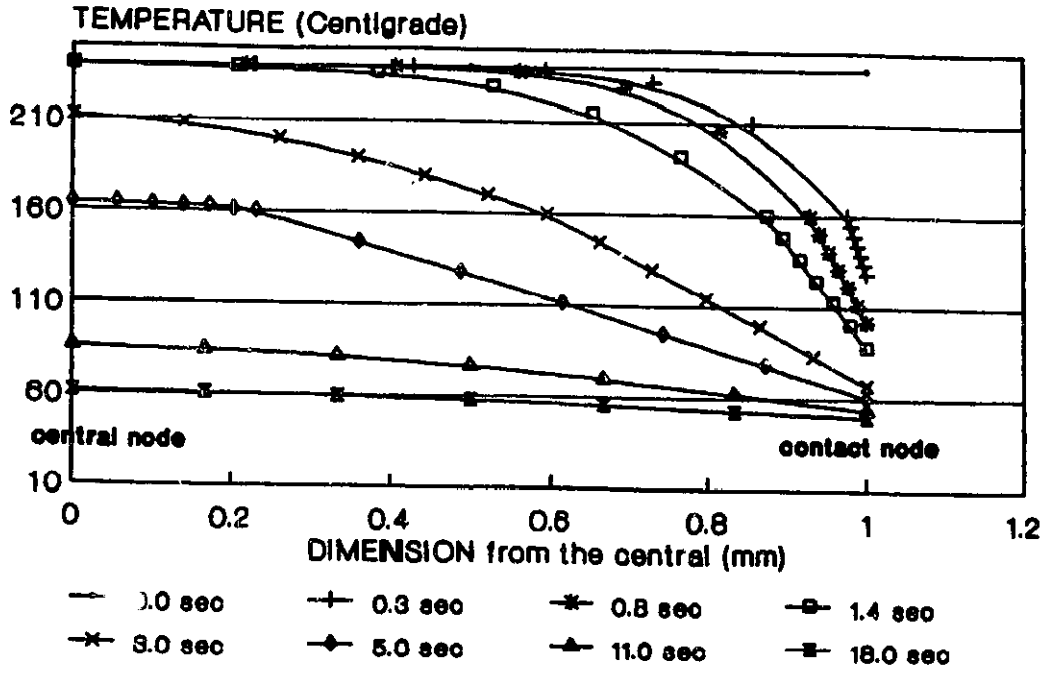

Figure A.I.4 Temperatures in the polymer along Grid #1 at various times during the 15th cycle.

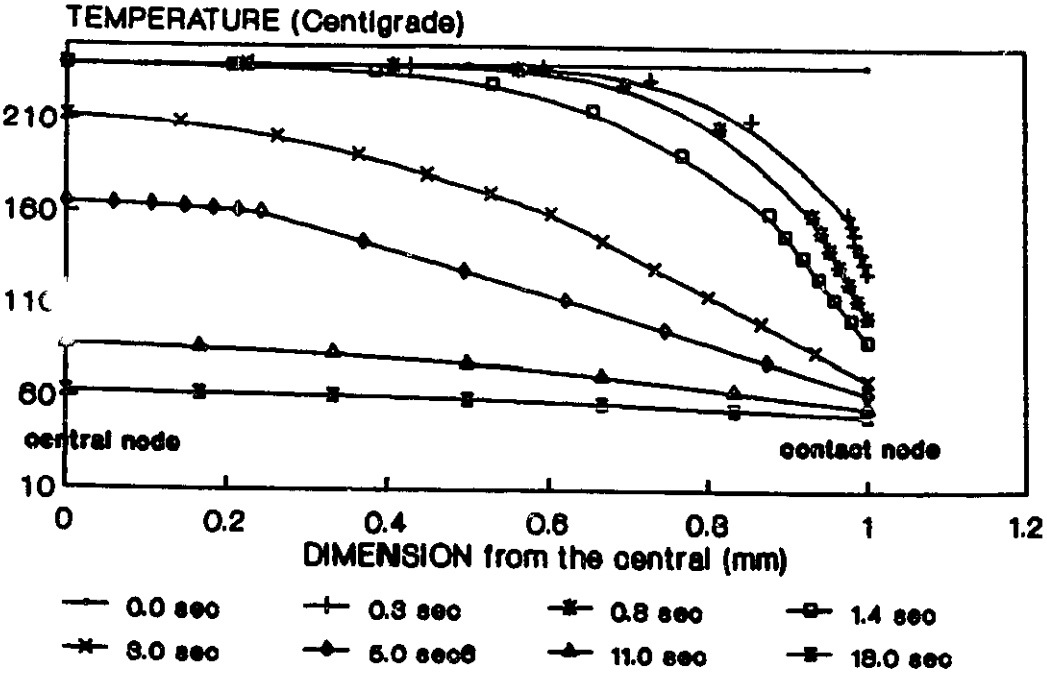

Figure A.I.5 Mold temperatures along Grid #12 at various times during the first cycle.

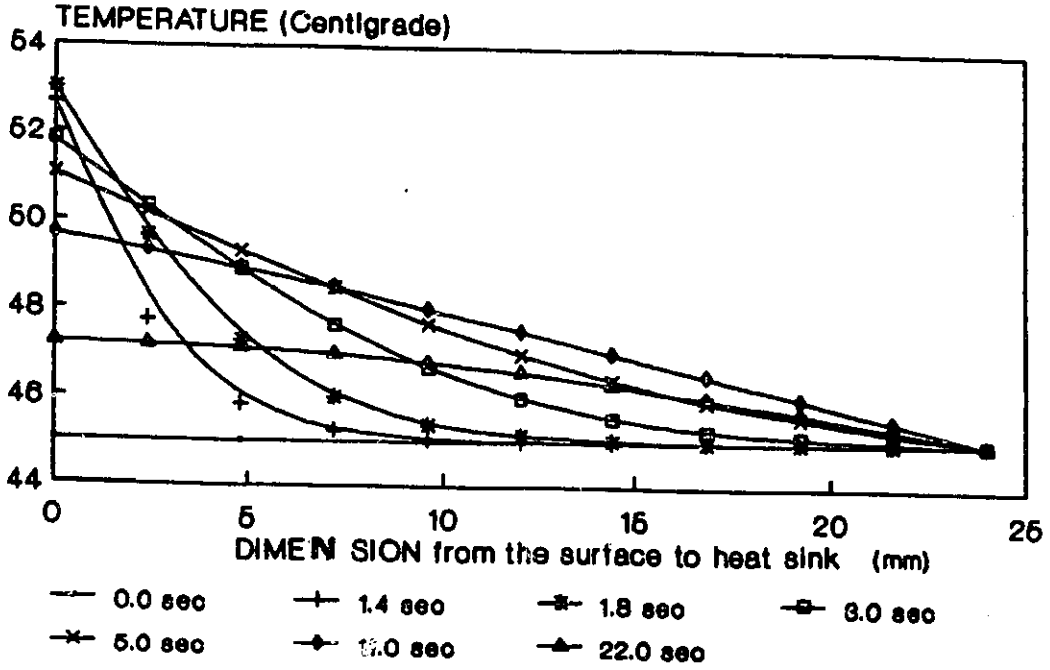

Figure A.I.6 Mold temperatures along Grid #12 at various times during the 15th cycle.

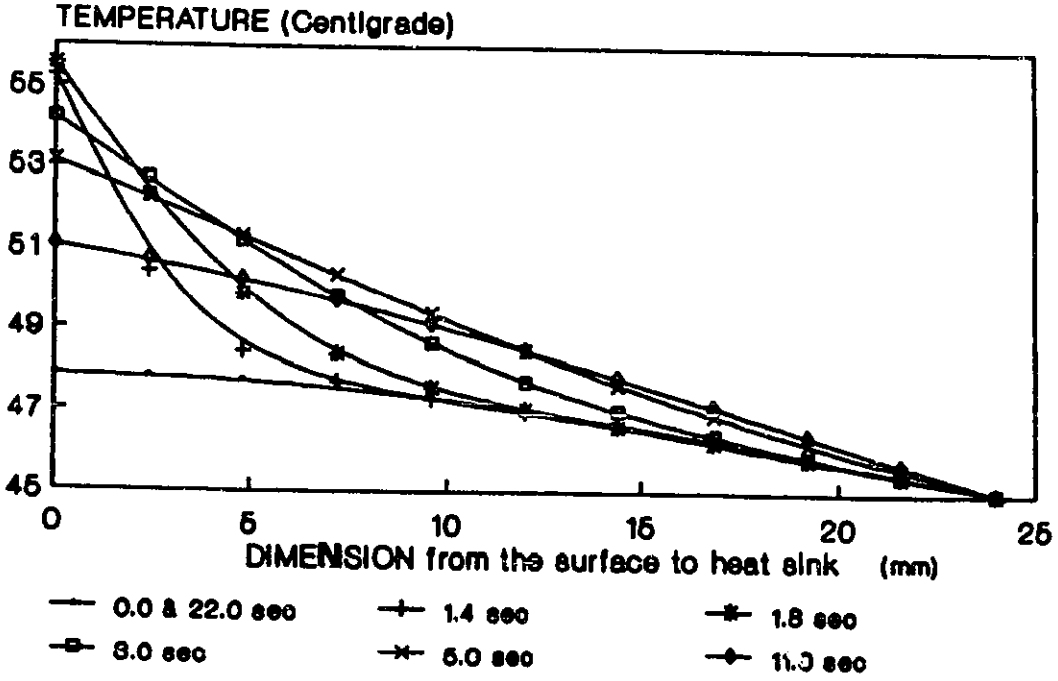

Figure A.I.7 Temperatures in the polymer along Grid #12 at various times during the first cycle.

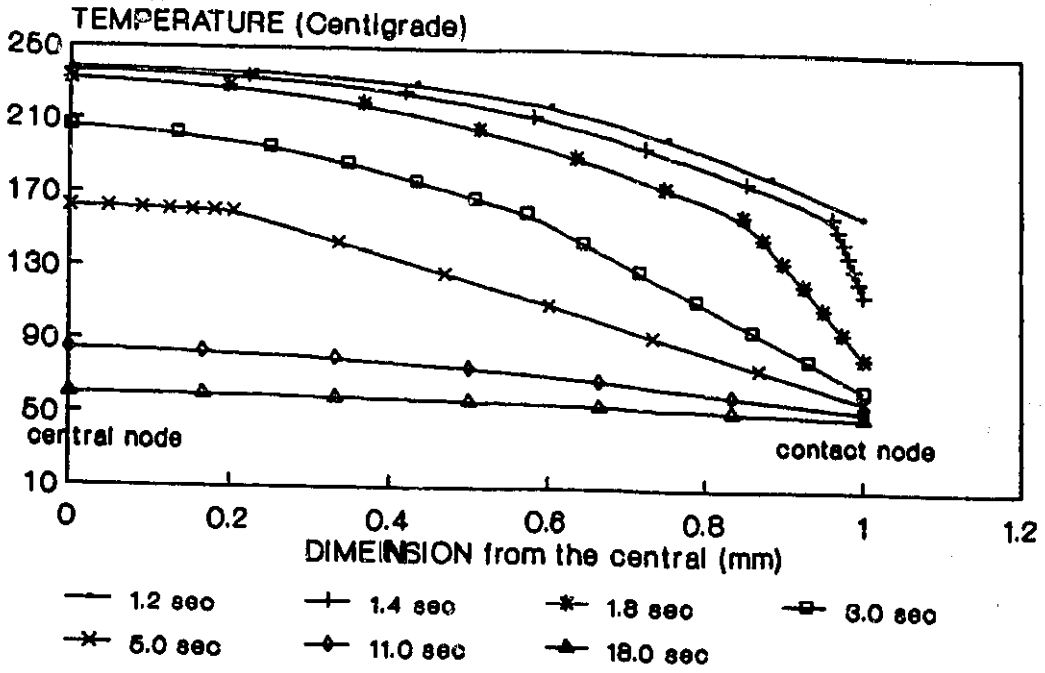

Figure A.I.8 Temperatures in the polymer along Grid #12 at various times during the 15th cycle.

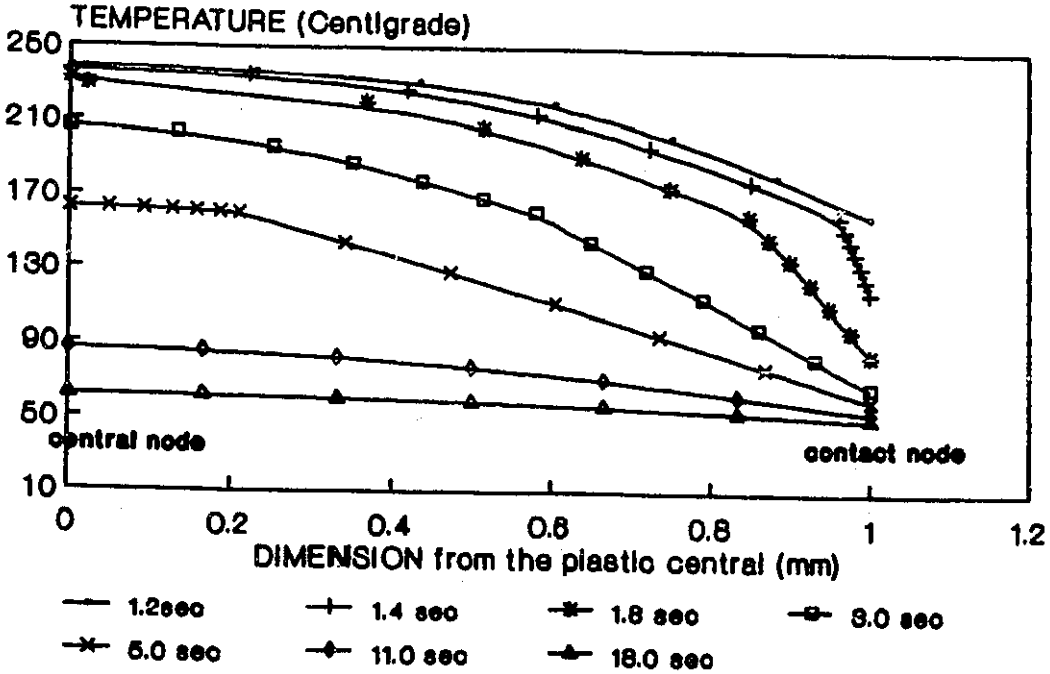

Figure A.II.1 Variation of the temperature distribution in the mold along the contact surface at various times during the first cycle (thickness of the part=2*1 mm)

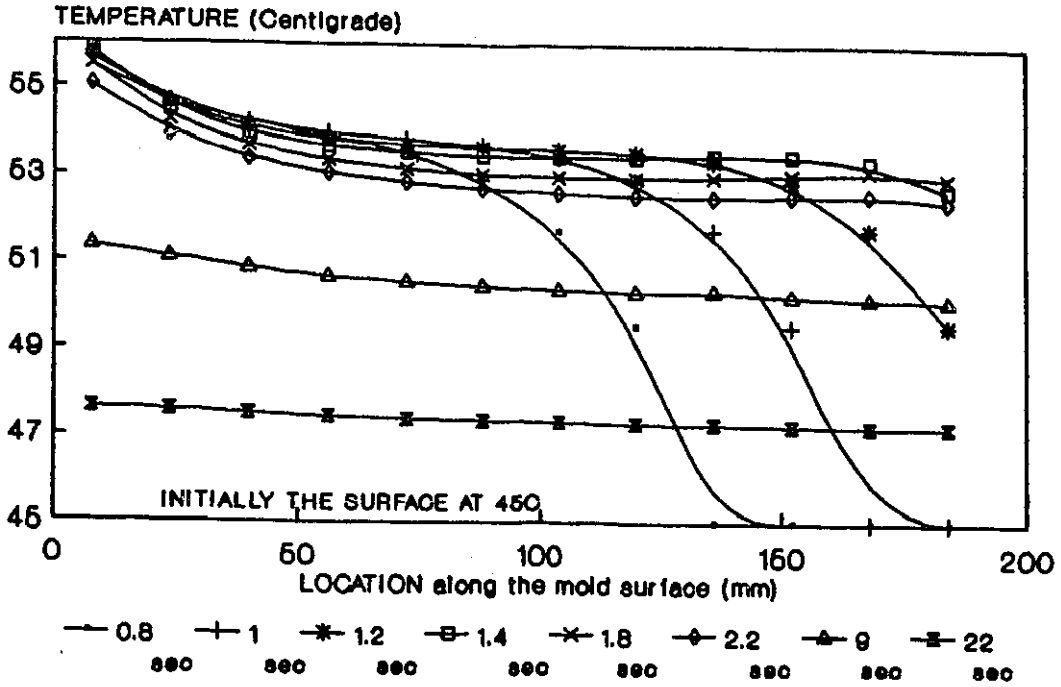

Figure A.II.2 Variation of the temperature distribution in the mold along the contact surface at various times during the 15th cycle.

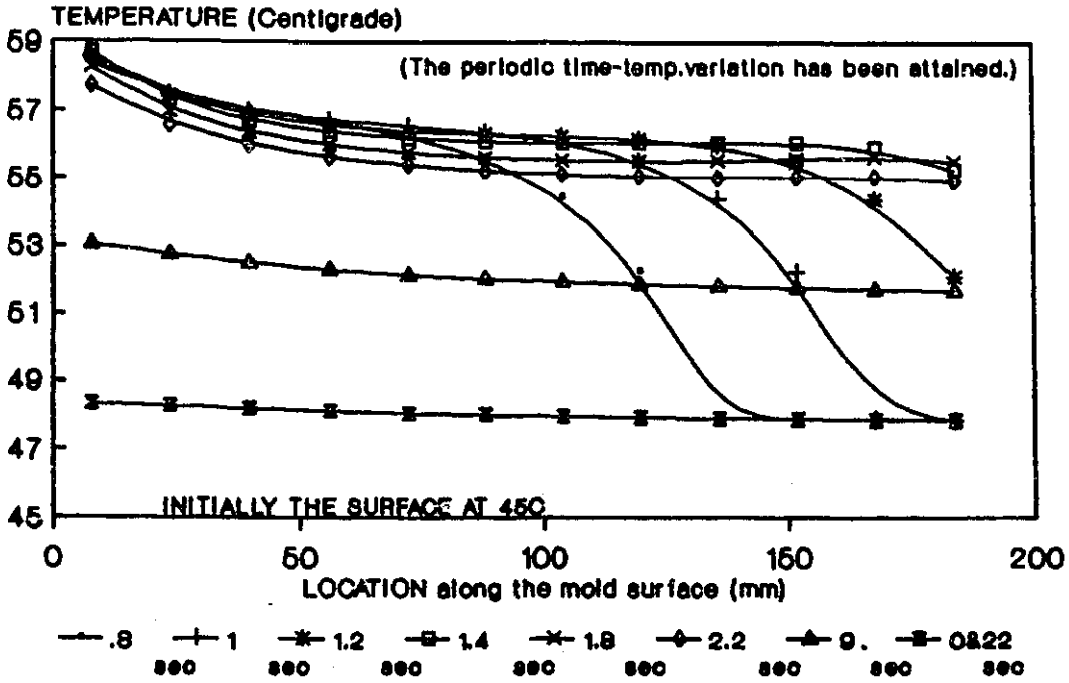

Figure A.II.3 Temperature distribution in the polymer at the mold contact surface at various times during the first cycle (part thickness = 2*1.0 mm).

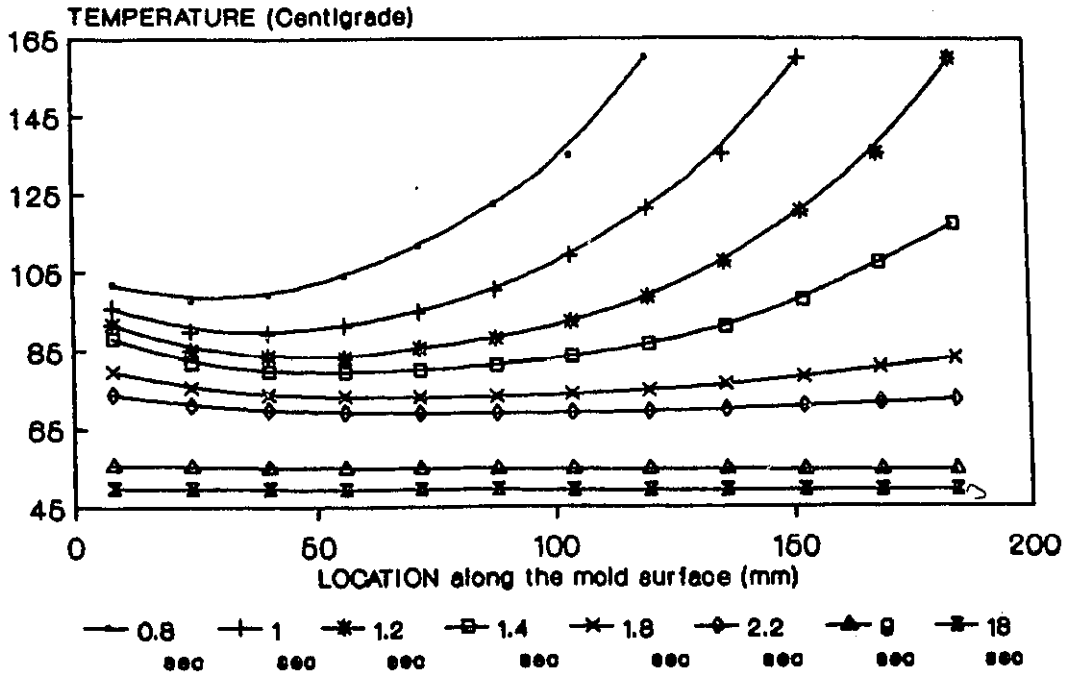

Figure A.II.4 Temperature distribution in the polymer at the mold contact surface at various times during the 15th cycle.

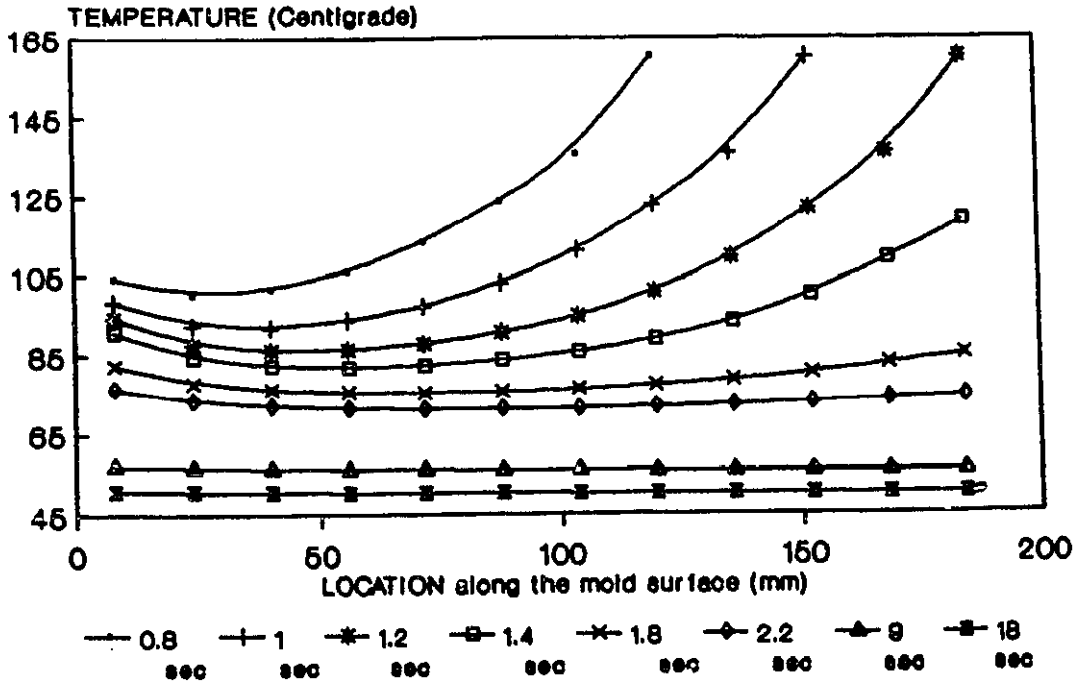

Figure A.III.1 The discontinuous temperature gap on Grid #1 at the mold/polymer interface during the first and 15th cycles.

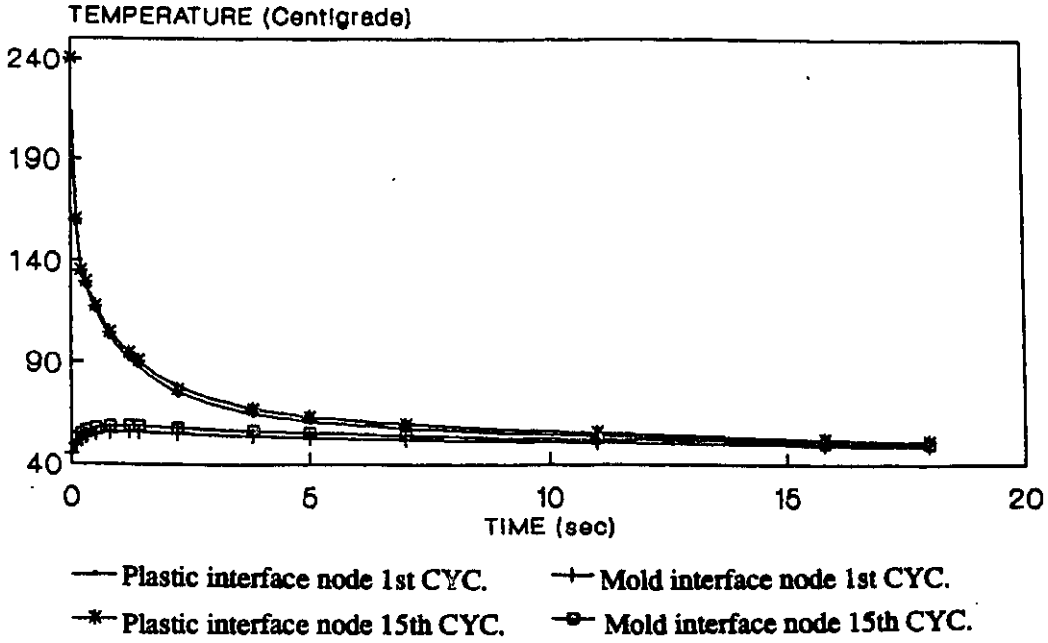

Figure A.III.2 The thermal response of the mold contact node on grid #1 for various molding cycles.

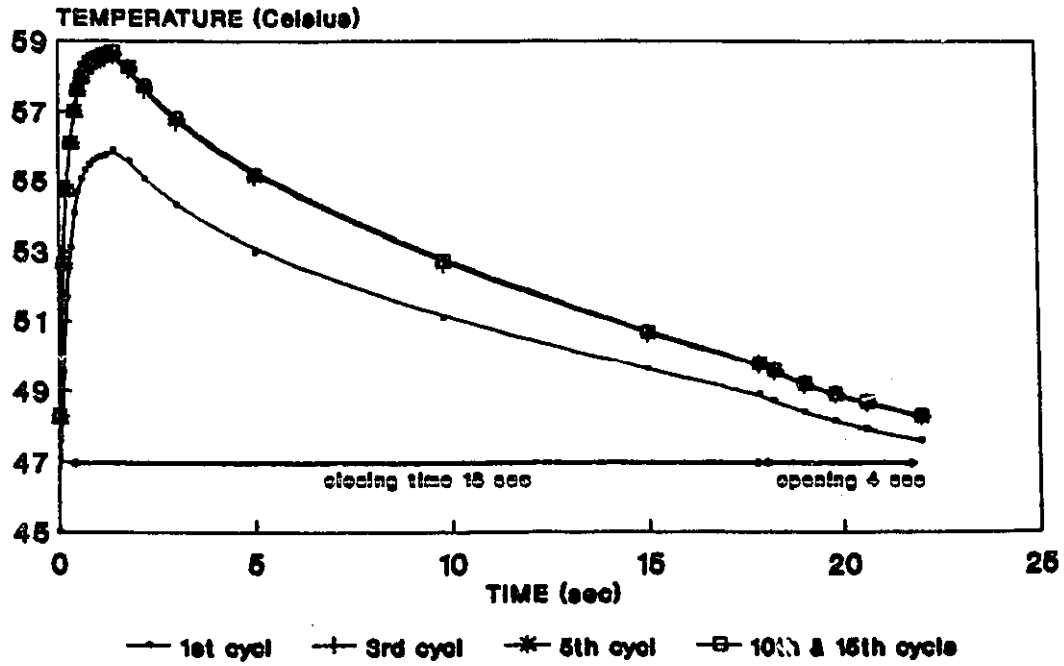

Figure A.III.3 The discontinuous temperature gap on Grid #12 at the mold/polymer interface during the first and 15th cycles.

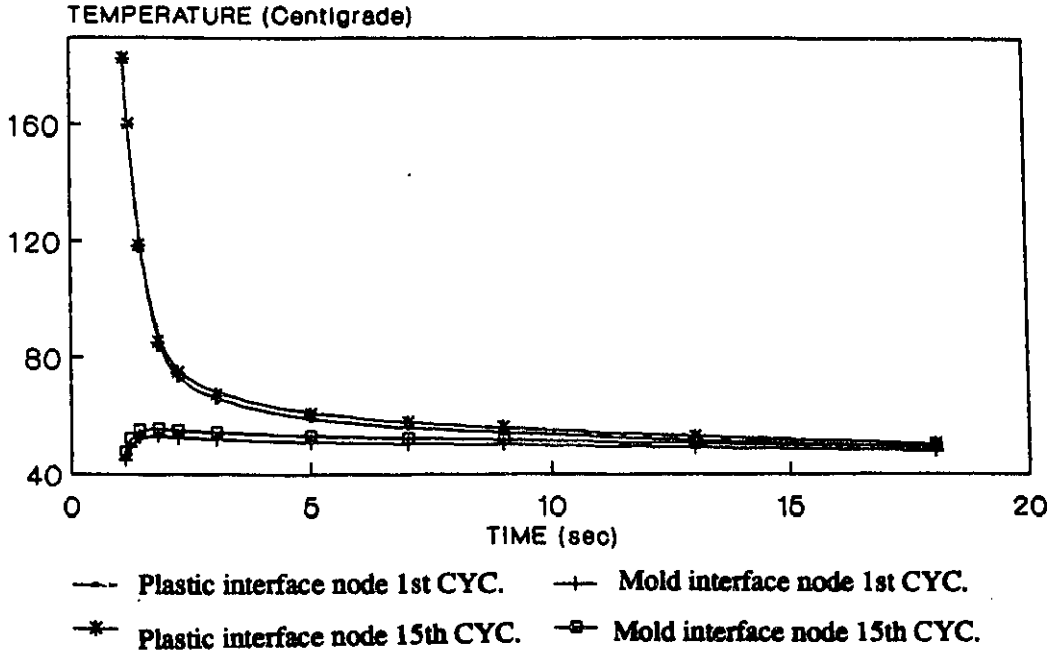

Figure A.III.4 The thermal response of the mold contact node on grid #12 for various molding cycles.

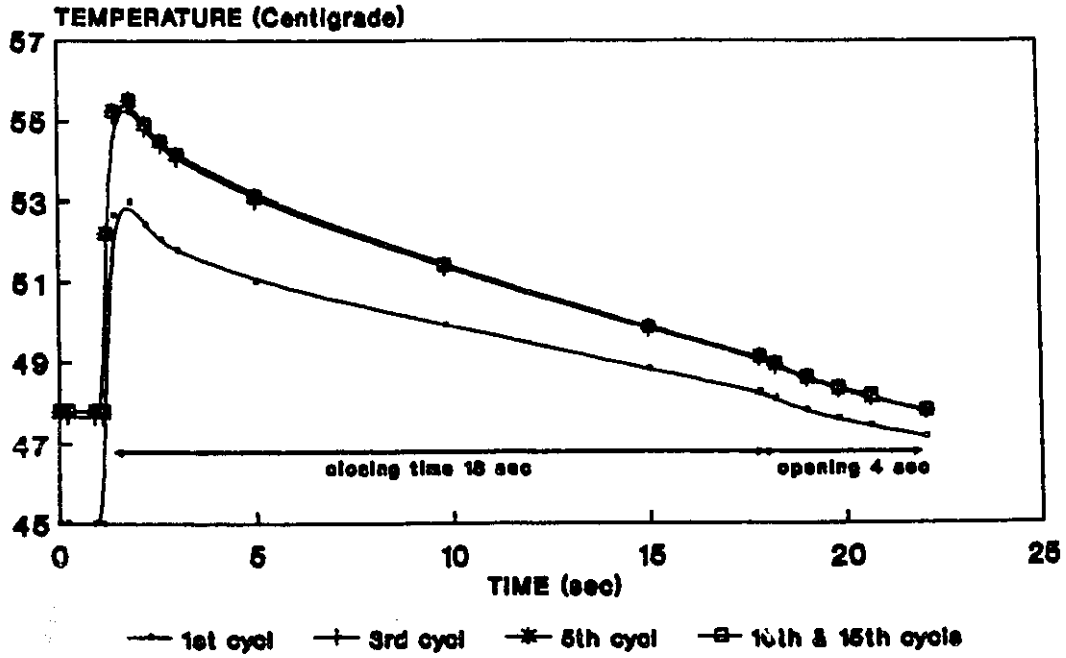

Figure A.IV Pressure gradients and the thickness of the frozen layers at the moment when the mold has just been filled on the first and fifteenth cycles.

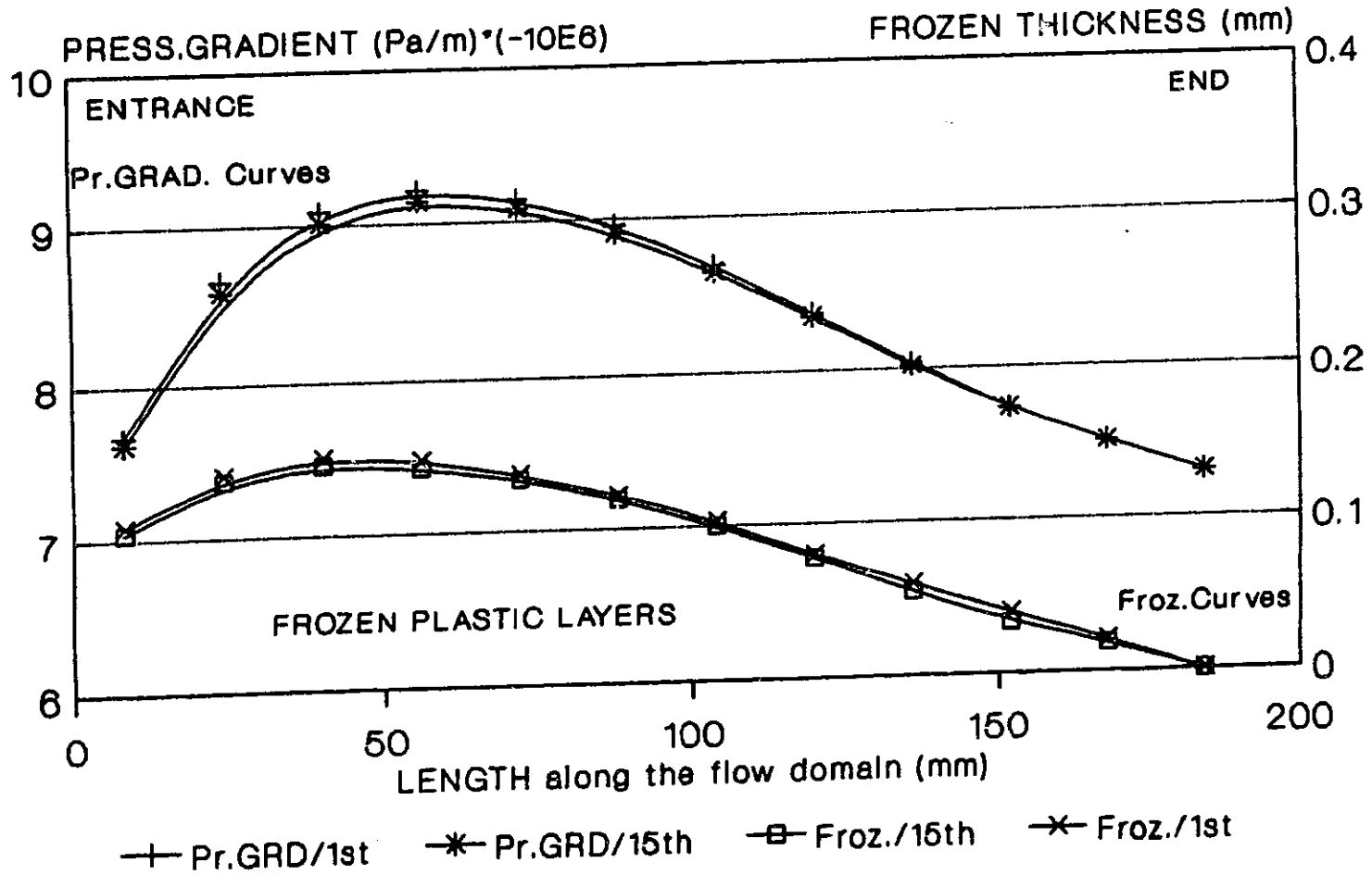

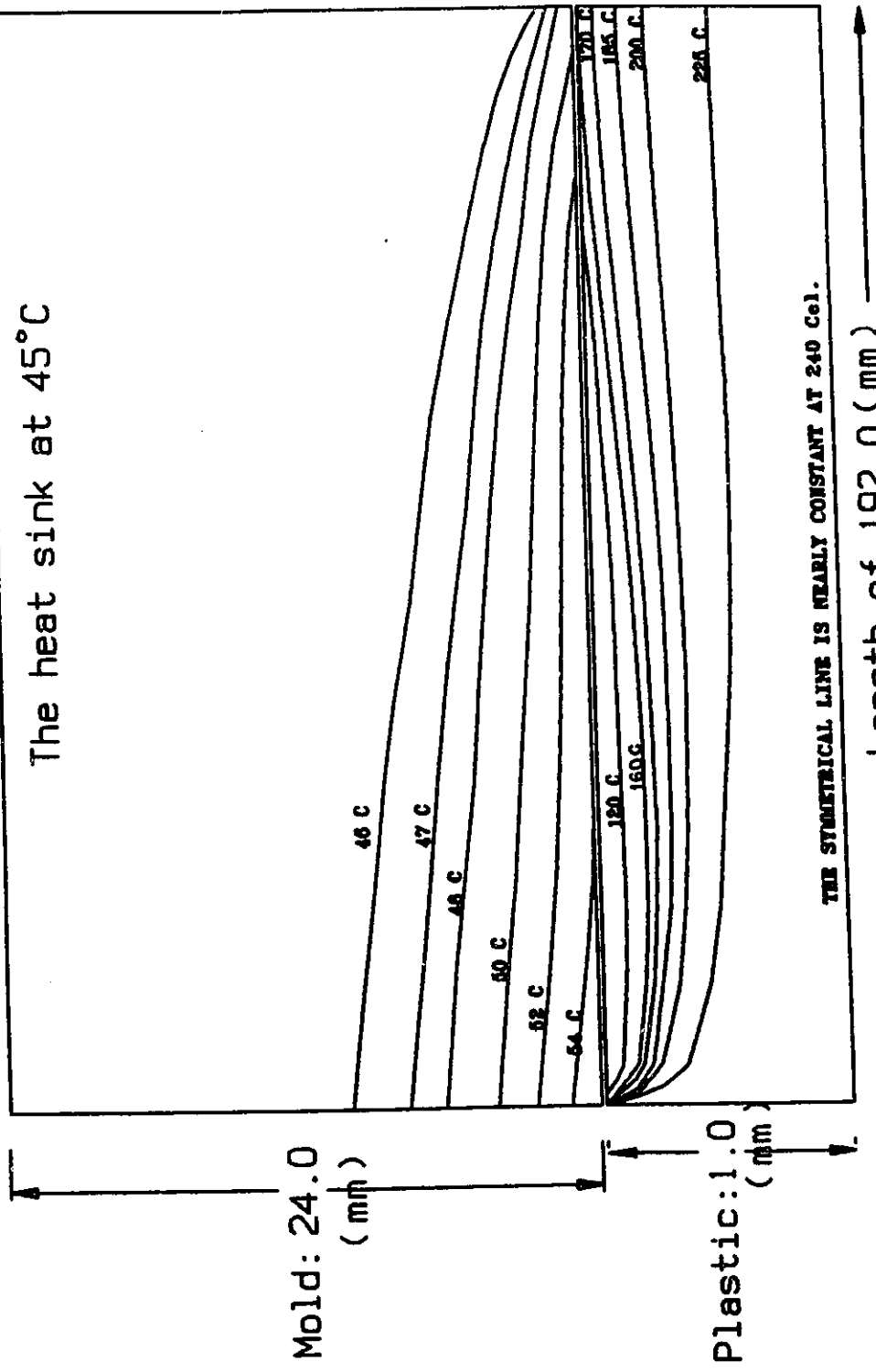

Figure A V.1 The isothermal profiles in the mold and the plastic at the moment when the mold has just been filled on the first cycle. (Injection speed = 0.16 m/sec)

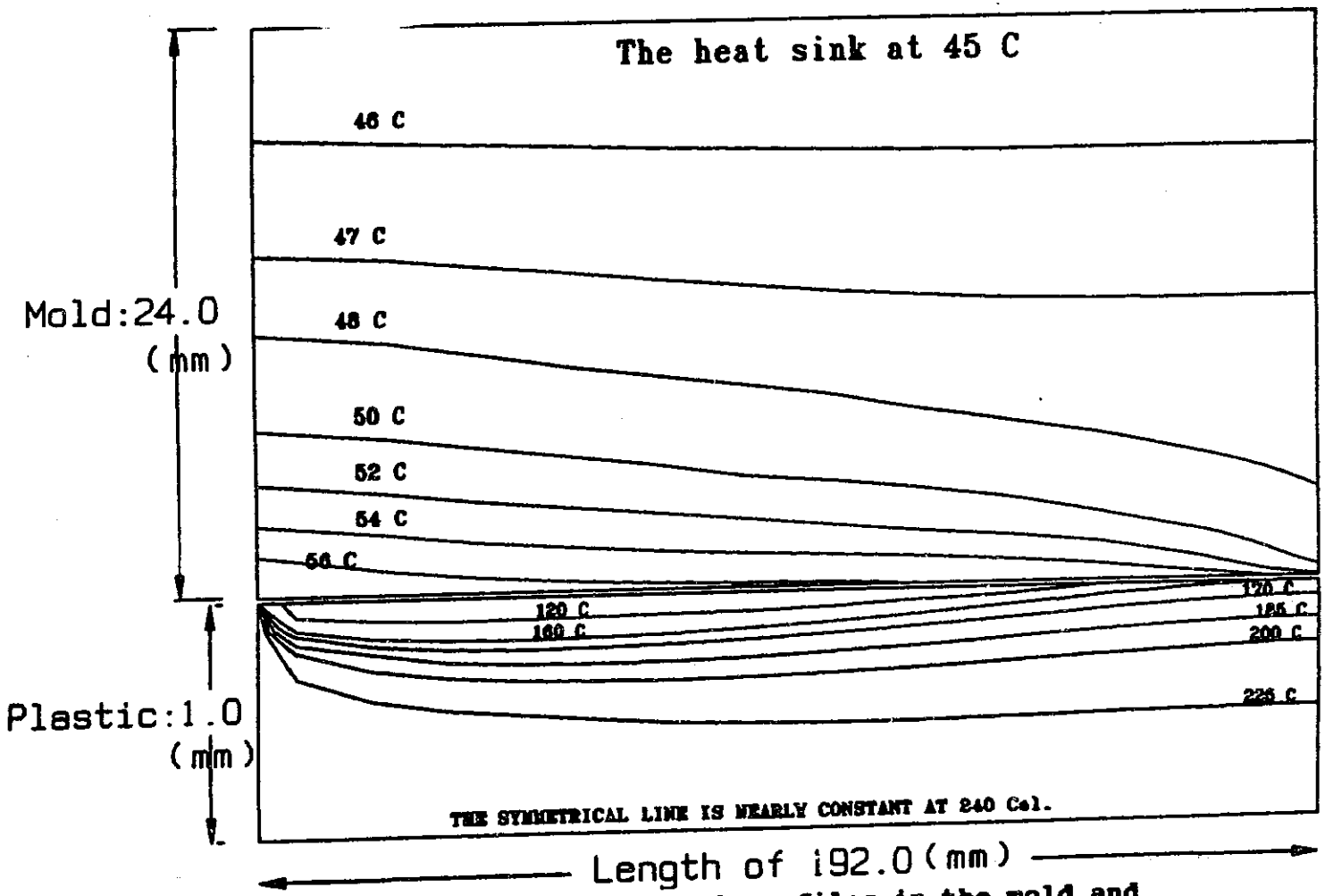

Figure A V.2 The isothermal profiles in the mold and the plastic at the moment when the mold has just been filled on the 15th cycle. (Injection speed = 0.16 m/sec)

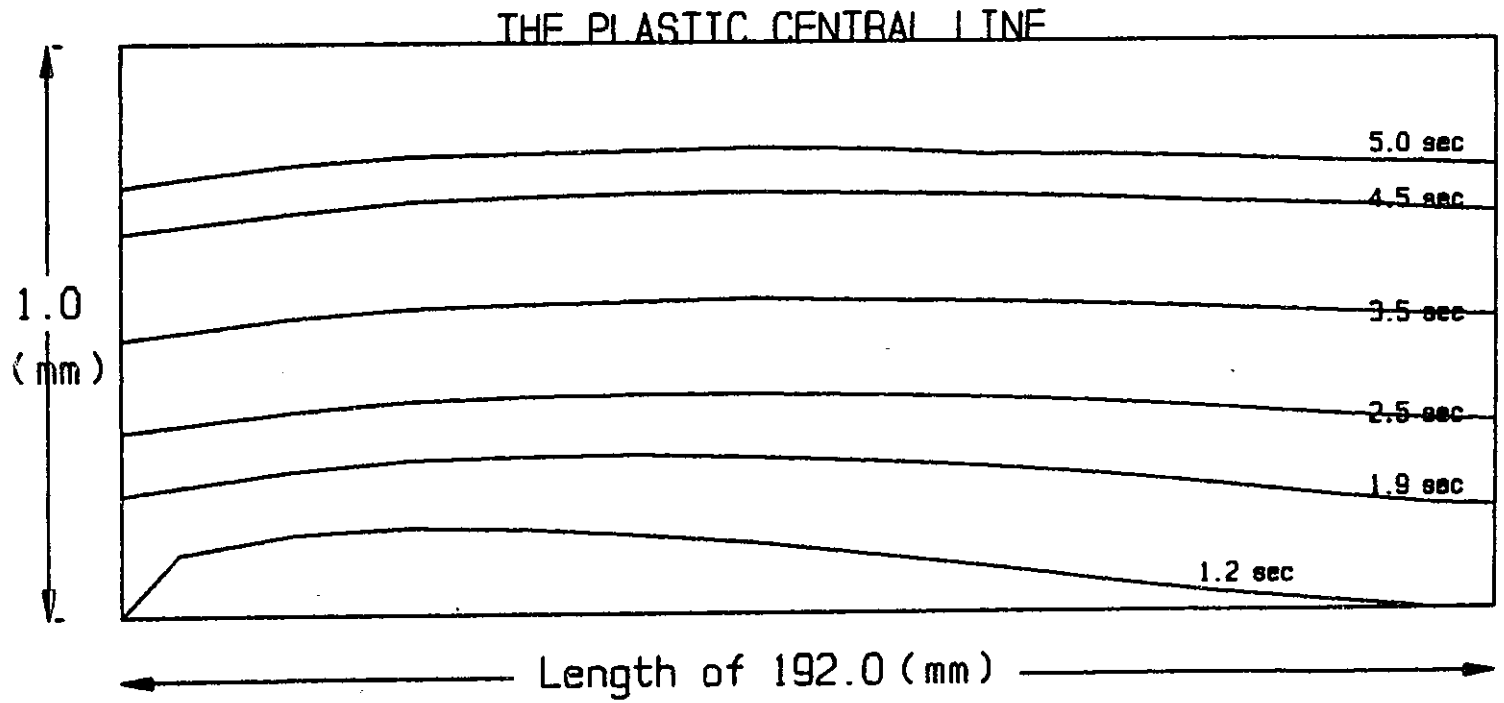

Figure A.VI.1 The growth position of the solid plastic layer at various times during the first cycle.(Injection speed=0.16 m/sec: Hr=2500 W/m.m.K)

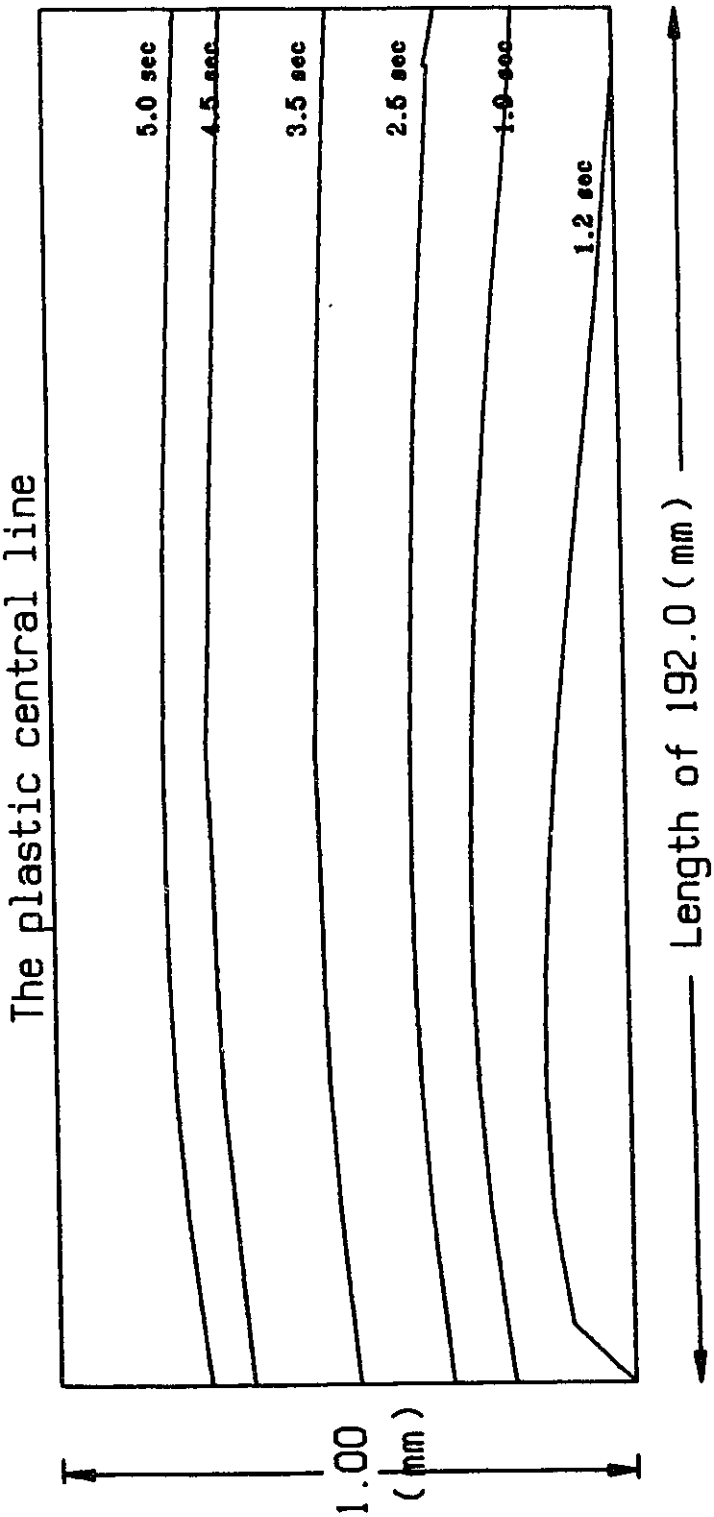

Figure A.VI.2 The growth position of the solid plastic layer at various times during the 15th cycle.(Injection speed=0.16 m/sec: Hr=2500 W/m.m.K)

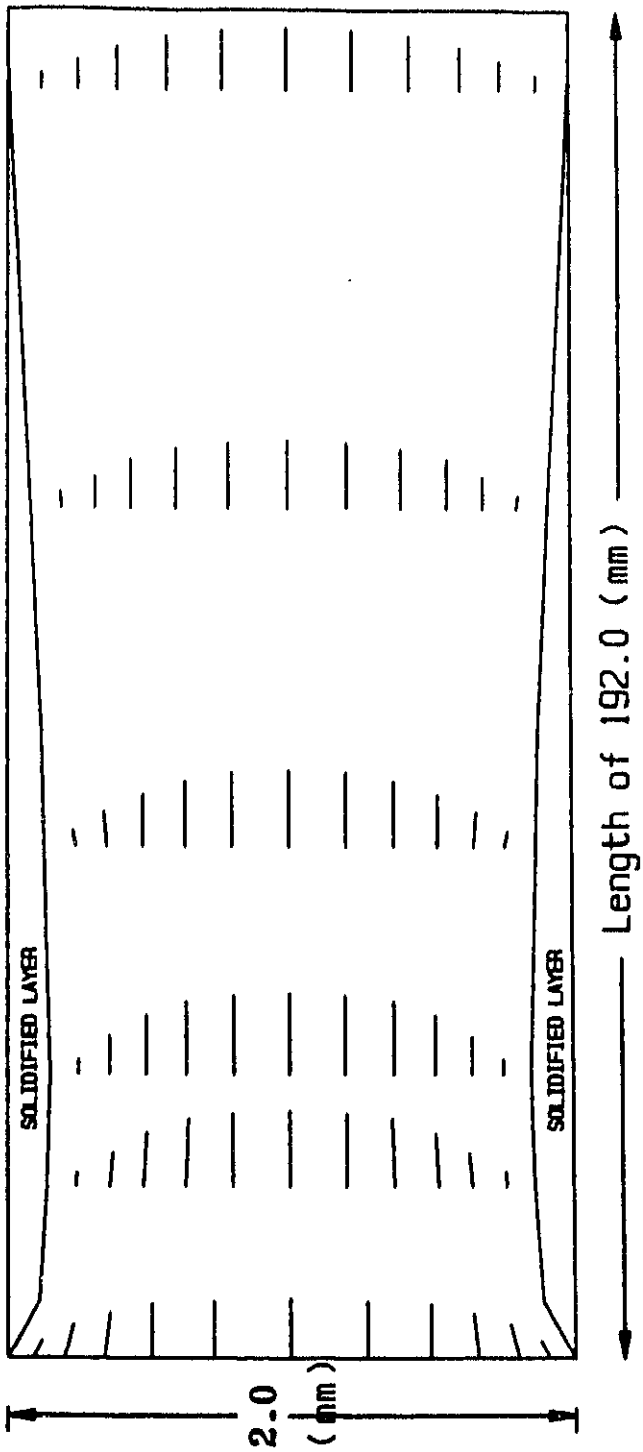

Figure A.VII.1 The velocity profile, indicated by the length and direction of the short lines, and the thickness of the solid plastic layer at the moment the mold is just filled on the first cycle.
(Injection speed 0.16 m/sec)

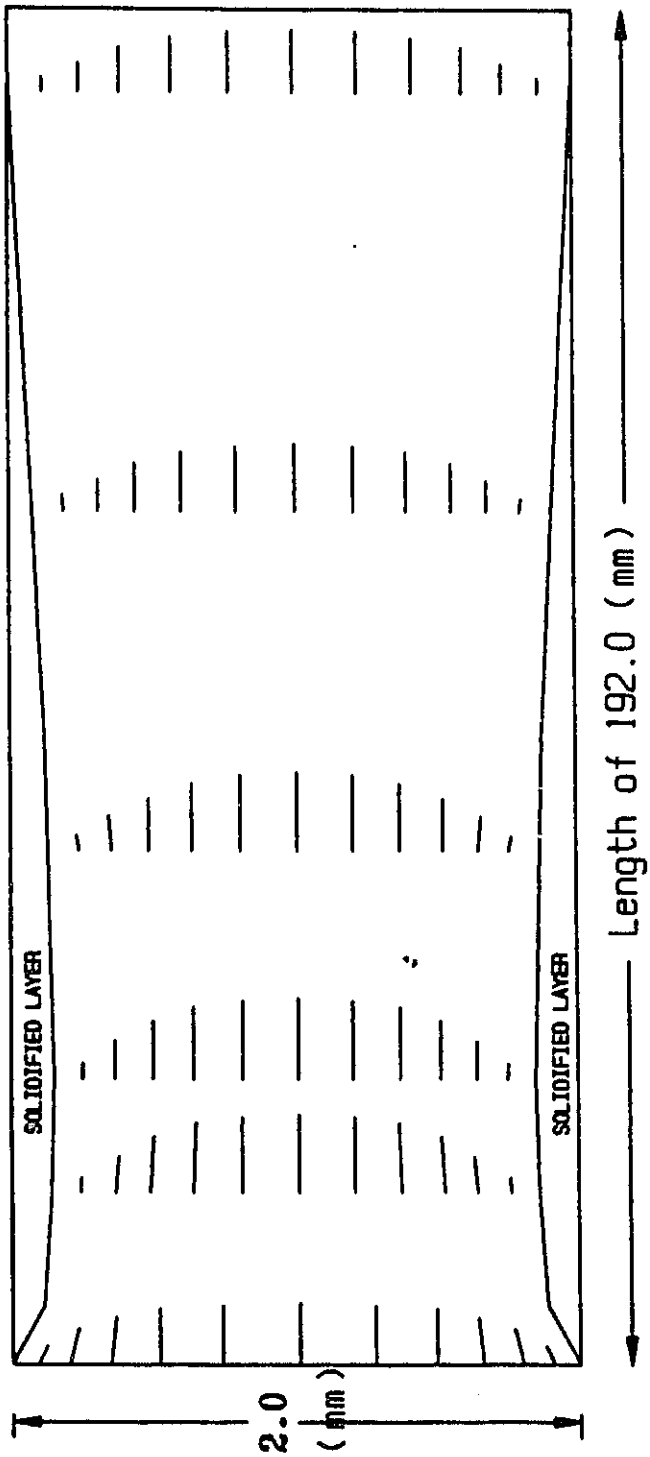

Figure A.VII.2 The velocity profile, indicated by the length and direction of the short lines, and the thickness of the solid plastic layer at the moment the mold is just filled on the 15th cycle. (Injection speed 0.16 m/sec)

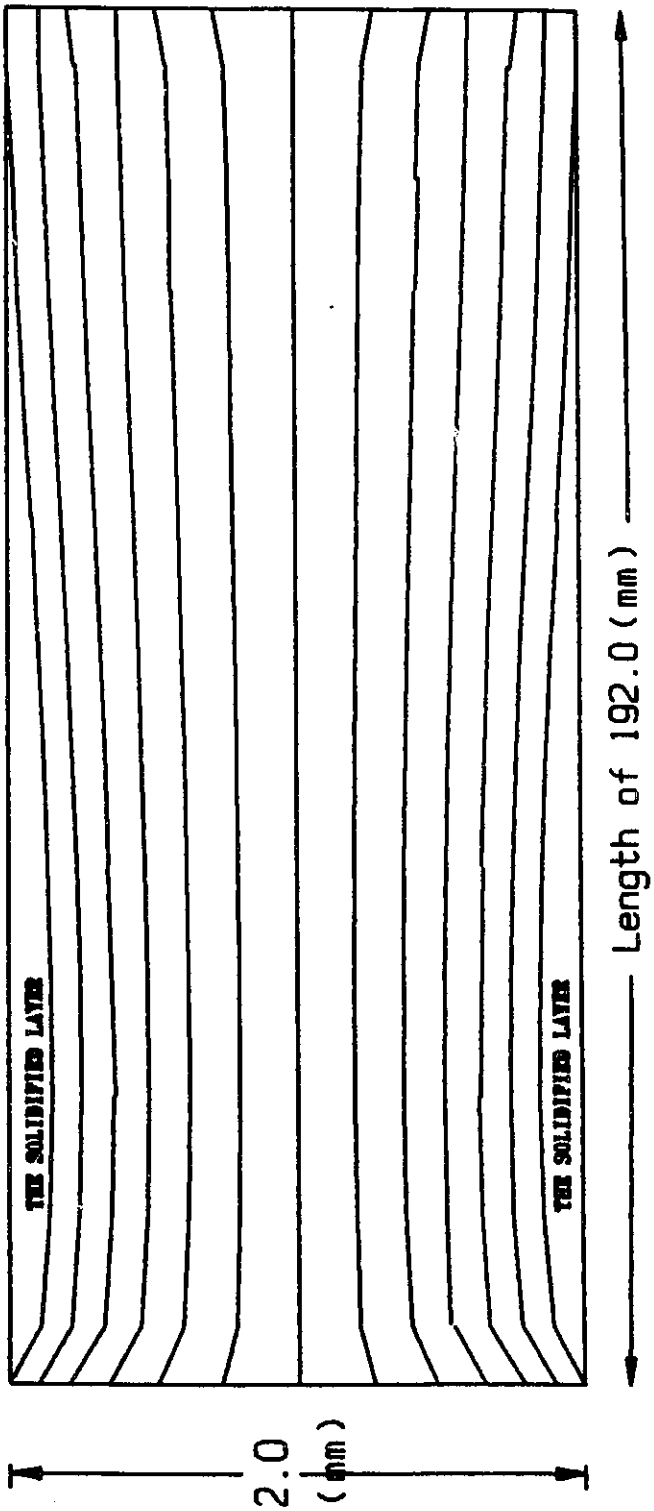

Figure A.VII.3 The streamline profile when the mold has just been filled on the first cycle. (Injection speed=0.16 m/sec)

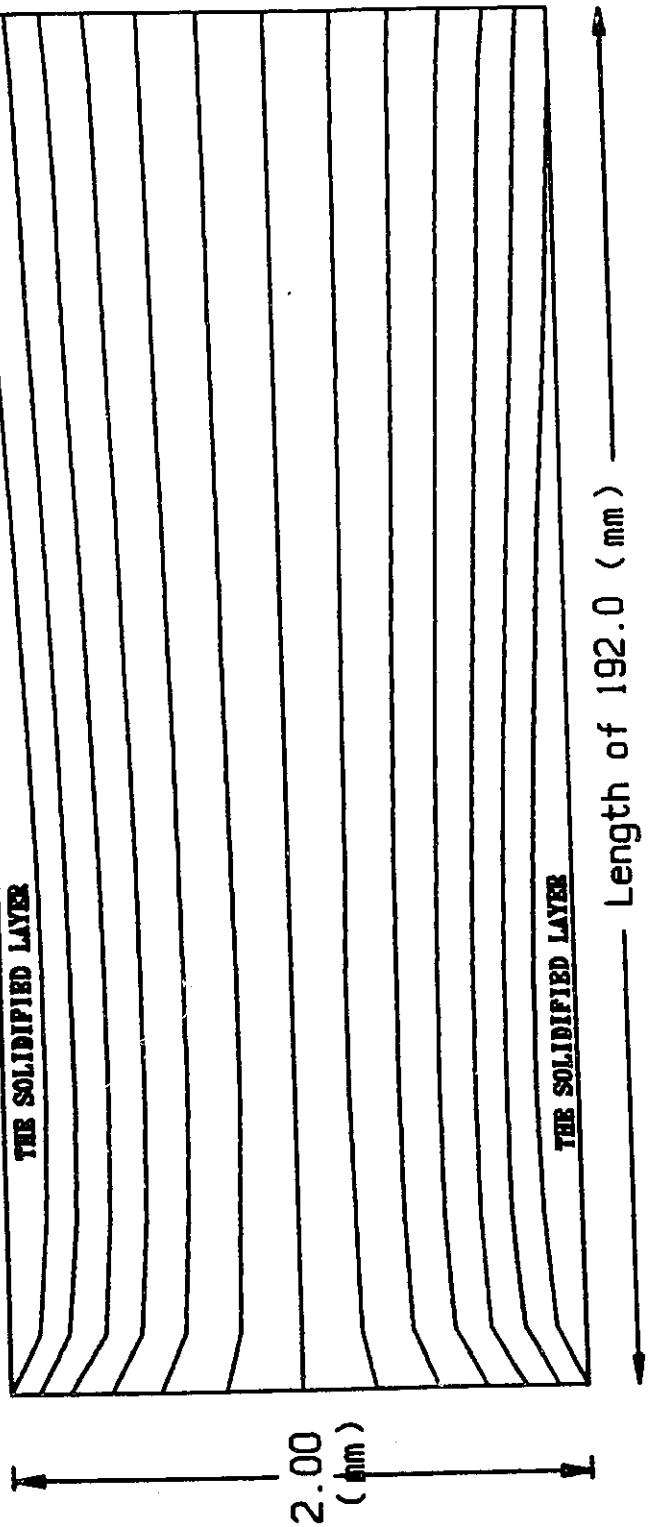

Figure A.VII.4 The streamline profile when the mold has just been filled on the 15th cycle. (Injection speed=0.16 m/sec)

4.2.2 GROUP B

The Effect of Varying the Mean Injection Velocity (V)

(The varied inputs are from Data Table 2)

(These are the outputs of the first cycle)

Note that a change in the injection velocity with a fixed grid size also requires the time step size to vary. The grid size = (injection velocity)(Time increment). If the time step is held constant then the grid size must change.

Figures B.I.1 to 2 : The thermal response of the mold contact nodes on grids 1 and 12 for various injection speeds 105

Figures B.II.1 to 4 : The thermal response of the mold contact nodes 8mm from the entrance and 8mm from the cavity end with different number of nodes per grid, different time step values 106

Figures B.III.1 and 2 : The thermal response of the mold contact nodes 8mm from the entrance and 8mm from the cavity end for different time step values at a constant injection speed 108

Figures B.IV.1 to 2 : The thermal response of the mold contact nodes on grids 1 and 12 for different numbers of nodes per grid at constant injection speed and time increment 109

Figures B.V : The pressure gradients and frozen layer thicknesses for different injection speeds and time increments at the moment when the mold is just filled 110

Figures B.VI.1 to 2 : The maximum shear rates lines along the

flow direction when the mold is just filled 111

Figures B.VII.1 to 2 : The isothermal profiles in the plastic and the mold when the cavity is just filled for different injection velocities and time increments 112

Figure B.I.1 The thermal response of the mold contact node on grid #1 for various injection speeds (mold cycle #1).

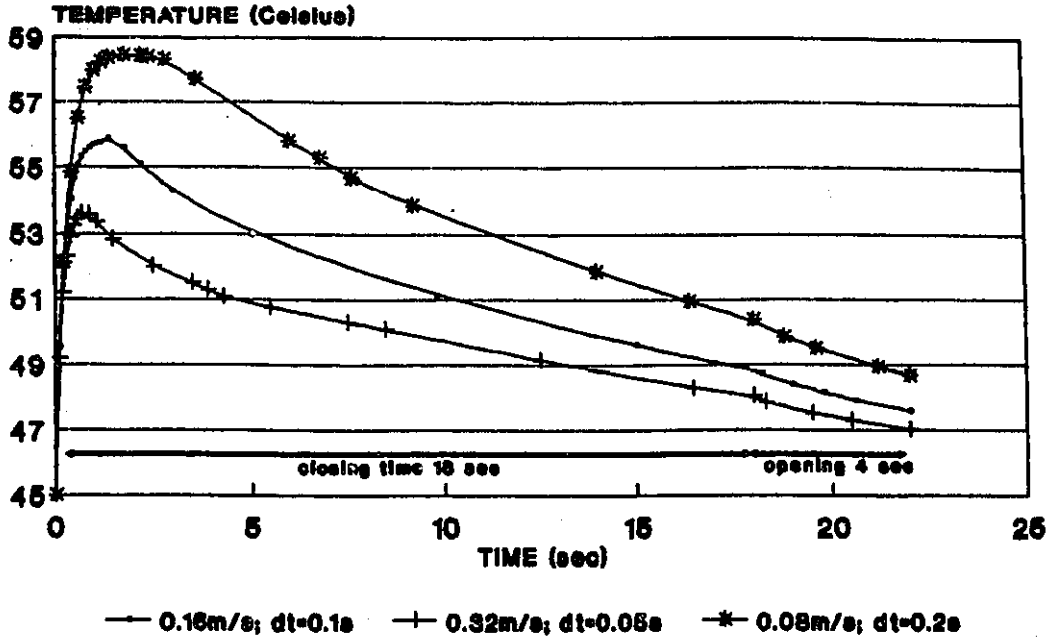

Figure B.I.2 The thermal response of the mold contact node on grid #12 for various injection speeds (mold cycle #1).

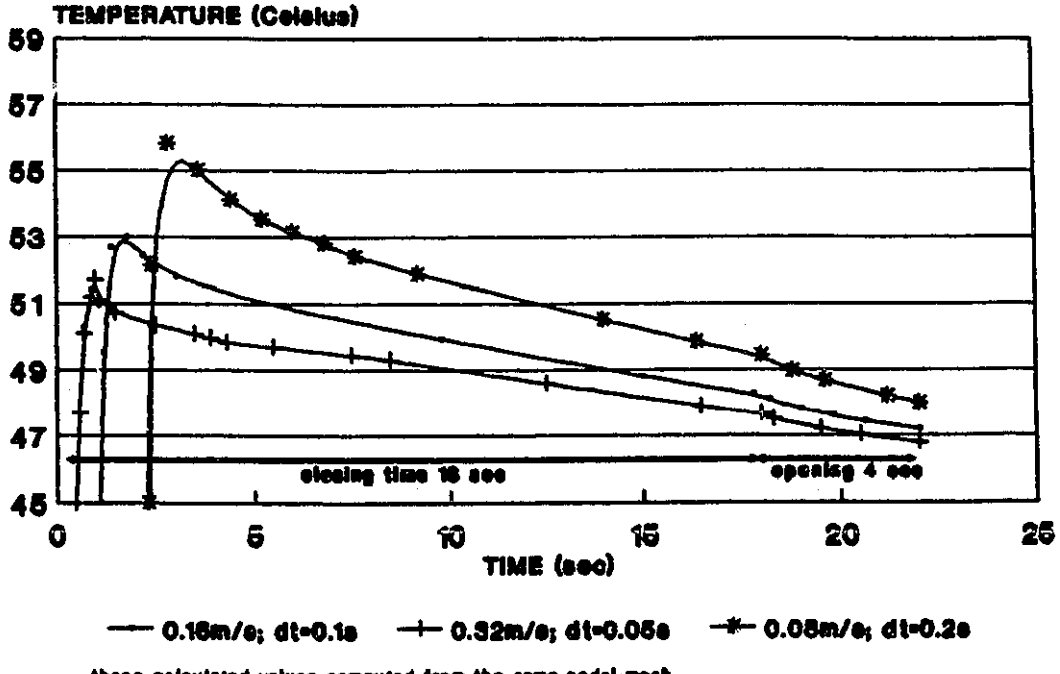

Figure B.II.1 The thermal response of the mold contact node 8mm from the entrance for various injection speeds and time step values.

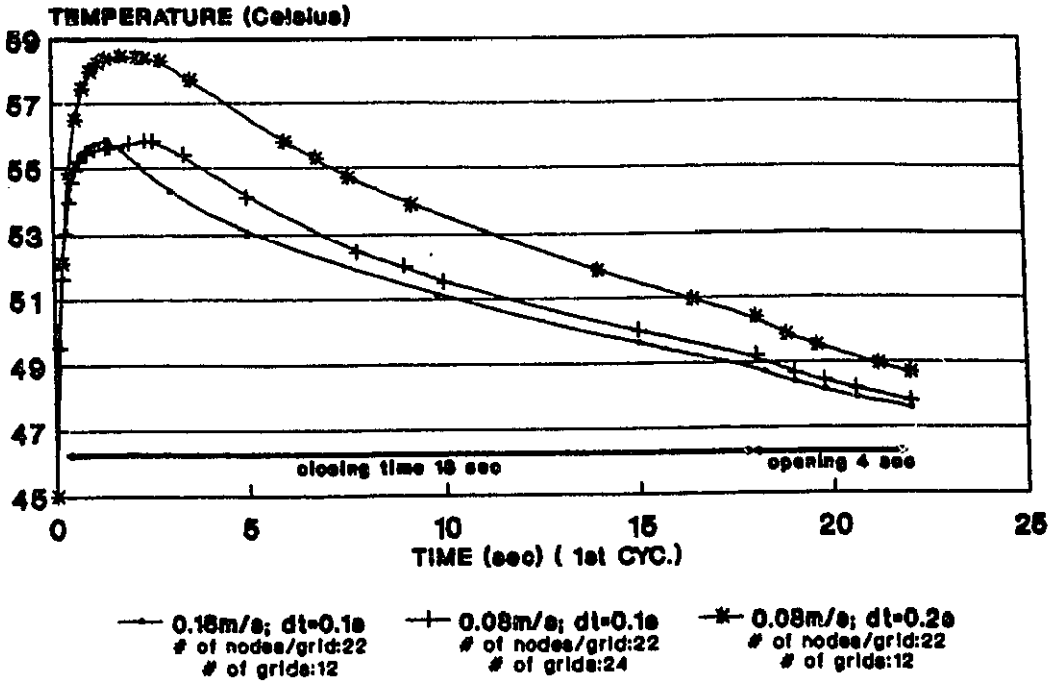

Figure B.II.2 The thermal response of the mold contact node 8mm from the entrance for various number of nodes per grid and different time step values.

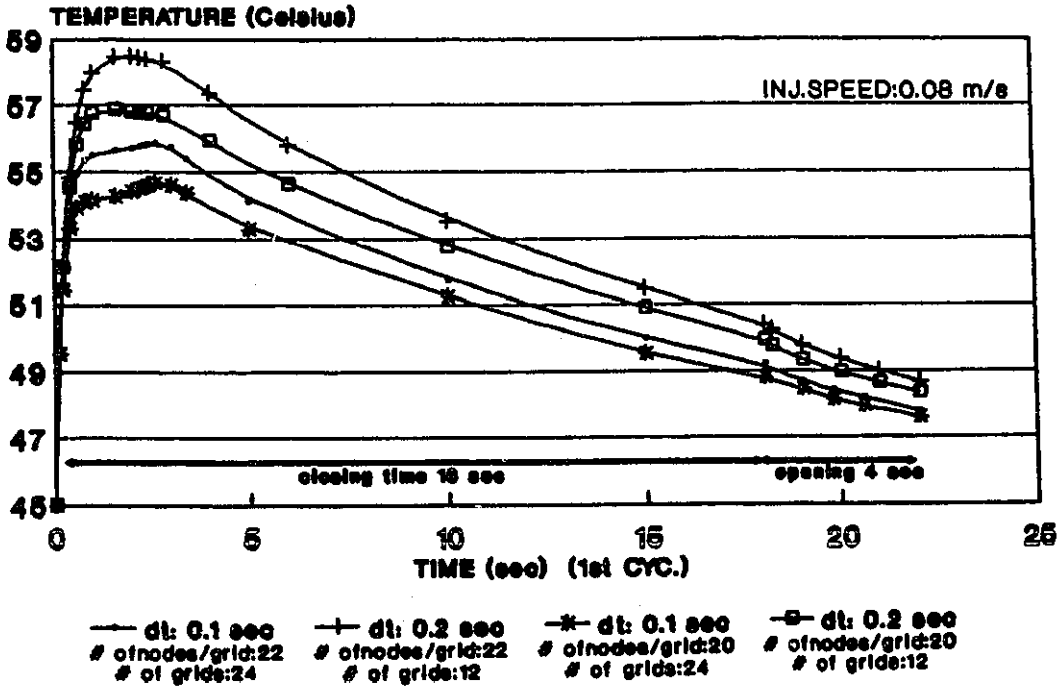

Figure B.II.3 The thermal response of the mold contact node 8mm from the cavity end for various injection speeds and time step values.

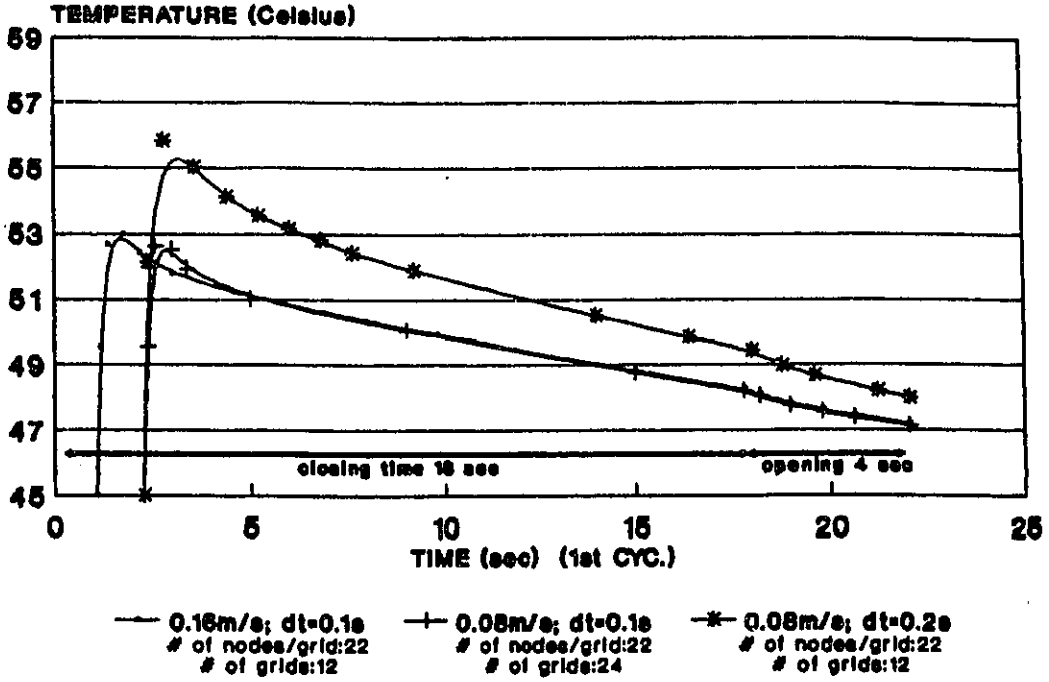

Figure B.II.4 The thermal response of the mold contact node 8mm from the cavity end for various number of nodes per grid and different time step values.

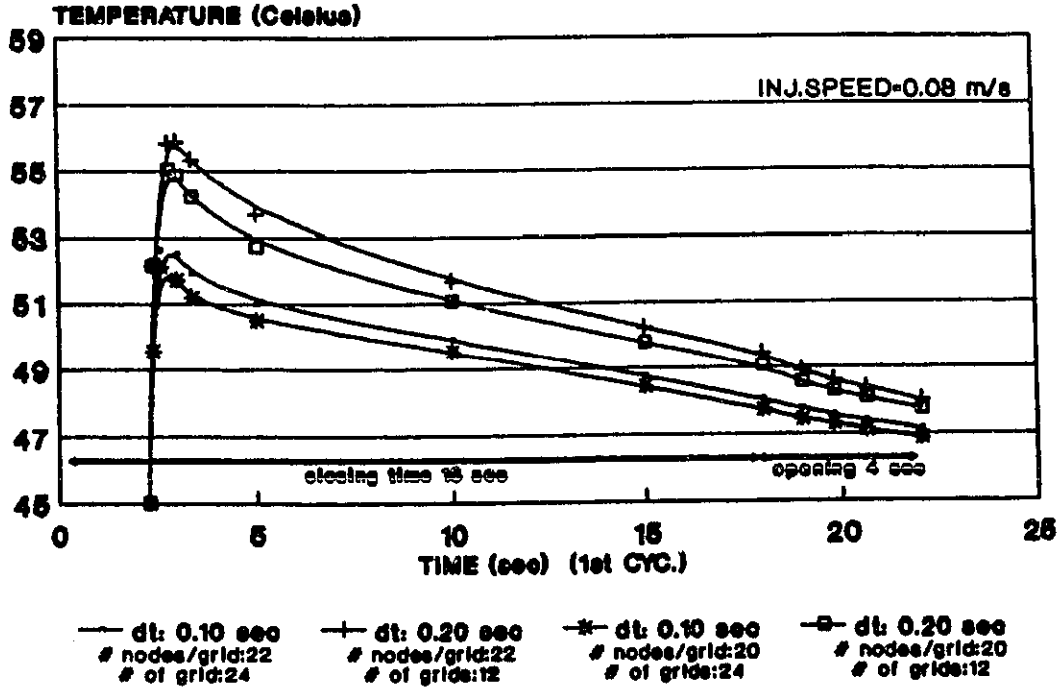

Figure B.III.1 The thermal response of the mold contact node on grid #1 for different time step values at constant injection velocity.

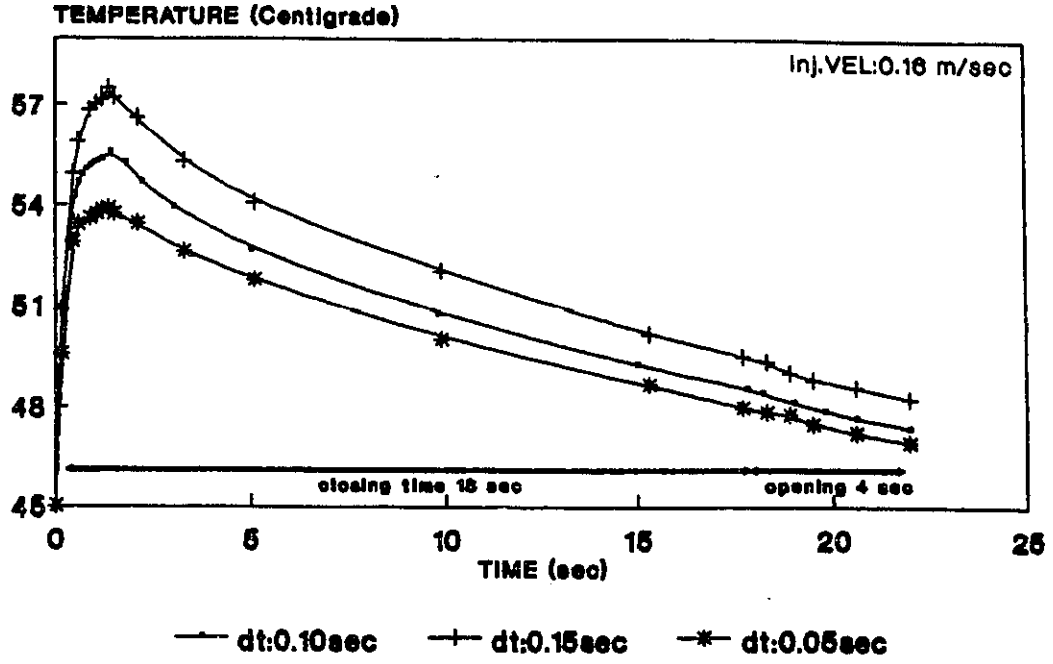

Figure B.III.2 The thermal response of the mold contact node on grid #12 for different time step values at constant injection velocity.

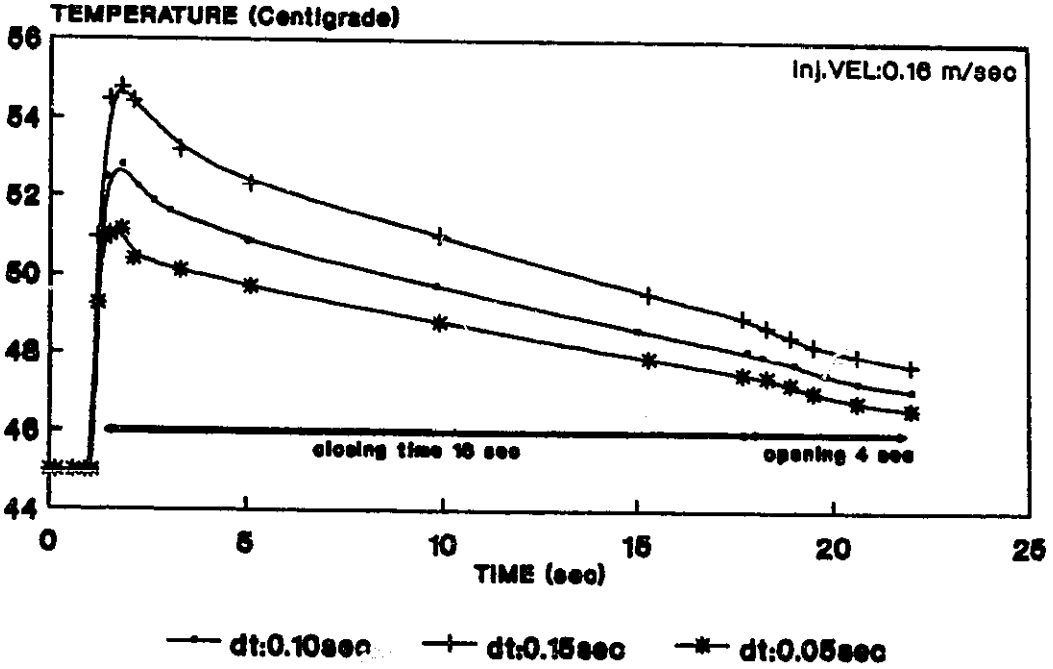

Figure B.IV.1 The thermal response of the mold contact node on grid #12 for different number of nodes per grid at constant injection velocity.

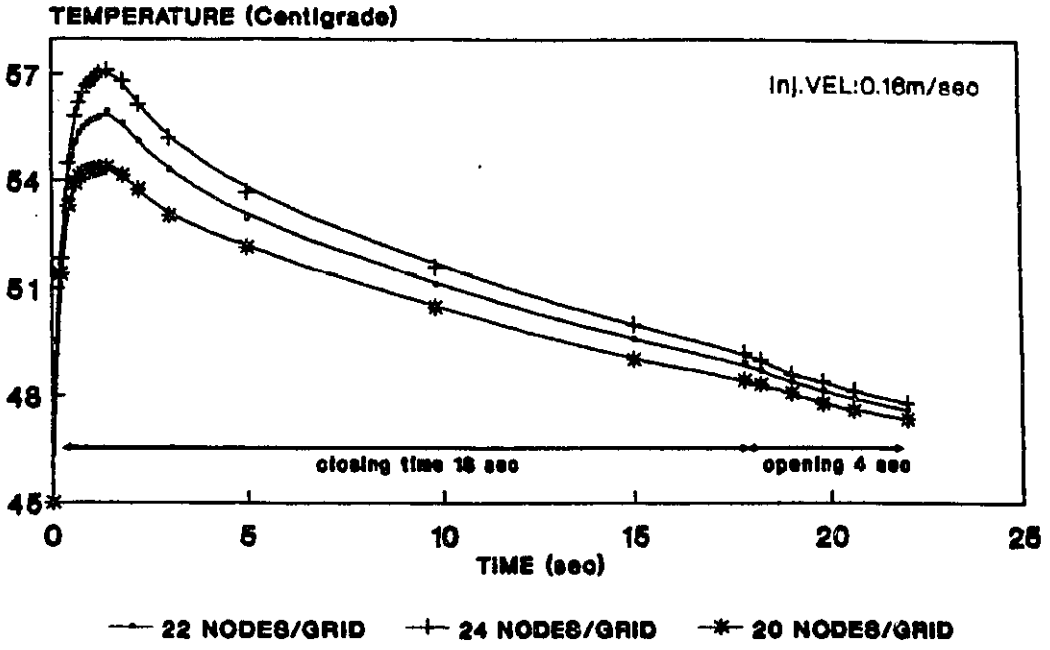

Figure B.IV.2 The thermal response of the mold contact node on grid #12 for different number of nodes per grid at constant injection velocity.

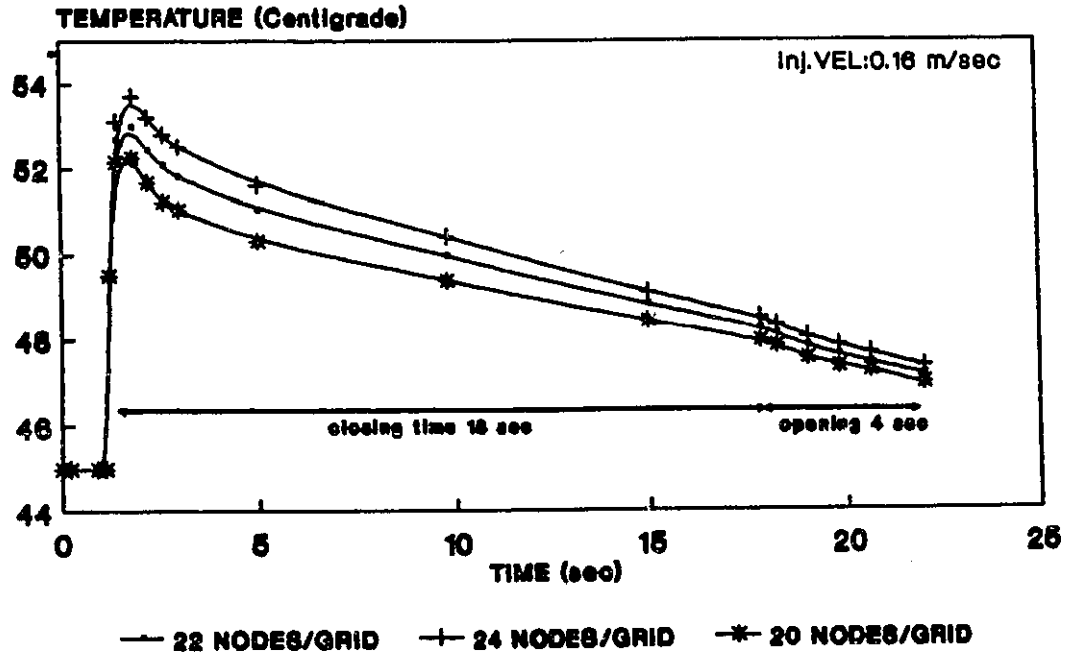

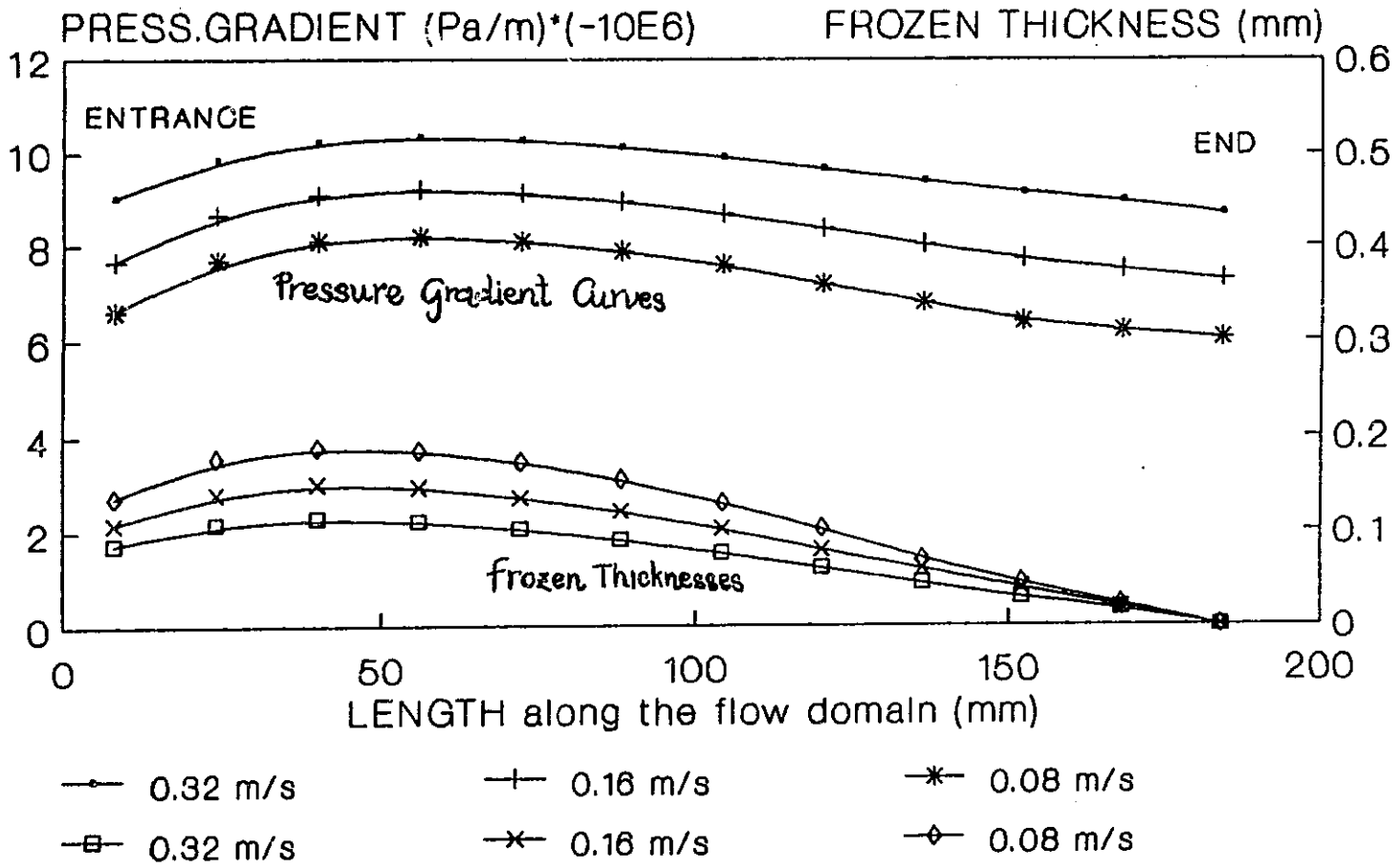

Those calculated values computed from the same nodal mesh but different dt-values due to different inj.speeds

Figure B.V The pressure gradients and frozen layer thicknesses for different injection speeds at the moment the mold is just filled.

Figure B.VI.1 The loci of maximum shear rates along the direction of flow at the moment the mold has just been filled (injection velocity=0.16 m/sec).

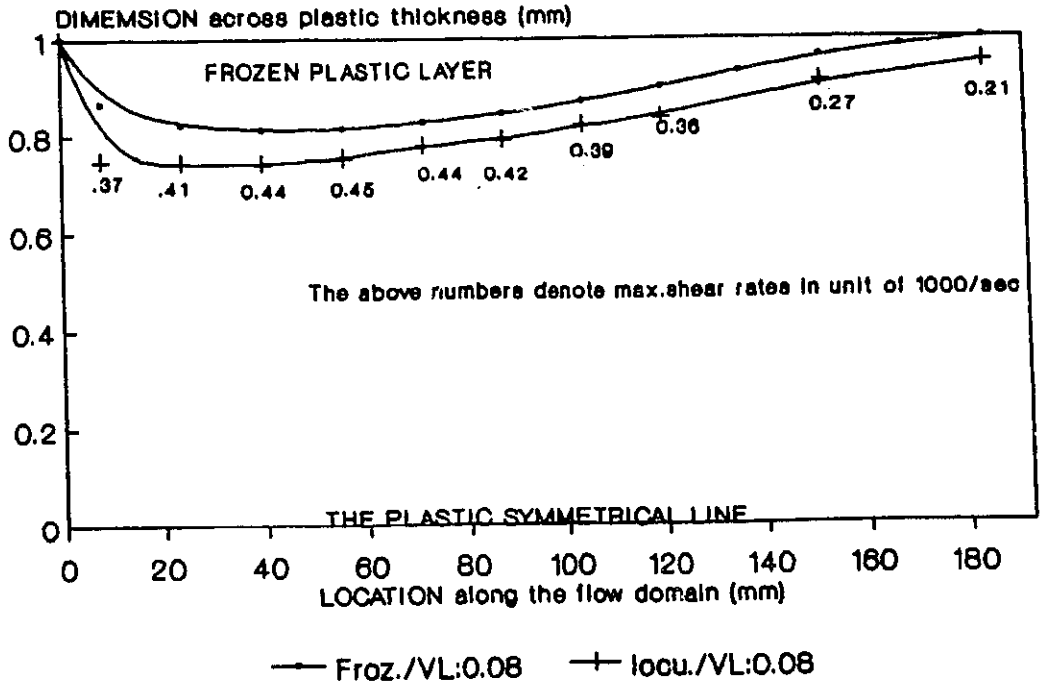

Figure B.VI.2 The loci of maximum shear rates along the direction of flow at the moment the mold has just been filled for various injection velocities.

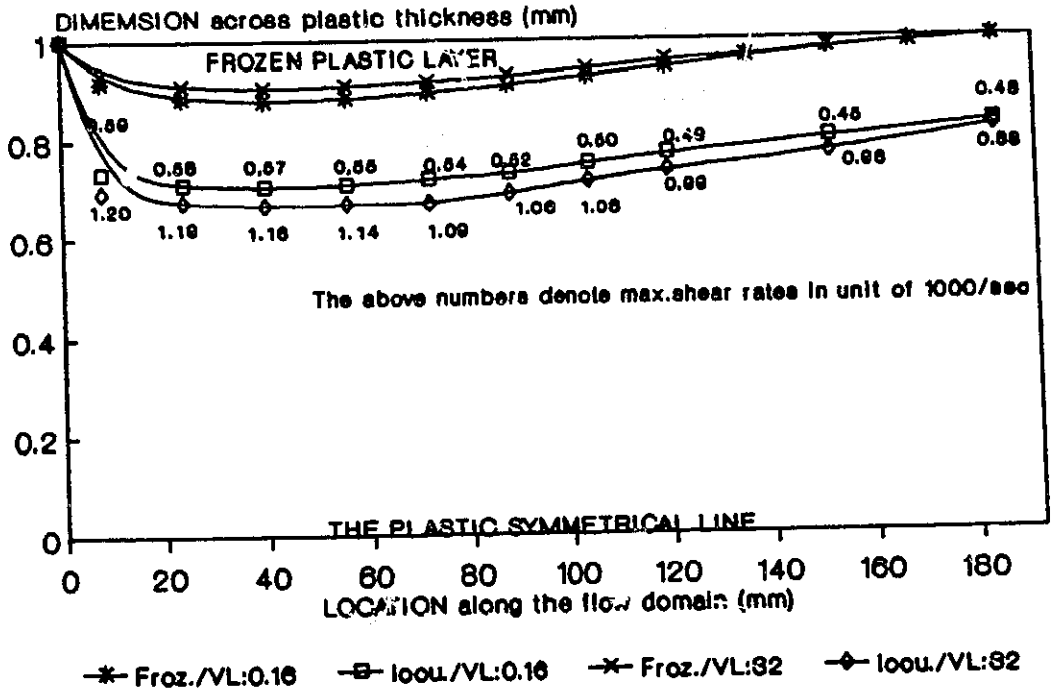

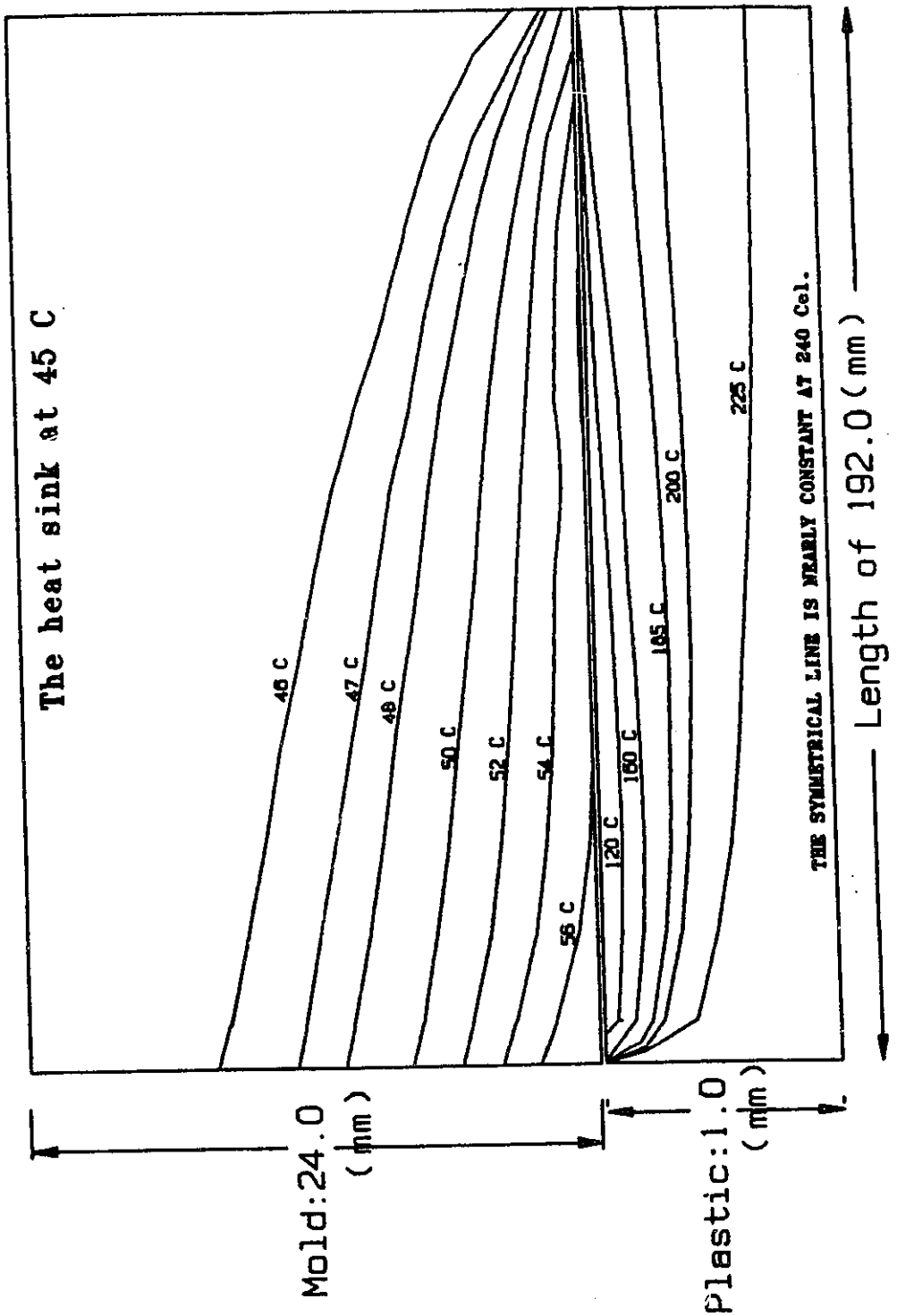

Figure B.VII.1 Isothermal profiles in the plastic and the mold at the moment when the mold has just been filled (Injection speed=0.08 m/sec)

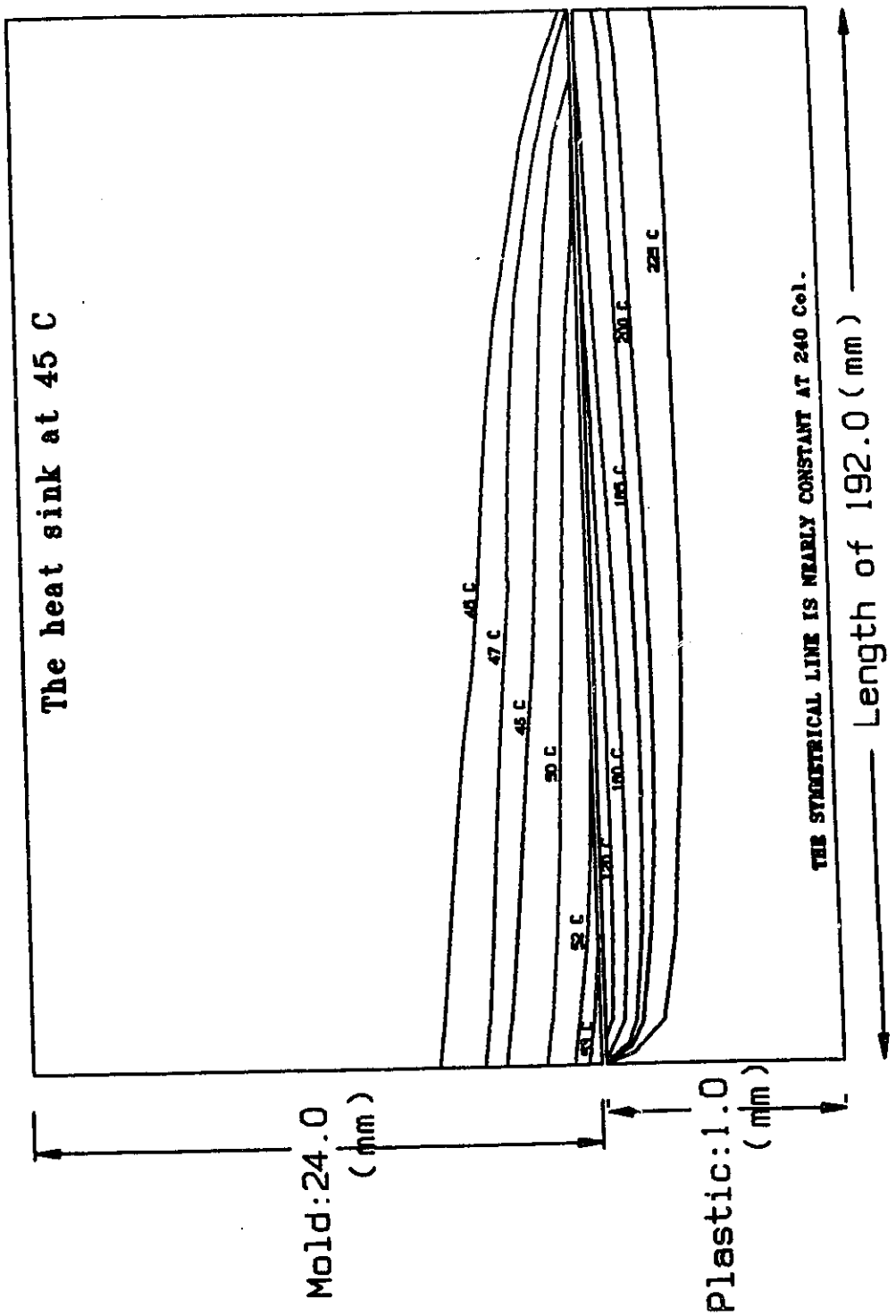

Figure B.VII.2 Isothermal profiles in the plastic and the mold at the moment when the mold has just been filled (Injection speed=0.32 m/sec)

4.2.3 GROUP C

The Effect of Varying the Cavity Thickness (2h)

(The varied inputs are from Data Table 2)

(These are the outputs for the first cycle only)

Figures C.I.1 to 4: Variation of the temperature distributions along the mold and the plastic interface at various times throughout the first cycle for different cavity thicknesses 115

Figures C.II.1 to 4 : The thermal response of the mold and plastic interfacial nodes and symmetrical nodes on grids 1 and 12 as a function of time for different cavity thicknesses 117

Figures C.III.1 to 3 : The maximum shear rates lines along the flow direction when the mold is just filled for various cavity thicknesses 119

Fig. C.IV : The pressure gradient distributions along the flow direction when the mold is just filled for various cavity thicknesses 120

Figure C.I.1 Variation of the temperature distribution in the mold along the contact surface at various times during the first cycle (thickness of the part=2*0.5 mm)

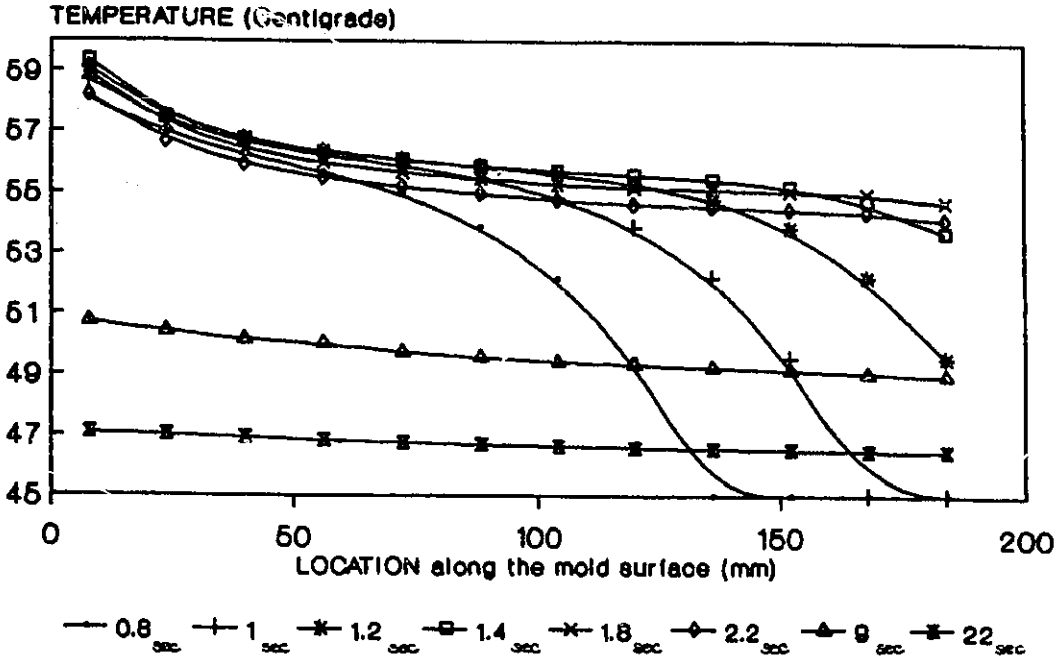

Figure C.I.2 Temperature distribution in the polymer at the mold contact surface at various times during the first cycle (part thickness=2*0.5 mm).

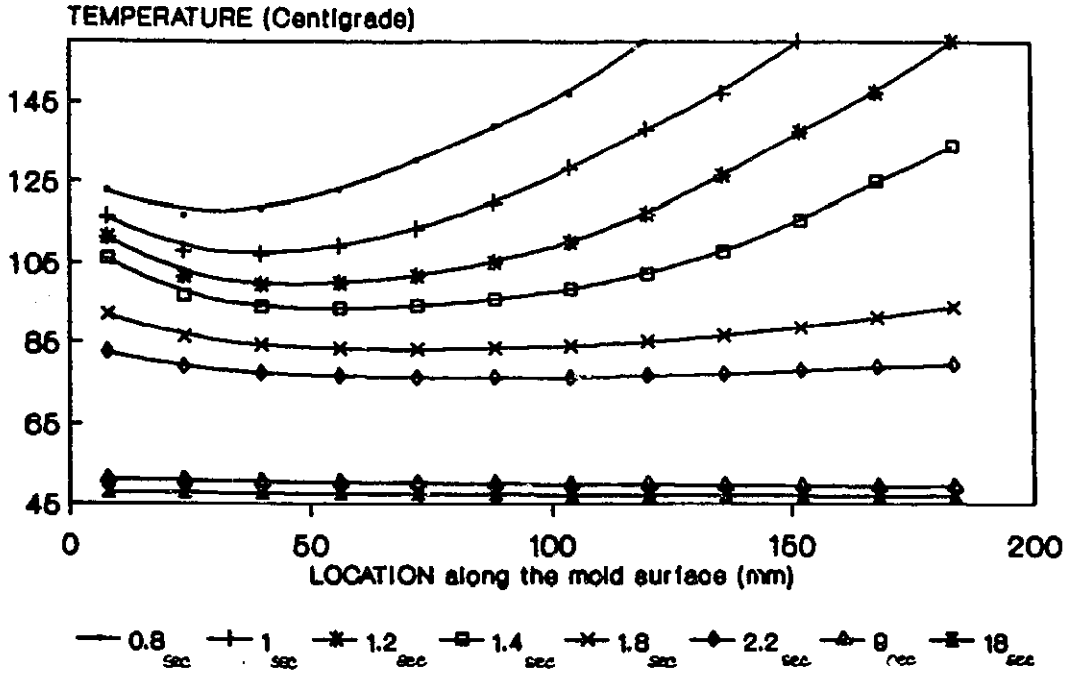

Figure C.I.3 Variation of the temperature distribution in the mold along the contact surface at various times during the first cycle (thickness of the part=2*0.2 mm)

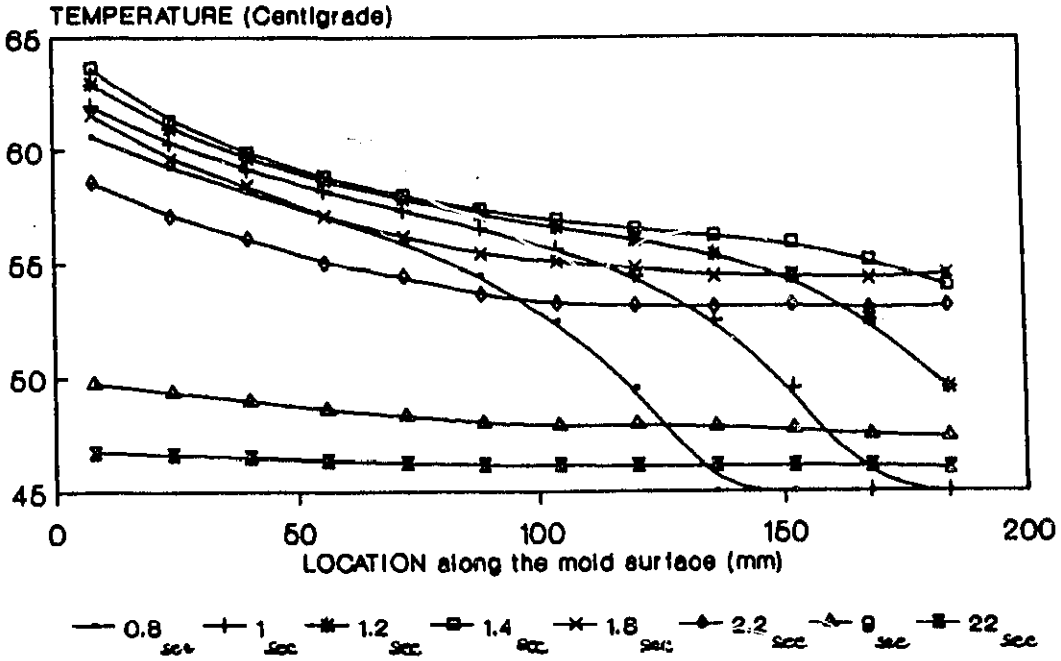

Figure C.I.4 Temperature distribution in the polymer at the mold contact surface at various times during the first cycle (thickness of the part = 2*0.2 mm).

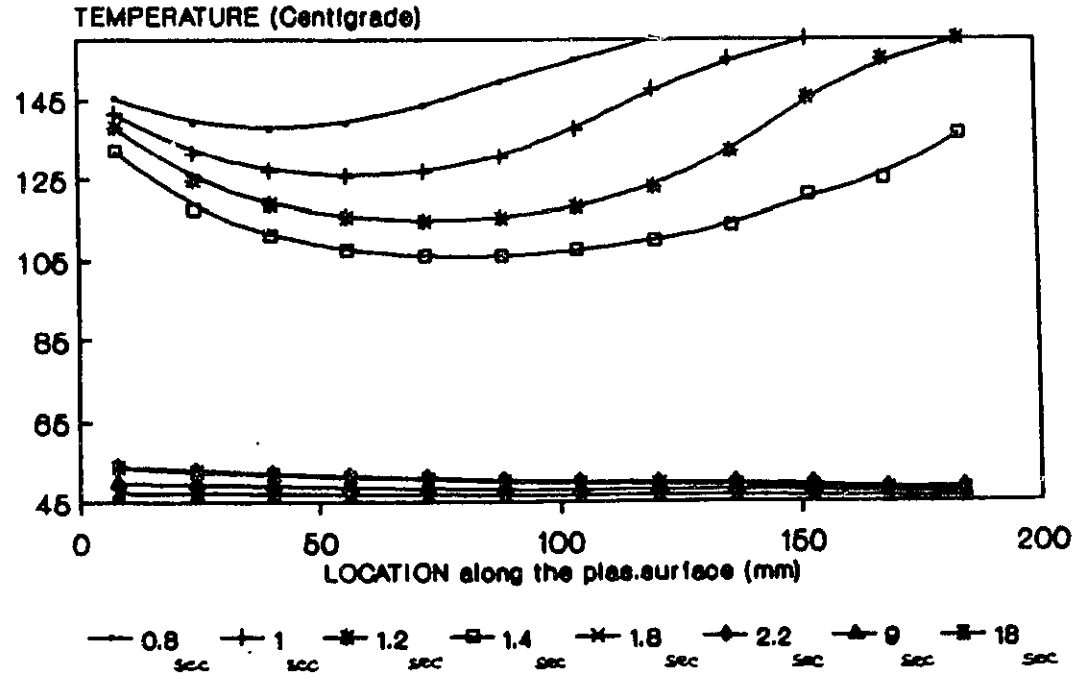

Figure C.II.1 The thermal response of the mold contact node on Grid # 1 for various part thicknesses.

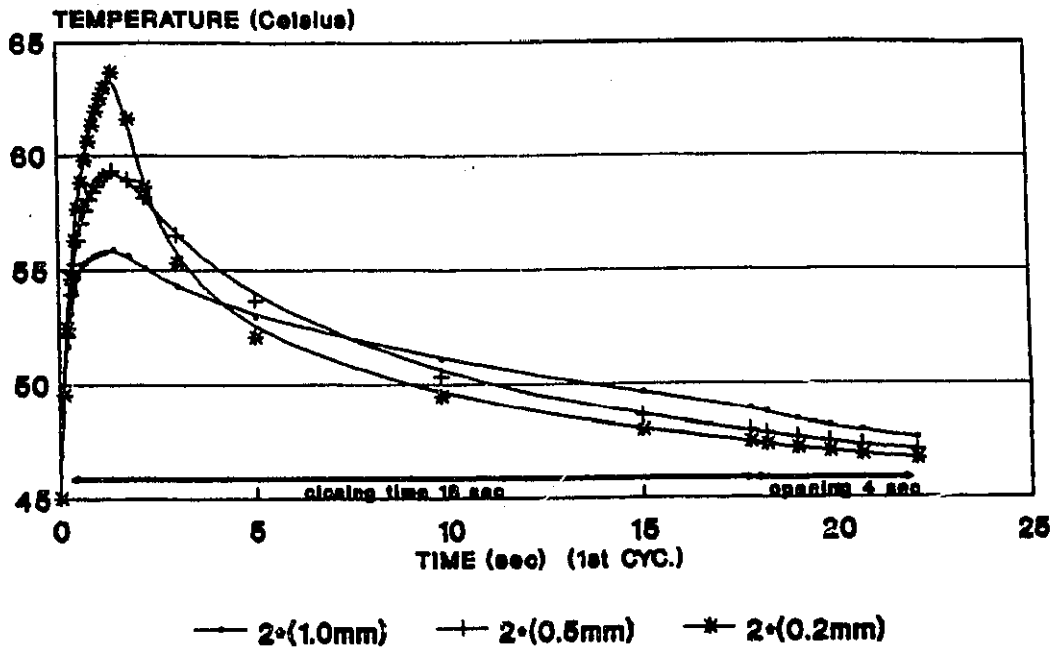

Figure C.II.2 The thermal response of the mold contact node on Grid # 12 for various part thicknesses.

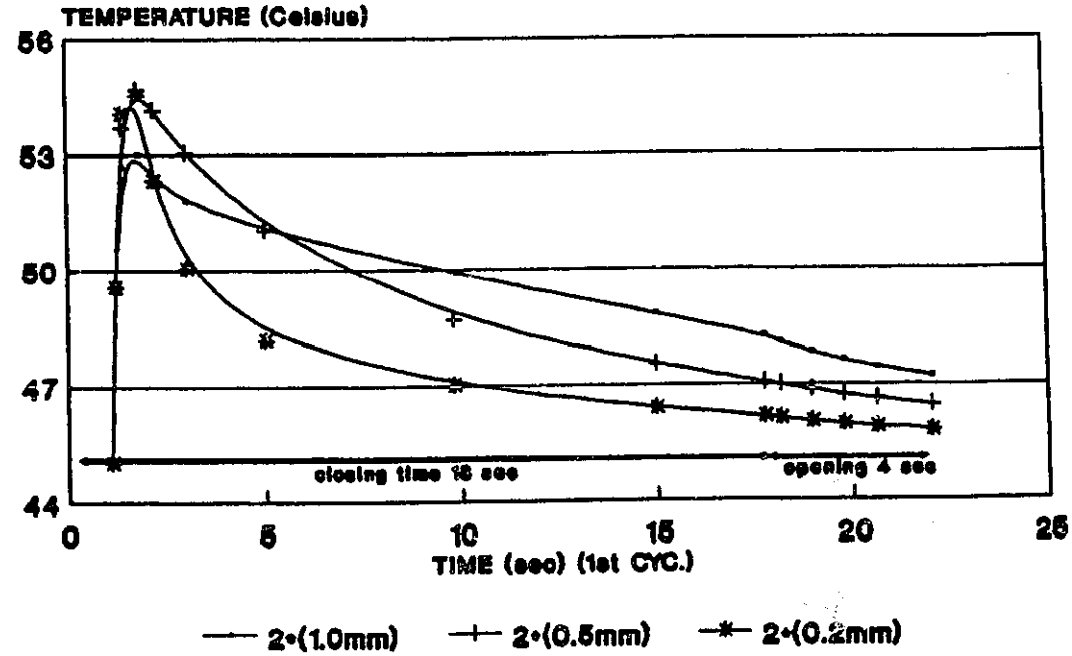

Figure C.II.3 The thermal response of the plastic at the symmetric centreline and at the plastic/mold interface at grid #1 for different part thicknesses.

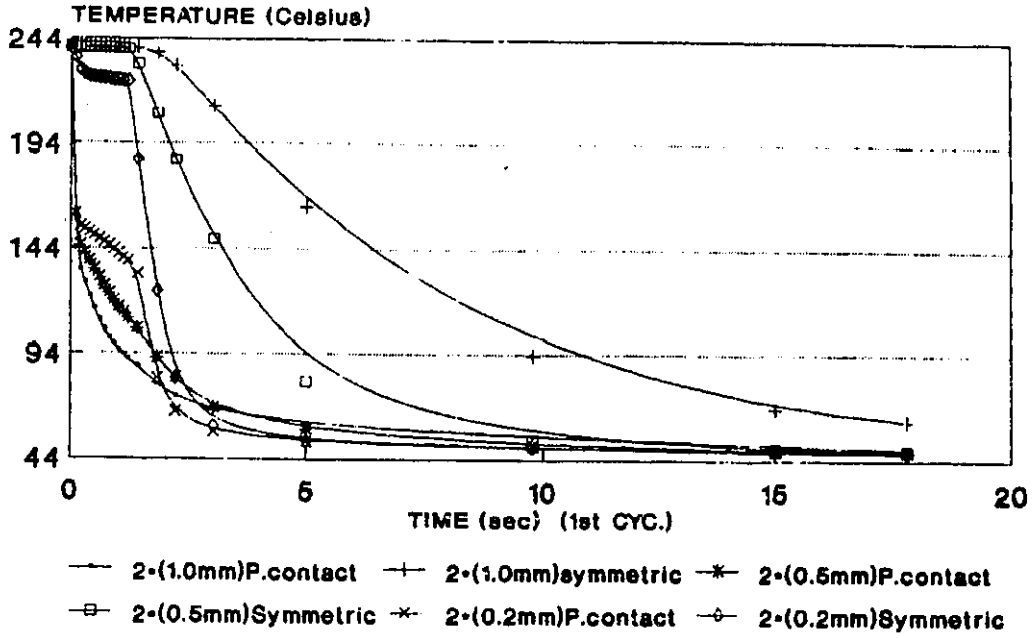

Figure C.II.4 The thermal response of the plastic at the symmetric centreline and at the plastic/mold interface at grid #12 for different part thickness.

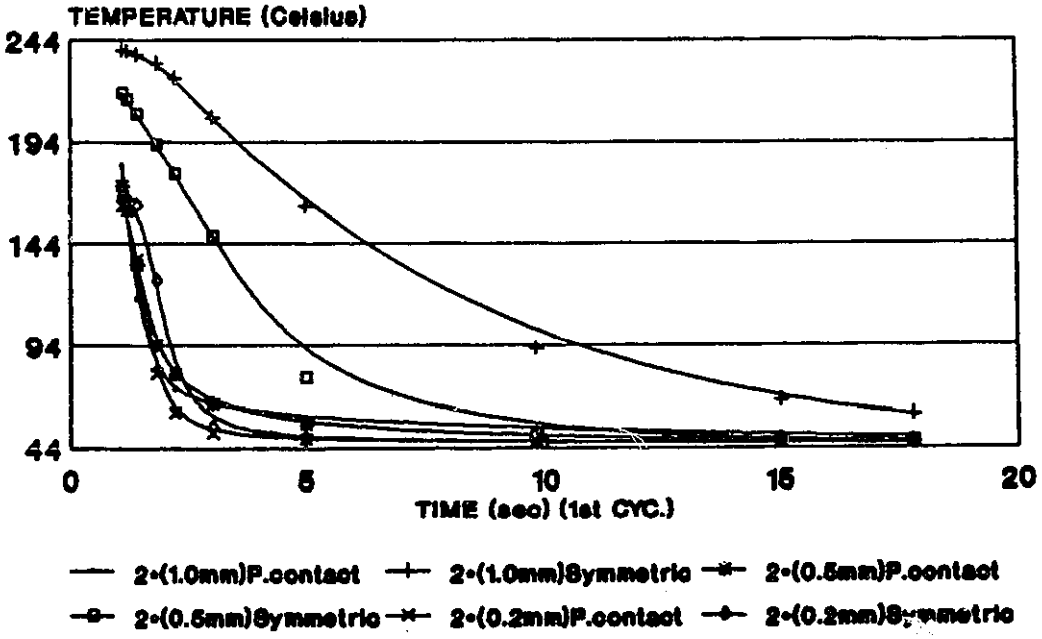

Figure C.III.1 The locus of maximum shear rates along the direction of flow at the moment the mold has just been filled for a part thickness=2*1.0 mm.

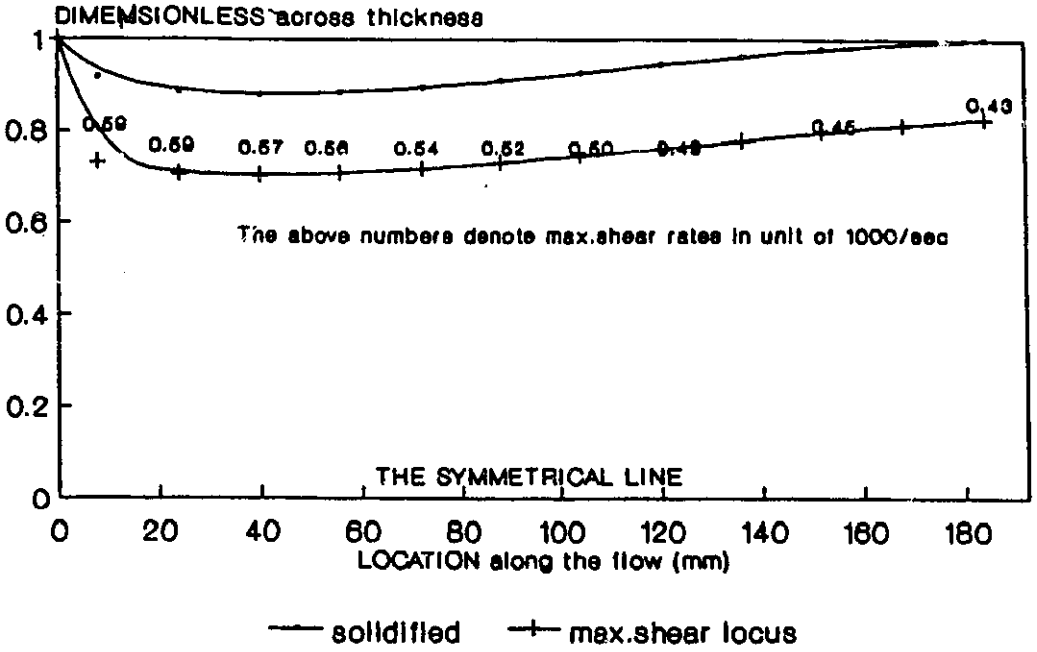

Figure C.III.2 The locus of maximum shear rates along the direction of flow at the moment the mold has just been filled for a part thickness=2*0.2 mm.

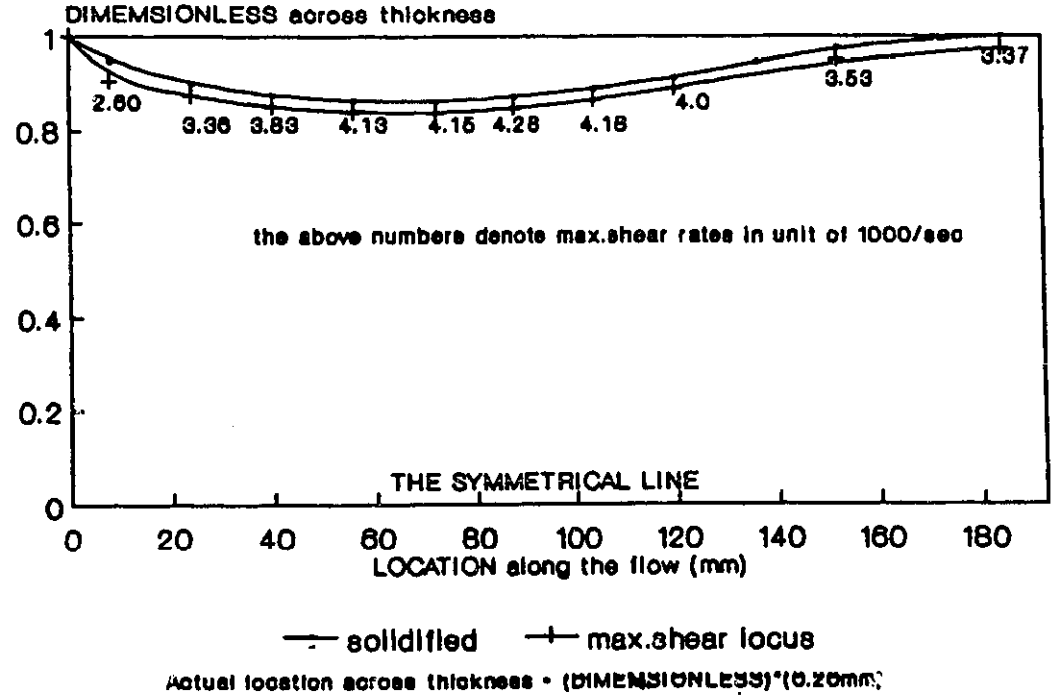

Figure C.III.3 The locus of maximum shear rates along the direction of flow at the moment the mold has just been filled for a part thickness=2*0.5 mm.

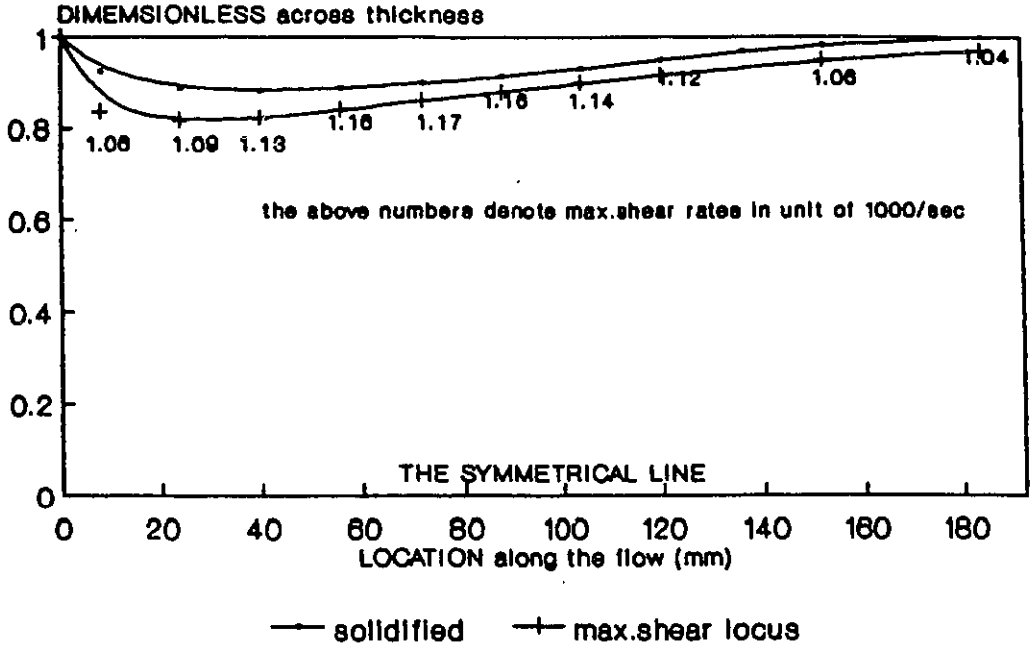

Figure C.IV The pressure gradient distribution along the direction of flow for different part thicknesses at the moment when the mold has just been filled.

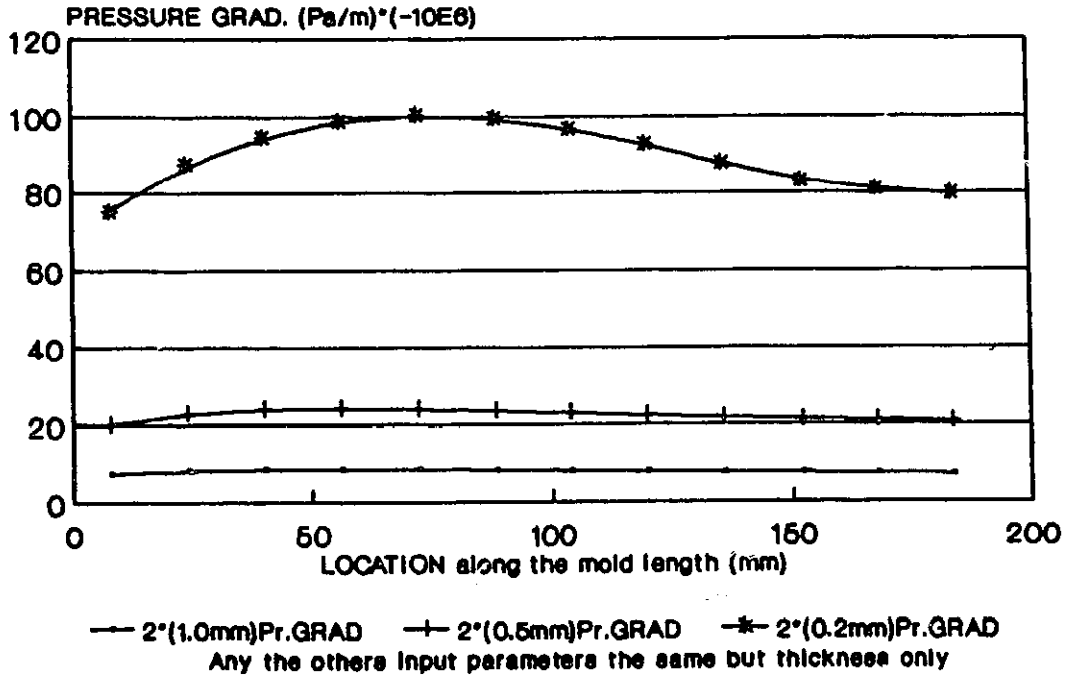

4.2.4 GROUP D

The Effect of Varying the Contact Conductance (Hr)

(The varied inputs are from Data Table 2)

Figures D.I.1 to 8 : Variation of the temperature distributions along the interface at various times for both the mold and plastic throughout the first cycle 122

Figures D.II.1 to 4 : The thermal response of the interfacial nodes on grids 1 and 12 for various contact conductances for the first cycle 126

Figure D.III : The maximum shear rates lines and frozen layer thicknesses when the mold is just filled for the first cycle 128

Figure D.IV : The pressure gradient distributions and frozen layer thicknesses when the mold is just filled for the first cycle 128

Figures D.V.1 to 7 : Temperature distributions and thermal response curves for the fifteenth cycle 129

Figure D.I.1 Variation of the temperature distribution in the mold along the contact surface at various times for a contact conductance of Hr=1000 W/m.m.K.

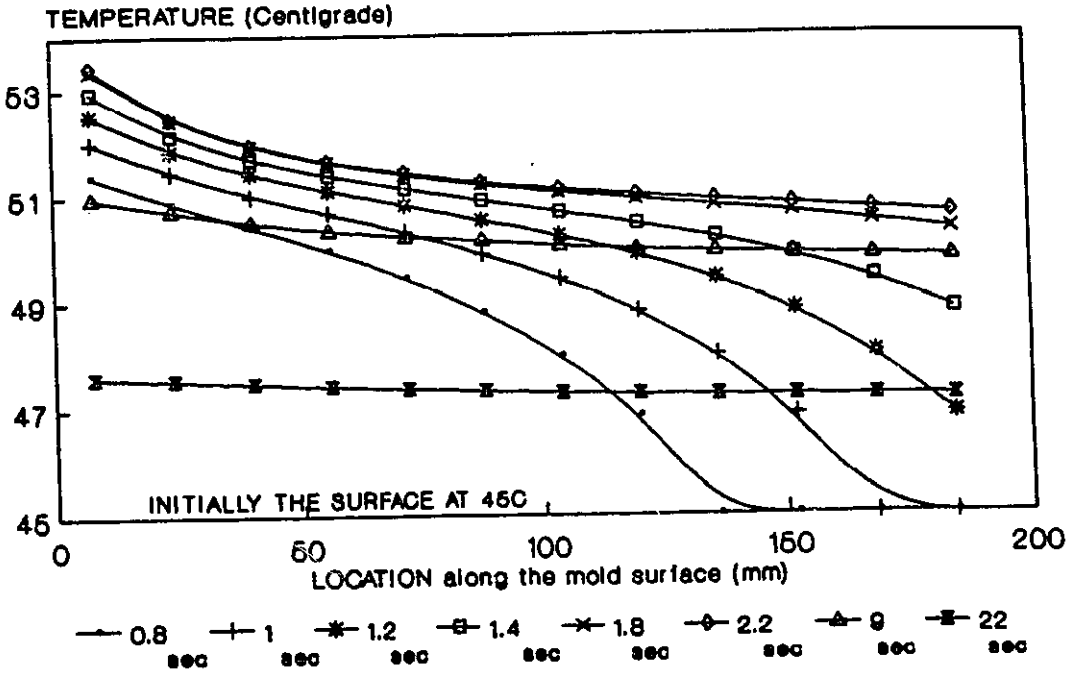

Figure D.I.2 Variation of the temperature distribution in the mold along the contact surface at various times for a contact conductance of Hr=2500 W/m.m.K.

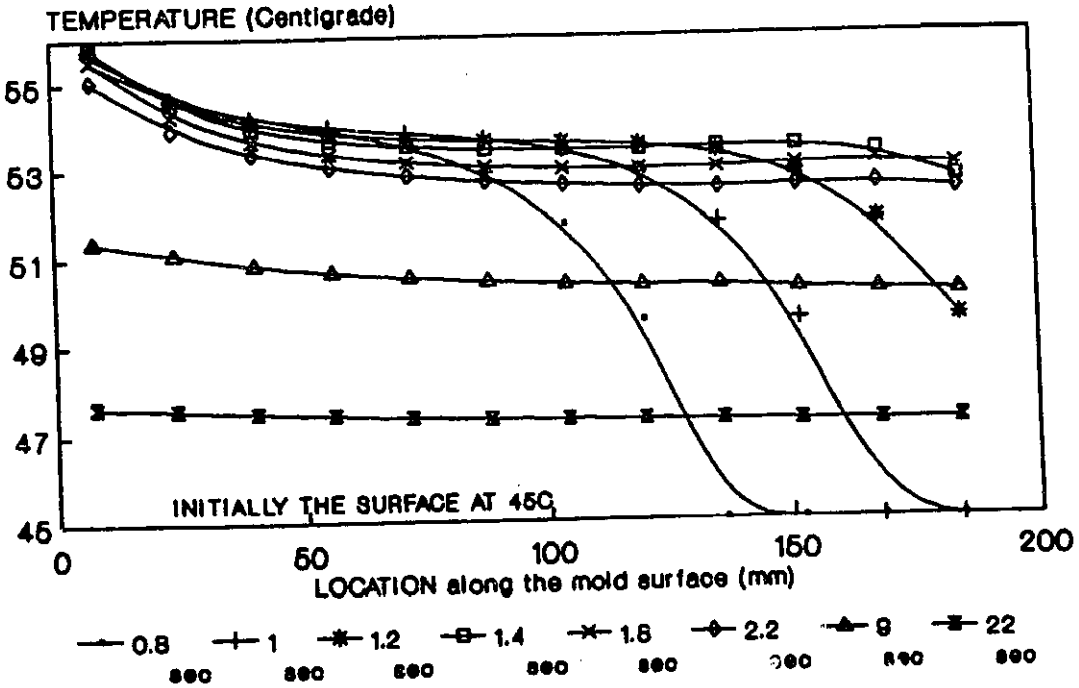

Figure D.I.4 Variation of the temperature distribution in the mold along the contact surface at various times for a varying contact conductance denoted Hr=10000* W/m.m.K.

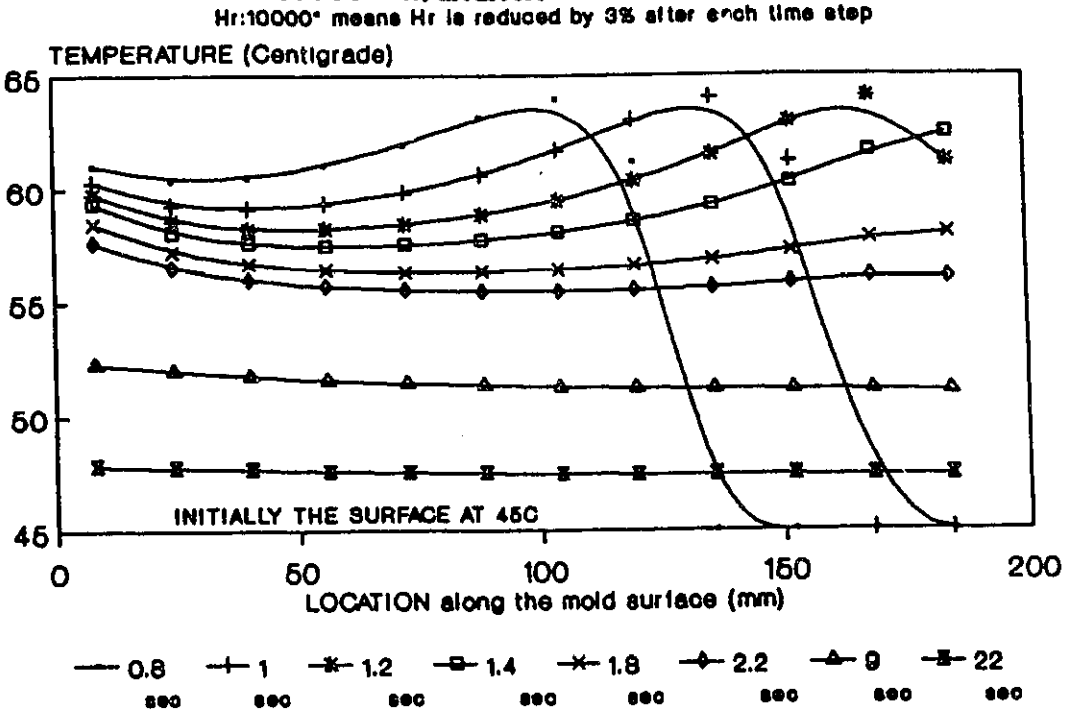

Figure D.I.3 Variation of the temperature distribution in the mold along the contact surface at various times for a contact conductance of Hr=10000 W/m.m.K.

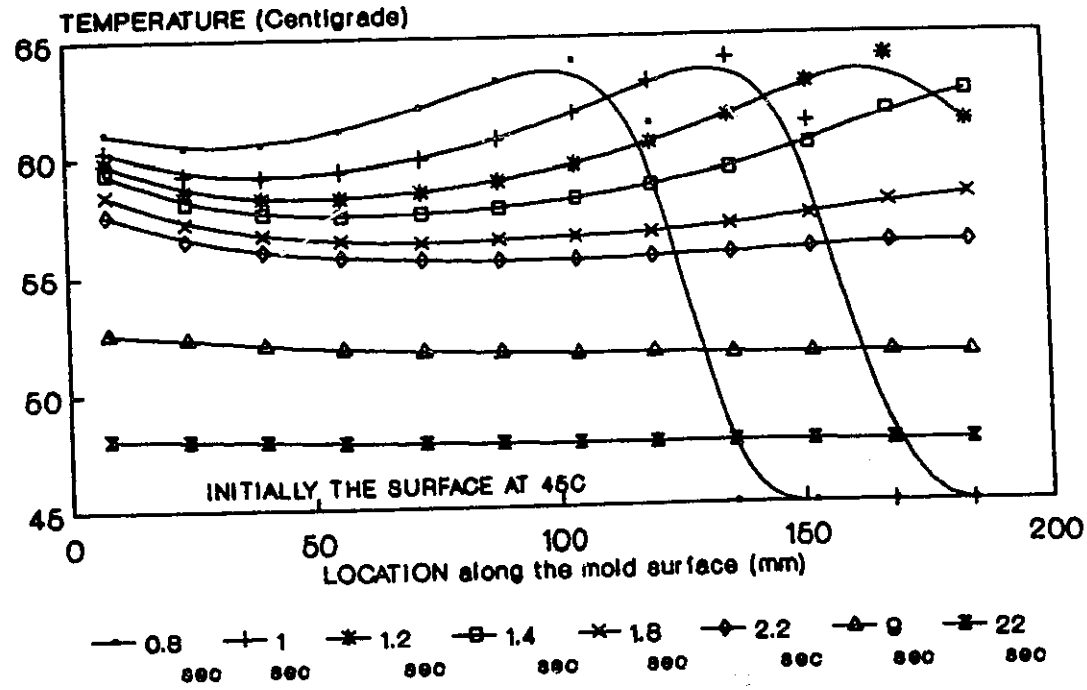

Figure D.I.5 Temperature distribution in the polymer at the mold contact surface at various times for a contact conductance Hr=1000 W/m.m.K.

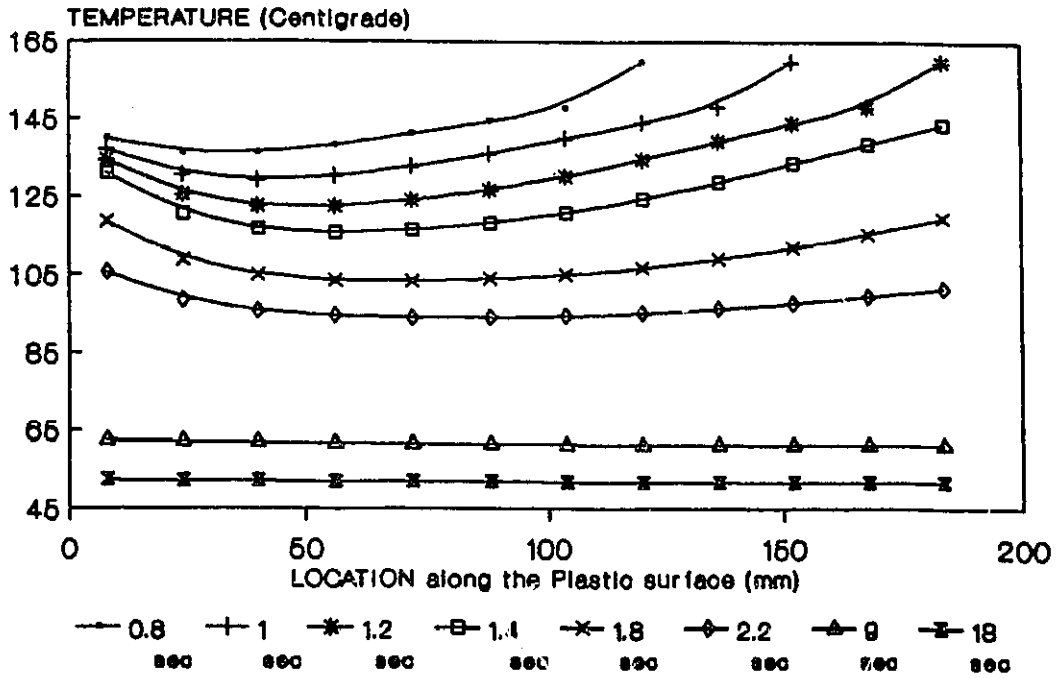

Figure D.I.6 Temperature distribution in the polymer at the mold contact surface at various times for a contact conductance Hr=2500 W/m.m.K.

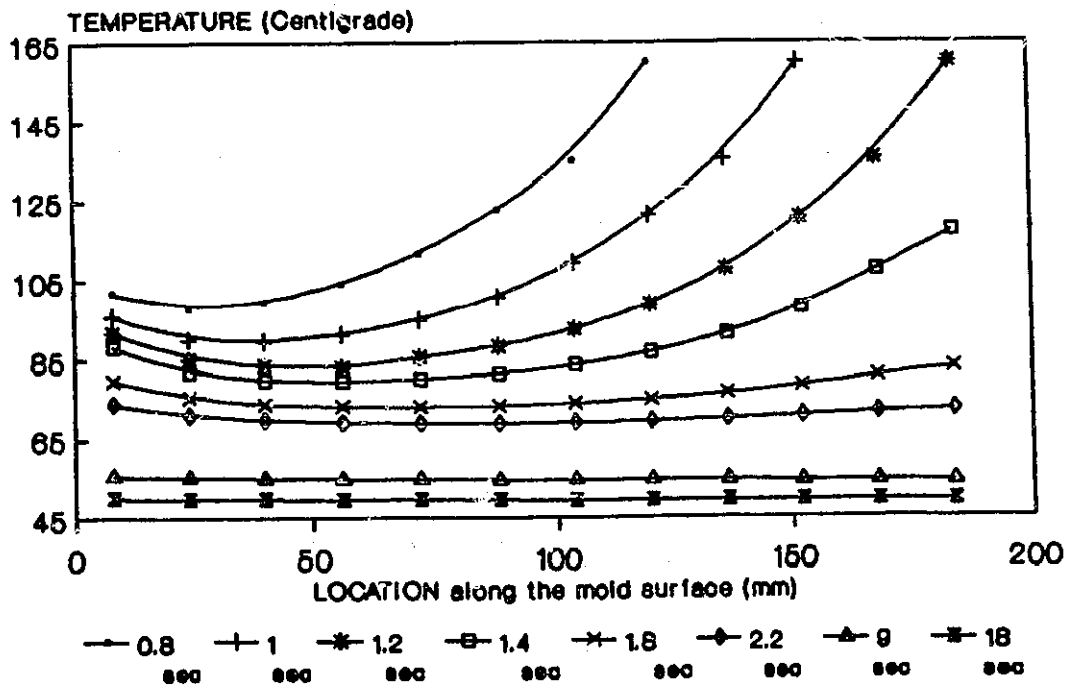

Figure D.I.7 Temperature distribution in the polymer along the mold contact surface at various times for a contact conductance of Hr=10000 W/m.m.K.(first molding cycle)

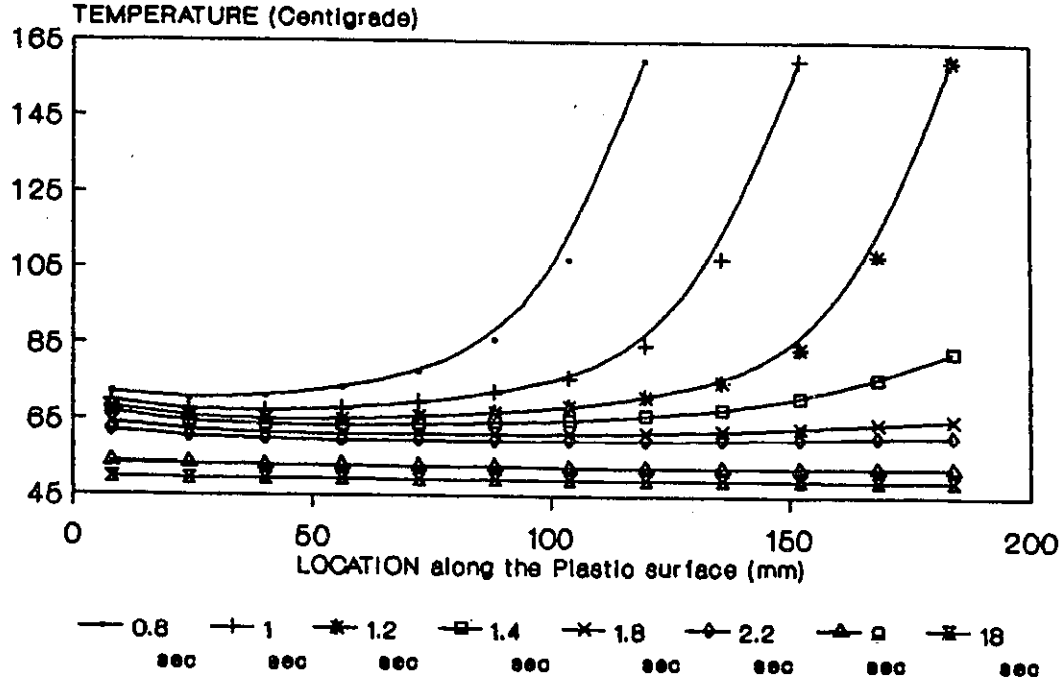

Figure D.I.8 Temperature distribution in the polymer at the mold contact surface at various times for a varying contact conductance of Hr=10000* W/m.m.K.

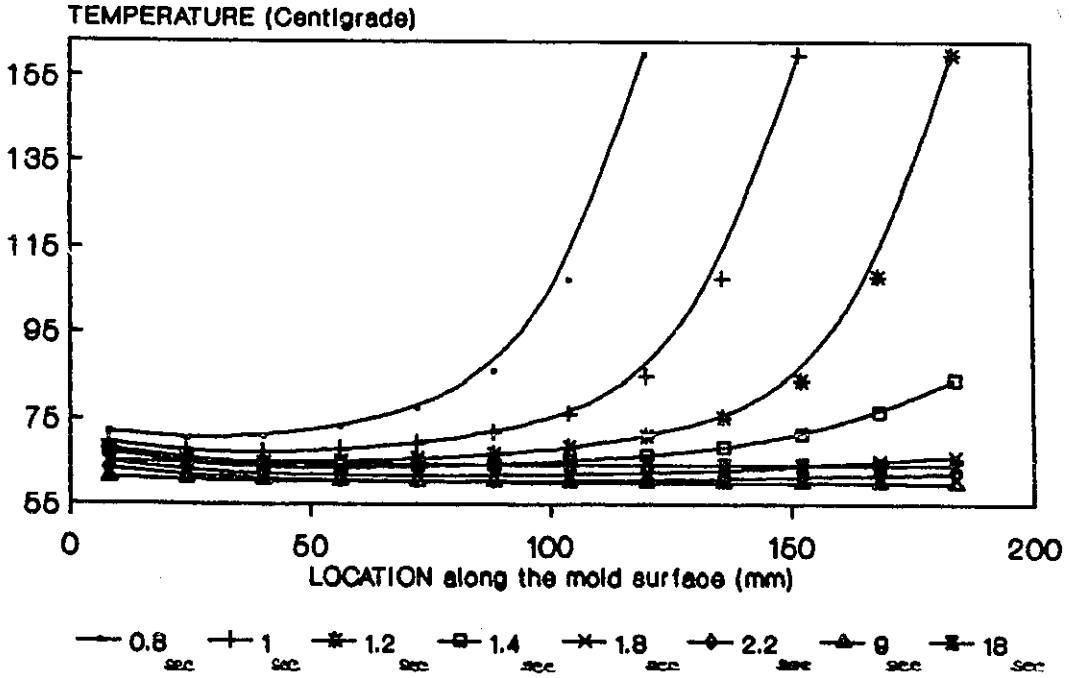

Figure D.II.1 The thermal response of the mold contact node on grid #1 for various contact conductances

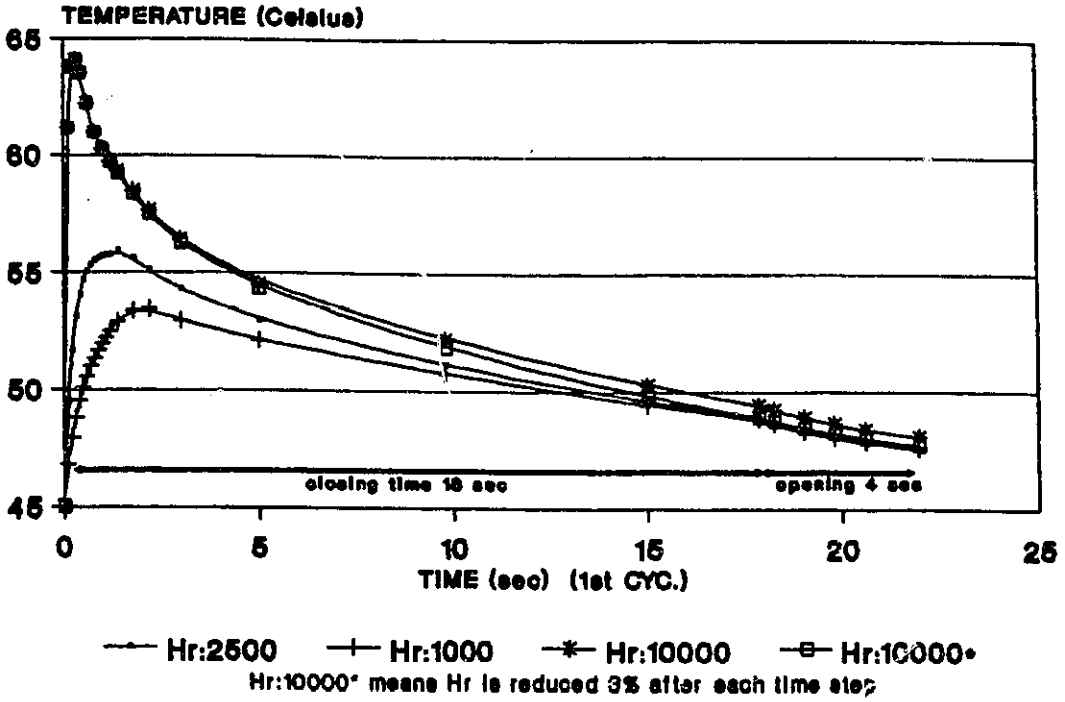

Figure D.II.2 The thermal response of the mold contact node on grid #12 for various contact conductances

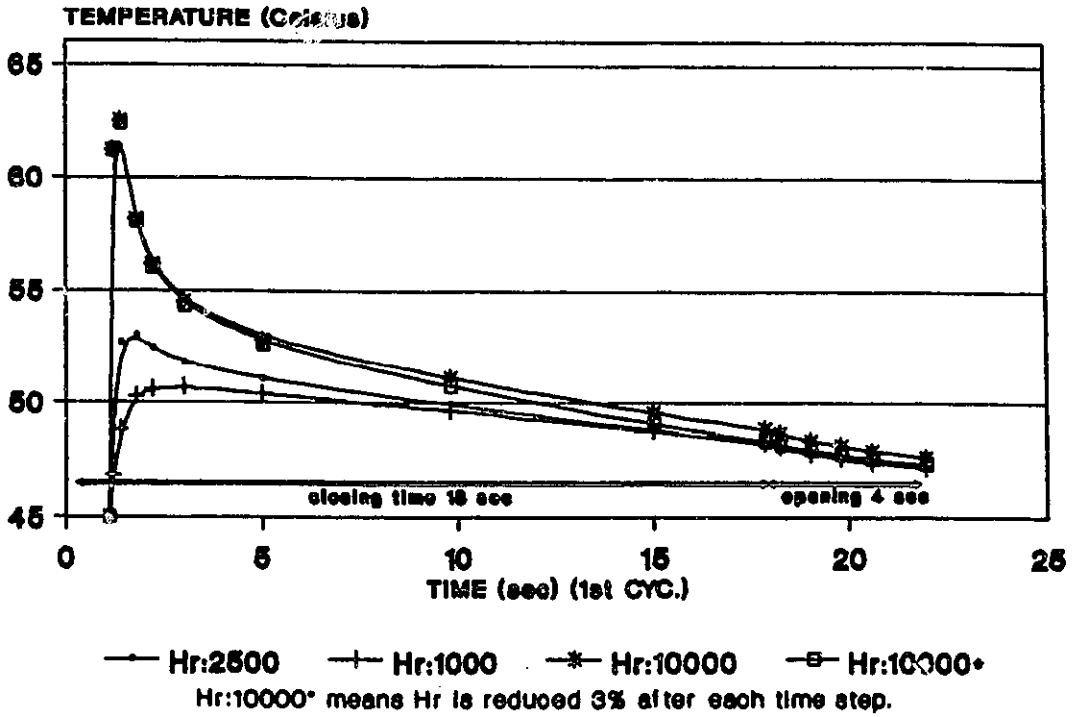

Figure D.II.3 The thermal response in the plastic at the interface node on grid #1 for various contact conductances.

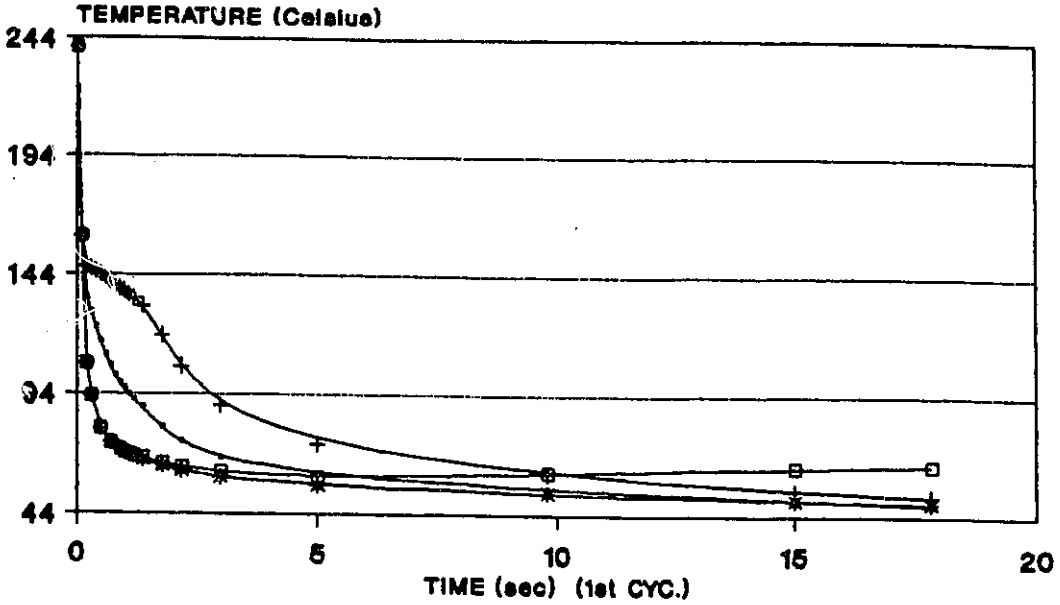

Hr:10000* means Hr is reduced by 3% after each time step.

Figure D.II.4 The thermal response in the plastic at the interface node on grid #12 for various contact conductances.

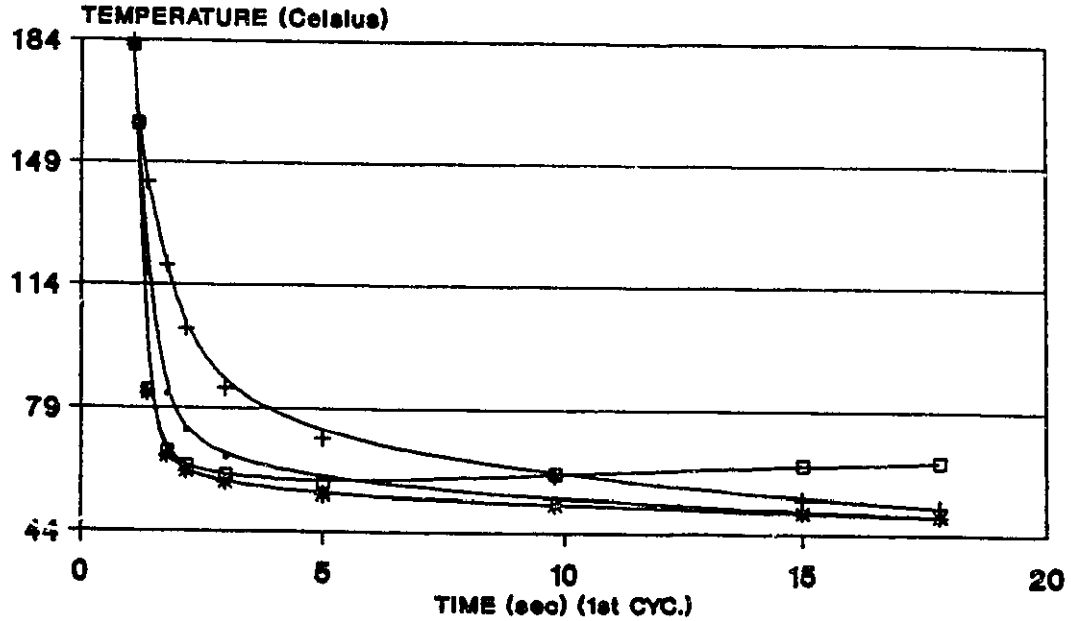

Hr:10000* means Hr is reduced by 3% after each time step.

Figure D.III The variation with different contact conductances of the loci of maximum shear rates at the moment the mold has just been filled.

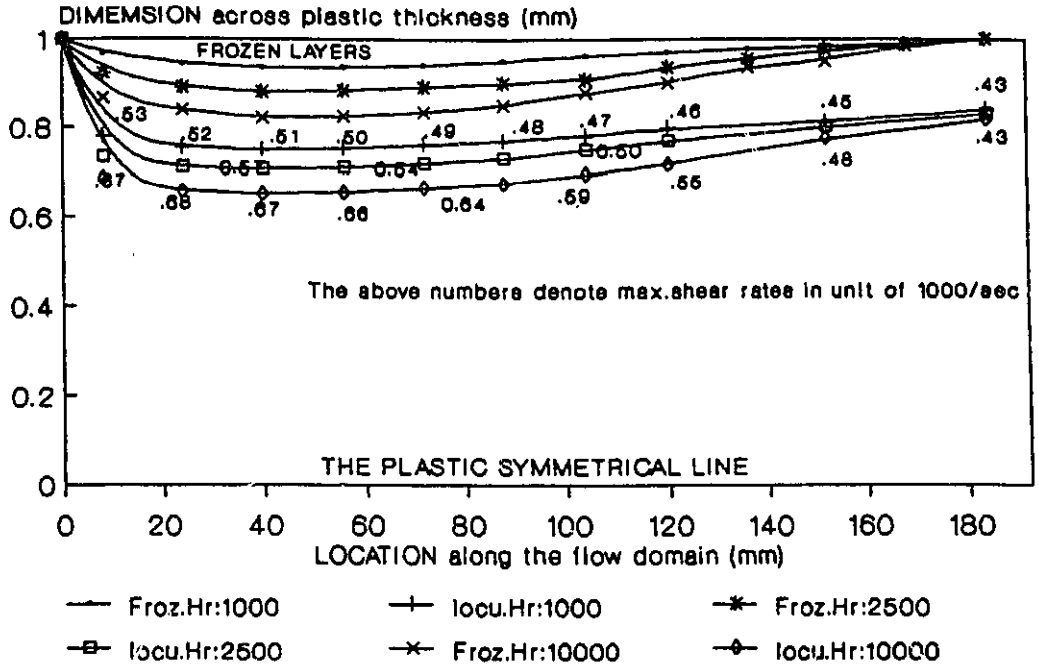

Figure D.IV The variation with different contact conductances of the pressure gradients and the frozen layer thicknesses at the moment the mold has just been filled.

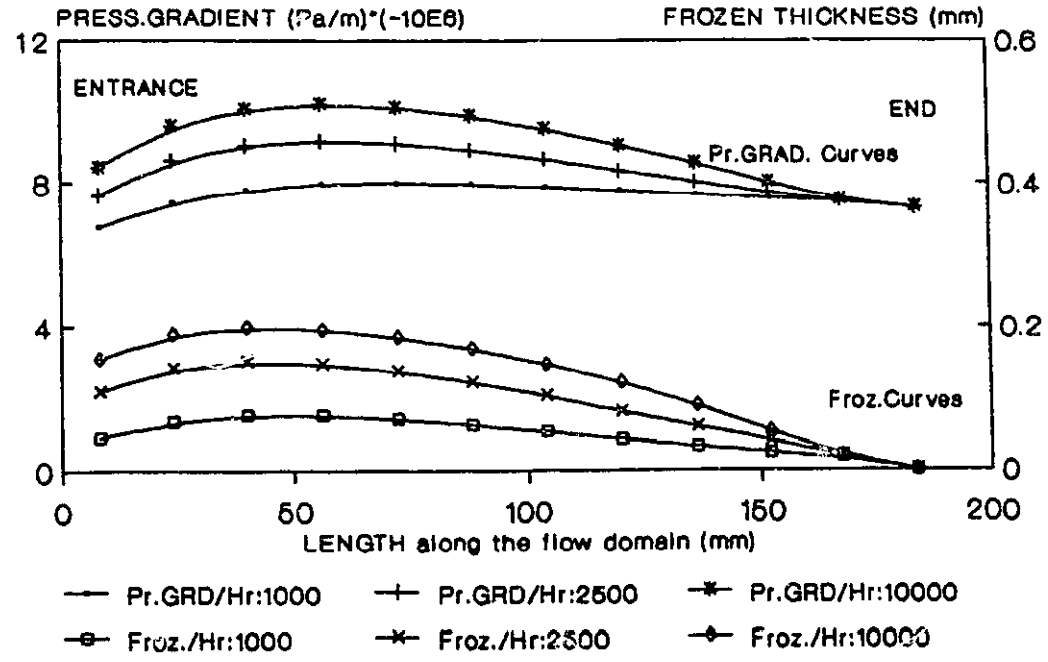

Figure D.V.1 Variation of the temperature distribution in the mold along the contact surface at various times for a contact conductance of Hr=10000 W/m.m.K. (during the 15th molding cycle)

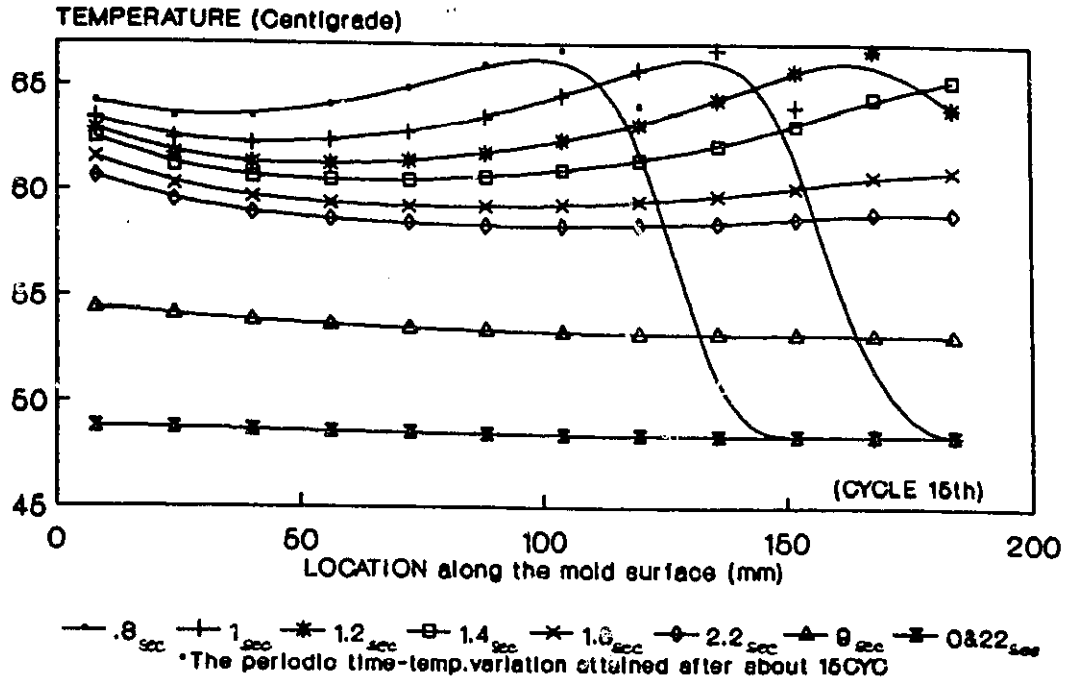

Figure D.V.2 Temperature distribution in the polymer along the contact surface at various times for a contact conductance of Hr=10000 W/m.m.K.(during the 15th molding cycle)

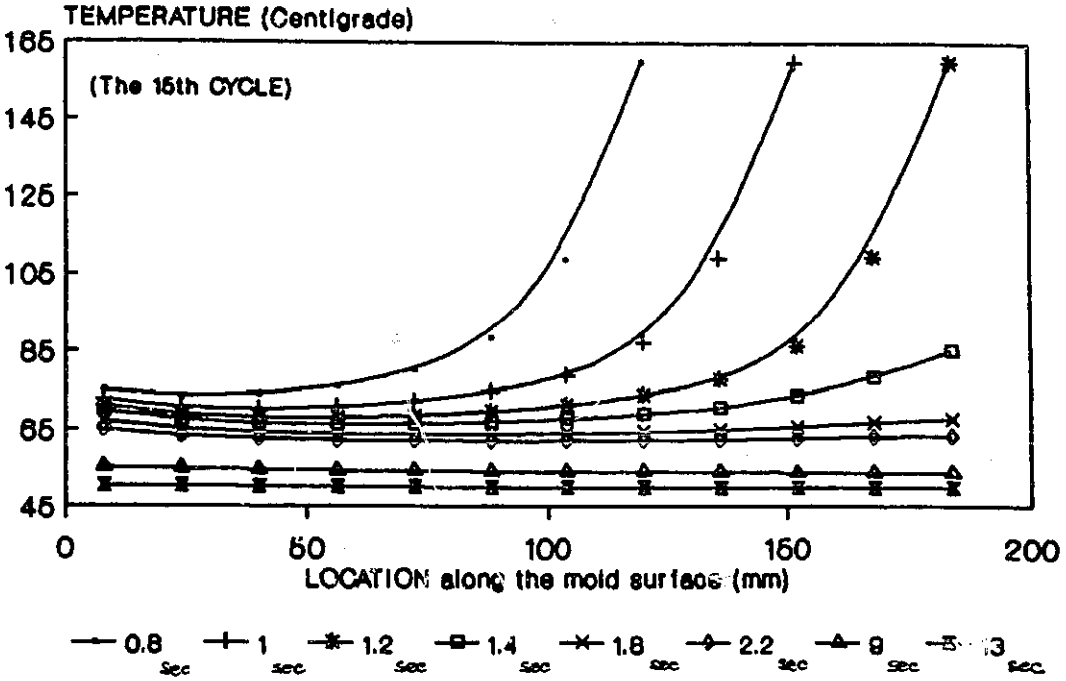

Figure D.V.3 The thermal response of the mold contact node on grid #1 for different contact conductances during the 15th molding cycle.

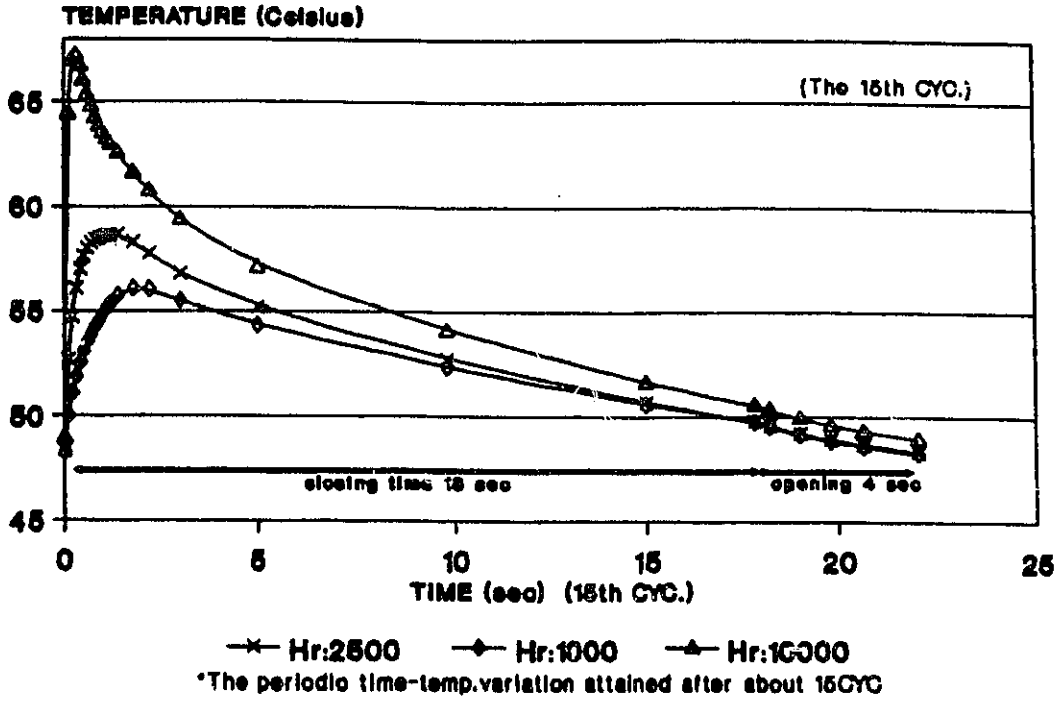

*The periodic time-temp.variation attained after about 15CYC

Figure D.V.4 The thermal response of the mold contact node on grid #12 for different contact conductances during the 15th molding cycle.

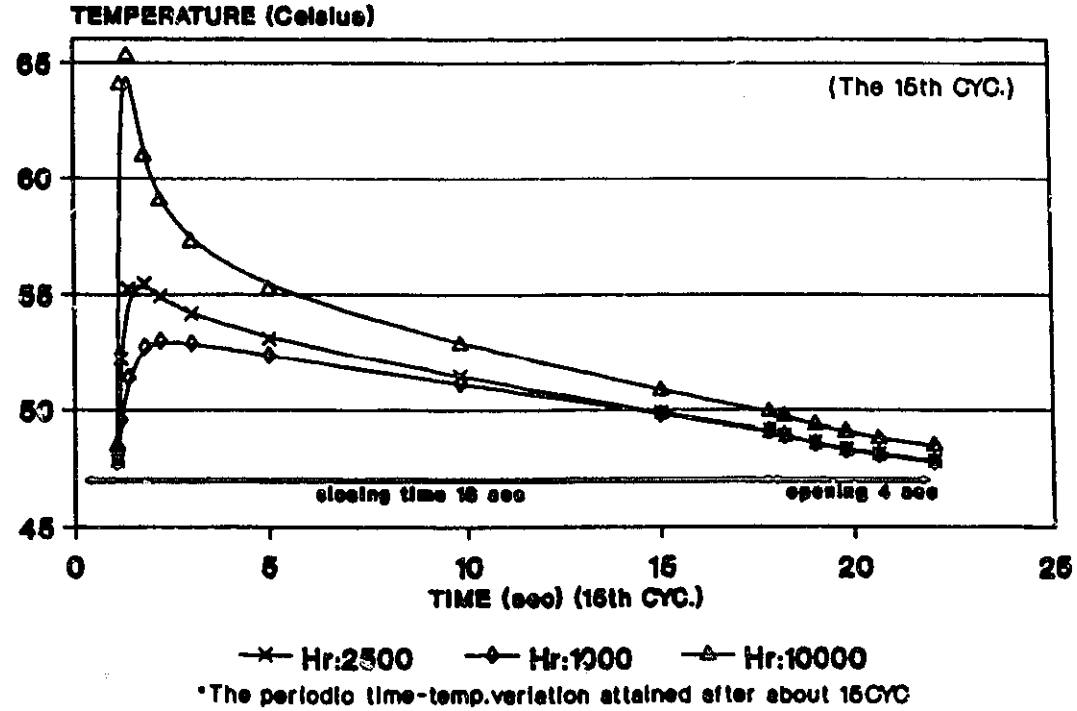

*The periodic time-temp.variation attained after about 15CYC

Figure D.V.5 The thermal response of the polymer node at the mold contact on grid #1 for different contact conductances during the first and 15th molding cycles.

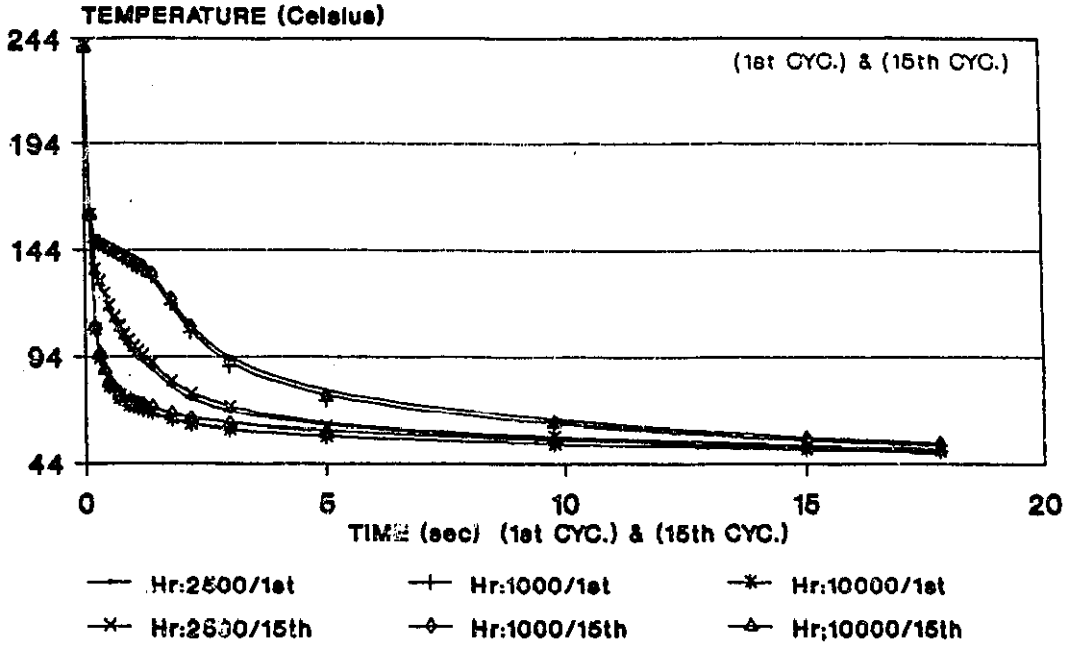

Figure D.V.6 The thermal response of the polymer node at the mold contact on grid #12 for different contact conductances during the first and 15th molding cycle.

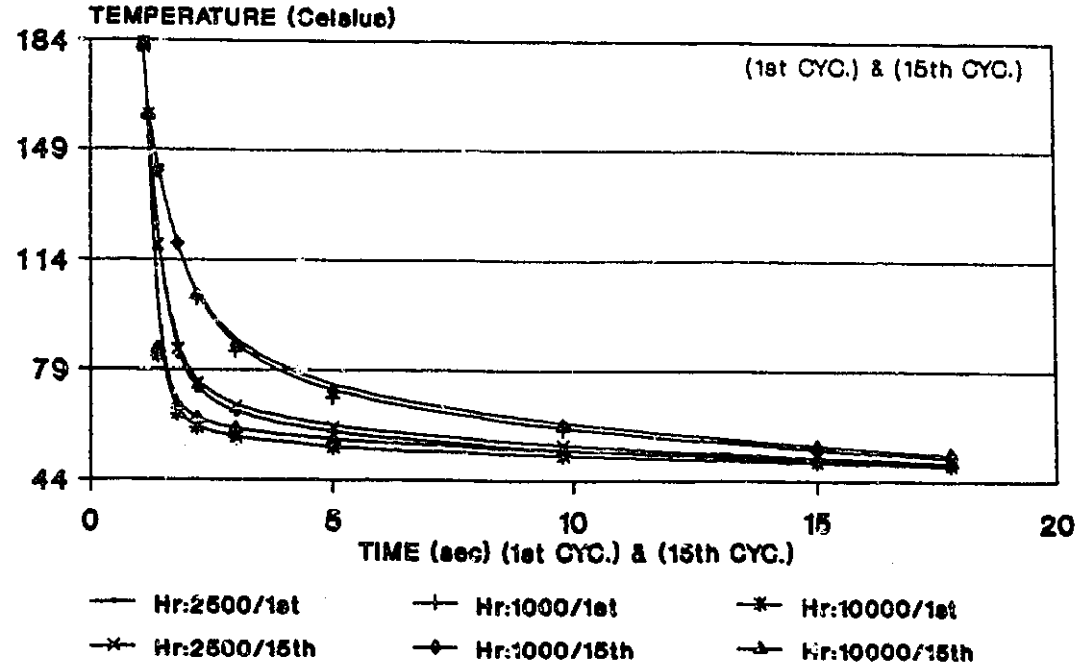

Figure D.V.7 The thermal response of the mold contact nodes on grids #1,3,6 & 12 for a contact conductance of 10000 W/m.m.K.cycle.

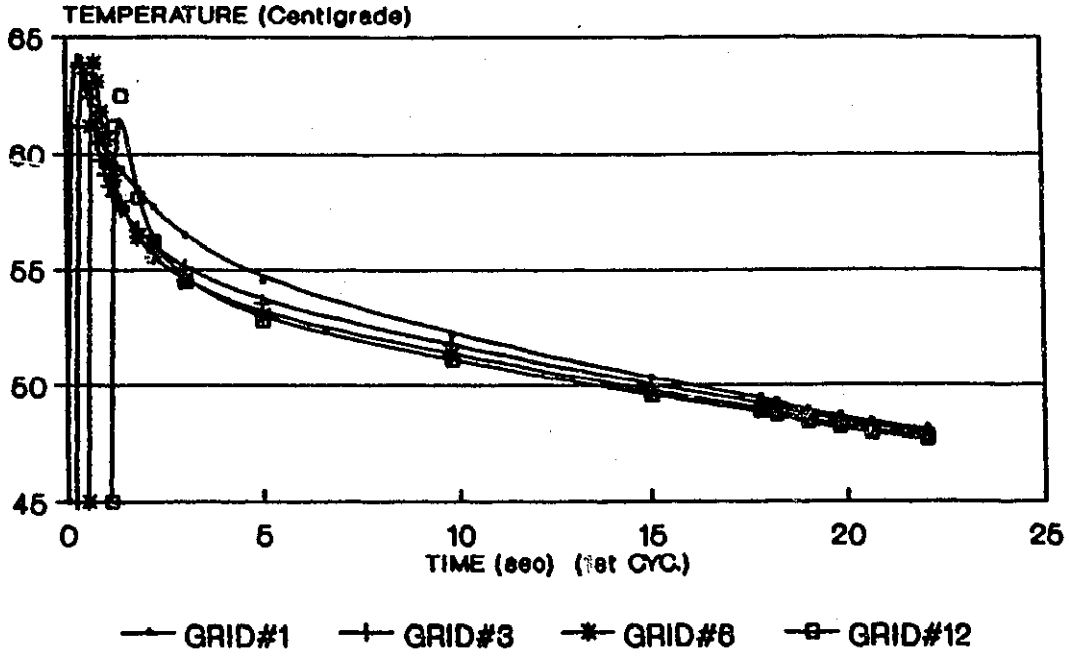

4.2.5 GROUP E

The Effect of Varying the mold sink Temperature (To)

(The varied inputs are from Data Table 2)

Figures E.I.1 to 4 : Variation of the temperature distributions along the interface at various times for the first cycle 134

Figures E.II.1 to 6 : The thermal response of some selected interfacial nodes at various times for the first cycle 136

Figure E.I.1 Variation of the temperature distribution in the mold along the contact surface at various times for an initial mold temperature of 65 °C.

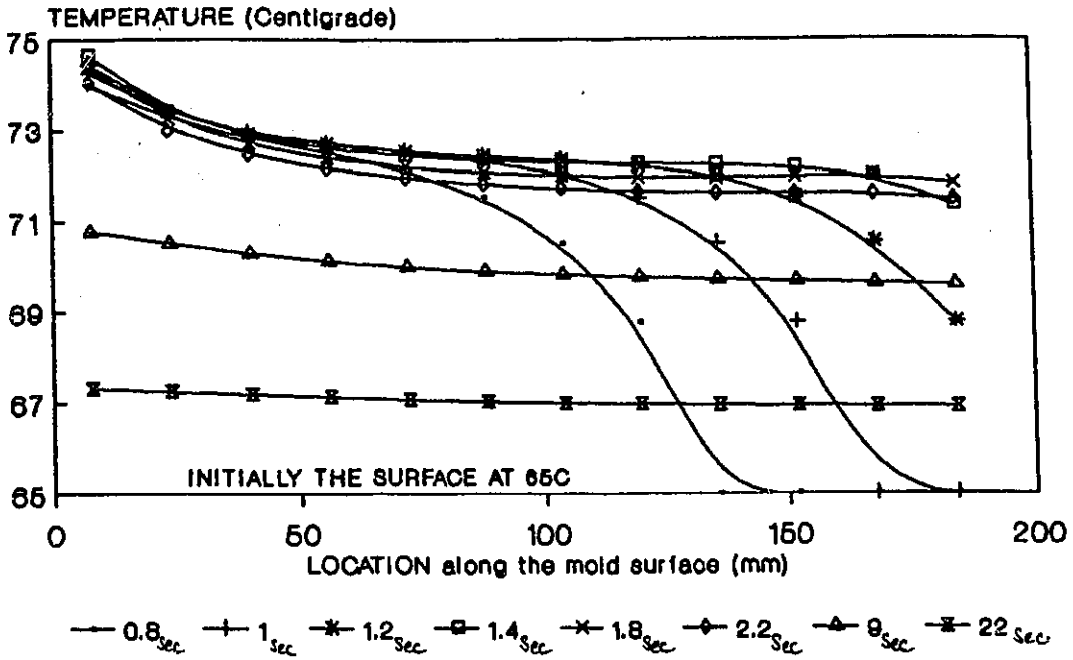

Figure E.I.2 Variation of the temperature distribution in the mold along the contact surface at various times for an initial mold temperature of 85 °C.

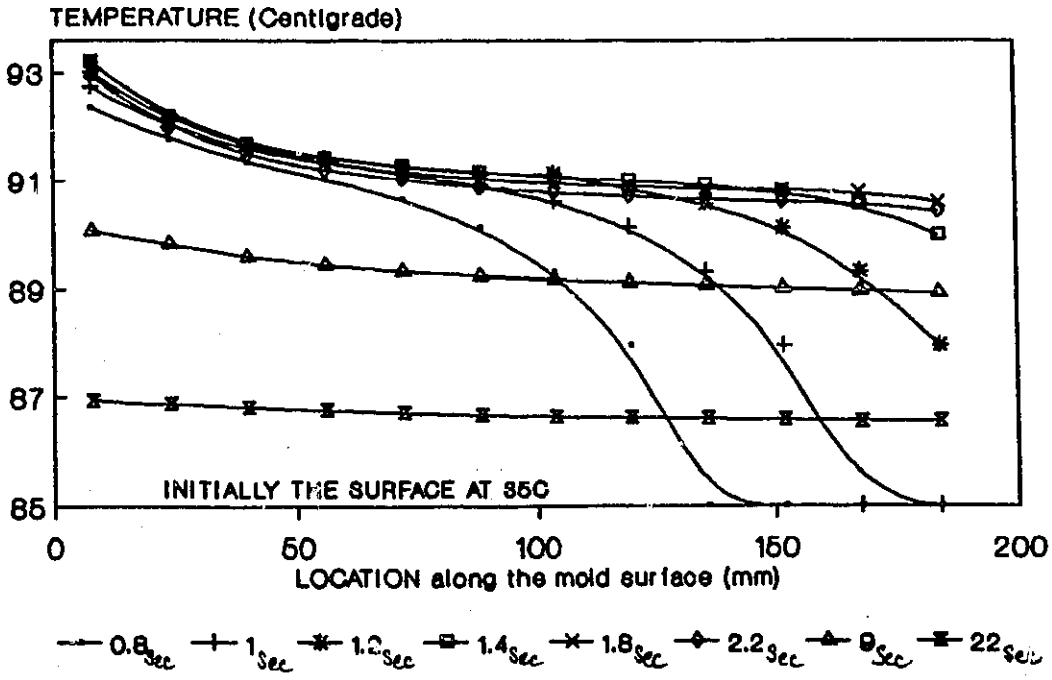

Figure E.I.3 Temperature distribution in the polymer along the mold contact surface at various times during the first cycle with an initial mold temperature of 65 C.

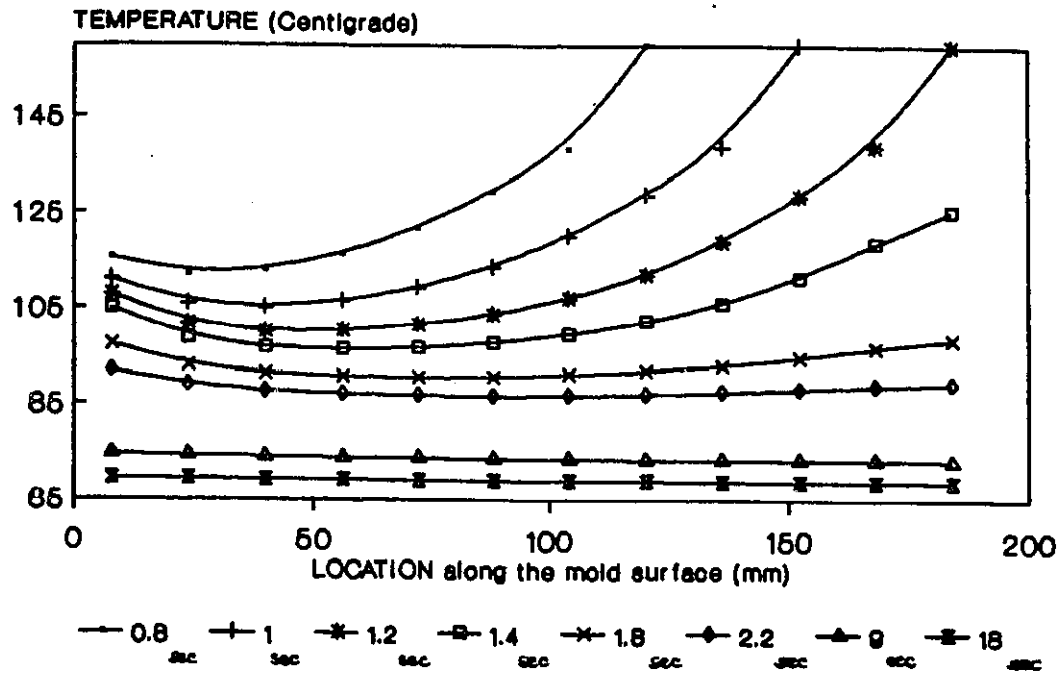

Figure E.I.4 Temperature distribution in the polymer along the mold contact surface at various times during the first cycle with an initial mold temperature of 85 C.

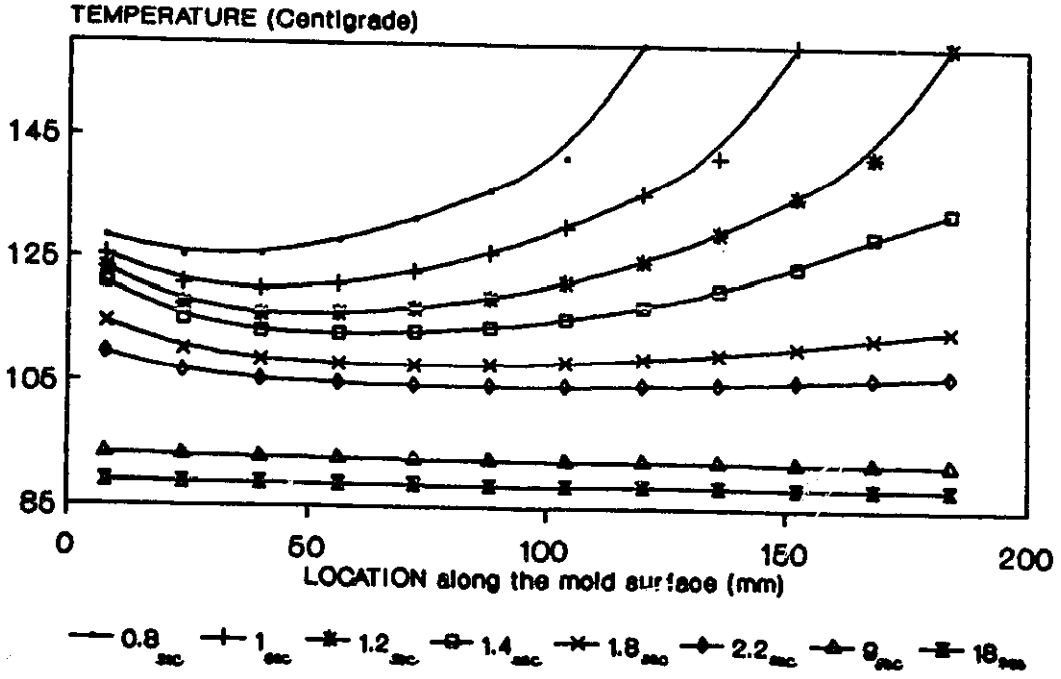

Figure E.II.1 The thermal response of the mold surface at selected locations (Grids 1,3,6 & 12) for an initial mold temperature of 45 C.

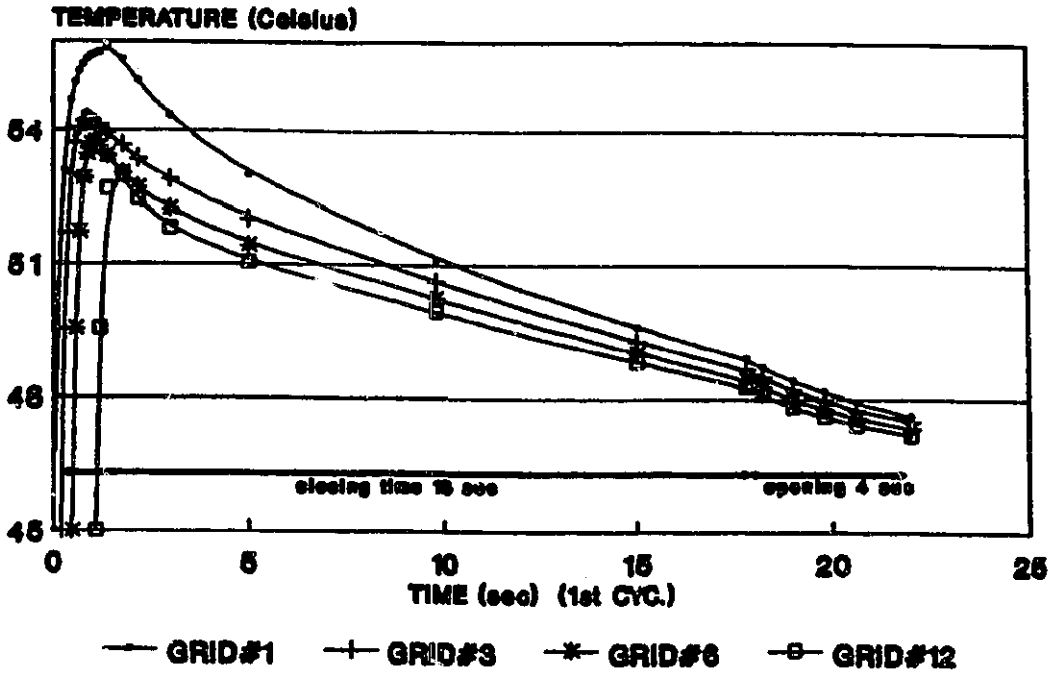

Figure E.II.2 The thermal response of the mold surface at selected locations (Grids 1,3,6 & 12) for an initial mold temperature of 85 C.

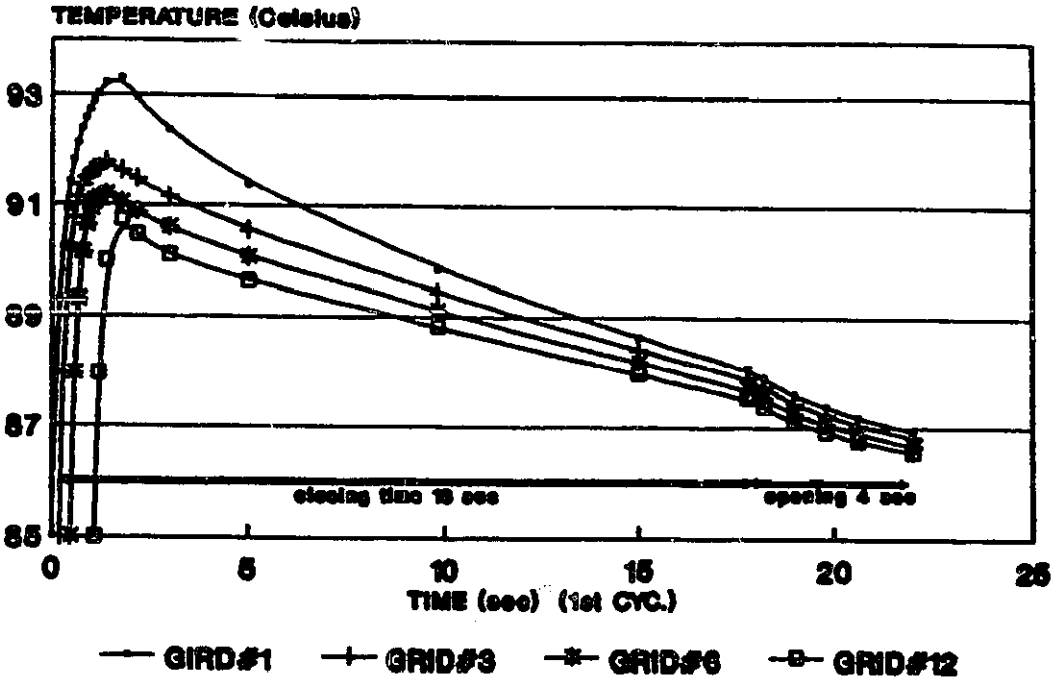

Figure E.II.3 The thermal response of the polymer interface node on Grids 1,3,6 & 12 for an initial mold temperature of 45 C.

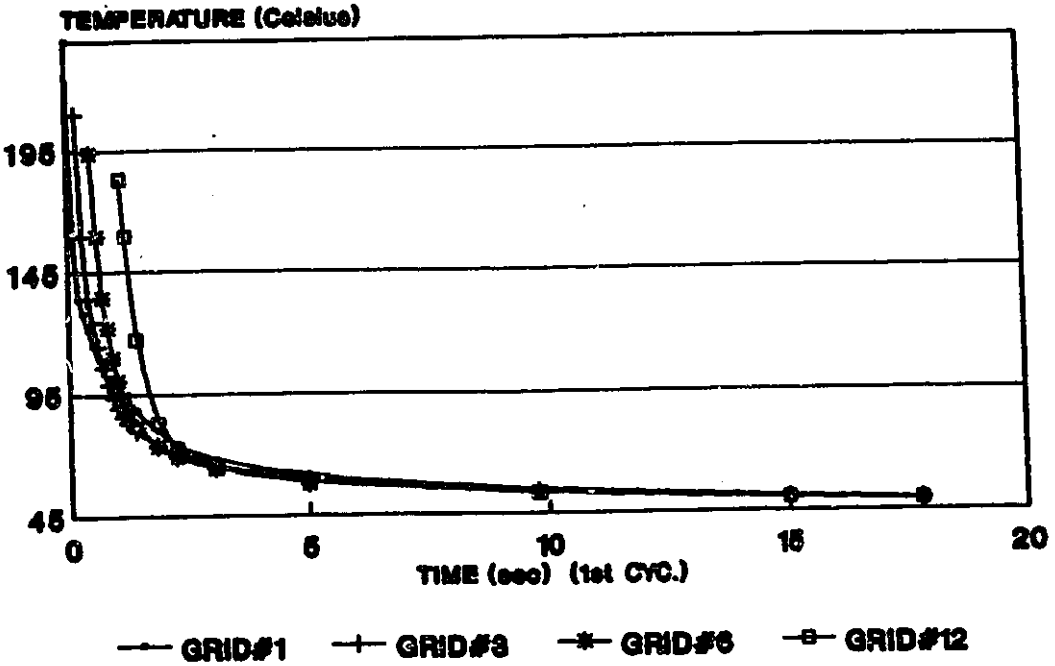

Figure E.II.4 The thermal response of the polymer interface node on Grids 1,3,6 & 12 for an initial mold temperature of 85 C.

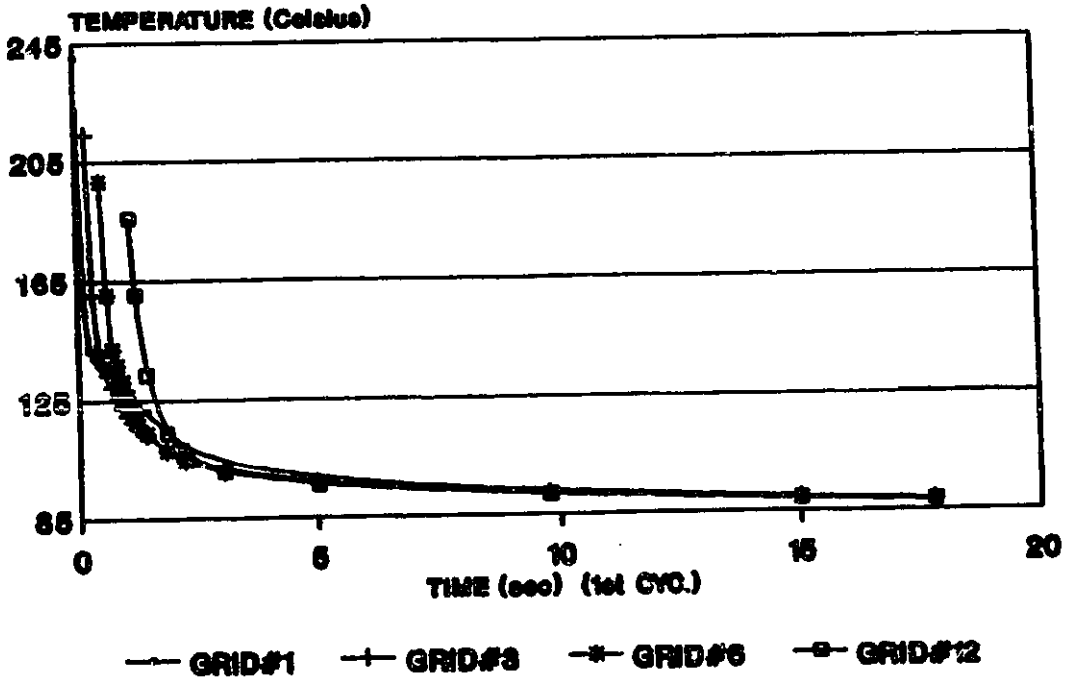

Figure E.II.5 The thermal response of the polymer interface node on Grids 1,3,6 & 12 for an initial mold temperature of 65 C.

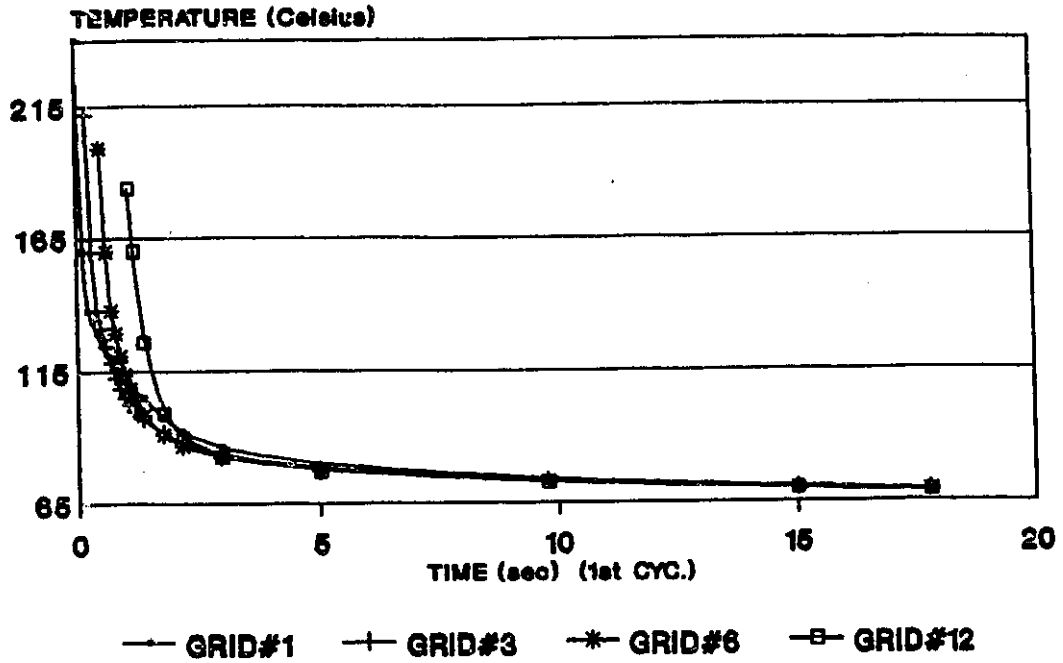

Figure E.II.6 The thermal response of the mold surface at selected locations (Grids 1,3,6 & 12) for an initial mold temperature of 65 C.

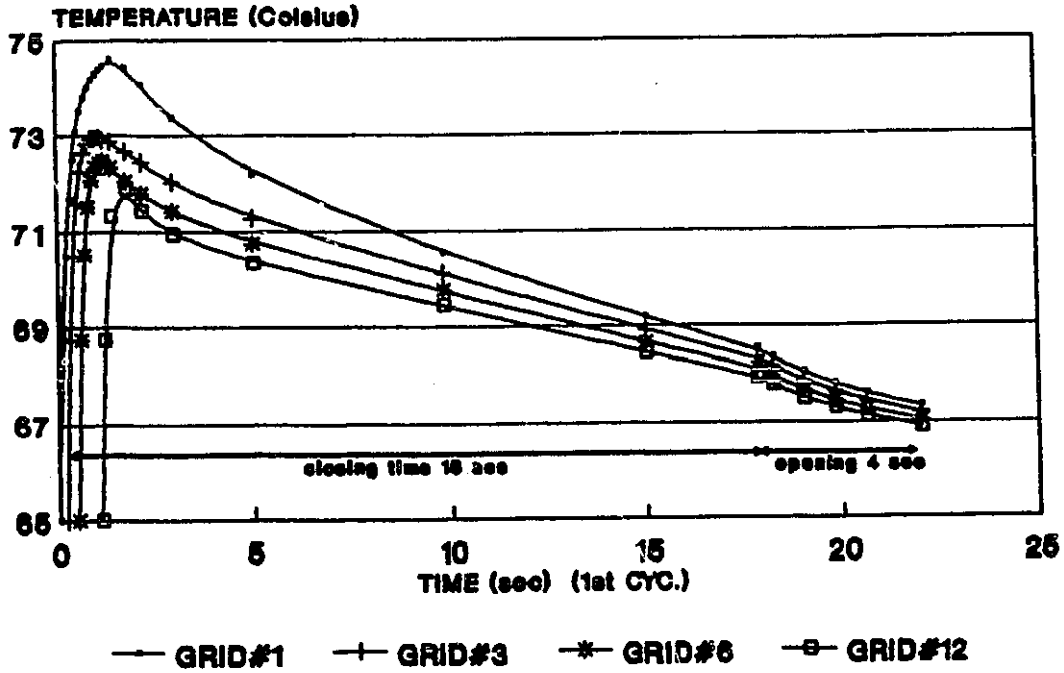

4.3 DISCUSSION OF RESULTS

A general discussion about the basic features of the outputs is made in order to assess the ability of the program and to determine whether or not the model is able to provide some reasonable answers to the main quest of the thesis.

4.3.1 Group A: Transient cyclic behaviour

When cold start up occurs, it takes a number of molding cycles before the mold temperatures throughout the system become repetitive. From Figures A.III.2 and 4 it is apparent that the interface temperatures have stabilized by the sixth cycle. When the interface temperatures have stabilized then all others throughout the plastic will also have stabilized since the interface temperatures are subject to the maximum fluctuations within the system. For the purpose of these results, the fifteenth cycle is used to represent the final periodic steady-state behaviour of the system. This warm up time is about three minutes comparable to that of the work of C.A. Hieber and K.K. Wang in the Ref.[37]. Obviously, the warm up time will be affected by the mold material, total cycle time and the location of cooling lines.

Figures A.V.1 and 2 show comparisons of the overall thermal behaviour of the system at the moment when the cavity is just filled for the first and fifteenth cycles. The temperature level of mold contact surface at the beginning (or end) of a cycle was found to increase three Celsius compared with the initial mold temperature level To (see Figure A.II.2). The mold surface temperature rises rapidly and then gradually falls periodically within a temperature range from 11 Celsius (48 to 59 C) at grid 1 to 8 Celsius (48 to 56 C) at grid 12 (see Figures A.I.2 and 6 and Figures A.III.2 and 4). Figure A.I.8 shows that all of the plastic is solidified in less than 11 seconds. Generally Figures A.I.1 to A.I.8 show us how

fast and how far the heat flux goes from the polymer part through the mold body to the heat sink at To, along the chosen grid lines 1 and 12 during the initial first cycle, and the fifteenth cycle where periodic steady-state has been attained. These temperature profiles indicate that there has been no significant change between the heat flux-time patterns of these molding cycles.

Figure A.II.2 shows the temperature variation along the length of the cavity. Notice that the temperature distribution of the mold surface becomes "equalized" very quickly after the mold cavity is filled up. It may partially be due to the simple geometry of the cavity.

If the molding cycle time is cut shorter, it is expected that the the mold surface temperature will increase, since the mold will have less time to cool. For this case there should be little change in the magnitude of the thermal fluctuation of the mold surface. In practice, the molding cycle time of this case is rather long. For economic reasons, the cycle time should be cut shorter if the quality control of molded parts permits this.

Figures A.II.3 and 4 show that the difference in temperature of plastic surfaces at the time of ejection between the first and fifteenth cycles is negligible. Notice that the cooling rate of the polymer surface during the last 9 seconds of this cycle is relatively very slow compared with that during the first 9 seconds and the temperature variation along the length of the the plastic surface during the last 9 seconds is negligible.

Figures A.III.1 and 3 show that the interface temperature gap, which is caused by the non-perfect thermal contact at the interface, declines nearly exponentially with time when the Hr value is kept constant. At the beginning of a cycle, the

temperature gap is very large and the mold surface temperature shoots up to its peak value, then rolls "down hill" as in Figures A.III.2 and 4, whereas the polymer surface temperature falls dramatically during the first few seconds , then slower and slower during the latter part of the cycle. Notice in Figure A.III.2 and Figure A.II.1 that the mold contact node at grid 1 reaches its peak value in approximately 1.7 seconds. This is about a half second after the filling stage ceases.

Figure A.IV and Figures A.VII.1 to 4 show that the plastic flow field does not change much during the cyclic computations except that the frozen plastic boundary of the 15th cycle is just slightly below that of the 1st cycle as shown in Figure A.IV. Generally the freezing boundary grows nearly linearly with time, Figures A.VI's . During the filling the fastest growth of the solidified plastic layer is not far from the entrance gate. But near the end of the solidification phase, the fastest growing layer is about half the distance along the cavity length from the gate.

Because of the stiffly implicit Euler method used, the freezing boundary growth within a time step will be limited by the liquid node adjacent to the freezing node. The calculation of the growth of the freezing boundary becomes unstable when the physical meaning of the calculation is violated at the latter part of the solidification phase. For this case we set 7 nodes in the liquid region. As this region becomes smaller and smaller, eventually it reaches to the point where all 7 nodes must suddenly solidify for the given fixed time step, this event can not be accommodated in the calculation. Hence, the calculation had to be stopped at a certain point, say the upper limit of the freezing boundary, before the solidification was actually completed to avoid the mathematical instability. This instability

occured when about 85% of plastic domain became solidified. We could "push" the upper limit further toward the central symmetrical line using a smaller time step, or reducing the number of nodes in the plastic liquid in the latter part of the solidification, if it were really necessary.

Figure A.IV shows that the pressure gradient curve has a similar shape to that of the frozen boundary. The maximum value of the pressure gradient occurs a little bit downstream from the location of the maximum thickness of frozen plastic layer. The total area under the pressure gradient curve is the injection pressure at the entrance (the ambient pressure taken as zero).

Generally, for this set of the input values of the Table 1, there is no significant change in the flow field and thermal field within the molten polymer between the first and fifteenth molding cycles.

4.3.2 Group B: Effect of varying the mean injection velocity (V)

In all of these tests carried out, the number of grid lines, the injection speed and the time step used are related by : (grid Size) = (Injection Velocity)(Time Increment). In the "Group B" study of the effect of injection velocity, it was therefore necessary to also modify either the grid size or the time increment. The studies shown in Figures B.I.1 and 2 held the grid size constant.

The result shown in Figure B.I.1 and 2 are contrary to what was expected. A faster injection speed should cause the mold to be a little bit hotter due to higher viscous heating.

As a result the author reran the program with different time steps and numbers of nodes per grid for injection speeds of 0.08 m/s and 0.16 m/s. Figures B.II.1 to B.IV.2 show that the solution of the numerical model is dependent upon the

selection of both the size of time step, and to the nodal spacing. The results of these graphs shows that the solution of the numerical calculation is merely a rough approximation to the exact solution of the simplified model equations in the chapter III. The results are still sensitive to the change in size of time step, and to the nodal spacing. Therefore both these parameters need to be reduced further to achieve a better approximation. The smaller the time step, the better the approximate solution obtained, and more "thermal pictures" of the domain solution will be generated. The greater the number of nodes per grid, the better will be the approximate solution obtained. Because of the restriction upon the virtual memory locations that could be accessed by the author for use, further study could not be carried out. Fortunately, these two factors have opposite shifting effects upon the temperature values of the interface as shown in Fig.B.III and B.IV, therefore it may be possible to obtain an approximate solution very close to the exact solution without using too fine a grid size and time increment. For now, what one can say is that the choice of a proper combination of the time step value and nodal spacing value on each grid is necessary for the effective use of this numerical analysis. How to determine the proper combination is a question that needs further study [50]

There are other ways to improve the approximation. For instance, one can use the unconditionally stable Crank-Nicolson scheme or Alternating Direction Methods to achieve second order accuracy for the transient term on the left-hand-side of equation, (C.3).

Figure B.V shows that a faster injection velocity requires a higher injection pressure even though the flow domain gets "less squeezed" by the thinner frozen

plastic layer in the shorter filling time. There is a non-linear relationship between the injection velocity and injection pressure. It is mainly due to the non-Newtonian characteristics and viscous heating effects of polymer flow. Figures B.VI.1 and 2 show the relative position between the maximum shear rate line with respect to the freezing boundary. The higher the injection speed (V), the larger the separation distance between these two lines. These calculated results can be checked with experimental work on the orientation of polymers. An interested reader can read Appendix F for more details about polymer orientation in injection molded objects.

The isothermal profiles of the total domain are presented in Figures B.VII.1 and B.VII.2 and may be compared with Figures A.V.1 and 2 for a 0.16 m/s injection speed. It is worth mentioning here that some researchers, such as F. Dupret and L. Vanderschuren [20], who worked on the macro-analysis calculation of the temperature field of plastic during the filling stage of injection molding cycle with a similar cavity, had to impose transient boundary conditions on the cavity surfaces and supposed that at some distance "e" away from the cavity surface inside the mold plate, the temperatures was constant and equal to Te in order to avoid any singularity in the temperature field. They located this isothermal temperature boundary (Te) parallel to the cavity surface at a distance "e" from this surface. According to Fig.B.VII.1 and 2, the location of an isothermal temperature boundary relative to the cavity surface is not constant but it depends on how far the heat from the plastic diffuses into the mold plate by the end of the filling time. Hence the longer the filling time , the further away from the cavity surface is the location of the isothermal boundary.

4.3.3 Group C: Effect of varying the cavity thickness (2h)

Notice that the relationship between the injection speed (V) and the volumetric flow rate is: $Q^* = (2h)V$. Therefore, for a thinner cavity, the volumetric flow rate will be smaller if the injection speed is kept constant.

Figures A.II.1, A.II.2 and C.I.1 to C.I.4 show the time-temperature varying patterns of the interface for three cavity thicknesses. Note how much warmer the mold region near the injection gate and the plastic become with the thinner cavities during the early portion of the cycle. This is shown more clearly in Figures C.II.1 and 2 where the transient behaviour of the temperature of the mold surface node at grid points 1 and 12 are shown. In Figure C.II.1 the temperature shoots up to a higher peak value, and then falls faster as the thickness decreases. This higher initial temperature rise is due to higher viscous heating in the thinner cavity. This manifests itself in a frozen layer at this location (Grid 1) that is much thinner for the thinner cavity. At the end grid (12), shown in Fig.C.II.2, the peak value of the curve for 2*(0.5mm) is slightly higher than that of the 2*(0.2mm) curve. This is due to the cooling of the smaller volume of plastic as it flows down the thinner cavity.

The thinner plastic part cools down much faster and the temperature difference between the core and the surface is much smaller after the solidification phase is completed. This can be seen by comparing the temperature difference between the core and the surface of the plastic as a function of time for grid 1 and 12 as shown in figures C.II.3 and C.II.4 respectively.

It is worth mentioning here that an approximate minimum cooling time required to reach a desired ejection temperature for this case can be calculated with the following expression [51]:

$$S = \frac{(2h)^2}{2\pi\alpha} \ln\left[\frac{\pi}{4}\frac{(T_p - T_m)}{(T_x - T_m)}\right] \qquad (4.1)$$

S : minimum cooling time

2h : mold cavity thickness

α : effective thermal diffusivity of plastic (including latent heat)

T_p : injection temperature of plastic melt

T_m : mold temperature

T_x : desired ejection temperature of plastic

Equation (4.1) states that the minimum cooling time is directly proportional to the square of the thickness of molded part. The plots in Fig.C.II.3 and Fig.C.II.4 show the possible and apparent difference in cooling time between these thicknesses. But they should be "magnified" to read their cooling time values at desired ejection temperatures accurate enough to compare with those calculated with the equation (4.1) above.

It is interesting to compare the relative locations of maximum shear rate lines in Fig.C.III.1 to Fig.C.III.3 and those in Fig.B.VI.1, Fig.B.VI.2. For the same injection speed V and with no pressure gradient across the cavity thickness, it is clear that the flow is able to respond to the "squeezing" change in the thickness of the flow path. As the flow path gets narrower, the relative size of the main core flow becomes larger to ease the flow resistance (by viscous effect) which is very high for the narrow flow path, and viscous heating increases thus initially impeding the solidification. The highest maximum value on the locus line is moved downstream, and the variation of the maximum value along the flow is greater when the cavity thickness 2h becomes smaller as shown in Fig.C.III.1 to Fig.C.III.3.

According to the macroscopic calculation for mold filling of an end gated rectangular cavity section, the relationship between the injection pressure and the injection volumetric flow rate is written as follows [51]:

$$P = Q^* \eta \frac{12L}{W(2h)^3} \qquad (4.2)$$

where P is the pressure at mold entrance, Q^* the volumetric flow rate , η is the resin viscosity and L , W , 2h are the mold cavity length, width and thickness respectively. Thus for constant flow rate Q^*, L, W and resin viscosity η, the injection pressure is inversely proportional to the cube of the cavity thickness 2h. In this model, the volumetric flow rate is $Q^* = (2h)V$. Therefore the (4.2) can be rewritten as follows

$$P = V \eta \frac{12L}{W(2h)^2} \qquad (4.3)$$

The output in Figure C.IV shows that the injection pressure (the area under the pressure gradient curve) is nearly inversely proportional to the square of the cavity thickness 2h. The relationship of the two is modified by the non Newtonian characteristics and the thermal field of the flow.

Since the model equations of the plastic domain are in dimensionless form, they allow the effect of changing cavity thickness to be evaluated relatively easily. Therefore the program can carry out its numerical analysis for any value of the mold cavity thickness as long as the molding conditions do not run into a situation of short shots (molten polymer flow gets frozen off before the cavity is filled). This is one of many advantages of using these convenient dimensionless forms.

4.3.4 Group D: Effect of varying the thermal contact conductance (Hr)

Figures D.I.1 to D.I.8 and D.II.1 to D.II.4 show the temperature distribution at the mold/plastic interface as a function of time for thermal contact conductance values equal to 1000.0, 2500.0 and 10,000.0 W/m.m.K. The magnitude of the thermal fluctuation range of the mold surface is about 7 centigrade, 9 centigrade and 15 centigrade degrees respectively as shown in Fig.D.I.1 to Fig.D.I.4. The initial temperature rise of the mold surface is higher and reaches its peak value earlier as the thermal contact value Hr increases, as shown in figures D.II.1 and D.II.2 . If the thermal contact of the interface were "perfect", the mold surface temperature would reach its peak value immediately after the polymer melt reaches it, and would then rapidly decrease. By definition, the two sides of the interface would have the same temperature value for perfect thermal contact.

Notice that the pattern of the post-peak temperature decline of the mold surface is not linear with time. The work of C.A.Hieber, K.K.Wang et al [37] on mold thermal analysis assumed a perfect thermal contact condition and that the temperature decline pattern was linear with time.

The plastic surface cools off very quickly after coming into contact with the mold surface when good thermal contact exists at their interface, as may be seen in figures D.I.5 to D.I.8. The large difference in thermal conductivity between the polymer the mold material partially assists the rapid cooling of the plastic surface although the interior of the plastic part is still rather hot. Good thermal contact is attained by having very good physical contact adherence at the interface. That however can bring about sticking of the plastic parts to the mold surface when the

mold opens. In practice, sometimes good contact conductance must be sacrificed in order to achieve quality control of the molded parts.

It has been suggested that the thermal conductance, Hr, may decrease during the latter part of the cooling stage due to the shrinkage of the plastic. To simulate this effect, the author reran the program with a conductance which was a function of time, denoted as Hr:10,000* in the Figures. The initial Hr value was set at 10,000 W/m.m.K and was then reduced by 3% after each time step of 0.10 sec.. This resulted in a value of Hr of 44 W/m.m.K at the time of ejection of the part. This was an arbitrary choice of Hr variation, but with this program the Hr can be any predetermined function of time . In Fig.D.II.3 and D.II.4, the curves of Hr:10,000* show that the greatly reduced contact conductance over the last 80% of the cycle actually cause the plastic surface to rise in temperature as the interior of the plastic cools. The amount of heat flow from the core of the part to the plastic surface is greater than that taken away by the mold surface in the latter part of the cooling stage.

In Fig.D.III and Fig.D.IV, the relative location of maximum shear rate line with respect to the freezing boundary, and pressure gradient distribution along the flow are as expected. The author expects that the variation of the Hr value will directly influence to the magnitude of the interface heat flux, hence the temperature level of the thermal field, but not the pattern of the temperature distribution of the thermal field.

The results in Fig.D.V.1 when compared with its counterpart Fig.D.I.3 shows that the effect of successive molding cycles is to raise the temperature of the mold interface at the start of the cycle from 45 Celsius to about 48.5 Celsius, and to shift

other temperatures throughout the cycle upwards by a few degrees. Aside from that, the temperature changes are generally similar, and beyond 15 cycles there is no significant change. These temperature shifts are more obvious if we compare Fig.D.V.3 with Fig.D.II.1 and Fig.D.V.4 with Fig.D.II.2. In Fig.D.V.5 and Fig.D.V.6 the curves for the first and fifteenth cycles are superimposed on the same graph and the shift of few degrees is made more obvious.

A similar shift in the temperature calculated for the plastic at the interface can be seen by superimposing Fig.D.V.2 onto its counterpart Fig.D.I.7.

4.3.5 Group E: Effect of varying the initial mold temperature (To)

A comparison of the figures in series E.I and E.II with figures A.II.1 and A.II.3 show the effect of the mold cooling water temperature (To) on the temperature distribution along the interface as a function of time. In general, the temperature level of the temperature-time varying pattern of the mold surface is shifted up for higher initial mold temperatures (To). The higher the initial mold temperature, the smaller will be the peak temperature rise of the mold surface, because of the smaller temperature difference between the melt and the cooling water line, as shown in figures E.II.1, E.II.2 and E.II.6. Also, the magnitude of the thermal fluctuation of the mold surface will be slightly reduced, as shown in Figure A.II.1 and Figures E.I.1, E.I.2.

The conditions that are most favourable for reaching the ultimate shrinkage in the shortest time are relatively high mold temperature and a lower rate of freezing of the molded material. Each material has its own rate of postmolding shrinkage as a function of time. The shrinkage data are available from material suppliers.

4.3.6 Some suggestions for the flow analysis

Upon reviewing all the plots of maximum shearing rate lines along the flow, an effort was made to determine whether or not some dimensionless number or expression could be used to estimate the relative location of the maximum shearing rate line when the molding parameters are changed. The relative size of the high shearing region is a function of the dimensionless numbers: Re and ε, the Reynolds number and the asymptotic parameter respectively. As an analogue with the Newtonian fluid analysis, see equation (4.3), the high shearing stress region is proportional to ε^{2n} . Using an exponential effect for the change in cavity thickness on the relative size of the high shearing stress region compared with that of the main core flow, we can suggest an expression as follows:

$$S_{sh} \propto (1-n)\, e^{-a(1/\varepsilon)^{2n}}$$

Similar arguments can be applied to the influence of Re to develop the following expression:

$$S_{sh} = D(1-n)\left(1-e^{-b(Re)}\right) e^{-a(1/\varepsilon)^{2n}}$$

where S_{sh} is the relative size of the high shearing stress region compared with that of the main core flow. The high shearing stress region is defined as the the distance from the frozen plastic layer to the locus line of the maximum shear rates along the plastic flow. And D, a and b are material factors to be determined by experiment.

Notice that the lines of the maximum shearing rate, the maximum shear stress and the maximum viscosity along the flow are not the same but are nearby one

another and the argument, so far, is confined to the generalized Newtonian fluid with the viscosity law given by equation (3.7). The viscosity is assumed to be not affected by the pressure. Nevertheless, we can extend the program to include the pressure dependence of viscosity if the pressure-viscosity relationship is known.

4.3.7 Possible sources of error in the model analysis

A total error analysis of the mathematical model is not trivial a task and is beyond the scope of the thesis. In order to improve the accuracy of the analysis, we have to be aware of the three main sources of error that come from the algorithm used in the analysis. These are briefly presented here in their order of relative importance according to the author.

1, *Numerical method error.* This source of error is inherent with the discretization process of the model equations into a set of finite difference equations as well as other numerical approximation calculations such as interpolation, numerical integration. There are various ways to reduce this type of error, such as using higher order terms, smaller time steps and smaller spacial increments.

2, *Model simplification error.* This error is the difference between the original mathematical equations and the simplified model equations in chapter III and can be called the truncation error of the model. This error is independent of the numerical method error. It may be estimated with the use of the program inputs and outputs to approximate all the terms in the original mathematical equations, and thus check the validity of the asymptotic approximation assumption.

The simplifying assumptions which are made during the derivation of the model equations have a major role in the limitation of the program analysis. The

conditions for the applicability of these assumptions will be briefly written below in point form :

(1) The Quasi-Steady State and Fully Developed flow assumptions are good for flows with the Reynolds number, Re, very small. In injection molding processes of plastic, the Reynolds number is typically very small.

(2) The asymptotic approximation assumption is the major simplifying step, very good with ε much smaller than unity. If the feedback check of the assumption with the original mathematical equations shows that the effect of some other terms can not be ignored as ε gets larger, an iterative computational scheme can be made to take other additional terms into account for a better approximation of the analysis at the expense of computational time.

(3) For the conditions studied, the molten polymer begins freezing as soon as it comes into contact with the mold cavity wall. This assumption is used to simplify the numerical algorithm which determines when the freezing boundary begins to be taken into account.

(4) The shrinkage of plastic may indirectly affect the thermal field, since the shrinkage can cause the thermal contact value Hr to decrease during the latter part of cooling stage. The shrinkage can be estimated with an equation of state relating P, V and T.

(5) The fountain effect was not taken into account. Several researchers working on the fountain effect during the filling flow reported that the size of the fountain zone is just over 2h, the plastic thickness. Hitherto, the time step values used in the program analysis were too large to sense the fountain effect with the flow front grid during the filling stage.

(6) The isothermal temperature To, or better, a constant heat transfer coefficient Hc of the heat sink is satisfactory for the turbulent flow of cooling medium.

(7) The central symmetrical plane of the model confines the numerical algorithm to the analysis of symmetrical flows only. For the asymmetrical flow, the determination of the flow front shape is a crucial task.

(8) The Power-law of the viscosity is commonly used for many engineering applications of polymeric flows. The exponential effect of temperature on the viscosity η over a wide temperature range is usually a rough approximation for most molten polymers.

In general, all the assumptions made in the thesis are quite satisfactory for the main purpose of the thesis thermal analysis.

3, *Accumulated machine error*. This results from the round-off error of the computing process as the computer carries out the numerical algorithm of the program. This error can be accumulated or random. It can be reduced by using a numerical scheme with the least number of arithmetical computations and/or more memory word locations to store a single value.

4.3.8 Critique of the main program

Successful coding of a computer program should possess these characteristics: clarity and efficiency. This computer coding procedure does not satisfy these two requirements due to the lack of a well prepared program design. The two characteristics depend mainly on the numerical algorithm and the structure of the program. In addition, a knowledge of the functional features of the hardware being used, and a appropriate computer language chosen for coding can help improve

the efficiency of the program. The type of computer used is also important. Some computers have very fast computing speed, but are not as good for data processing of inputs/outputs.

The present program, which has over a thousand lines of Fortran 77 coding, consists of 4 modules in a logical sequence-structure. Each module has its own function, but lacks flexibility due to its "compressed" structure. For flexibility, each module could be decomposed into a number of next level sub-modules. For instance, the Tau 2 subroutine for the filling stage could have the freezing boundary and interpolation computations, the viscosity computation, the coefficient matrix, the pressure gradient, and velocity profile integrations as separate subroutine units to handle these computational functions separately.

The main difference in the numerical algorithm between this program and the others mentioned in the literature review is that it uses a direct solution technique and interpolations instead of the iterative method for the streamline values. It seems that the former should be more efficient than the iterative method. The Gaussian elimination algorithm for solving matrices is not efficient in use of computer memory locations, but it is unconditionally stable. The Gaussian elimination solver can be replaced by an appropriate fast converging iterative solver in order to use main computer memory locations in a more efficient manner. Notice that most of the iterative solvers are conditionally stable and require initially guessed values of the unknowns stored in an input file.

The main weakness of the current program which can affect the program efficiency is that it exhausts the main memory storage of the CPU. It keeps all calculated values of the unknowns in the CPU main memory storage. The

resolution to this weakness is to "dump" all calculated values out of the main storage into a backing storage, such as internal hard disc or external floppy disc/magnetic tape. If the program is to be run with the CMS environment at the computer centre of the University of Windsor, consultants of this facility are available to demonstrate how to handle the dumping job. The graphical outputs of the program can be extended and greater utilization made of the graphical software facility available to a user.

Testing and Validation: To be useful, the model must predict the outcome of physical experiments. Before relying upon the program for design, it must be tested against experimental results. Good experimental work measures all of the inputs quantities required for the program, as well as the outputs. A comparison with an idealised problem tests the accuracy of the numerical method and the correctness of the program. A comparison with experimental results also tests the validation of the mathematical model. Poor agreement with experiments could indicate a problem in the numerical method, the programming or in the model itself. Only a thorough testing program, using a wide variety of cases, can identify and correct the possible errors in the model [53].

Chapter V
CONCLUSIONS AND RECOMMENDATIONS

The original purpose of this study was to set up a computer program which would permit a study of the thermal behaviour of the interface between the metal face of a mold and the molten plastic injected into the mold cavity. To do this, it was necessary to create a program capable of a complete cyclical two-dimensional analysis of both the molten plastic and the mold. In the analysis of this program, there are about ten variables which directly affect the results of the analysis of the program. The effect of varying the injection speed (V), the thickness (2h), the thermal contact conductance (Hr) and the initial mold temperature (To) presented in the thesis make sense and are informative. Unfortunately, the program has not yet been validated against experimental data and hence any of the following conclusions, which are solely based on the program outputs, must be suspect until they are ultimately supported by experimental evidence.

5.1 CONCLUSIONS

1. The interfacial mold surface temperature varies substantially with time throughout each cycle but is less sensitive to variation along the length of the rectangular cavity. The magnitude of the temperature excursion varied from 9^o to 20^o centigrade at the inlet end and from 6^o to 18^o centigrade at the other end of the cavity when the contact conductance was varied from

1 to 10 kW/m.m.K (For temporal and spacial variations, see figures D.V.3 and D.V.4 and figures A.V.2 , B.VII.1 and B.VII.2 respectively).

2. Viscous heating can cause the injected plastic temperature in a thin mold to exceed that of a thicker mold and hence cause higher mold interface temperature excursions (see figures C.II.1 and C.II.3).

3. Increasing the mold cooling water temperature shifts all the temperatures throughout the cycle up, slows down the freezing rate, and decreases the temperature variations (see figures E.I.1 to E.II.6).

4. Increasing the injection rate resulted in a decrease in the interface temperature excursion, an unexpected illogical result. It was subsequently found that the results were sensitive to the choice of time increment and number of nodes selected along each grid line. Decreasing the time interval and increasing the number of nodes had opposite shifting effects on the results. As a result it must be concluded that the numerical values of all of the results are questionable. Unfortunately, because of limited funds and the virtual memory available to the author, further studies could not be carried out.

5.2 RECOMMENDATIONS

1. Carry out further tests to determine a suitable combination of time increment and number of nodes per grid to eliminate the current sensitivity to these values.

2. The validity of the viscosity law should be checked.

Chapter VI
POSSIBLE APPLICATIONS AND FUTURE WORKS

6.1 APPLICATIONS

Suppose that the program analysis works fairly well. What can it be used for ?. The lengthy literature review of CAE packages in injection molding in the Chapter II shows that there are possible applications for this type of program analysis. For the aim of the investigation of the thesis, the possible applications are:

1. For the filling flow analysis, this program analysis can predict the location of the isothermal boundary (Te) which is away from the cavity surface, somewhere inside the mold wall as a function of location of flow pattern and of filling time. Perhaps, this prediction could be made directly by an analytical approach !
2. For the thermal analysis, the program can calculate the amount of heat flow through a non-perfect thermal contact mold/plastic interface as a function of time and position if the thermal contact conductance Hr is a known function of time.

For a constant thermal contact value Hr, the heat flux through the interface at a given point, right after the interface of that point is formed, can be approximated by the following semi-empirical function of time which was developed based on the result generated in this study.

$$\frac{Q''_{interf.}}{Hr} = \Delta T_{interf.} = \frac{(\Delta T)_{init.}}{Cosh\left[\,(ho\sqrt{t})^{m}\,\right]} \qquad Eq.(6.1)$$

$$where \quad ho = \frac{Hr(\kappa_p + \kappa_m)}{\kappa_p \kappa_m}$$

$$\kappa_p = [(\rho Cp)_p k_p]^{1/2}$$

$$\kappa_m = [(\rho Cp)_m k_m]^{1/2}$$

$$(\Delta T)_{init.} = (T_p - T_m) \quad \text{at t = 0.0 sec}$$

$\Delta T_{interf.}$ is the temperature drop across the plastic/mold interface due to a finite value of Hr.

The power index "m" of the argument of the hyperbolic cosine function is adjustable and the subscripts, "p" and "m" in this case, stand for the plastic and mold respectively.

Figures 6.1 to 6.6 show a comparison of $\Delta T_{interface}$ as a function of time calculated using equation (6.1) and by the program.

Suppose that, when the time approaches infinity, the temperature of the molded part approaches the mold temperature To. The total amount of heat flow through the interface must be equal to the heat removed from the molded part. The area under the program curves in Fig.6.1 to Fig.6.6 can used to find out whether the program analysis satisfies the conservation law of energy.

Figure 6.1 The temperature gap at the interface at Grid #1 predicted by the numerical analysis compared with that calculated from Equation 6.1. (Hr=2500 W/m.m.K; m=0.52)

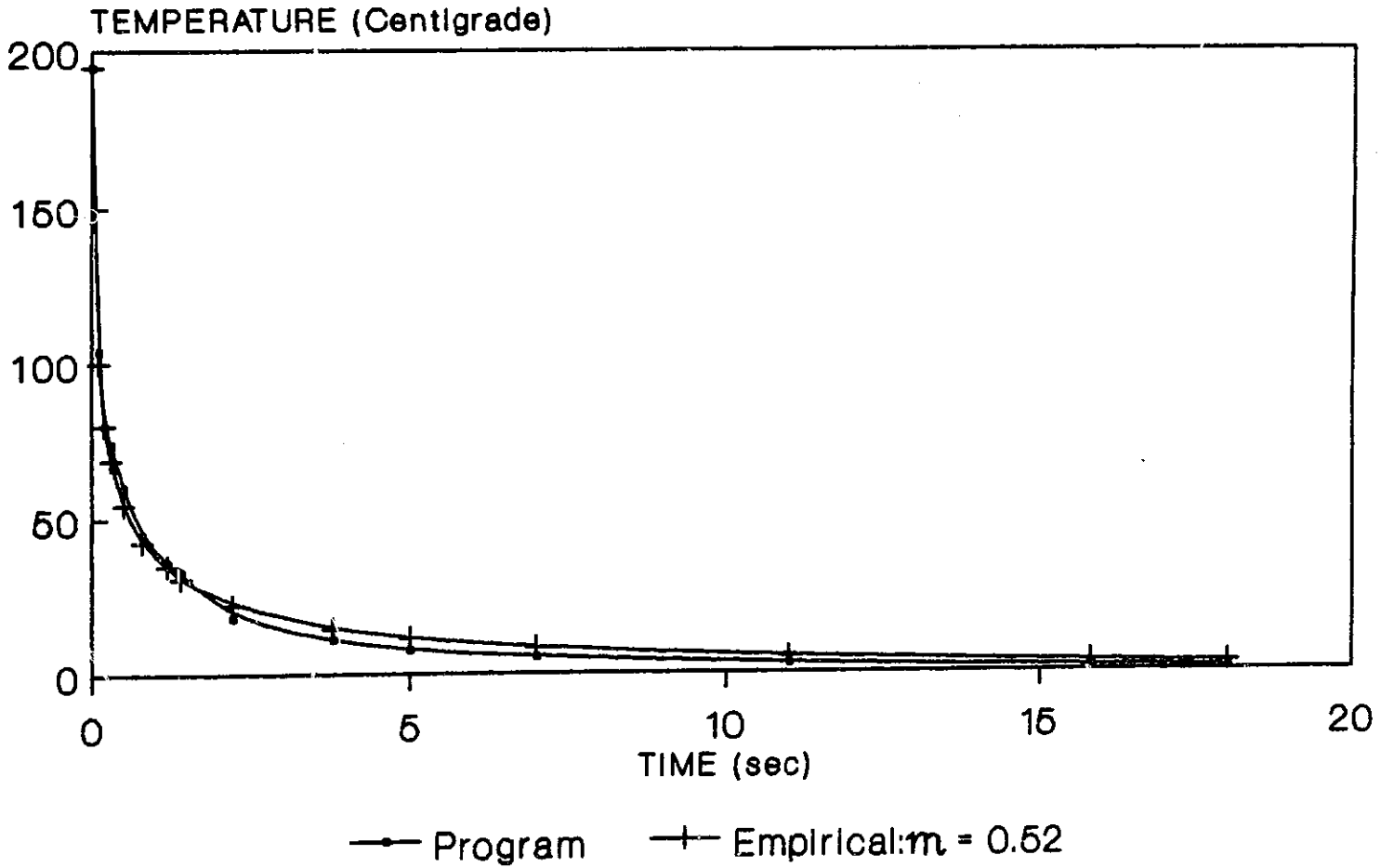

Figure 6.2 The temperature gap at the interface at Grid #1 predicted by the numerical analysis compared with that calculated from Equation 6.1. (Hr=2500 W/m.m.K; m=0.53)

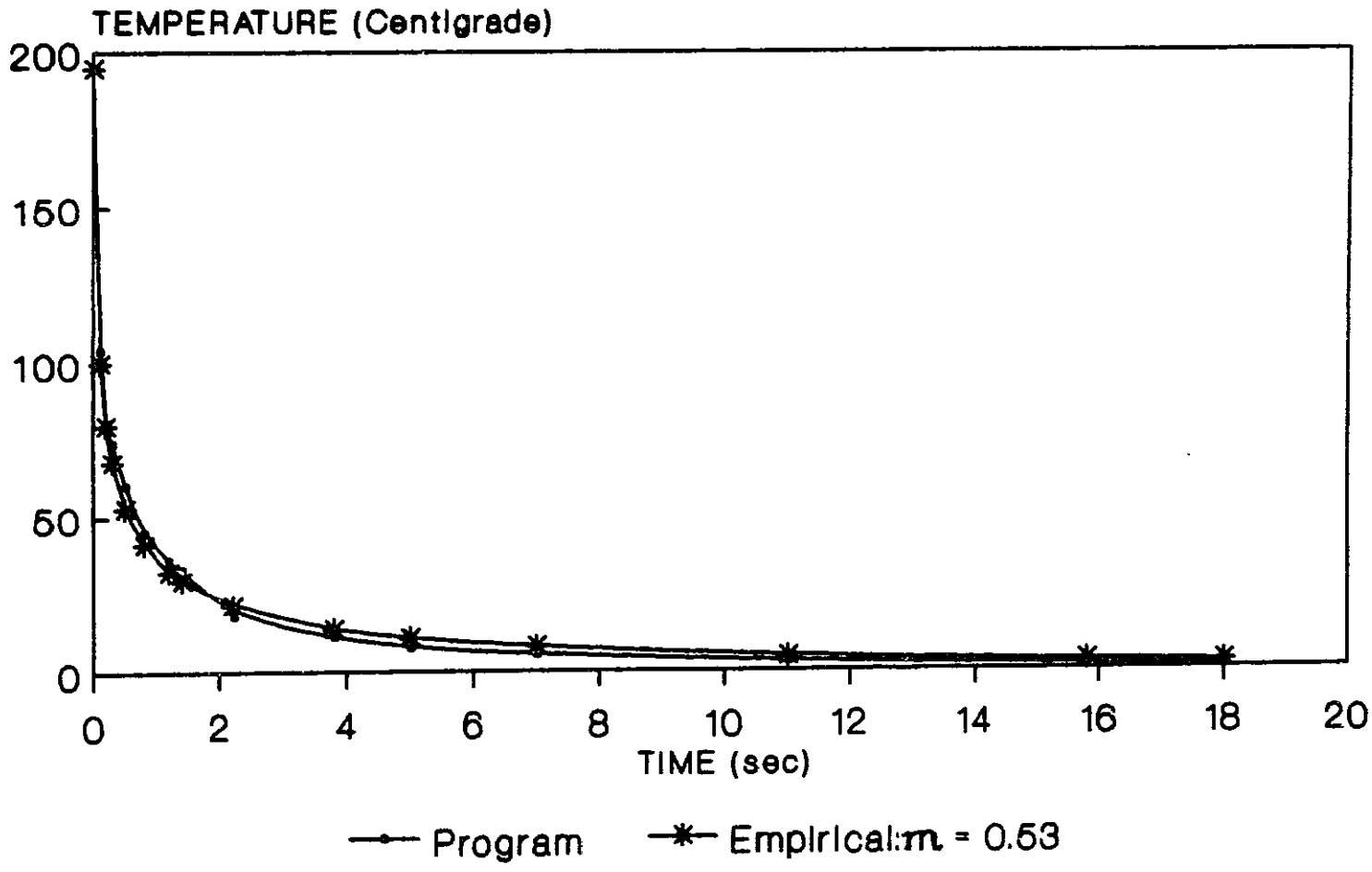

Figure 6.3 The temperature gap at the interface at Grid #1 predicted by the numerical analysis compared with that calculated from Equation 6.1. (Hr=2500 W/m.m.K; m=0.54)

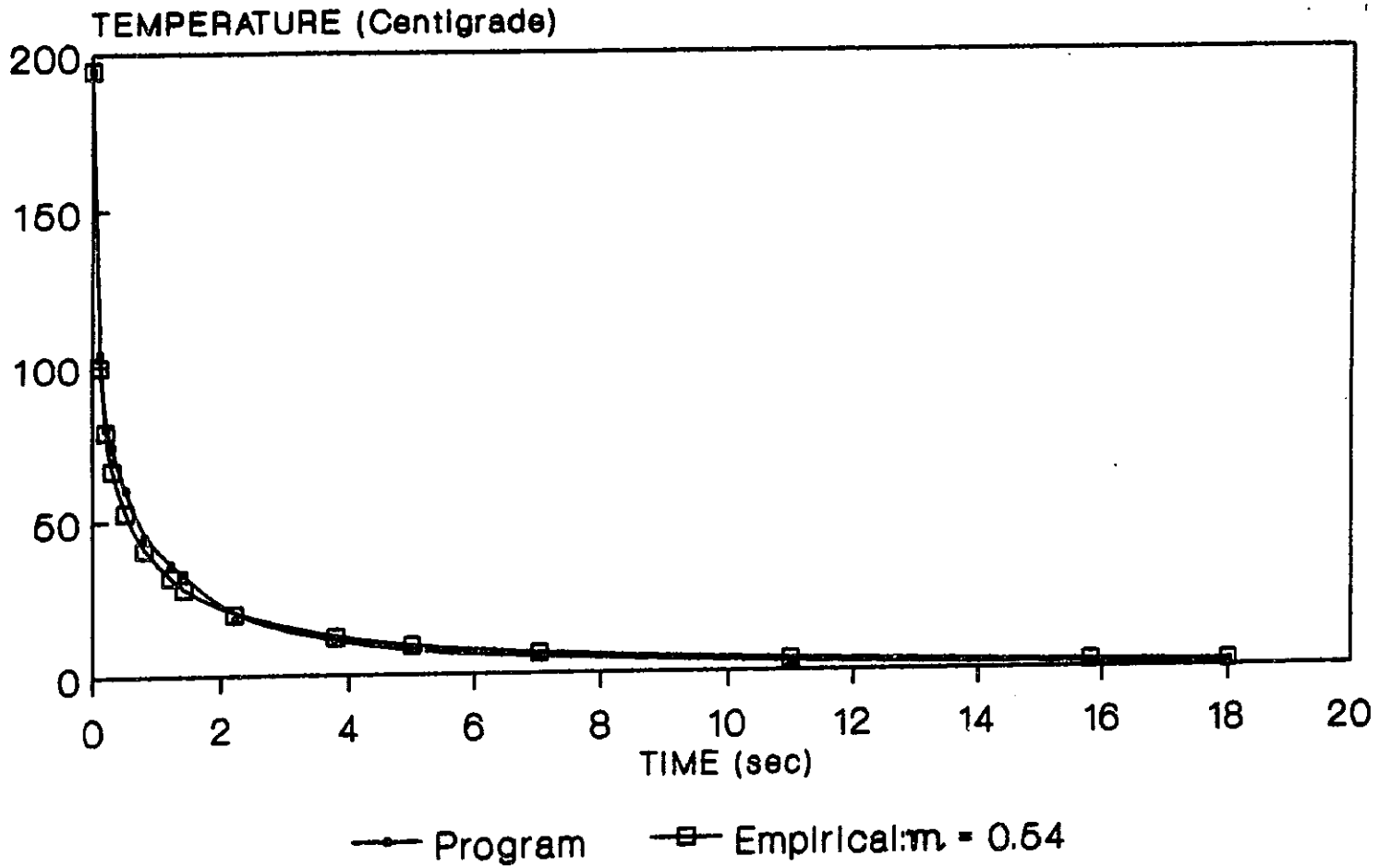

Figure 6.4 The temperature gap at the interface at Grid #1 predicted by the numerical analysis compared with that calculated from Equation 6.1. (Hr=10000 W/m.m.K; m=0.40)

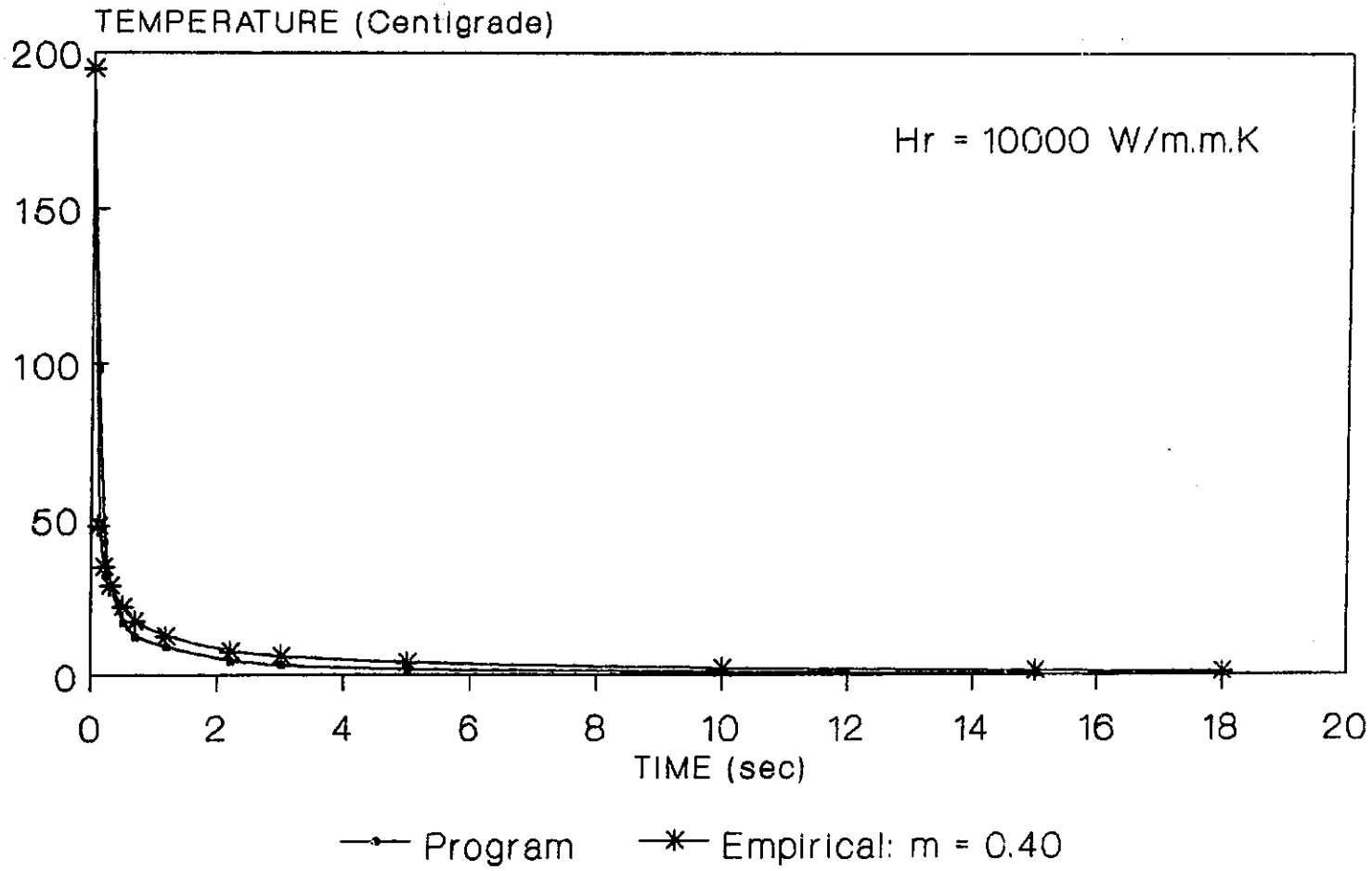

Figure 6.5 The temperature gap at the interface at Grid #1 predicted by the numerical analysis compared with that calculated from Equation 6.1. (Hr=10000 W/m.m.K;n=0.41)

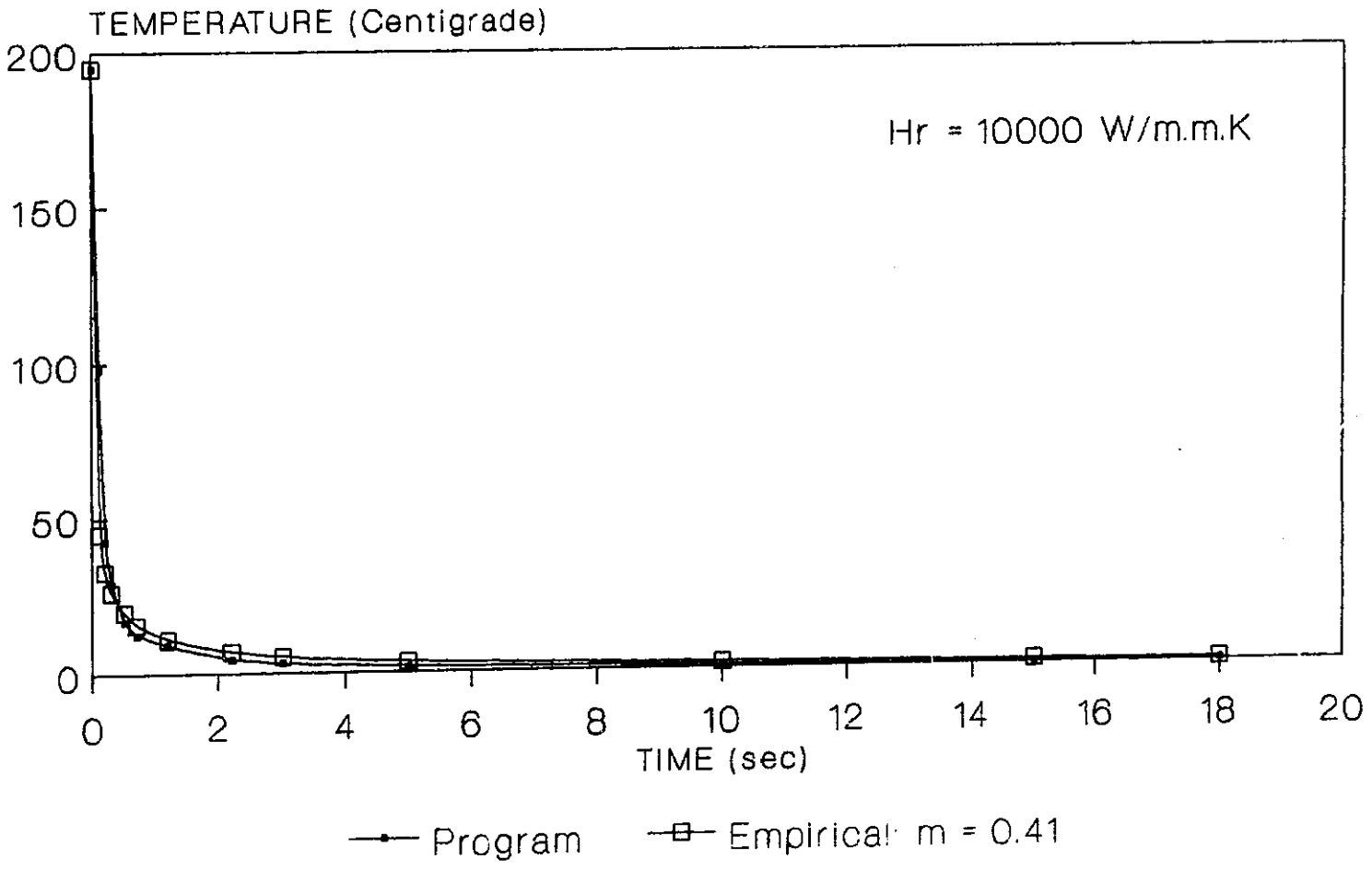

Figure 6.6 The temperature gap at the interface at Grid #1 predicted by the numerical analysis compared with that calculated from Equation 6.1. (Hr=10,000 W/m.m.K; m=0.42)

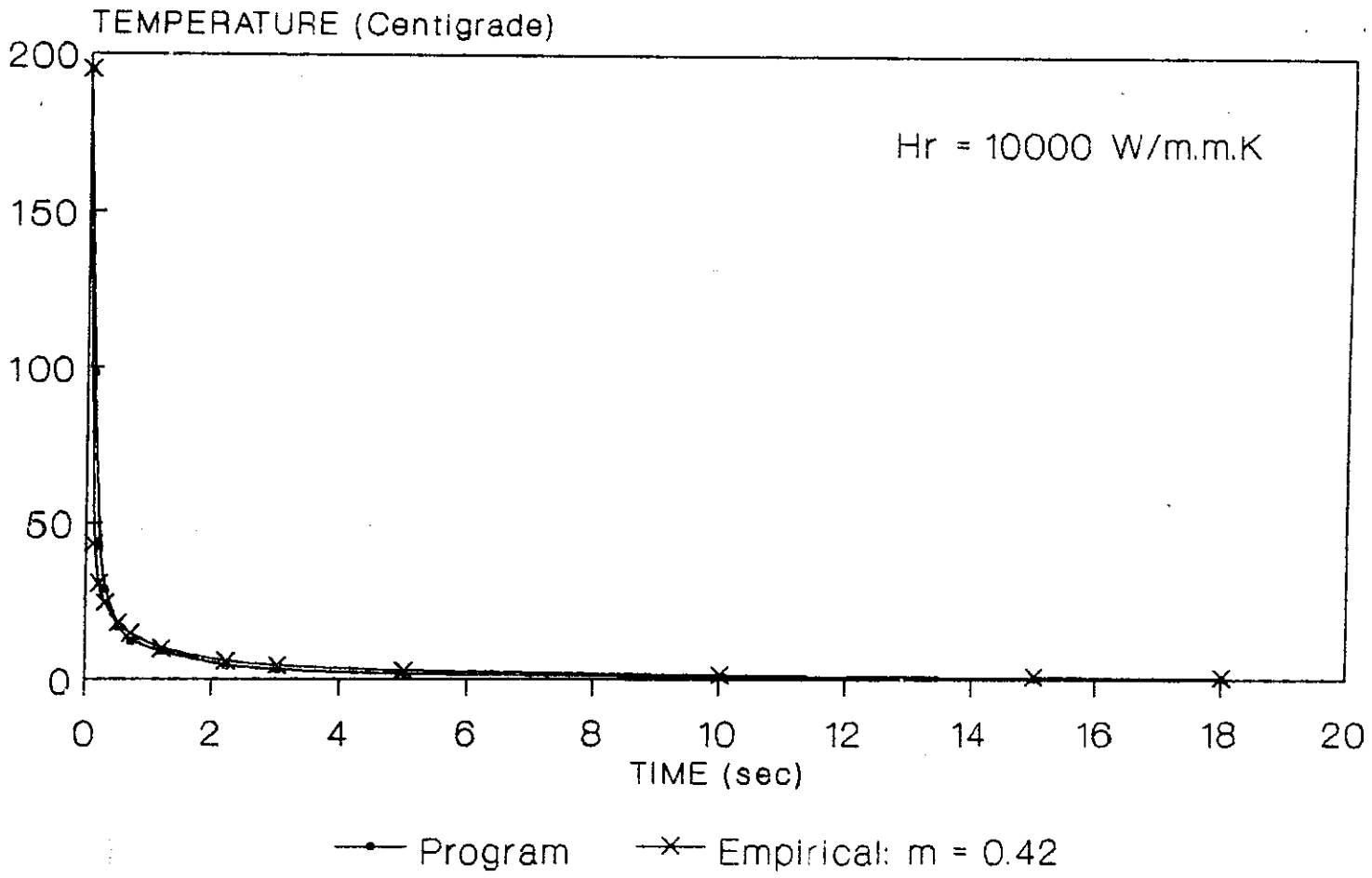

For the conservation of energy, the product of:

(Area under the program curve)(Hr value)

should be equal to the sum of the following terms:

The sensible heat : $(h\ \rho\ Cp)\ (\Delta T)_{init.}$ and the heat of fusion : $(h\ \rho)\lambda$

Usually, The sensible heat term is much greater than the other.

Figures 6.1 to 6.3, for the thermal contact value Hr = 2500.0, show that when the power index m is increased, all the values calculated using Eq.(6.1) decrease. At the first few seconds the temperature gap at the interface calculated by Eq.(6.1) reduces slightly faster than that of the program but after that it is vice versa. The value of the power index m should be chosen so that the areas under these two curves are the same. Similar results between the program and semi-empirical curves are observed in Figures 6.4 to 6.6 for Hr = 10,000.

A few researchers, mentioned in the literature review assuming interface heat fluxes that decline linearly or exponentially with time, do not agree with the program results which are shown in Fig.6.1 to Fig.6.6. The rate of linear decline with time was constant whereas that of the exponential decline was too rapidly. Eq.(6.1) however agreed quite well with the program results and is recommended.

It is possible that the agreement between the Eq.(6.1) curve and the program curve is no longer obtained when the value of the molded part thickness gets larger than some upper limit. Then, an additional factor and/or additional term will be necessary to modify the Eq.(6.1), or it should be replaced by another expression during the latter part of the cooling stage for better curve fitting. To answer this question needs a little further study.

In order to take the non-isothermal effect into account, the heat flow analysis and the filling flow analysis are strongly coupled together for better results. The location of the isothermal line for the mold filling analysis and/or the heat flux through the interface are very important for the coupling of the two analyses while each analysis is carried out as a separate work, independent of the other as in many current CAE injection molding packages do.

Besides that the program analysis has a potential to estimate the degree of orientation of the microstructure of polymers that is very important in quality control, and residual stress analysis of molded parts, and can help establish the optimum total cycle time.

6.2 FUTURE WORKS

6.2.1 Domain decoupling

In the thesis work, a composite solution domain of both the mold and plastic together was carried out. There are several technical disadvantages of such a composite domain that can be overcome by decoupling the domain into two separate ones, the plastic domain and the mold domain. Then one can work on each domain as if each were a separate analysis without losing the coherent features of the composite domain solution.

In the current state of the numerical analysis in injection molding process, the boundary element method (BEM) is a promising means for carrying out a thermal analysis of the 3-D mold part domain. On the other hand, the finite element method (FEM) provides many advantages to carry out the macro-analysis of the filling flow within a 3-D domain with complicated geometry. The finite difference

technique is very handy to analyse the transient heat flow out of the plastic part domain. Thus the domain decoupling approach has many technical advantages in the practical terms. There are various ways to decoupling the composite domain. For this case the author suggest three decoupling schemes that will be briefly presented in the following paragraphs.

(1) The melt and solidified plastic domain are separately analysed by the implicit scheme with the boundary temperatures of the mold side interface nodes kept constant during each time step period. This means that these nodes are perfectly conductive (influx always equals outflux, hence no accumulated heat) for heat flow into the mold body during each time step, so that the decoupling along the mold/plastic interface can be carried out. After solving for the plastic temperatures, we can calculate the heat flux flows out of each of the plastic nodes on the interface. Then these nodal heat flux values are used as the thermal boundary condition imposed upon the mold surface for the thermal analysis of the mold body implicitly. The calculated temperatures of mold side interface nodes at the end of each current time step will be used as the thermal boundary value of the interface for the plastic domain computation in next time step. An iterative procedure can be made to improve the accuracy of the interface heat flux computation. The interactive procedure above can be repeated n times. In this approach of decoupling, we "cheat" a little bit at the interface as we assume that the temperatures of the mold surface are constant during the interface heat flux within each time step.

(2) We use the same approach of decoupling as above but the computations for both plastic domain and mold domain will be carried out by explicit schemes. With this approach, there is no "cheating" problem at the interface. But we have to be careful to consider the stability of the numerical scheme. For a linear problem, the stability criterion is determined by requiring that the coefficient associated with the node of interest at the previous time step is greater or equal to zero. In this case:

$$\left[\frac{1}{\Delta\tau} - \frac{(u^*)^l_{k-1}}{\Delta X} - \frac{2}{Gz(\Delta^l_k \Delta^{l+1}_k)}\right] \geq 0$$

The precise computation of the above condition is not trivial, since we must also pay attention to the nonlinear effects of the problem for the stability.

(3) We can use either the interface heat flux of the program analysis or the simple Eq.(6.1) to impose the thermal boundary condition of heat flux out of cavity surface and onto the mold surface at any location as soon as the interface is formed at that location.

6.2.2 Possible Extend of the Model Development

The informative details of the theoretical background and the numerical analysis presented in chapter II and chapter III can give us some clues about possible research directions into the future of the CAE tools in injection molding technology, and maximum confidence about the capability of the model development up to this time.

The program analysis can be modified and extended in the way we want. The possible extension of the program analysis is mainly dependent upon the research

direction that we aim for. The program analysis has a potential to develop into a more sophisticated numerical analysis.

First of all, the program analysis should be extended to include the case of constant maximum pressure at the entrance gate; the material thermal properties can be function of temperatures. The viscosity law as a function of pressure and the change in density during the phase transformation of plastic are also possible. The utilization of an equation of state, PVT, can be used to compute shrinkage during the latter part of cooling stage. Notice that an accurate and precise calculation of shrinkage should go hand in hand with a residual stress analysis of the molded part. The viscoelastic effect can be taken into account with an appropriate modification of the constitutive equations of σ_{ji} . The fountain effect upon the plastic thermal field only needs a minor modification, whereas the calculation of the shape of the fountain flow zone needs a entirely new numerical algorithm. The chief problem is how to extend the analysis to deal with 3-D domain of arbitrary shapes.

The Macro-analysis of the problem is explicitly desired to accomplish the 3-D analysis of the filling flow as well as the heat transfer. The point is to develop the macro-analysis so that it can cooperate with the micro-analysis of the thesis in order to obtain a more detailed picture of the molding process. It would be useful to access and use some commercial packages and to analyse and learn how they deal with different aspects of the injection molding process. But, in the long term, for the academic interest and the technical advancement of numerical analysis applied to the injection molding industry, we should develop our own numerical algorithms for these analyses in a competitive sense. A devoted research group

with an intimate intercourse between the academic work and the technical demand of the quality control of injection molding processes is definitely needed to build up a better injection molding CAE package.

In the Chapter II, the literature review outlines some of the principal approachs for the macro-analyses. When the author read through the academic papers of the macro-analysis, he had foggy idea about the basic technical steps of the numerical algorithms in these papers as if he were a guy hanging around the conference table around which the researchers were discussing about their simulation works. But, in order to *know precisely how* to design one of these numerical algorithms and to understand better what is going on around the conference table, he had to go ahead and develop one numerical algorithm scheme for the problem on his own. Having done his home work, he is now ready to join the table.

6.2.3 Experimental Works

A physical cavity model of injection molding can be built up, such as the one shown in Figure 3.1, to provide data for a verification of the program. The feasibility of the experimental measurement of the thermal contact conductance value Hr has been considered. An experimental design to locate the isothermal boundary Te for the filling flow analysis is possible. There are several experimental techniques currently used to measure the degree of the orientation of polymers[52]. How fast and how easy it is to set up the experimental work and the reliability of experimental measurements are mainly dependent on the possible facilities available to us. It certainly takes time and costs money to carry out these jobs. Besides that, the experimental data on the properties of polymers commonly used in injection molding industry should be compiled, and verified.

Closure: This thesis work is merely an initial sweeping work paving the way for possible future works leading to a better CAE package. Through the thesis work, the author has gained some experience with numerical dynamic simulation analysis and has learned how to use scientific methods as well as an engineering approach to study and solve some aspects of the physics of an industrial process.

:REFERENCES:

[1] Dominick V. Rosato & Donald V. Rosato, Injection Molding Handbook , Section III, Van Nostrand Reinhold Company, New York (1986).

[2] Louis T. Manzione, " Applications of CAE in Injection Molding", Chapter I, Hanser Publishers, Munich, Vienna, New York (1987).

[3] Ernest C. Bernhardt, G. Bertacchi, A. Moroni, "TMCONCEPT SYSTEM" chapter II in "Applications of CAE in Injection Molding", Edited by L.T. Manzione, Hanser Publishers, Munich, Vienna, New York (1987)

[4] Selcuk I. Guceri, "Finite Difference Solution of Field Problems" chapter 5 in "Fundamentals of Computer Modeling For Polymer Processing" Edited by Charles L. Tucker III, Hanser Publishers (1989)

[5] Colin Austin, "Computer Aided Engineering in Injection Molding" chapter 4 in "Applications of CAE in Injection Molding", Edited by L.T. Manzione , Hanser Publishers, Munich, Vienna, New York (1987)

[6] Colin Austin, "Flow of Plastic Into a Mold", p349-355 in "Injection Molding Handbook" edited by Dominick V. Rosato & Donald V. Rosato, Van Nostrand Reinhold Company, NY (1986).

[7] Thomas E. Burton, Mohsen Rezayat, "POLYCOOL2 A Three Dimensional Transient Mold Cooling Simulator", chapter 9 in "Applications of CAE in Injection Molding", Edited by L.T. Manzione, Hanser Publishers, Munich, Vienna, New York (1987)

[8] Brebbia C.A., Telles J.C.F., Wrobel L.C., Boundary Element Techniques, Springer-Verlag, New York (1984).

[9] Keith R. Schauer, AEC Corporation, p358-381 in Injection Molding Handbook edited by Dominick V. Rosato, Donald V. Rosato, Van Nostrand Reinhold Company, NY (1986).

[10] V.W. Wang, "A CAE Package With High Level Interactive Graphics", chapter 7 in "Applications of CAE in Injection Molding", Edited by L.T. Manzione, Hanser Publishers, Munich, Vienna, New York (1987)

[11] M.R. Kamal, "A Comprehensive, Integrated Computer Simulation of The Injection Molding Process", The McGill University Model(McKAM-II), chapter 9 in "Applications of CAE in Injection Molding", Edited by L.T. Manzione, Hanser Publishers, Munich, Vienna, New York (1987)

[12] W.D. Murray, Fr. Landis, " Numerical and Machine Solutions of Transient Heat Conduction Problems ", Transaction of ASME, Vol.81, p106-112, (1959)

[13] Ozisik, M. Necati, Boundary Value Problems of Heat Conduction, chapters 7 & 13, (1968).

[14] A.A. Tseng, P.F. Sun, S.P. Kolluri, Computer Aided Modeling of Polymer Processing: A Review, ANTEC'89, published by The Society of Plastics Engineers, p267-270

[15] R.B.Bird, E.W. Lightfood, W.E. Stewart; " Transport Phenomena "; chapters 3 & 9, Published by John Wiley & Sons (1960)

[16] R.B. Bird, R.C. Armstrong, O. Hassager; "Dynamics of Polymeric Liquids"; Published by John Wiley & Sons (1977)

[17] H.V. Wijngaarden, J.F. Dijksman and P. Wesseling; " Non-isothermal Flow of A Molten Polymer in A Narrow Rectangular Cavity" J. of Non-Newtonian Fluid Mechanics; 11, 175 (1982)

[18] C.A. Hieber and S.F. Shen, J. of Non-Newtonian Fluid Mechanics, 7, 1-32(1980)

[19] V.W. Wang, C.A. Hieber and K.K. Wang; "Dynamic Simulation and Graphics for the Injection Molding of Three-Dimensional Thin Parts"; J. of Polymer Engg., 7, No.1, p21-45, (1986)

[20] F.Dupret and L.Vanderschuren, AIChE J., 34, No.12, (1988)

[21] A.Couniot, L.Dheur, O.Hansen and F.Dupret, Numiform 89,Thompson et al. (eds.), p235-241, 1989 Balkema, Rotterdam.

[22] M.R.Kamal, S.K.Goyal, E.Chu, AIChE J., 34, No.1, (1988)

[23] Shan-fu Shen, Numiform 89, Thompson et al eds., p55-63, 1989 Balkema, Rotterdam.

[24] D.J.Coyle, J.W.Blake, C.W.Macosko; "The kinematics of fountain flow in mold-filling"; AIChE J., 33, No.7, p1168-1177, (1987)

[25] J.M.Castro, C.W.Macosko; "Studies of mold filling and curing in the reaction injection molding process"; AIChE J., 28, No.2, p250-260, (1982)

[26] J.S.Yu and D.M.Kalyon, A.H.Wagner; "Simulation of Microstructure Development in Injection Molding of Amorphous Engineering Plastics"; ANTEC'89, p281-285

[27] A.H.Wagner, J.S.Yu and D.M.Kalyon; "Orientation and residual stress distributions in injection molded engineering plastics"; ANTEC'89, p303-307.

[28] A.Davidoff, S.C.Schen, H.Bung; "PROCOP_ An advanced 2D and 3D flow simulation package in injection molding"; ANTEC'89, p295-298.

[29] A.Garcra-Rejon, G.Salloum, P.Girard and A.Vinet; "Modeling of the filling and cooling stages in thin wall injection moulding"; ANTEC'89, p348-351.

[30] M.Sobhanie and A.I.Isayev; "Two Dimensional Viscoelastic Simulation of Injection Molding of Thermoplastic Materials"; ANTEC'89, p286-290.

[31] P.Singh and M.R.Kamal;"Analysis of the Crystalline Morphology of Injection Molded Short Glass Fiber Polypropylene"; ANTEC'89, p235-239

[32] E.Chu, M.R.Kamal and S.K.Goyal; "A Computer Simulation of The Injection Molding Process Including Filling, Packing and Solidification" ANTEC'89, p344-347.

[33] W.Dietz, J.L.White, E.S.Clark; "Orientation Development and Relaxation in Injection Molding of Amorphous Polymers"; Polymer Engineering and Science; 18, No.4, p273-281, (1978)

[34] K.Palit and I-J. Chen; "How to Assess CAE Injection Mold Design Softwares for Production Applications"; ANTEC'89, p356-359.

[35] G.A.Campbell, H.Devanathan, T.Kenny, J.D.Small and A.L.Fricke et al; "The effect of injection molding parameters on the properties of molded parts"; ANTEC'89, P312-315

[36] J.L.S.Wales, J.V.Leeuwen, R.V.Der Vijgh; "Some Aspects of Orientation in Injection Molded Objects"; Polymer Engineering and Science; 12, No.5, p358-363 (1972)

[37] K.Himasekhar, C.A.Hieber and K.K.Wang; "Computer-Aided Design Software for Cooling System in Injection Molding"; ANTEC'89, p352-355.

[38] H.J-Kriegl; "Injection Molding of Plastics: II. Analytical Solution of Heat Transfer Problem"; Rheol.Acta 18, p693-701, (1979)

[39] S.M.Richardson; "Injection molding of thermoplastics: Freezing during mould filling"; Rheol.Acta 22, p223-236, (1983).

[40] E.T.Severs, Polymer Rheology, Reinhold Publishing Corporation, New York, 1962.

[41] Methods of Experimental Physics of Polymers; Vol.16, Part C; edited by R.A.Fava-Marton, Academic Press (1980).

[42] A.E.Lever, J.A.Rhys; "The Properties and Testing of Plastic Materials"; p158-192, CRC Press, (1968).

[43] Carslaw H. S. and J. C. Jaeger ; Conduction of heat in solids 2nd Ed., Oxford, University Press, London, pg89 (1959)

[44] R. B. Bird, R. C. Amrstrong, O. Hassager ; Dynamics of Polymeric Liquids ; Wiler, NY., Ch. 1 & 5 (1977)

[45] F. Neuwmann, C. P. Frank, and R. Von Mises ; Die Differential und Integral Gleichungen der Mechanik und Physik ; Vol.2 Viewg, Braunschweig 1927.

[46] Anthony , Ralston ; A first course in numerical analysis Publisher: McGraw-Hill Book company , Ch.: 3 & 8 (1965)

[47] Injection Moulding Handbook edited by Dominick V. Rosato and Donald V. Rosato ;Ch: 11; Van Nostrand Reinhold company INC. NY.1986

[48] T. E. Shoup, Applied numerical methods for the microcomputer Prentice-Hall, INC., Englewood Cliff ; Ch:6 (1984)

[49] S. M. Richardson ; Injection thermal plastics: freezing during mould filling ; Rheol. Acta 22, 223-236 (1983).

[50] Charles Tucker III; Fundamental of computer modeling for polymer processing ; Hanser Publisher (1989); Ch.V, section.5.4 & Ch.VIII.

[51] Glanvill A. B., The Plastics Engineer's Data Book. Machinery Publ. Co. ,1971.

[52] J.L.S Wales, J. Van Leeuwen and R. Van Der Vijgh; some aspects of orientation in injection molded objects ; Polymer Eng.& Sc. Vol.12, No.5

[53] Charles Tucker III; Fundamental of computer modeling for polymer processing ; Hanser Publisher (1998); Chater VIII.

Appendix A

Some Results of The Third Preliminary Study:

Fig. F.a1 & F.a2 : The thermal distribution of the mold part 181

Fig. F.b1 & F.b2 : The thermal distribution of the plastic part .. 182

Fig. F.c1 & F.c2 : The thermal history of contact nodes and symmetrical node 183

Fig. F.d : The freezing plastic front position Vs. time 184

THE THERMAL DISTRIBUTION OF THE MOULD
PART DURING THE 1st COMPUTATIONAL CYCLE
(To = 25 C ; Hr = 2000 W/m.m.K)

Fig.F.a1

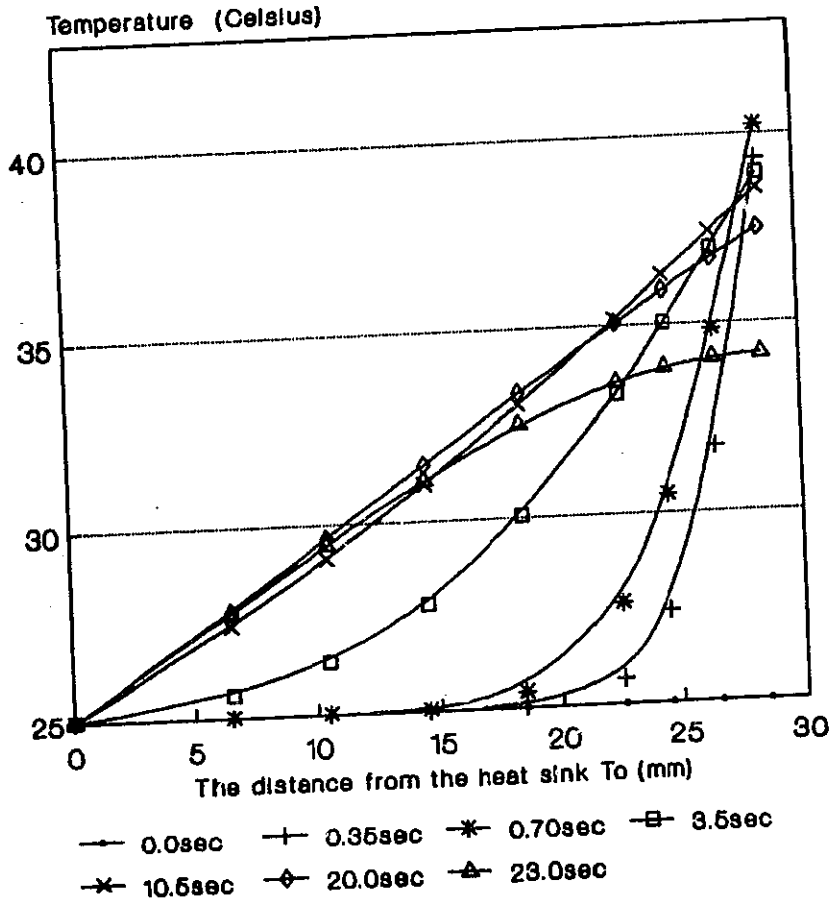

THE THERMAL DISTRIBUTION OF THE MOULD
PART DURING THE 15th COMPUTATIONAL CYCLE
(To = 25 C ; Hr = 2000W/m.m.K)

Fig.F.a2

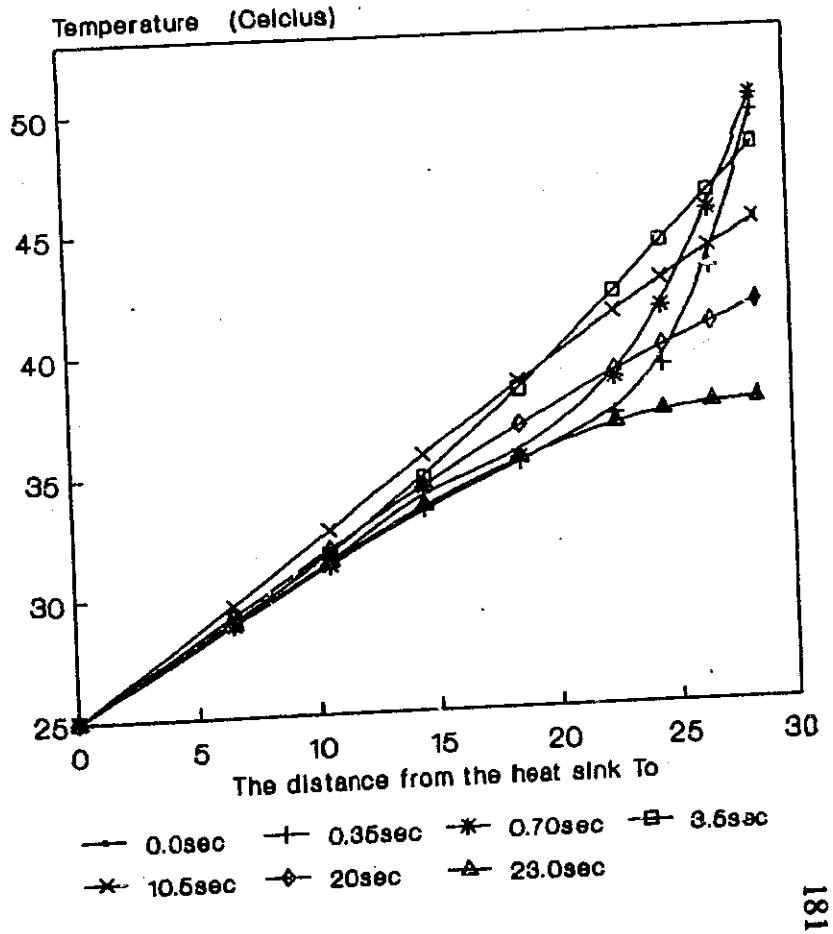

THE THERMAL DISTRIBUTION OF THE PLASTIC
PART DURING THE 1st COMPUTATIONAL CYCLE
(Tp = 265 C ; Hr = 2000W/m.m.K)

Fig.F.b1:

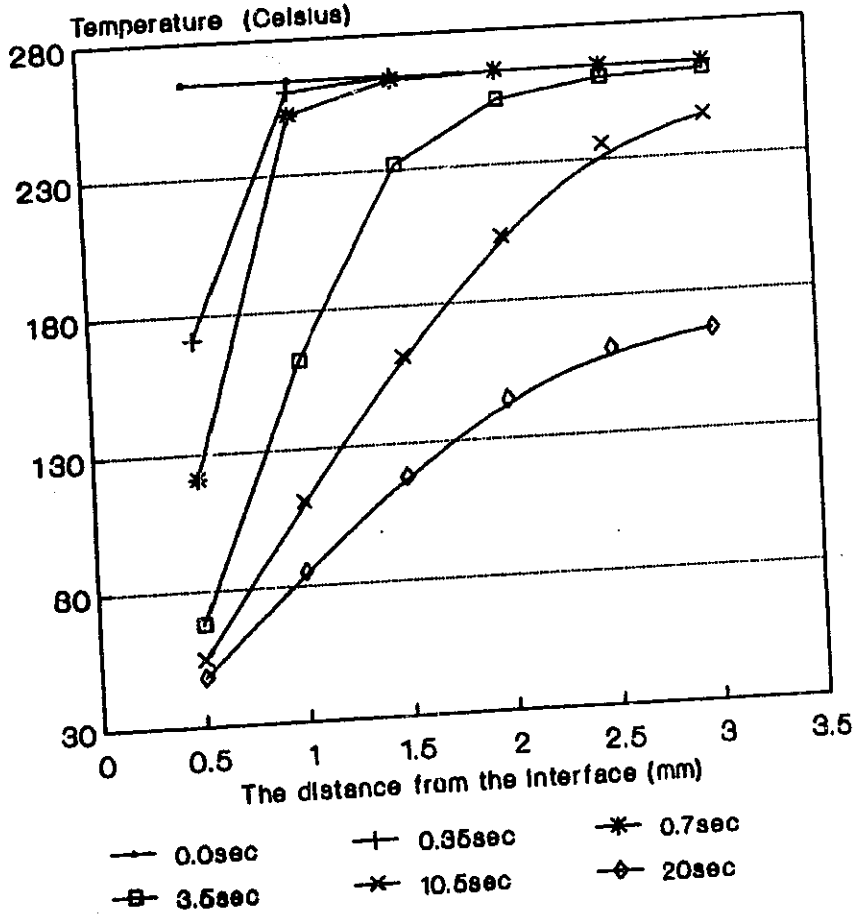

THE THERMAL RESPONSE OF THE PLASTIC PART
DURING THE 15th COMPUTATONAL CYCLE
(Tp = 265 C ; Hr = 2000W/m.m.K)

Fig.F.b2

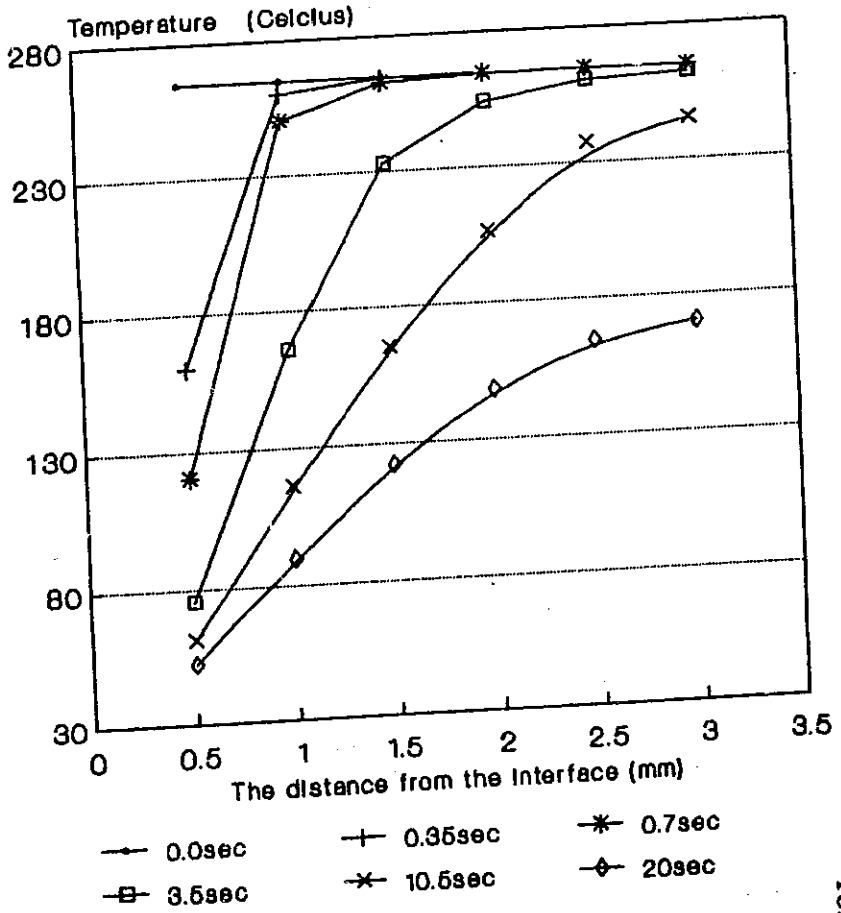

THE THERMAL HISTORY OF THE MOLD
INTERFACE DURING THERMAL CYCLES

Fig.F.c1:

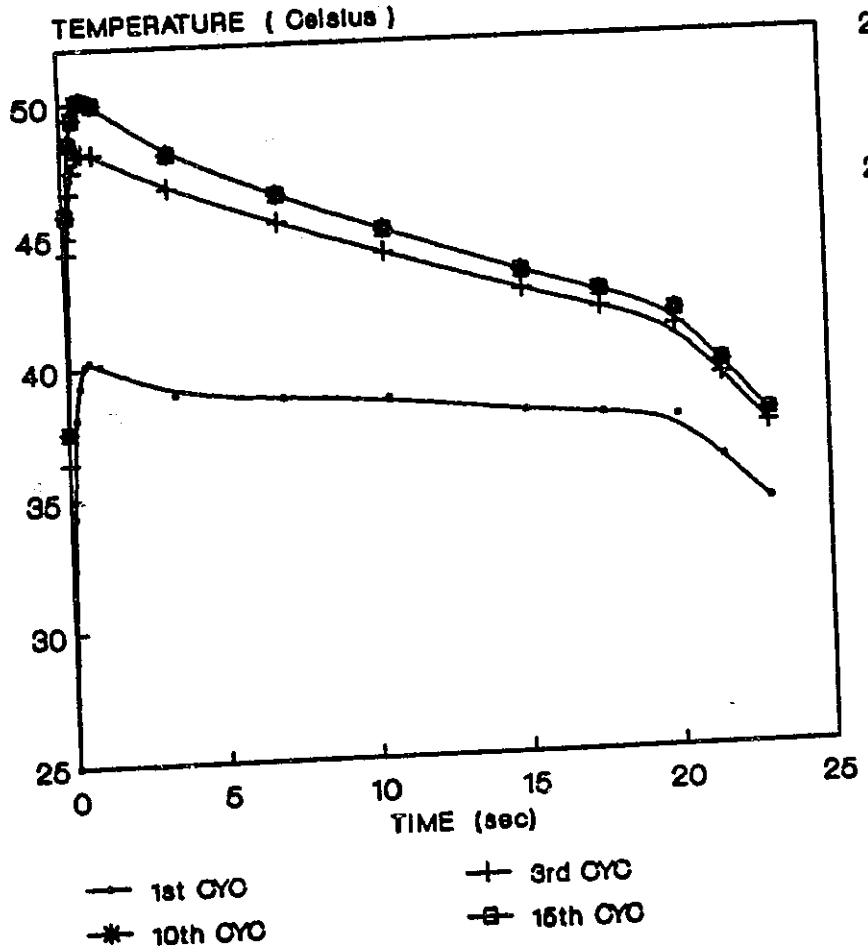

THE THERMAL HISTORY OF THE PLASTIC
INTERFACE AND ADIABATIC NODES

Fig.F.c2

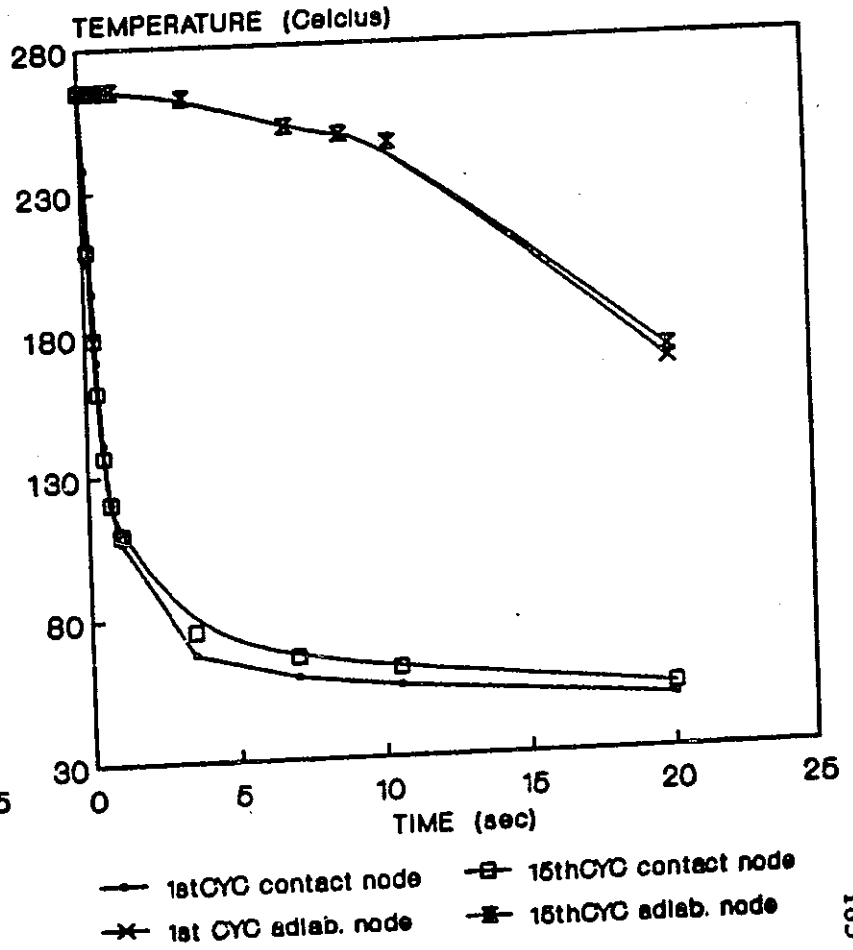

FREEZING FRONT POSITION VS. TIME
DURING THE 1st & 15th CYCLES

Fig.F.d

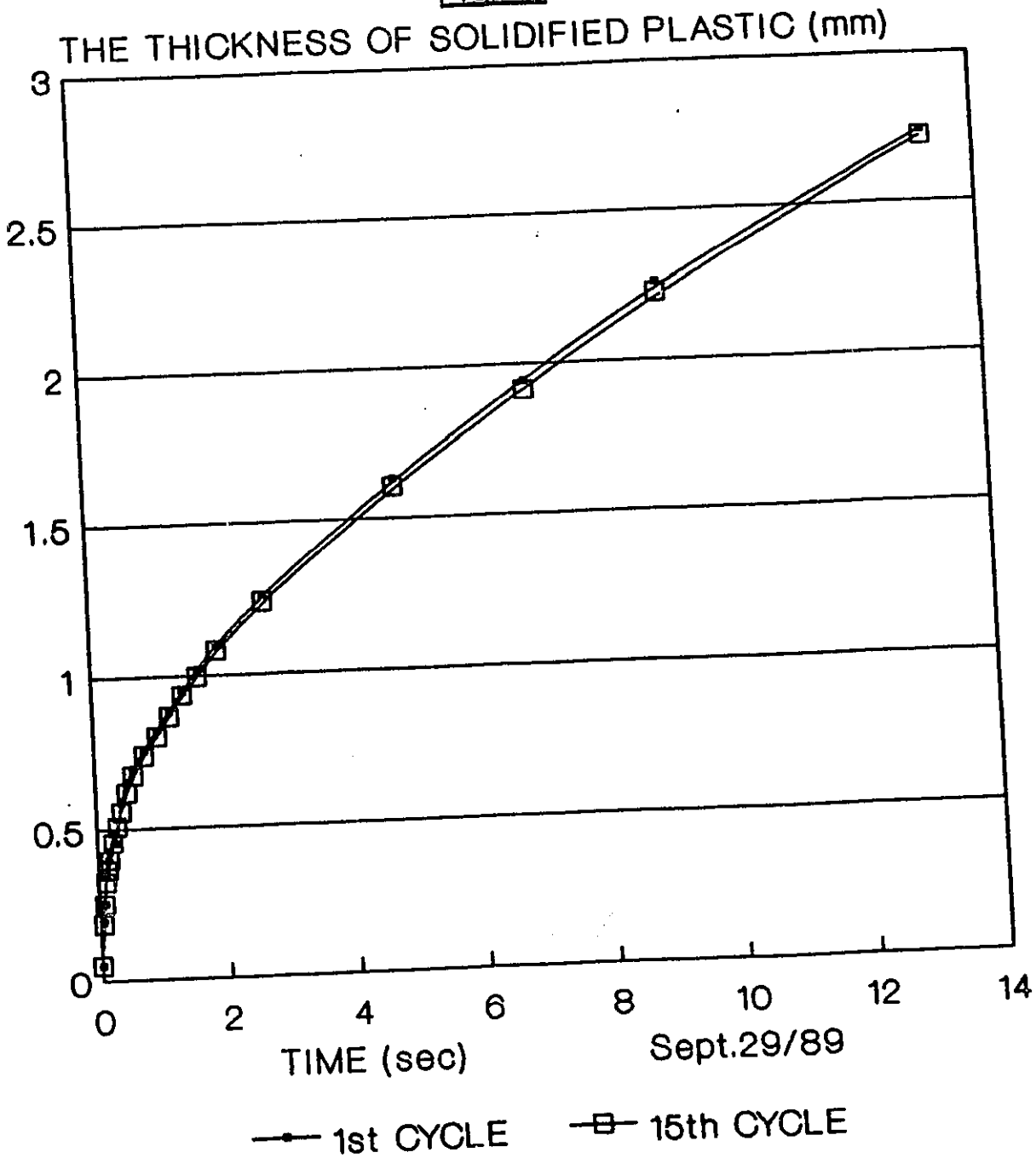

THE INPUTS OF THE PROGRAM OF THE THIRD STUDY:

(in SI units)

```
READ*, Tm, Tp, Tf, Thm, Thp
READ*, Km, Cpm, Dm,  Kp, Kps,  Cp, Cps,  Dp,Dps
READ*, Hr, Hc, LH,
READ*, Time, OPen, Tair
```

THE DATA FILE

```
25.0,  265.0,  245.0, 0.00275, 0.02825
58.0,  440.0, 7860.0, 2*0.280, 2*1270.0, 2*1360.0
2000.0, 20.0, 10000.0
20.0,   3.0,  25.0
```

THE DESCRIPTION OF THE INPUTS VALUES:

```
c   Tm :  initial mould temperature
c   Tp :  initial plastic temperature
c   Tf :  fusion temperature
c   Thm :  mould thickness
c   Thp :  plastic thickness
c   Km  :  mould thermal conductivity
c   Cpm :  mould specific heat capacity
```

```
c   Dm  :  mould material density
c   Kp, Kps : plastic thermal conductivities of liquid & solid
c   Cp, Cps : plastic specific heat capacities of liquid & solid
c   Dp, Dps : plastic densities of liquid & solid respectively
c   Hr  :  thermal contact conductance at interface
c   Hc  :  heat convection coefficient of surrounding air
c   LH  :  latent heat of fusion
c   Time : the time of mould/plastic contact
c   Open : the time of mould/plastic detach
c   Tair : surrounding air temperature
```

Appendix B
The Approximation of Thermal Contact Conductance Value Hr

If one assumes an average air gap δ at the Mold/Plastic interface. The amount of heat flow through this air gap is due to two main mechanisms as follows:

B.1 The Radiation Across The Interface Air Gap:

$$Q_r^{"} = \frac{\sigma(T_p^4 - T_m^4)}{\frac{1}{\varepsilon_p} + 1 + \frac{1}{\varepsilon_m}} = H_{R_r}(T_p - T_m) \quad Hence: \quad H_{R_r} = \frac{\sigma(T_p + T_m)(T_p^2 + T_m^2)}{\frac{1}{\varepsilon_p} + 1 + \frac{1}{\varepsilon_m}}$$

The subscript p and m in this case stand for the plastic and mold respectively. $Q_r^{"}$ is the heat flux due to radiation; H_{R_r} is the contact conductance due to radiation; σ is the Stefan-Boltzmann constant = $5.67\times10^{-8}\ W/m^2\ K^4$, and ε_p and ε_m are the emissivities of plastic and mold surfaces respectively. The additional one at the denominator is the view factor for parallel plates.

B.2 The Conduction Across The Interface Air Gap:

$$Q_c'' = k_a \frac{\partial T}{\partial y} \approx k_a \frac{(T_p - T_m)}{\delta} = H_{R_c}(T_p - T_m) \quad where \quad H_{R_c} = \frac{k_a}{\delta}$$

Q_c'' is the heat flux due to conduction; H_{R_c} is the contact conductance due to conduction; k_a is the thermal conductivity of the micro air gap.

For example, if $\delta \approx 5\times10^{-6} m$ *and* $k_a \approx 34\times10^{-3}$W/m.K, then H_{R_c} is approximately 6800 W/m.m.K. And if $T_p = 200\ Celsius$, $T_m = 50\ Celsius$, $\varepsilon_p = \varepsilon_m = 4/5$, then H_{R_r} approximately about 0.3 W/m.m.K.

Letting: Hr = $H_{R_c} + H_{R_r}$, The physical value of H_{R_r} is usually about four orders smaller than that of H_{R_c}, therefore we can assume that: Hr $\approx H_{R_c}$

The value of δ, the interface gap, is obviously a function of mold pressure, surface roughness.

Appendix C

The Simplified Freezing Boundary Condition

Equation (3.8) used to derive the equation (3.25) as follows:

$$\lambda \rho v_n = k_s \frac{\partial T_s}{\partial n} - k \frac{\partial T}{\partial n} \qquad (3.8)$$

$$= \left(k_s \frac{\partial T_s}{\partial x_1} - k \frac{\partial T}{\partial x_1} \right) n_{x_1} + \left(k_s \frac{\partial T_s}{\partial x_2} - k \frac{\partial T}{\partial x_2} \right) n_{x_2}$$

$$= n_{x_2} \left[\left(k_s \frac{\partial T_s}{\partial x_1} - k \frac{\partial T}{\partial x_1} \right) \frac{n_{x_1}}{n_{x_2}} + \left(k_s \frac{\partial T_s}{\partial x_2} - k \frac{\partial T}{\partial x_2} \right) \right]$$

$$= (1 + \delta'^2)^{-1/2} \left[(-\delta') \left(k_s \frac{\partial T_s}{\partial x_1} - k \frac{\partial T}{\partial x_1} \right) + \left(k_s \frac{\partial T_s}{\partial x_2} - k \frac{\partial T}{\partial x_2} \right) \right]$$

$$= (1 + \delta'^2)^{-1/2} \left[\left(-\delta' \frac{\partial}{\partial x_1} + \frac{\partial}{\partial x_2} \right) (k_s T_s - k T) \right]_{x_2 = \delta} \qquad (C.1)$$

Where: $\delta' = \partial \delta / \partial x_1$

The dimensionless form of equation (C.1) is

$$\frac{v_n}{V} = \varepsilon \frac{Ste}{Gz} (1 + \varepsilon^2 \alpha'^2)^{-1/2} \left(-\varepsilon^2 \alpha' \frac{\partial}{\partial x} + \frac{\partial}{\partial y} \right) \left(\frac{k_s}{k} \theta_s - \theta \right)_{y = \alpha} \qquad (C.2)$$

where $\alpha' = \partial \alpha / \partial x$ and the Stefan number is given by $Ste = (T_m - \text{To}) C_p / \lambda$.

The components of v_n are $(1+\varepsilon^2\alpha'^2)v_n(-\varepsilon^2\alpha',1)$, hence to leading order, $v_n \approx \vec{v}_2$. From (C.2) one can conclude that $v_n = O(\varepsilon)$ which is consistent with the asymptotic channel approximation. Accordingly, one puts $\vec{v}_2 = \vec{v}\,\varepsilon\, V$. In this way, The approximation of (C.2) is found to be:

$$\vec{v} = \frac{Ste}{Gz}\frac{\partial}{\partial y}\left(\frac{k_s}{k}\theta_s - \theta\right)_{y=\alpha} \qquad (3.25)$$

Appendix D
The Derivations of Velocity and Pressure Gradient Integrations

With the assumption of ($\partial\pi / \partial x < 0$) the model momentum equation is written as:

$$\frac{\partial \pi}{\partial x} = \mathrm{Re}^{-1} \frac{\partial}{\partial y} e^{-A\theta} \left| \frac{\partial u}{\partial y} \right|^n \qquad (D.1)$$

At any point in the flow field, we can write $u = \partial Q / \partial y$ then :

$$\frac{\partial \pi}{\partial x} = \mathrm{Re}^{-1} \frac{\partial}{\partial y} e^{-A\theta} \left| \frac{\partial^2 Q}{\partial y^2} \right|^n \qquad (D.2)$$

Because of $\partial\pi / \partial y = 0$, then :

$$\frac{\partial^2 Q}{\partial y^2} = \mathrm{Re}^{1/n} e^{\frac{A\theta}{n}} \left(\frac{\partial \pi}{\partial x} \right)^{1/n} y^{1/n} \qquad (D.3)$$

Take anti-derivative , anti-derivative constants are neglected :

$$\frac{\partial Q}{\partial y} = \mathrm{Re}^{1/n} e^{\frac{A\theta}{n}} \left(\frac{\partial \pi}{\partial x} \right)^{1/n} y^{(1+1/n)} \qquad (D.4)$$

Take integration along y-axis from 0 to α , integration constant neglected :

$$Q = \mathrm{Re}^{1/n}\left(\frac{\partial \pi}{\partial x}\right)^{1/n}\int_0^{\alpha} e^{\frac{A\theta}{n}} y^{(1+1/n)}dy \qquad (D.5)$$

Take power of n for both sides , then solve for $\partial\pi / \partial x$:

$$\frac{\partial \pi}{\partial x} = Q^n \mathrm{Re}^{-1}\left[\int_0^{\alpha} e^{\frac{A\theta}{n}} y^{(1+1/n)}dy\right]^{-n} \qquad (D.6)$$

Substituting (I.6) into (I.3) then take integration along y-axis :

$$u(x,y,\tau) = Q\frac{\int_y^{\alpha} e^{\frac{A\theta}{n}} y^{1/n}dy}{\int_0^{\alpha} e^{\frac{A\theta}{n}} y^{(1+1/n)}dy} \qquad (D.7)$$

The expression (D.7) satisfies the entrance boundary condition , so it is acceptable. An interested reader can check it himself. The two main mathematical reasons for neglecting the above constants :

* There are not sufficient information about the boundary condition.

* The $\partial\pi / \partial x$ is not yet determined.

For this case, the entrance velocity profile is :

$$u(0,y,\tau) = Q\frac{2n+1}{n+1}\left(1 - y^{(1+1/n)}\right) \qquad (D.8)$$

Appendix E

Simpson's Rule For Numerical Integration of Unequal Spaced X-Data

Simpson's rule uses a parabolic curve to approximate the actual segment of the integrand over any three points, say X_{i-1}, X_i, X_{i+1} on the integrand curve. The general quadratic function is $y = ax^2 + bx + c$. Three equations, namely $Y_{i-1}(X_{i-1})$; $Y_i(X_i)$ and $Y_{i+1}(X_{i+1})$ may be used to solve for the coefficients "a", "b" and "c" as follows :

$$a = \frac{Y_i(X_{i-1} - X_{i+1}) + X_i(Y_{i+1} - Y_{i-1}) + Y_{i-1}X_{i+1} - Y_{i+1}X_{i-1}}{X_i^2(X_{i-1} - X_{i+1}) + X_{i-1}^2(X_{i+1} - X_i) + X_{i+1}^2(X_i - X_{i-1})}$$

$$b = \frac{(Y_i - Y_{i+1})}{(X_i - X_{i+1})} - a(X_i + X_{i+1}) \quad \text{, and} \quad c = Y_i - aX_i^2 - bX_i$$

The area between the three points and the x-axis can be determined as follows:

$$A(X_{i-1}\ X_{i+1}) = \int_{X_{i-1}}^{X_{i+1}} (ax^2 + bx + c)dx = \frac{a}{3}(X_{i+1}^3 - X_{i-1}^3) + \frac{b}{2}(X_{i+1}^2 - X_{i-1}^2) + c(X_{i+1} - X_{i-1})$$

Appendix F
The Polymer Orientation in Injection Molded Objects

Orientation in polymers simply refers to the alignment of polymer chains whether they are stretched or not. In the molten state, polymer chains have a preferred relaxed state, and with randomly coiled up configuration and oriented distribution. In shearing flowing, the shear stress of flow will distort coiled up configuration of polymers and have a tendency of aligning and stretching the polymer chains parallel to the shearing direction. This parallel alignment creates strong and weak directions in a molded part. Polymers are stronger in the alignment direction because the atom to atom bonds are much stronger than the weak forces attracting neighboring chains. Usually shrinkage is greater along the alignment direction than in any other direction. Due to the characteristics of shearing flow, injection molded parts are not uniformally oriented. The degree of orientation of polymer chains varies considerably through the cross section from the surface to the core of the part. It also varies slightly along the length of the part. The magnitude of these variations also depends on the temperature, pressure, injection flow rate and the mold temperature.

In general, the cavity shearing flow usually defines three distinctable layers of orientation : surface , sub-surface and core regions.

1, The boundary between the advancing melt and the still empty portion of the cavity is called the melt front. Due to the surface tension effect, this melt front behaves like a stretching membrane of polymer as a balloon. Note that the direction of stretching at the front is tangential to the front surface and normal to the flow direction. This stretching creates considerable orientation of the polymer molecules The melt front rolls out (like a bull dozer tread) onto the surface of the mold cavity, creating a thin region of surface orientation on the plastic part.

2, Behind the melt front, more polymer is flowing to keep the advancing melt front "inflated". In this zone, the polymer orientation is caused by shearing of one polymer layer over another which is a consequence of the unavoidable velocity difference resulting from the central plane flowing faster than the edges. This shearing flow creates another band of high orientation just under the surface layer which came from the stretching front. One edge of this band is hung up on the frozen surface layer, while the other edge is trying to go along with the main core flow. this edge is about the maximum shear stress line along the flow. Thus the relative position of the calculated maximum shear rate line can be compared with the thickness of this oriented sub-surface region.

3, Finally the core of the part is also oriented to some degree due to shearing and velocity gradations; the orientation gradually diminishes to nothing at the central line.

The program can not estimate the thickness of the oriented surface layer which is caused by the fountain effect of melt front. What we can say about it is that its

thickness is strongly dependent on the shape of the moving melt front. It is worth noting that the shearing and stretching forces essentially disappear after the flow ceases and the polymer orientation can relax out to various degrees. The relaxation is affected by the melt temperature, the mold temperature and the packing pressure. A birefringence measurement technique is usually used to determine the orientation pattern of polymer chains across the thickness of a molded plastic part [52].

VITA AUCTORIS

The author was born in 1963, in Vietnam.

His high school was H.B. Beal School in London, Ontario.

He received his Bachelor of Applied Science in Engineering Materials in the summer of 1988, and then he spent one year studying research in the fracture toughness of A-2 chromoloy tool steel, 3 months on polymer scrap reinforced concrete, and finally he started working on this thesis topic in Aug/1989, solo. He completed his M.A.Sc degree at the same school, University of Windsor, in the spring of 1991.

The same pyrenee ranges , this side is true, the other side is false

Blaise Pascal

Possunt, quia posse videntur.

[Mathematician Aeneid, V]

They can, because they know they can.